

Electronic Thesis and Dissertation Repository

9-29-2014 12:00 AM

Numerical and Experimental Studies of Transmission Lines Subjected to Tornadoes

Ahmed Hamada
The University of Western Ontario

Supervisor
Ashraf El Damatty
The University of Western Ontario

Graduate Program in Civil and Environmental Engineering
A thesis submitted in partial fulfillment of the requirements for the degree in Doctor of
Philosophy
© Ahmed Hamada 2014

Follow this and additional works at: <https://ir.lib.uwo.ca/etd>



Part of the [Structural Engineering Commons](#)

Recommended Citation

Hamada, Ahmed, "Numerical and Experimental Studies of Transmission Lines Subjected to Tornadoes" (2014). *Electronic Thesis and Dissertation Repository*. 2479.
<https://ir.lib.uwo.ca/etd/2479>

This Dissertation/Thesis is brought to you for free and open access by Scholarship@Western. It has been accepted for inclusion in Electronic Thesis and Dissertation Repository by an authorized administrator of Scholarship@Western. For more information, please contact wlsadmin@uwo.ca.

NUMERICAL AND EXPERIMENTAL STUDIES OF TRANSMISSION LINES
SUBJECTED TO TORNADOES

(Thesis format: Integrated Article)

by

Ahmed Hamada

Graduate Program in Engineering Science
Department of Civil and Environmental Engineering

A thesis submitted in partial fulfillment
of the requirements for the degree of
Doctor of Philosophy

The School of Graduate and Postdoctoral Studies
The University of Western Ontario
London, Ontario, Canada

© Ahmed Hamada 2014

ABSTRACT

The majority of worldwide weather-related transmission line failures have been attributed to High Intensity Wind (HIW) events in the form of tornadoes and downbursts. The research conducted in the current thesis presents a significant development in the understanding of the structural behaviour of transmission line systems under tornado loading. A comprehensive in-house numerical model that combines the data of computational fluid dynamic (CFD) simulations of tornado wind fields with three dimensional nonlinear structural analysis modelling is developed. A three dimensional four-noded cable element is first formulated to simulate the nonlinear large deformation behaviour of the conductors. The support provided to the conductors through the towers and the insulators is modelled using a three dimensional nonlinear spring system with stiffness dependent on the rotation experienced by the insulators. This lines model is used to assess the importance of accounting for the flexibility of the insulators and supporting towers on the lines behaviour, the effect of the tornado loads acting on conductors on the overall response of transmission towers, and the behaviour of conductors under the most critical tornado configurations. The in-house model formulation is extended by including a simulation for members of the lattice towers using three dimensional nonlinear frame elements. By including a failure model, the numerical model is employed to predict the tornado velocities at which failure initiates and to describe the progress of collapse. The in-house numerical model provides a lot of flexibility, in term of computational efficiency and in term of implementation of various failure models. A sophisticated aeroelastic model of a three span transmission line system is designed and constructed to perform a boundary layer wind tunnel test. The results of the test are used to investigate

the dynamic response of the transmission line system under boundary layer wind, and to validate the developed numerical model. Finally the numerical model is used to develop a set of load configurations simulating the critical effect of F2 tornado on Lattice transmission line structures that can be implemented in the codes of design and can be used by line design engineers.

KEYWORDS

Transmission line, Tornado, Wind load, Finite element, Aeroelastic, Design, Failure, Wind tunnel, Transmission tower

CO-AUTHORSHIP

This thesis has been prepared in accordance with the regulations for an Integrated Article format thesis stipulated by the School of Graduate and Postdoctoral Studies at the University of Western Ontario. Statements regarding the co-authorship of individual chapters are as follows:

Chapter 2: ANALYSIS AND BEHAVIOUR OF GUYED TRANSMISSION LINES UNDER TORNADO WIND LOADS

All the numerical work was conducted by A. Hamada under close supervision of Dr. A. A. El Damatty. Drafts of Chapter 2 were written by A. Hamada and modifications were done under supervision of Dr. A. A. El Damatty. A paper co-authored by A. Hamada and A. A. El Damatty was submitted and published in the *Canadian Society of Civil Engineers (CSCE) 2013 Conference*.

Chapter 3: NONLINEAR FORMULATION OF FOUR-NODED CABLE ELEMENT AND ANALYSIS OF TRANSMISSION LINES CONDUCTORS UNDER TORNADO WIND LOADS

All the numerical work was conducted by A. Hamada under close supervision of Dr. A. A. El Damatty. Drafts of Chapter 3 were written by A. Hamada and modifications were done under supervision of Dr. A. A. El Damatty. A paper co-authored by A. Hamada and A. A. El Damatty was submitted and published in the *2014 International Conference on Advances in Wind and Structures (AWAS14) - ACEM14*.

Chapter 4: BEHAVIOUR OF TRANSMISSION LINE CONDUCTORS UNDER TORNADO WIND LOADS

All the numerical work was conducted by A. Hamada under close supervision of Dr. A. A. El Damatty. Drafts of Chapter 4 were written by A. Hamada and modifications were done under supervision of Dr. A. A. El Damatty. A paper co-authored by A. Hamada and A. A. El Damatty will be submitted to the *Journal of Wind and Structures*.

Chapter 5: FAILURE ANALYSIS OF GUYED TRANSMISSION LINES DURING TORNADO EVENTS

All the numerical work was conducted by A. Hamada under close supervision of Dr. A. A. El Damatty. Drafts of Chapter 5 were written by A. Hamada and modifications were done under supervision of Dr. A. A. El Damatty. A paper co-authored by A. Hamada and A. A. El Damatty has been submitted to the *Engineering Structures Journal*.

Chapter 6: DEVELOPMENT AND TESTING OF AN AEROELASTIC MODEL OF GUYED TRANSMISSION LINE SYSTEM

All wind tunnel experiments were designed and carried out by A. Hamada under the supervision of Dr. A. A. El Damatty, Dr. Girma T. Bitsuamlak, and Dr. J. Peter C. King, and with the help of Mohamed Hamada. All the numerical work was conducted by A. Hamada. Drafts of Chapter 6 were written by A. Hamada and modifications were done under supervision of Dr. A. A. El Damatty and Dr. Girma T. Bitsuamlak. A paper co-authored by A. Hamada, M. Hamada, A. A. El Damatty, Dr. Girma T. Bitsuamlak, J. Peter C. King will be submitted to the *Journal of Fluids and Structures*.

**Chapter 7: EQUIVALENT F2 TORNADO LOADING ON LATTICE
TRANSMISSION LINE SYSTEMS**

All the analytical work was conducted by A. Hamada under close supervision of Dr. A. A. El Damatty. Drafts of Chapter 7 were written by A. Hamada and modifications were done under supervision of Dr. A. A. El Damatty. A paper co-authored by A. Hamada and A. A. El Damatty has been submitted to the *Journal of Structural Engineering*.

To my lovely wife *Sarah*

To my beloved parents *Shadia* and *El Sayed El Mahdy*

To my brother *Mohamed*

For patiently enduring, support, encouragement, patience, and sharing these years of hard
work

To my supervisor, *Dr. Ashraf A. El Damatty*

For his support as well as his sharing knowledge and expertise during these years

ACKNOWLEDGMENTS

I would like to express my appreciation and gratitude to the people who have helped me. Without them, this thesis would have not been completed.

First, Dr. Ashraf El Damatty, for his valuable guidance, advice, and encouragement throughout the course of this research work. It has been a privilege to work under his supervision.

Second, I would like to thank Dr. Girma T. Bitsuamlak and Dr. J. Peter C. King for their support, patience, and continuous encouragement throughout the experimental part of this research. I would like to express my gratitude to Mr. Gerry Dafoe and everyone at the Boundary Layer Wind Tunnel Laboratory (BLWTL) for helping me and making these past years an enjoyable and fruitful experience.

The author gratefully acknowledges the Vanier Canada Graduate and the Natural Science and Engineering Research Council of Canada (NSERC) for the financial support provided for this research. The author is indebted to Hydro One Inc. for the in-kind support, the collaboration, and the financial support provided for this research.

The author would like also to express his appreciation to Dr. Horia Hangan, Dr. Eric Ho, and Dr. Eric Savory for their constructive criticism and valuable comments throughout the course of this work. For all the graduate students who supported me and shared their valuable experience with me, thank you.

Above all, I thank my wife and my family for their tremendous support throughout this time. For all the love and encouragement provided, I deeply thank my wife, my parents, and my brother.

TABLE OF CONTENTS

ABSTRACT	II
CO-AUTHORSHIP	IV
ACKNOWLEDGMENTS	VIII
LIST OF TABLES	XVII
LIST OF FIGURES	XIX
LIST OF SYMBOLS	XXVIII
CHAPTER 1	1
1.1 General.....	1
1.2 Literature Review.....	4
1.2.1 Tornadoes Wind Profiles	4
1.2.2 Behaviour of Transmission Lines under Normal and High Intensity Wind	8
1.3 Background.....	12
1.4 Objectives of Thesis.....	15
1.5 Scope of Thesis.....	16
1.5.1 Chapter 2 – Analysis and Behaviour of Guyed Transmission Lines under Tornado Wind Loads – Case Studies.....	16
1.5.2 Chapter 3 – Nonlinear Formulation of Four-Noded Cable Element and Application to Transmission Lines under Tornadoes	17
1.5.3 Chapter 4 – Behaviour of Transmission Line Conductors under Tornado Wind Loads.....	18
1.5.4 Chapter 5 – Failure Analysis of Guyed Transmission Lines during Tornado Events.....	18
1.5.5 Chapter 6 – Development and Testing of an Aeroelastic Model of a Guyed Transmission Line System.....	19
1.5.6 Chapter 7 – Equivalent F2 Tornado Loading on Lattice Transmission Line Systems	20

1.6	References.....	20
CHAPTER 2.....		27
2.1	Introduction.....	27
2.2	Finite Element Modelling of Transmission Line Systems.....	29
2.3	F2 Tornado.....	31
2.3.1	F2 Tornado Wind Field.....	31
2.3.2	Evaluation of the Tornado velocity Components at Various Locations of the Transmission Lines System	32
2.4	ASCE No. 74 Guidelines Wind Field.....	33
2.5	CIGRE` Overhead Lines Design Guidelines Wind Field.....	35
2.6	Evaluation of Tornado and Wind Forces on Transmission Line Nodes.....	36
2.7	Parametric Study.....	37
2.7.1	Analysis of Transmission Line Type T1 under F2 Tornado, ASCE 2010, CIGRE`, and Downburst Wind Fields	38
2.7.2	Analysis of Transmission Line Typ2 T2 under F2 Tornado, ASCE 2010, and Downburst Wind Fields	40
2.7.3	Discussion.....	40
2.8	Analysis of Transmission Line System – Broken Wire.....	41
2.8.1	Tower T1.....	42
2.8.2	Tower T2.....	43
2.8.3	Broken Wire Discussion	43
2.9	Conclusion	44
2.10	Acknowledgement	45
2.11	Reference	46
CHAPTER 3.....		49
3.1	Introduction.....	49

3.2	Cable Element Formulation	51
3.2.1	Four-Noded Cable Element and Linear Derivation	51
3.2.2	Geometric Nonlinear Formulation of the Cable Element	55
3.2.3	Steps of Nonlinear Analysis.....	57
3.3	Finite Element Modelling of Transmission Line’s Cables	58
3.3.1	Derivation of Spring System.....	59
3.3.2	Cables Modelling	62
3.4	Tornado Velocity Profile and Loading	62
3.5	Model Validation	64
3.6	Effect of Conductors’ Supports on the Force Transmitted to Transmission Towers	66
3.7	Conclusion	67
3.8	Acknowledgement	68
3.9	Reference	68
3.10	Appendix.....	70
3.10.1	Appendix I	70
3.10.2	Appendix II.....	70
3.10.3	Appendix III.....	70
CHAPTER 4	77
4.1	Introduction.....	77
4.2	F2 Tornado Wind Field on Tower and Conductors	78
4.3	Description of Transmission Lines and Finite Element Model	81
4.4	Effect of Conductors on the Transmission Towers Behaviour	84
4.5	Effect of Various Parameters on Conductors’ Longitudinal Reaction	90
4.5.1	Effect of Magnitude of Load.....	93

4.5.2	Effect of Conductors' Pretension and Sag	98
4.5.3	Effect of Insulator Length	100
4.5.4	Effect of Conductor Self-Weight	101
4.6	Conclusion	102
4.7	Acknowledgement	104
4.8	References	104
CHAPTER 5		106
5.1	Introduction.....	106
5.2	F2 Tornado Wind Fields	109
5.3	Description of the Two Considered Guyed Transmission Line Systems	110
5.4	Components and Validation of the Numerical Model	111
5.4.1	Modeling of Conductors and Ground-wires	113
5.4.2	Simulation of Insulators	116
5.4.3	Simulation of Guys	118
5.4.4	Simulation of Tower Members	119
5.4.5	Numerical Model Validation	120
5.5	Failure Analysis	121
5.5.1	Failure Analysis – No Post Yield Strength.....	125
5.6	Effect of Material Model	135
5.7	Comparison between Failure Studies of the two Lines	136
5.8	Effect of Geometric Nonlinearities	138
5.9	Conclusion	139
5.10	Acknowledgement	141
5.11	References.....	141
5.12	Appendices.....	144

5.12.1	Appendix A.....	144
5.12.2	Appendix B.....	146
5.12.3	Appendix C.....	146
CHAPTER 6	151
6.1	Introduction.....	151
6.2	Description of the Aeroelastic Model of Transmission Line System.....	156
6.2.1	Description of Transmission Line System.....	156
6.2.2	Dynamic Properties of Full-scale Transmission Line System.....	158
6.2.3	Aeroelastic Model and Testing Plan.....	161
6.3	Results and Discussion.....	176
6.3.1	Mode Shapes Frequencies and Damping.....	176
6.3.2	Accelerometer Results.....	177
6.3.3	Tower Supporting Guy Forces.....	179
6.3.4	Bending Moments.....	190
6.4	Validation of an In-house Three Dimensional Finite Element Model of Transmission Line System.....	200
6.4.1	Validation of the Numerical Model without Conductors.....	201
6.4.2	Validation of the Numerical Model with Conductors.....	203
6.5	Effect of Conductors on the Structural Response of the Transmission Line System	206
6.5.1	Transmission Tower’s Supporting Guys.....	206
6.5.2	Transmission Tower’s Internal Forces.....	207
6.6	Conclusions.....	210
6.7	Acknowledgement.....	212
6.8	References.....	212
CHAPTER 7	216

7.1	Introduction.....	216
7.2	Description of the Transmission Line Systems Used to Develop Critical Load Cases	221
7.2.1	Finite Element Modelling.....	225
7.2.2	F2 Tornado Wind Field.....	225
7.3	Parametric study.....	228
7.3.1	Critical tornado configuration on transmission tower’s main body.....	230
7.3.2	Critical tornado configuration on cross-arms	232
7.4	Velocity Profiles for Critical Load Cases for the Towers – Tower Profiles.....	237
7.5	Velocity Profiles for Critical Load Cases for Cross-arms – Line Profiles	239
7.6	Steps of Applying Critical Load Cases on Transmission lines.....	240
7.7	Verification using different towers configurations	241
7.7.1	Description of the Two Transmission Line Systems	242
7.7.2	Analysis and Discussion	243
7.8	Conclusion	245
7.9	Acknowledgment	247
7.10	References.....	247
7.11	Appendices.....	251
7.11.1	Appendix I	251
7.11.2	Appendix II.....	256
7.11.3	Appendix III.....	264
7.11.4	Appendix IV.....	267
	CHAPTER 8.....	272
8.1	Summary.....	272
8.2	Conclusions.....	274

8.3	Recommendation for Future Work	280
	CURRICULUM VITAE.....	281

LIST OF TABLES

Table 1-1 Comparison of Tornado Categorizations from Design Guides (ASCE 2010 and CIGRÉ 2009) and the Enhanced Fujita Scale for Tornadoes	6
Table 2-1 Results of the Parametric Study due to F2 Tornado, Downburst, Conventional Wind, and CIGRE` Wind.....	39
Table 2-2 Results of the Parametric Study due to F2 Tornado, Downburst, and Conventional Wind Fields (Tower T2).....	41
Table 2-3 Results of Broken Wire Cases – Tower T1	44
Table 2-4 Results of Broken Wire cases – Tower T2.....	44
Table 3-1 Physical Parameters Employed for Conductors and Ground-wires	59
Table 3-2 In-house and SAP 2000 Conductor’s Reactions Comparison (F2 Tornado Configuration $R= 125$ and $\theta = 180^\circ$).....	65
Table 4-1 Physical Parameters Employed for Conductors and Ground-wires	84
Table 4-2 Results of the Parametric Study Conducted for Transmission Tower T1	87
Table 4-3 Results of the Parametric Study Conducted for Transmission Tower T2	89
Table 5-1 Cable Properties and Axial Forces	115
Table 5-2 <i>FTTHIW</i> and SAP 2000 Transmission Tower (T1) Peak Internal forces of Selected Members ($R = 125$ (m) and $\theta = 0$).....	121
Table 5-3 <i>FTTHIW</i> and SAP 2000 Conductor’s Reactions ($R = 125$ (m) and $\theta = 0$).....	121
Table 5-4 Summary of Failure Velocities Predicted by Both Material Models	136
Table 5-5 Comparison between Linear and Nonlinear Analyses of Tower T1 under F2 Tornado Wind Loads	139

Table 6-1 Frequencies and Damping of Full-scale Tower.....	160
Table 6-2 Scaling Ratio of Physical Parameters of the Aeroelastic Model.....	165
Table 6-3 Matching Tower Mass to Spine Mass	169
Table 6-4 Normalized Mean Wind Speed at Reference Height and the Longitudinal Turbulence at the Different Velocity Measurement Locations.....	175
Table 6-5 Supporting Guys Forces, Tower Base Reactions, and Tower’s Bending Moments of the Aeroelastic and the Numerical Models – without Conductors Case	201
Table 6-6 Supporting Guys Forces, Tower’s Bending Moments, Conductor’s Longitudinal Reaction of the Aeroelastic and Numerical Model – with Conductors.....	206
Table 7-1 Recommended Twelve Case of Loading of Transmission Towers and Lines for Peak Internal Forces in the Tower of Interest.....	238
Table 7-2 Recommended Six Case of Loading of Transmission Towers and Lines for Maximum Longitudinal and Transverse Reactions of Transmission Lines	239
Table 7-3 Parametric Study and Equivalent Loading Cases Results for Tower T5	244
Table 7-4 Parametric Study and Equivalent Loading Cases Results for Tower T6	245

LIST OF FIGURES

Fig. 1-1 Schematic View of Guyed Transmission Line System	3
Fig. 2-1 Geometry of the Modelled Guyed Towers.....	30
Fig. 2-2 Vertical Profile of Tangential Component for Different Radial Distances from Tornado Centre	31
Fig. 2-3 Horizontal Projection of Transmission Tower and F2 Tornadoes	33
Fig. 2-4 Recommended Torsional Wind Load Case Recommended by CIGRE'	37
Fig. 3-1 Cable Element Coordinate and Systems and Nodal Degrees of Freedom	53
Fig. 3-2 Finite Element Model for Transmission Line Systems.....	59
Fig. 3-3 Conductors' Cross-arms and Insulators Configurations	61
Fig. 3-4 Horizontal Projection of F2 Tornado Located at Relative Distance $R = 125$ (m) and $\theta = 180^\circ$	63
Fig. 3-5 Transverse Velocity Profile – Conductors ($R = 125$ (m), and $\theta = 180^\circ$).....	64
Fig. 3-6 Conductors Axial (Vertical) Velocity Profile ($R = 125$ (m), and $\theta = 180^\circ$).....	64
Fig. 3-7 Cable Displacements in Elevation and Plan View using SAP 2000 and Current Numerical Code (F2 Tornado $R= 125$ and $\theta = 180^\circ$).....	66
Fig. 3-8 Iterations to Convergence at Load Level R^t , Newton – Raphson Method.....	71
Fig. 4-1 Vertical Profile of Tangential Velocity Component for Different Radial Distances from Tornado Center (F2 Tornado).....	80
Fig. 4-2 Variation of the Three Velocity Components of F2 Tornado along the Height at Distance 100 (m) from Tornado Center.....	80

Fig. 4-3 Variation of the Three Velocity Component of F2 Tornado along the Height at Distance 150 (m) from Tornado Center.....	81
Fig. 4-4 Geometry of the Modelled Guyed Transmission Lines	82
Fig. 4-5 Cable Element Coordinate and Systems and Nodal Degrees of Freedom	83
Fig. 4-6 Tornado Parameters (Configurations) R and θ	84
Fig. 4-7 Geometry of Guyed Tower T1 – Transmission Line L1.....	85
Fig. 4-8 Geometry of Guyed Tower T2 – Transmission Line 2	86
Fig. 4-9 Horizontal Projection of F2 Tornado Located at Relative Distance $R = 125$ (m) and $\theta = 180^\circ$	91
Fig. 4-10 Transverse Velocity Distribution along the Conductors – $R = 125$ (m) and $\theta = 30, 45, 60, 90, 180^\circ$	91
Fig. 4-11 Vertical Velocity Distribution along the Conductors – $R = 125$ (m) and $\theta = 180^\circ$	92
Fig. 4-12 Deformed Shape of Transmission Line L1 due to F2 Tornado Configurations $R = 125$ (m) and $\theta = 180^\circ$	93
Fig. 4-13 Deformed Shape of Transmission Line L2 due to F2 Tornado Configurations $R = 125$ (m) and $\theta = 180^\circ$	93
Fig. 4-14 Transmission Line System L1 Longitudinal Reactions due to the Variation of the Applied F2 Tornado Loads	95
Fig. 4-15 Transmission Line System L2 Longitudinal Reactions due to the Variation of the Applied F2 Tornado Loads	95
Fig. 4-16 Transmission Line System L1 Transverse and Vertical Reactions due to the Variation of the Applied F2 Tornado Loads.....	96

Fig. 4-17 Transmission Line System L2 Transverse and Vertical Reactions due to the Variation of the Applied F2 Tornado Loads.....	97
Fig. 4-18 Variation of Transmission Line's Transverse Reaction with Pretension Force and Sag – $R = 125$ (m) (Transmission Line System L1)	98
Fig. 4-19 Variation of Transmission Line's Vertical Reaction with Pretension Force and Sag – $R = 125$ (m) (Transmission Line System L1)	99
Fig. 4-20 Variation of Transmission Line's Longitudinal Reaction with Pretension Force and Sag – $R = 125$ (m) (Transmission Line System L1)	99
Fig. 4-21 Variation of Longitudinal Reaction with Pretension force	100
Fig. 4-22 Variation of Longitudinal Reaction with Insulator Lengths	101
Fig. 4-23 Variation of Longitudinal Reaction with Conductor's self-weight.....	102
Fig. 5-1 Transmission line system (L1) – Tower Type (T1)	110
Fig. 5-2 Transmission line system (L2) – Tower Type (T2)	110
Fig. 5-3 Finite Element Model for L1 and L2 Transmission Lines (Conductors and Ground wires)	113
Fig. 5-4 Cable Element Coordinate System and Nodal Degrees of Freedom	113
Fig. 5-5 Cable Geometry and Loading	114
Fig. 5-6 Cable Displacements in Elevation and Plan View using SAP 2000 and Current 4-Nodes Cable Element.....	114
Fig. 5-7 Conductors' Cross-arms and Insulators Configurations of Tower T1	117
Fig. 5-8 Equivalent Cable Element.....	118
Fig. 5-9 Tornado Configurations R and θ Relative to the Tower of Interest	123

Fig. 5-10 Failure Analysis (First Method) L1 – T1, Analysis Case $R = 125$ (m) and $\theta = 180^\circ$	127
Fig. 5-11 Transverse Velocity Profile – Conductors	127
Fig. 5-12 Simulation of the Tower as an Over-hanging Beam - Failed Members L1 – T1, Analysis Case $R = 125$ (m) and $\theta = 180^\circ$	128
Fig. 5-13 Failure Analysis (First Method) L1 – T1, Analysis Case $R = 125$ (m) and $\theta = 30^\circ$	129
Fig. 5-14 Transverse Velocity profile – Conductors	130
Fig. 5-15 Failed Members L1 – T1, Analysis Case $R = 125$ (m) and $\theta = 30^\circ$	130
Fig. 5-16 Failure Analysis L2 – T2, Analysis Case $R = 125$ (m) and $\theta = 330^\circ$	132
Fig. 5-17 Failed Members L2 – T2, Analysis Case $R = 125$ (m) and $\theta = 330^\circ$	133
Fig. 5-18 Failure Analysis L2 – T2, Analysis Case $R = 125$ (m) and $\theta = 180^\circ$	134
Fig. 5-19 Vertical Profile of F2 Tornado Three Velocity Components at $R = 100$ (m) .	134
Fig. 5-20 Failed Members L2 – T2, Analysis Case $R = 125$ (m) and $\theta = 180^\circ$	135
Fig. 5-21 Equivalent Cable Element in Local Coordinates	145
Fig. 5-22 Degrees of Freedom on Three Dimensional Frame Element in Local Coordinates	150
Fig. 6-1 Schematic of the Full-scale Guyed Transmission Tower.....	157
Fig. 6-2 Schematic View of the Three Dimensional Finite Element Model	158
Fig. 6-3 First Two Mode Shapes of the Transmission Tower – (Pretension Force 10 and 7 (kN)).....	161

Fig. 6-4 Assembled Aeroelastic Transmission Line Model ($\Psi = 30^\circ$)	163
Fig. 6-5 Schematic of the Transmission line Full Aeroelastic Model	163
Fig. 6-6 Aeroelastic model Yaw angle ($\Psi = 90, 75, \text{ and } 30^\circ$).....	164
Fig. 6-7 The 1:50 Scale of Transmission Tower Aeroelastic Model.....	167
Fig. 6-8 Assembled Transmission Tower Aeroelastic Model	168
Fig. 6-9 Supporting Guys Anchorage and Pretension Adjustment and Measurements..	170
Fig. 6-10 2-DOF Universal Base Support.....	171
Fig. 6-11 Vertical Profile of Mean Wind Speed and Longitudinal Turbulence Intensity Measured at the Center Location, (Reference Wind 46.7 m/sec).....	174
Fig. 6-12 Wind Profile Test Locations	175
Fig. 6-13 Assembled Aeroelastic Transmission Line Model ($\Psi = 90^\circ$)	176
Fig. 6-14 Relation between Accelerometers rms and Wind Speeds (m/sec) for Both Towers – Case of Towers only	177
Fig. 6-15 Relation between Accelerometers rms values and Wind Speeds (m/sec) for Both Towers – Case of Towers with Conductors	178
Fig. 6-16 Time Histories of Measured Supporting Guy 2 Axial Force for Different Wind Speeds – without Conductors Case.....	181
Fig. 6-17 Boundary Layer Supporting Guy 2 Response Spectra due to Reference Mean Wind Speed of 9.4, 18.0, 27.0, and 36.6 (m/sec), Respectively	184
Fig. 6-18 Variation of the Internal Force of the Supporting Guy 2 with Different Wind Speeds	185

Fig. 6-19 Time Histories of Measured Supporting Guy 2 Axial Force for Different Wind Speeds – with Conductors Case	187
Fig. 6-20 Boundary Layer Supporting Guy 2 Response, with Conductors Case, Spectra due to Reference Mean Wind Speed of 9.4, 18.0, 27.0, and 36.6 (m/sec), Respectively	190
Fig. 6-21 Time Histories of Measured Mid. Far Tower Bending Moment for Different Wind Speeds – without Conductors Case.....	192
Fig. 6-22 Boundary Layer Far Tower Mid. Bending Moment Response Spectra due to Reference Mean Wind Speed of 9.4, 18.0, 27.0, and 36.6 (m/sec), Respectively.....	195
Fig. 6-23 Time Histories of Measured Mid. Far Tower Bending Moment for Different Wind Speeds – with Conductors Case	197
Fig. 6-24 Boundary Layer Far Tower Mid. Bending Moment, with Conductors Case, Response Spectra due to Reference Mean Wind Speed of 9.4, 18.0, 27.0, and 36.6 (m/sec), Respectively	200
Fig. 6-25 Time History of Measured Conductor’s Longitudinal Reaction on Tower’s Cross-arm (N) – Near Tower	203
Fig. 6-26 Boundary Layer Conductor’s Longitudinal Reaction on Tower Cross-arms Response Spectra due to Reference Mean Wind Speed of 36.6 (m/sec).....	205
Fig. 6-27 Simulation of the Guyed Tower as an Overhanging Beam.....	208
Fig. 6-28 Conductor’s Cross-arms Orientation and Longitudinal Reaction	209
Fig. 7-1 Vertical profile of tangential velocity component for different radial distances from F4 tornado center.....	217
Fig. 7-2 Guyed Towers T1 and T2.....	223
Fig. 7-3 Self-supported Towers T3 and T4.....	224

Fig. 7-4 Vertical profile of tangential velocity component for different radial distances “ r ” from tornado center – F2 Tornado	227
Fig. 7-5 Vertical profile of radial velocity component for different radial distances “ r ” from tornado center – F2 Tornado	227
Fig. 7-6 Vertical profile of axial (vertical) velocity component for different radial distances “ r ” from tornado center – F2 Tornado	228
Fig. 7-7 Tornado Configurations R and θ Relative to the Tower of Interest	229
Fig. 7-8 Variation of Transmission Line’s Transverse Reaction with R and θ (T1 Tower)	233
Fig. 7-9 Schematic View of Critical Tornado Configuration $R = 250$ (m) and $\theta = 60^\circ$ (T1 Tower).....	234
Fig. 7-10 Variation of Transmission Line’s Vertical Reaction with R and θ (T1 Tower)	234
Fig. 7-11 Variation of Transmission Line’s Longitudinal Reaction with R and θ (T1 Tower).....	236
Fig. 7-12 Variation of Transmission Line’s Longitudinal Reaction with R and θ (T2 Tower).....	237
Fig. 7-13 Verification Transmission Towers – Tower T5 and T6.....	243
Fig. 7-14 Tower Velocity Profile A along Tower Height – F2 Tornado.....	251
Fig. 7-15 Tower Velocity Profile B along Tower Height – F2 Tornado	252
Fig. 7-16 Tower Velocity Profile C along Tower Height – F2 Tornado	252
Fig. 7-17 Tower Velocity Profile D along Tower Height – F2 Tornado.....	253

Fig. 7-18 Tower Velocity Profile F along Tower Height – F2 Tornado.....	253
Fig. 7-19 Tower Velocity Profile G along Tower Height – F2 Tornado.....	254
Fig. 7-20 Line Velocity Profile H – F2 Tornado Transverse Velocity Profile along the Lines.....	256
Fig. 7-21 Line Velocity Profile I – F2 Tornado Transverse Velocity Profile along the Lines.....	256
Fig. 7-22 Line Velocity Profile J – F2 Tornado Transverse Velocity Profile along the Lines.....	257
Fig. 7-23 Line Velocity Profile K – F2 Tornado Transverse Velocity Profile along the Lines.....	257
Fig. 7-24 Line Velocity Profile L – F2 Tornado Transverse Velocity Profile along the Lines.....	258
Fig. 7-25 Line Velocity Profile M – F2 Tornado Transverse Velocity Profile along the Lines.....	258
Fig. 7-26 Line Velocity Profile N – F2 Tornado Transverse Velocity Profile along the Lines.....	259
Fig. 7-27 Line Velocity Profile O – F2 Tornado Transverse Velocity Profile along the Lines.....	259
Fig. 7-28 Line Velocity Profile P – F2 Tornado Transverse Velocity Profile along the Lines.....	260
Fig. 7-29 Line Velocity Profile Q – F2 Tornado Transverse Velocity Profile along the Lines.....	260
Fig. 7-30 Line Velocity Profile R – F2 Tornado Transverse Velocity Profile along the Lines.....	261

Fig. 7-31 Line Velocity Profile S – F2 Tornado Transverse Velocity Profile along the Lines.....	261
Fig. 7-32 Tower Velocity Profile C1 along Tower Height – F2 Tornado	264
Fig. 7-33 Tower Velocity Profile C2 along Tower Height – F2 Tornado	264
Fig. 7-34 Tower Velocity Profile C3 along Tower Height – F2 Tornado	265
Fig. 7-35 Tower Velocity Profile C4 along Tower Height – F2 Tornado	265
Fig. 7-36 Tower Velocity Profile C5 along Tower Height – F2 Tornado	266
Fig. 7-37 Line Velocity Profile C6 – F2 Tornado Transverse Velocity Profile along the Lines.....	267
Fig. 7-38 Line Velocity Profile C7 – F2 Tornado Transverse Velocity Profile along the Lines.....	268
Fig. 7-39 Line Velocity Profile C8 – F2 Tornado Transverse Velocity Profile along the Lines.....	268
Fig. 7-40 Line Velocity Profile C9 – F2 Tornado Transverse Velocity Profile along the Lines.....	269
Fig. 7-41 Line Velocity Profile C10 – F2 Tornado Transverse Velocity Profile along the Lines.....	269
Fig. 7-42 Line Velocity Profile C11 – F2 Tornado Transverse Velocity Profile along the Lines.....	270

LIST OF SYMBOLS

Symbol	Units	Description
A_i	m^2	Projected area perpendicular to “ i “ direction at the loaded Node
A_x	m^2	Projected area perpendicular to X - direction at the loaded Node
A_y	m^2	Projected area perpendicular to Y - direction at the loaded Node
A_z	m^2	Projected area perpendicular to Z - direction at the loaded Node
C_f	--	Drag Force coefficient
C_{fx}	--	Average of drag force coefficients in X - direction
C_{fy}	--	Average of drag force coefficients in Y - direction
C_{fz}	--	Drag force coefficients in Z - direction
E	N/m^2	Modulus of elasticity
E_{eq}	N/m^2	Equivalent modulus of elasticity
F_c	kN	Reaction force of the conductors on the tower
F_g	kN	Reaction force of the ground wire on the tower

F_{wi}	N	Nodal point wind force in “ i ” direction
F_x	N	Total tornado wind force component in global X - direction
F_y	N	Total tornado wind force component in global Y - direction
F_z	N	Total tornado wind force component in global Z - direction
G	--	Gust response factor
h_o	m	Height of the fluid computational domain
K	--	Shielding factor
K'	--	Wind parameter for G gust response factor calculations
K_z	--	Exposure coefficient
K_{zt}	--	Topographic coefficient
L	m	Total lines (conductors) span – Tower members length
L_c	m	Inclined equivalent cable element length
L_l	m	Insulator length
L_s	--	Wind parameter for G gust response factor calculations
L_x	m	Horizontal lines (conductors) length
P	N/m	Distributed tornado force on the tower – Axial force in tower members

P_y	N/m	Weight per unit length of adjacent conductors
R	m	Radial distance between the tower center and the tornado center
r	m	Radial distance relative to the tornado center in the CFD
r_o	m	Radius of the fluid computational domain
R_{fa}	m	Radial full-scale distance between point “a” and the tornado centre
R_{ma}	m	Radial distance in the CFD model between point “a” and The tornado centre
S	--	Swirl ratio – $S = 0.5 (V_t / V_r)$ at the CFD boundaries
S'	m or ft	Design Span
T	sec or N	Fundamental natural period – Cable Tension
V	m/sec	Wind velocity
V_o	m/sec	Reference velocity for CFD model
V_{ama}	m/sec	CFD axial velocity components of point “a”
V_{AX}	m/sec	Full-scale axial velocity component of point “a”
V_i	m/sec	Tornado velocity component in “ i “ direction - 10 m reference 3-sec wind speed in “ i ” direction
V_m	m/sec	Velocity resulting from the CFD model

V_{ma}	m/sec	Axial velocity resulting from the CFD model
V_{mr}	m/sec	Radial velocity resulting from the CFD model
V_{mt}	m/sec	Tangential velocity resulting from the CFD model
V_r	m/sec	Radial velocity at the boundary layer profile inlet
V_{RD}	m/sec	Full-scale radial velocity of point “a”
V_{rma}	m/sec	CFD radial velocity components of point “a”
V_t	m/sec	Tangential velocity at the boundary layer profile inlet
V_{tma}	m/sec	Tangential CFD velocity components of point “a”
V_{TN}	m/sec	Full-scale tangential velocity of point “a”
V_x	m/sec	Nodal tornado velocity component in global X-direction
V_y	m/sec	Nodal tornado velocity component in global Y-direction
z	m	Cartesian coordinate of the point in global Z-direction in the CFD model
Z	m	Cartesian coordinate of the point of interest in global Z – direction
Z_o	m	Reference height of the reference velocity in CFD model

Z_{fa}	m	Cartesian full scale coordinate of point “a” in global Z – direction
Z_{ma}	m	Cartesian coordinate of point “a” in global Z-direction in the CFD model
Z_h	m or ft	Effective height
Z_h	m or ft	Gradient height
ρ_a	kg/m ³	air density
θ	degree	angle between a vertical plane that contains the centre of the tower and the tornado and a vertical plane perpendicular to the transmission line
α	--	Power law exponent
α_{FM}	--	Wind parameter for G gust response factor calculations
θ_{fa}	degree	angle between a vertical plane that contains the centre of the tornado and point “a” and a vertical plane perpendicular to the transmission line
θ_{ma}	degree	angle between a vertical plane that contains the centre of the tornado and point “a” and a vertical plane perpendicular to the transmission line
θ_L	degree	Insulator rotation angle in the longitudinal direction

θ_T	degree	Insulator rotation angle in the transverse direction
Ψ	degree	Wind angle of attack – Aeroelastic test

CHAPTER 1

INTRODUCTION

1.1 General

Electricity plays a vital and essential role in our daily life as almost all business and activities depend on having a reliable source of electricity. Transmission lines are responsible of carrying electricity from the source of production to the distribution system and ultimately to the end users. Failure of transmission lines can have devastating social and economical consequences, so it is imperative to understand how failure occurs, and how to prevent it. The structural components of a transmission line system, as shown in Fig. 1-1, are the towers, the conductors, the ground-wires, and the insulator strings. The towers are slender and flexible structures, which makes them vulnerable to strong wind loads. With respect to structural behaviour, transmission towers can be classified as either self-supported or guyed towers, depending on how they are attached to the ground. Self-supported towers are most commonly used; however, guyed towers tend to be more economical. Majority of transmission towers are made of lattice steel members. Conductors are attached to the towers via insulators strings. For lightning protection, the ground wires are attached directly to the top of the towers. The current study focuses on the behaviour of both types of towers mainly under tornado wind loads.

In Canada, tornadoes occur in almost all the southern regions of the country, such as in southern Alberta, Manitoba, Saskatchewan, Ontario, and Quebec. Ishac and White (1994) reported that of all the populated areas in Canada, southwestern Ontario experiences the

highest rate of tornado incidences. About two tornadoes per 10,000 (km²) occur every year in this region, and most of transmission line failures are caused by tornadoes. 92% of these tornadoes are F2 or less on the Fujita scale. The electrical company Ontario Hydro reported that five out of six weather related line failures in their territory are due to tornadoes (Behncke and White 2006). Newark (1984) concluded that on an average an F3 tornado occurs in southwestern Ontario every five years. In the United States, 800 to 1,000 high-intensity wind storms occur each year leading to extensive damage and/or failure of transmission structures (Behncke and White 2006). The CIGRÉ (2006) questionnaire on line failures indicated that 65% of weather-related events on transmission lines were caused by tornadoes. Twisdale (1982) suggested that tornado wind loads should dominate the design of most transmission lines over 10 miles in central areas of the United States. Despite these facts, the codes of practice, design guidelines, and utilities design methodologies are based solely on the loads resulting from large-scale synoptic events with conventional boundary layer wind profiles. Those profiles are characterized by a monotonic increase in velocity with height, which is different than the wind profiles attributed to tornadoes where the maximum wind speed occurs near the ground. Based on metrological studies, Kareem (2010) concluded that winds developed by thunderstorms, both tornadoes and downbursts, fundamentally differ from the conventional boundary layer wind. A main difference is in the velocity profile along the height. The same conclusion about an inverted velocity profile for tornadoes and downbursts was mentioned by Holmes and Oliver (2000) and Letchford and Chay (2002). Tornadoes and downbursts, which are often referred to as High Intensity Wind

(HIW), are localized events. This leads to a spatial variation in their wind fields, unlike large scale wind events such as hurricanes and cyclones.

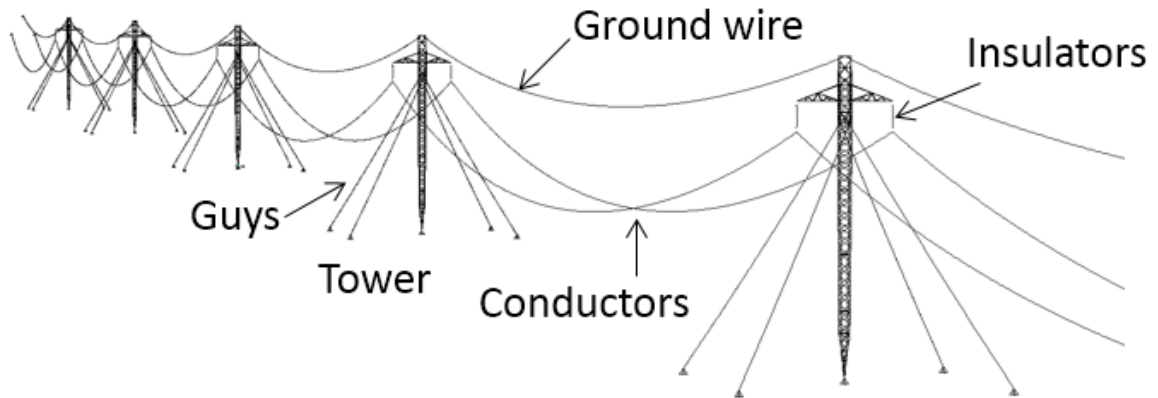


Fig. 1-1 Schematic View of Guyed Transmission Line System

The tornado wind profile has three velocity components. These are the tangential, radial, and vertical components. Unlike conventional wind, the vertical component of a tornado wind profile has a significant effect on the behaviour of transmission line (ASCE 2010). The complexity in analyzing transmission line structures under HIW arises from the fact that tornadoes are localized events with relatively narrow path width and complex wind profile. Due to the localized nature of tornadoes, the forces acting on the tower and the conductors vary based on the location of the event relative to the tower. In fact, some incidences of transmission line failures were attributed to tornadoes with centers located far from the transmission line as documented in the ASCE (2010). The behaviour of the conductors is complicated due to its highly nonlinear behaviour. As a result, the ASCE (2010) recommends that the tornado loads on the lines should be neglected because of such complexity. An extensive study is conducted in the current thesis to develop and validate numerical tools that can be used to determine the behaviour, study the failure

under tornadoes and to design lattice transmission towers to resist the critical loads associated with such events.

1.2 Literature Review

1.2.1 Tornadoes Wind Profiles

Tornadoes are rotating wind vortices with high wind speeds affecting relatively narrow paths as defined by Fujita (1981). They originate from convective clouds that generate rotating columns of air (Twisdale 1982). The Fujita scale (Fujita and Pearson 1973) is the most widely tornado scale currently used. It categorizes tornadoes between F0 to F5 based on maximum wind speed, path length, path width, and level of damage. In 2001, the Texas Tech University Wind Science and Engineering Research Center recommended an alternative categorization, known as the Enhanced Fujita Scale (McDonald et al. 2004 and Ramsdell, Jr. and Rishel, 2007). The Enhanced Fujita Scale is based on the highest wind speed estimated in the tornado path, but the damage classification is still based on the criteria recommended by the original Fujita Scale. The Enhanced Fujita Scale is not widely used yet and the intent to implement it in design codes and manuals of practice has been considered as perhaps being premature due to wind speed estimates being based upon design practices specific to the USA (Doswell III et al. 2009). In Table 1-1, a comparison of tornado categorizations from different design codes, such as ASCE (2010), Enhanced Fujita Scale, and CIGRE` (Council of Large Electric Systems 2009), are presented.

The size and intensity of tornadoes cannot be measured in the field by traditional recording stations due to the severity and the localized nature of these events. Photographic analysis using videos of moving objects in tornadoes, Doppler radar, and damage investigations are the only available methods to estimate the tornado wind speeds (McCarthy and Melsness 1996). This explains the lack of full-scale data for tornadoes available in the literature. Recently, field measurements were recorded by Wurman (1998) and were introduced by Sarkar et al. (2005) for the 1998 Spencer South Dakota F4 tornado and by Lee (2005) for the 1999 Mulhall F4 tornado. Doppler radars are used to obtain the tornado field measurements but the recorded data is not very accurate for the near ground region. Laboratory simulations of tornadoes have been used to obtain the behaviour in the near ground region and to describe the characteristics of the tornado-like-vortices phenomena. The first laboratory attempts were made by Ward (1972) by developing the Ward-type simulator. Tornado simulators were developed over time and led to the creation of Tornado Vortex Chambers (TVC), which provide a good simulation of the characteristics inside a tornado. However, the results from the laboratory simulation are sensitive to the applied boundary conditions. Numerical simulations, using Computational Fluid Dynamics (CFD), can provide a good assessment of the flow field near the ground.

Harlow and Stein (1974) developed one of the first numerical models to simulate tornado-like vortices. The two-dimensional axisymmetric model produced both the one-cell and two-cell vortices using a free-slip lower boundary condition. Rotunno (1977) and Rotunno (1979) was able to capture the vortex break down of a tornado-like vortices using a no-slip lower boundary condition. The simulations showed the vortex core size to

be function of the swirl ratio (S), where S is half the ratio between the tangential and radial velocities at the computational domain boundaries. Rotunno (1984) was able to simulate multiple vortices by introducing random noise to a three dimensional modal of Ward-type tornado vortex chamber (TVC). The simulation showed secondary vortices with 20–30% more tangential velocity than the mean flow. Fiedler (1994), Fiedler (1997), and Trapp and Fiedler (1995) used an axisymmetric model to study vortices that form within a domain with rigid boundaries by introducing the concept of buoyancy in a rotating cylinder of fluid. The study showed that the vortex touchdown produces wind speeds that exceed the thermodynamic speed limit by a factor of 5 and at higher swirl ratios produced multiple vortices. Lewellen et al. (1997) and Lewellen et al. (2000) modelled real scale tornado flow using Large Eddy Simulations (LES) and analyzed the flow dynamics close to ground surface. The results showed the production of multiple vortices at high swirl ratios.

Table 1-1 Comparison of Tornado Categorizations from Design Guides (ASCE 2010 and CIGRÉ 2009) and the Enhanced Fujita Scale for Tornadoes

Scale	Fujita Scale Fastest Quarter-mile wind speeds				3 - sec gust (mph)	Enhanced Fujita Scale	CIGRÉ (2009) Tornadoes			
	Wind Speed	Path length	Path width	Cumulative Percentage		3 - sec gust (mph)	Gust Wind (2-3 sec gust) (m/sec)	Potential Wind Gust Width	Frequency of Occurance (average)	Notes
F0	72 (mph) 32.2 (m/sec)	< 1.0 (mile) 1.61 (km)	< 50 (ft) 15.2 (m)	22.9	45 - 78	65 - 85				
F1	73 - 112 (mph) 32.6 - 50 (m/sec)	1.0 - 3.1 (mile) 1.61 - 5.0 (km)	51 - 170 (ft) 15.2 - 52 (m)	57.6	79 - 117	86 - 110				
F2	113 - 157 (mph) 50 - 70.2 (m/sec)	3.2 - 9.9 (mile) 5.0 - 15.9 (km)	171 - 530 (ft) 52 - 162 (m)	86.1	118 - 161	111 - 135	45 - 70	1000 (m)	1/5	Torsional Loading
F3	158 - 206 (mph) 70.6 - 92.1 (m/sec)	10 - 31 (mile) 16 - 50 (km)	531 - 1,670 (ft) 162 - 509 (m)	96.8	162 - 209	136 - 165	70 - 95	400 (m)	1/1000	
F4	207 - 260 (mph) 92.1 - 116.2 (m/sec)	32 - 99 (mile) 51 - 159 (km)	1,671 - 4,750 (ft) 509 - 1,448 (m)	99.5	210 - 261	166 - 200	95 - 120	200 (m)	1/4000	
F5	261 - 318 (mph) 116.2 - 142.2 (m/sec)	100 - 315 (mile) 160 - 507 (km)	4,751 - 6,000 (ft) 1,448 - 1,829 (m)	100	262 - 317	> 200	> 120	200 (m)	1/10,000	

The tornado wind field used in this study is obtained from a three dimensional CFD conducted by Hangan and Kim (2008). They related the swirl ratio (S) used in the CFD simulation to the Fujita scale. The CFD simulation was conducted using the commercial program FLUENT (FLUENT Inc. 2005). Hangan and Kim (2008) modeled tornadoes using three dimensional RANS simulations with the Reynolds Stress Model (RSM) turbulence closure. The simulations of tornado-like vortices included the formation of a laminar vortex at low swirl ratio, followed by turbulent vortex breakdowns and vortex touch downs at higher swirl ratio values. The simulation was initially conducted using a swirl ratio $S = 0.28$. This is the same swirl ratio applied in the experimental program conducted by Baker (1981) using a Ward-type vortex chamber. The results of the CFD analysis with $S = 0.28$ were validated by Hangan and Kim (2008) through a comparison with Baker's experimental results. The numerical analysis was then extended by Hangan and Kim (2008) by considering values of $S = 0.10, 0.4, 0.7, 0.8, 1.0$ and 2.0 , respectively. An extensive study was conducted by Hangan and Kim (2008) to estimate the proper swirl ratio that provides good matching between the numerical results and the F4 tornado field measurements. Hangan and Kim (2008) also introduced a geometric scale and a velocity scale which can be applied to CFD data to estimate the F4 tornado field. They concluded that the F4 tornado approximately corresponds to a swirl ratio S of 2.0 . Very few field measurements are yet available in the literature for F2 tornadoes. This is despite the fact that 86% of categorized tornadoes are associated with F2 tornadoes or less as stated in the ASCE (2010). Hamada et al. (2010) presented a procedure to estimate the velocity field for F2 tornado using Hangan and Kim (2008) CFD data and the parameters of F2 tornadoes defined in the Fujita scale. It should be mentioned that the CFD velocity

field for tornadoes were developed assuming smooth ground surface, i.e. without considering the topographical effect. In addition, This CFD model does not include a turbulence component.

1.2.2 Behaviour of Transmission Lines under Normal and High Intensity Wind

Many investigators and hydro companies conducted valuable research in the area of transmission line systems behaviour under wind loads. The majority of the research focused on assessing the response of transmission line components separately to large scale boundary layer wind events. Few attempts have been made in the literature to investigate the behaviour of transmission line systems under HIW events. The modelling and assessment of the behaviour of transmission lines under downburst loading was conducted by Shehata et al. (2005) and Shehata and El Damatty (2007). In this study, a three dimensional finite element model simulating the towers and a two-dimensional model simulating the conductors were developed to assess the structural performance of transmission towers under downburst loading. An extensive parametric study was conducted in the same investigations to determine the critical downburst loading cases. The studies done by Shehata et al. (2005) and Shehata and El Damatty (2007) were extended by Shehata and El Damatty (2008) to investigate the structural performance of the tower under these critical downburst loading cases. The failure of a transmission tower during a downburst event, which occurred in Manitoba, Canada in 1996, was assessed by Shehata and El Damatty (2008). In this study, a numerical scheme, which included a failure model, was developed to study the progressive collapse of the guyed

tower. Shehata et al. (2008) extended the numerical model by including an optimization routine. This model is capable of predicting the critical downburst parameters and the corresponding forces. The failure of a self-supported lattice tower under modelled tornado and microburst wind profiles was investigated by Savory et al. (2001). The analytical tornado wind model used in this study is based on the model developed by Wen (1975). Only the horizontal wind profile corresponding to F3 tornado was used in the analysis without considering the vertical component of the tornado wind field. The turbulence component associated with the tornado and the downburst wind loading was neglected. The tower members were modelled using three dimensional truss elements. The dynamic analysis was done for the tower alone, including its self-weight, without modelling the lines. The failure observed in this study under tornado loads was a shear failure, which was observed in some field observations. Ladubec et al. (2012) studied the effect of large displacement on the response of transmission towers under downburst wind field. The analysis used nonlinear space frame elements to simulate the towers members. The study showed an increase of 20% compared to linear analysis in the peak axial forces in the tower main leg chord members. The study is considered as an extension to the linear analysis of transmission towers that was performed by Shehata and El Damatty (2008).

Loredo-Souza and Davenport (1998) investigated experimentally, through wind tunnel testing, transmission line failures. The experimental results compared successfully with the theoretical predictions obtained from a statistical method combined with using influence lines. The study shows that the dynamic behaviour of the conductors is affected significantly by the value of aerodynamic damping, which can be as high as 60% of the

critical damping. The aerodynamic damping is directly proportional to the wind velocity and inversely proportional to the line mass. The study concluded that the background response is indeed the main contributor for the total fluctuating response. Darwish et al. (2010) modified the two-dimensional nonlinear finite element model of the transmission lines developed by Shehata et al (2005) to study the dynamic characteristics of the conductors under turbulent downburst loading. The modified model accounted for the large deformations and the pretension loading, and was used to predict the natural frequencies and mode shapes. In this study, the turbulence component was extracted from full-scale data and then added to the mean component of the downburst wind field developed by Kim and Hangan (2007). The study concluded that the resonant component due to turbulence is negligible as a result of the large aerodynamic damping. In addition, the study discussed the effect of the pretension force on the natural period and mode shapes of the conductors. Loredo-Souza and Davenport (2003) reviewed the influence of the design procedure, such as the statistical method and the influence lines procedure, for the establishment of wind loading on transmission tower response. In this study, a comparison was carried out between Davenport's gust response and the statistical method that uses the influence lines procedure for estimating wind loading on transmission line structures. The second approach accounts for the effect of the higher modes. Loredo-Souza and Davenport (2003) concluded that the dynamic response of transmission towers depends strongly on both the structural and aerodynamic damping of the towers. Hamada (2009) studied the dynamic behaviour of a guyed transmission line system under the translation motion of F4 and F2 tornadoes. Without considering the turbulence component, it was concluded that the dynamic analysis has a minor effect on the towers.

This conclusion was explained by the high aerodynamic damping of the conductors, and the significant difference between the loading period associated with a moving tornado (minimum of 13 sec) and the towers' period (about $T = 0.5$ sec). Lin et al. (2012) studied an aeroelastic model of a single transmission line span and a single guyed tower under boundary layer and downdraft flow. The study was conducted at a length scale of 1:100. The analysis of the test results concluded that the aeroelastic model responded quasi-statically to both types of wind loading. In addition, the study showed that the resonant dynamic response was less significant with the downdraft flow wind load than the boundary layer wind load.

Hamada and El Damatty (2011) conducted a comprehensive study to assess and understand the performance of transmission line structures under tornado loading. The study investigated the variation of the tower members' internal forces with the tornado locations relative to the transmission line system. In addition, the study provided an insight about the structural response of the towers under tornado wind loads. The dynamic effect associated with the translation motion of the tornado was assessed and the results of the parametric study were used to assess the sensitivity of the members' peak forces with the parameters defining the location of the tornado relative to the transmission line. Altalmas et al. (2012) and El Damatty and Hamada (2013) assessed the transmission lines' failure mechanisms under critical tornado configurations. In addition, the studies predicted the maximum tornado velocity that various lines can withstand before experiencing global failure. The study also described different failure modes as well as their progression. Hamada and El Damatty (2013) assessed the behaviour of two guyed transmission line structures under F2 tornado wind field, boundary layer wind,

electrical companies' recommended wind field, and CIGRE` recommended tornado loading cases. In addition, a comparison was carried out between the forces in the transmission tower members, resulting from the tornado, and those obtained in the case of broken wires under F2 tornado wind loads.

1.3 Background

The Author during his Master of Engineering Science (M.E.Sc.) thesis developed a procedure to model and predict the structural performance of lattice tangential guyed transmission lines subjected to tornado wind loads. The tornado wind field was based on a model scale CFD analysis developed and validated by Hangan and Kim (2008). The CFD results, together with the full-scale tornado measurements and different manual of practices recommendations, were used to establish wind fields associated with F4 and F2 tornadoes as discussed in detail by Hamada et al. (2010). These tornado wind fields vary spatially in a three dimensional manner and are time independent representing the steady-state status of a tornado. The data along the circumference at different heights and radii from the tornado center was averaged leading to axisymmetric set of F4 and F2 tornado data. A tornado wind field has three main components; radial, tangential, and axial (vertical) components. The procedures used to obtain the wind forces due to these three components of the wind field acting on the transmission lines and towers nodes were described by Hamada et al. (2010). A numerical code was developed by the author to calculate the F4 and F2 tornado forces acting on the components of a lattice transmission line system. A three dimensional nonlinear finite element model for the transmission line system was developed using the commercial software SAP 2000 (CSI Inc. 2008). The

model included a simulation of the transmission tower, in addition to two towers and three spans of transmission lines (conductors and ground-wires) on each side of the middle tower (the tower of interest). The model accounted for the geometric nonlinearity resulting from the large deformations experienced by the lines and the towers. A two-noded cable element was used to model the lines and the supporting guys, while including the effect of tension stiffening and sagging. Only one guyed tower was used in the study, which is the generic tangent lattice tower A-402-0 belonging to the electrical company Manitoba Hydro. The analysis procedure and various steps were discussed in detail by Hamada et al. (2010) and Hamada (2009).

The study proceeded by studying the dynamic response of transmission lines under tornado loads. In this study, the time history variation of the loading resulted from the translation of the tornado. The numerical code simulating the tornado loading was modified to produce the required loading time histories associated with a tornado movement perpendicular, parallel, and oblique to the lines. The natural period and mode shapes of the considered transmission line system were first determined by conducting free vibration analyses. The static finite element model was modified to account for the time history variation of the tornado forces resulting from the translation motion of the tornado event. In addition, the model accounted for the structural and the aerodynamic damping of the transmission towers and lines. Time history analyses were conducted and results were compared with quasi-static analyses results. The study showed no significant dynamic effect associated with the translation motion of the tornado. This resulted mainly from the large aerodynamic damping of the conductors and the low fundamental period

of the towers in comparison to the loading period. More details regarding the dynamic analyses and the obtained results are provided by Hamada and El Damatty (2011).

The developed numerical model was then used to conduct an extensive parametric study to investigate the structural performance of the guyed transmission tower under loads resulting from different F4 and F2 tornado events. The parametric study was conducted in a quasi-static manner based on the dynamic analysis conclusions. The parametric study was conducted by carrying out a large number of analyses; each analysis corresponded to a specific tornado location relative to the transmission line system. Firstly, the study assessed the behaviour of transmission lines under an F4 tornado wind field. Secondly, the behaviour was assessed under an F2 tornado wind field. In the third part of the study, the structural behaviour of the guyed transmission tower under various critical tornado locations was described. Lastly, the results of the parametric study results were used to assess the sensitivity of the member forces to the variation of the tornado location relative to the transmission line system. More details regarding the extensive parametric study results and the sensitivity analyses are provided by Hamada and El Damatty (2011).

The research conducted in the current Ph.D. thesis represents a significant extension to the study carried on by the author in his M.E.Sc. Thesis. As mentioned earlier, the structural analysis previously conducted in the Master thesis relied on a commercial software. A major step accomplished in this Ph.D. thesis is that a comprehensive in-house numerical model that combines the CFD data with nonlinear structural analysis modelling is developed. This provides a lot of flexibility, in term of computational

efficiency and in term of implementation of various failure models as described later. The objective and scope of the thesis are provided below.

1.4 Objectives of Thesis

The major objectives of the thesis can be summarized in the following:

- 1- Develop an in-house comprehensive numerical model for the analysis and prediction of failure of transmission line systems under tornado loading. The numerical model includes the tornado wind field obtained from CFD simulations together with nonlinear three dimensional finite element simulation for the transmission line system.
- 2- Study the behaviour of the conductors under tornado loading and assess the effect of various parameters that might affect this behaviour.
- 3- Design an aeroelastic model of a multi span guyed transmission line system that can be used for better understanding of the behaviour of such structures under wind loads and also to validate the developed numerical model.
- 4- Use the developed model to conduct a number of case studies in order to gain an insight about the resilience of lattice transmission towers against failures when experiencing an F2 tornado event. Also, use those case studies to assess and describe the failure modes of the towers under F2 tornadoes.
- 5- Develop a set of load cases that simulate and provide an envelope for the effect of tornadoes on tangent transmission line structures for possible implementation in the design guidelines.

1.5 Scope of Thesis

The thesis has been prepared in ‘Integrated-Article’ format. In the present chapter, a review of the studies related to transmission lines and tornadoes and the objectives and thesis’s scope are provided. The following six chapters address collectively the thesis objectives. Chapter eight presents the conclusion of the study together with suggestions for further research work. A description of scope of each chapter is provided below.

1.5.1 Chapter 2 – Analysis and Behaviour of Guyed Transmission Lines under Tornado Wind Loads – Case Studies

This chapter builds on the research done by the author during his Master thesis. The analyses are conducted in this chapter using the commercial software SAP 2000. The main purpose is to assess the significance of F2 tornado loading on tangent transmission line systems in comparison with the loading cases recommended by design codes, manuals of practice, and other HIW events such as downbursts. Numerical models are developed to study the behaviour of two guyed transmission lines under F2 tornado and several other wind loads. The F2 tornado wind field used is based on a full three dimensional CFD model that was developed and validated in earlier studies. Three dimensional nonlinear finite element models of existing transmission lines belonging to electrical utilities are developed. This chapter studies the behaviour of two guyed transmission line structures under F2 tornado wind field, boundary layer wind, downbursts, and CIGRE` recommended tornado loading cases. In addition, a comparison is carried out between the internal forces induced in the transmission tower members, resulting from the tornado, and those obtained in the case of broken wires during a F2

tornado event. The study reveals the importance of considering tornadoes when designing lattice transmission line structures.

1.5.2 Chapter 3 – Nonlinear Formulation of Four-Noded Cable Element and Application to Transmission Lines under Tornadoes

Transmission line conductors and ground-wires are sensitive to wind loads as they typically have long spans and are very flexible compared to the supporting towers. The analysis of transmission lines is challenging due to the nonlinearity introduced by large displacements that are often much larger than the conductors' diameter and of same order of magnitude compared to the initial sagging. A powerful three dimensional four-noded cable element is developed in the current chapter. After validating this nonlinear formulation, the element is used to model multi-span conductors. In this simulation, the support provided to the conductors through the towers and the insulators is modelled using a three dimensional spring system with stiffness dependent on the rotation experienced by the insulators. This numerical development is used to study the behaviour of transmission line conductors under tornadoes. The study is confined to F2 tornadoes since the vast majority of tornadoes are equal to or less than this level. The effect of boundary conditions and the importance of accounting for the flexibility of the insulators and the supporting towers are then assessed.

1.5.3 Chapter 4 – Behaviour of Transmission Line Conductors under Tornado Wind Loads

The study conducted in the Chapter builds on the development of the sophisticated model of transmission line conductors accomplished in the previous chapter. Many codes of practice recommend neglecting the tornado forces acting on the conductors and ground-wires because of the complexity in predicting the conductor's response to such loads. As such, the current chapter assesses the effect of tornado loads acting on conductors on the overall response of transmission towers. Then, the behaviour of the conductors under the most critical tornado configuration is described. In addition, the sensitivity of the lines' behaviour to the magnitude of tornado loading, the level of initial sag, the insulator's length, and lines self-weight is investigated.

1.5.4 Chapter 5 – Failure Analysis of Guyed Transmission Lines during Tornado Events

In this chapter, an in-house numerical model simulating lattice towers is developed. This is coupled with the numerical model of the conductor developed in Chapter 3 together with the tornado wind field to form a comprehensive package for the analysis of transmission lines under tornado loads. The numerical model is also extended in order to predict the tornado velocities at which failure might initiate and to describe the progress of collapse under this type of loading. Two different assumptions regarding the post yielding behaviour of members under tension are included in the numerical models. Two transmission line systems are considered in this chapter as case studies. Using the developed numerical models, failure studies are conducted for each transmission line

system. For each system, the failure studies included two critical tornado configurations, determined in view of previous studies. In addition, each failure study case is repeated twice using the two material models describing the post yield behaviour of tensions members. The study gives an insight about the resilience of transmission against failures when experiencing F2 tornadoes, describe the failure modes under such events, assess the effect of different assumptions regarding post yield tension behaviour, and quantify the effect of inclusion of geometric nonlinearities in this type of analysis.

1.5.5 Chapter 6 – Development and Testing of an Aeroelastic Model of a Guyed Transmission Line System

The objective of the current study is to develop and perform a boundary layer wind tunnel test of a full aeroelastic model of a guyed transmission line system. The same guyed transmission line system that was investigated by the author during his Master thesis and in previous chapters of this thesis is used. The aeroelastic model is designed for a geometry scale of 1:50 and tested in the Boundary Layer Wind Tunnel Laboratory (BLWTL) at the University of Western Ontario, Canada. The aeroelastic model simulates the behaviour of four transmission towers with three full spans in between. The model is tested using an open exposure conventional boundary layer wind and for different wind directions. In addition, the model is tested with and without the transmission lines (conductors and ground-wires) to investigate the effect of the lines on the structural response of the towers. The results are used to understand the behaviour of transmission towers under wind loads and are used to validate the numerical model developed in the previous chapters.

1.5.6 Chapter 7 – Equivalent F2 Tornado Loading on Lattice Transmission Line Systems

There is a lack of procedures in the design codes and manuals of practice related to the estimation of tornado forces on transmission line systems. As such, the purpose of this Chapter is to present load cases that simulate the critical effect of F2 tornadoes on tangent lattice transmission line structures. The current Chapter builds on the extensive research previously conducted on this subject. A main challenge in this application of localized wind events is that the forces acting on the structure vary significantly based on the location of the tornado and a large parametric study involving varying the tornado location has to be conducted for each system to determine critical cases. Critical load cases are determined in this Chapter based on parametric studies carried out in previous investigations as well as others conducted in the current Chapter. The vertical profile of three velocity components associated with each critical load case as well as the horizontal profile of the associated transverse velocity along the lines are provided. A procedure that will allow practicing engineers to use those profiles for analyzing lattice transmission lines under F2 tornadoes is described. Validation of the developed procedure is conducted by considering two independent transmission line systems. The results indicate that the developed load cases estimates peak internal forces that are either slightly higher or 5% less than the values predicted by the detailed parametric studies.

1.6 References

Altalmas, A., El Damatty, A. A., and Hamada, A. (2012). "Progressive failure of transmission towers under tornado loading." *Annual Conference of the Canadian Society*

for Civil Engineering 2012: Leadership in Sustainable Infrastructure, CSCE 2012, June 6, 2012 - June 9, Canadian Society for Civil Engineering, Edmonton, AB, Canada, 2220-2229.

American Society of Civil Engineers (ASCE), 1997. Design of Latticed Steel Transmission Structures. Standard ANSI/ASCE 10-90, New York, NY, USA.

American Society of Civil Engineers (ASCE), 2010. Guidelines for Electrical Transmission Line Structural Loading, third edition. ASCE Manuals and Reports on Engineering Practice, vol. 74. Reston, VA, USA.

Baker, G. L., and Church, C. R. (1979). "Measurements of core radii and peak velocities in modeled atmospheric vortices." *J. Atmos. Sci.*, 36, 2413-2424.

Behncke, R.H., and White, H. B. (2006). "Applying Gust Loadings to Your Lines." *Proceedings of the 9th International Conference on Overhead Lines*, American Society of Civil Engineers (ASCE), Fort Collins, Colorado

CIGRÉ (Conseil International des Grands Réseaux Électriques/ International Council on Large Electrical Systems) SC-22 WG22-06 (2006). "Review of IEC 826: Loading and Strength of Overhead Lines. Part 3: Analysis of Recent Transmission Line Failures." Scientific Committee B2 on Overhead Lines.

CIGRÉ (Conseil International des Grands Réseaux Électriques/ International Council on Large Electrical Systems) (2009). "Overhead line design guidelines for mitigation of severe wind storm damage." Scientific Committee B2 on Overhead Lines, B2. 06.09.

Darwish, M. M., Damatty, A. A. E. I., and Hangan, H. (2010). "Dynamic characteristics of transmission line conductors and behaviour under turbulent downburst loading." *Wind and Structures, an International Journal*, 13(4), 327-346.

Doswell III, C.A., Brooks, H.E. and Dotzek, N. (2009), "On the implementation of the enhanced Fujita scale in the USA." *Atmospheric Research* 93, 554-563.

El Damatty, A. A., and Hamada, A. (2013). "Behaviour of guyed transmission line structures under tornado wind loads - Case studies." *Electrical Transmission and Substation Structures 2012: Solutions to Building the Grid of Tomorrow*, November 4, 2012 - November 8, American Society of Civil Engineers (ASCE), Columbus, OH, United states, 193-204.

Fiedler, B. H. (1997). "Compressibility and Wind speed Limits in Tornadoes." *Atmosphere - Ocean*, 35(1), 93-93.

Fiedler, B. H. (1994). "The thermodynamic speed limit and its violation in axisymmetric numerical simulations of tornado-like vortices." *Atmosphere-Ocean*, 32(2), 335-359.

Fujita, T. T. (1981). "Tornadoes and downbursts in the context of generalized planetary scales." *J.Atmos.Sci.*, 38(8), 1511-34.

Fujita, T. T., and Pearson, A. D. (1973). "Results of FPP classification of 1971 and 1972 tornadoes." *8th Conference on Severe Local Storms (abstracts only)*, USA, 609.

Hamada, A. (2009). "Analysis and behaviour of guyed transmission line structure under tornado wind loading." M.E.Sc. thesis, School of Graduate and Postdoctoral Studies, University of Western Ontario, London, Ont.

Hamada, A., El Damatty, A. A., Hangan, H., and Shehata, A. Y. (2010). "Finite element modelling of transmission line structures under tornado wind loading." *Wind and Structures*, 13(5), 451-469.

Hamada, A., and El Damatty, A. A. (2011). "Behaviour of guyed transmission line structures under tornado wind loading." *Computers and Structures*, 89(11-12), 986-1003.

Hamada, A., and El Damatty, A. A. (2013). "Analysis and Behaviour of Guyed Transmission Lines under Tornado Wind Loads – Case Studies." *Annual Conference of the Canadian Society for Civil Engineering 2013: General Conference, CSCE 2013*, May 29, 2013 - June 1, Canadian Society for Civil Engineering, Montreal, QC, Canada.

Hangan, H., and Kim, J. -. (2008). "Swirl ratio effects on tornado vortices in relation to the Fujita scale." *Wind and Structures*, 11(4), 291-302.

Harlow, F. H., and Stein, L. R. (1974). "Structural analysis of tornado-like vortices." *J.Atmos.Sci.*, 31(8), 2081-98.

Holmes, J. D., and Oliver, S. E. (2000). "An empirical model of a downburst." *Eng.Struct.*, 22(9), 1167-1172.

Ishac, M. F., and White, H. B. (1994). "Effect of tornado loads on transmission lines." *Proceedings of the 1994 IEEE Power Engineering Society Transmission and Distribution Conference, April 10, 1994 - April 15*, Publ by IEEE, Chicago, IL, USA, 521-527.

Kareem, A. (2010). "Bluff Body Aerodynamics and Aeroelasticity: A Wind Effects Perspective." *Journal of Wind Engineering*, 7(1), 30-74.

Kim, J., and Hangan, H. (2007). "Numerical simulations of impinging jets with application to downbursts." *J.Wind Eng.Ind.Aerodyn.*, 95(4), 279-298.

Ladubec, C., El Damatty, A. E., and El Ansary, A. E. (2012). "Effect of geometric nonlinear behaviour of a guyed transmission tower under downburst loading." *2012 International Conference on Vibration, Structural Engineering and Measurement, ICVSEM 2012, October 19, 2012 - October 21*, Trans Tech Publications, Shanghai, China, 1240-1249.

Letchford, C. W., and Chay, M. T. (2002). "Pressure distributions on a cube in a simulated thunderstorm downburst. Part B: Moving downburst observations." *J.Wind Eng.Ind.Aerodyn.*, 90(7), 733-753.

Lewellen, D. C., Lewellen, W. S., and Xia, J. (2000). "The influence of a local swirl ratio on tornado intensification near the surface." *J.Atmos.Sci.*, 57(4), 527-44.

Lewellen, W. S., Lewellen, D. C., and Sykes, R. I. (1997). "Large-eddy simulation of a tornado's interaction with the surface." *J.Atmos.Sci.*, 54(5), 581-605.

Lin, W. E., Savory, E., McIntyre, R. P., Vandelaar, C. S., and King, J. P. C. (2012). "The response of an overhead electrical power transmission line to two types of wind forcing." *J.Wind Eng.Ind.Aerodyn.*, 100(1), 58-69.

Loredo-Souza, A., and Davenport, A. G. (2003). "The influence of the design methodology in the response of transmission towers to wind loading." *J.Wind Eng.Ind.Aerodyn.*, 91(8), 995-1005.

Loredo-Souza, A., and Davenport, A. G. (1998). "The effects of high winds on transmission lines." *J.Wind Eng.Ind.Aerodyn.*, 74-76 987-994.

McCarthy, P., and Melsness, M. (1996). "Severe weather elements associated with September 5, 1996 hydro tower failures near Grosse Isle, Manitoba, Canada. Manitoba Environmental Service Centre, Environment Canada."

McDonald, J.R., Forbes, G.S. and Marshall, T.P. (2004), "The enhanced Fujita (EF) scale." Preprints of the 22nd Conference on Severe Local Storms, 3-8 October, Hyannis, MA, USA, American Meteorological Society, CD-ROM B (Vol. 3).Mason, M.S., Wood, G.S., Fletcher, D.F. (2009), "Numerical simulation of downburst winds", *Journal of Wind Engineering and Industrial Aerodynamics* 97(11-12), 523-539.

Newark, M. J., 1984. Canadian tornadoes, 1950-1979. *Atmospheric-Ocean* 22, 243-253.

Ramsdell, Jr., J.V. and Rishel, J.P. (2007), "Tornado Climatology of the Contiguous United States.", PNNL-15112 Revision 1, Pacific Northwest National Laboratory, Richland, WA, USA. Prepared for U.S. Nuclear Regulatory Commission, NUREG/CR-4461 Revision 2, Washington, DC, USA.

Rotunno, R. (1984). "An investigation of a three dimensional asymmetric vortex." *J.Atmos.Sci.*, 41(2), 283-98.

Rotunno, R. (1979). "A study in tornado-like vortex dynamics." *J.Atmos.Sci.*, 36(1), 140-55.

- Rotunno, R. (1977). "Numerical simulation of a laboratory vortex tornado theory." *J.Atmos.Sci.*, 34(12), 1942-56.
- Sarkar, P., Haan, F., Gallus, Jr., W., Le, K. and Wurman, J. (2005). "Velocity measurements in a laboratory tornado simulator and their comparison with numerical and full-scale data." *37th Joint Meeting Panel on Wind and Seismic Effects*, .
- Savory, E., Parke, G. A. R., Zeinoddini, M., Toy, N., and Disney, P. (2001). "Modelling of tornado and microburst-induced wind loading and failure of a lattice transmission tower." *Eng.Struct.*, 23(4), 365-375.
- Shehata, A. Y., and El Damatty, A. A. (2008). "Failure analysis of a transmission tower during a microburst." *Wind and Structures*, 11(3), 193-208.
- Shehata, A. Y., and El Damatty, A. A. (2007). "Behaviour of guyed transmission line structures under downburst wind loading." *Wind and Structures, an International Journal*, 10(3), 249-268.
- Shehata, A. Y., El Damatty, A. A., and Savory, E. (2005). "Finite element modeling of transmission line under downburst wind loading." *Finite Elements Anal.Des.*, 42(1), 71-89.
- Shehata, A. Y., Nassef, A. O., and El Damatty, A. A. (2008). "A coupled finite element-optimization technique to determine critical microburst parameters for transmission towers." *Finite Elements Anal.Des.*, 45(1), 1-12.
- Trapp, R. J., and Fiedler, B. H. (1995). "Tornado-like vortexgenesis in a simplified numerical model." *J.Atmos.Sci.*, 52(21), 3757-3778.
- Twisdale, L. A. (1982). "Wind Loading Underestimates in Transmission Line Design." *Transmission and Distribution*, 40 - 46
- Ward, N. B. (1972), " The exploration of certain features of tornado dynamic using a laboratory model', *journal of the Atmospheric Science*, 26 (6), 1194-1204

Wen, Y. (1975). "Dynamic tornadic wind loads on tall buildings." *ASCE Structural Division*, 101(1), 169-185.

Wen-Chau Lee, and Wurman, J. (2005). "Diagnosed three dimensional axisymmetric structure of the Mulhall tornado on 3 May 1999." *J.Atmos.Sci.*, 62(7), 2373-93.

Wurman, J. (1998). "Preliminary results from the ROTATE-98 tornado study", *Preprints, 19th Conf. On severe local storms*, Minneapolis, MN, 14-18 September.

CHAPTER 2

ANALYSIS AND BEHAVIOUR OF GUYED TRANSMISSION LINES UNDER TORNADO WIND LOADS - CASE STUDIES

2.1 Introduction

The 2003 Northwest blackout demonstrated how heavily our societies rely on electricity nowadays. Transmission lines are considered the backbone of electricity distribution, from the source to the customers. More than 80% of weather-related transmission line failures world-wide are attributed to high intensity wind (HIW) events in the forms of downburst, microburst, and tornadoes (McCarthy and Melsness 1996). Li (2000) mentioned that 90 % of transmission line failures in Australia are caused by HIW events. McClure et al. (2008) reported that in many regions of the world, localized high intensity winds and icing pose a great risk for transmission lines failures. Ishac and White (1994) concluded that of all populated areas in Canada, South western Ontario experiences the highest rate of tornadoes. Most of transmission line failures in this area are mainly caused by tornadoes. Despite these facts, the codes of practice and design guidelines for transmission line structures are based on wind loads resulting from conventional boundary layer wind profiles and large-scale events. The conventional wind profile is characterized by a monotonic increase in velocity along the height. Wind profiles attributed to tornadoes and downbursts have maximum wind speed near the ground, with a decrease in the velocity along the height in the case of tornadoes. In addition, a significant vertical wind component exists in the tornado wind profile along with the tangential and radial wind components. McClure et al. (2008) proposed some simplified

design loading cases to account for the effect of localized HIW on transmission line supports.

In the current study, the tornado wind field is obtained from a three dimensional computational fluid dynamics (CFD) simulations conducted by Hangan and Kim (2008). The numerical tornado models were validated by Hangan and Kim (2008) with field measurements recorded by Lee and Wurman (2005) and introduced by Sarkar et al. (2005) for the 1998 Spencer South Dakota F4 tornado. The CFD velocity field for tornadoes assumes smooth ground surface, and does not include turbulence component. Hamada et al. (2010) estimated an F2 tornado velocity field from the CFD data provided by Hangan and Kim (2008).

Very few attempts had been made in the literature to investigate the behaviour and failure of transmission line structures during HIW events. Savory et al. (2001) studied the failure of a self-supported lattice tower under mathematical models simulating F3 tornadoes and microbursts. The mathematical tornado wind model used by Savory et al. (2001) was developed by Wen (1975). The behaviour and failure analysis of transmission lines under downburst wind loads were conducted by Shehata et al. (2005), Shehata and El Damatty (2007), and Shehata and El Damatty (2008). The modelling and assessment of the behaviour of transmission lines under F2 and F4 tornadoes were conducted by Hamada et al. (2010) and Hamada and El Damatty (2011). In these studies, a three dimensional nonlinear finite element model simulating the towers and six spans of the conductors was developed to assess the structural performance of guyed transmission lines under F2 and F4 tornado loading.

In the current study, the nonlinear three dimensional finite element model developed by Hamada et al. (2010) and Hamada and El Damatty (2011) is used to conduct an extensive parametric study to assess the behaviour of two guyed transmission line systems under different wind fields. These wind profiles include F2 tornado wind field, conventional boundary layer wind field, CIGRE` (2009) recommended tornado loading cases, and downbursts. The behaviour of the two-guyed towers is assessed for all these wind profiles in a quasi-static manner. The study compares between the peak member forces resulting from F2 tornado and the other loading cases used in the design by utility companies. The objective is to assess the significance of F2 tornado loading on tangent transmission lines in comparison with the loading cases recommended by the design codes, manual of practices, and other HIW events such as downbursts. In addition, a comparison is carried out between the forces in the guyed transmission towers' cross-arms, resulting from F2 tornado, and those obtained in the case of broken-wire under F2 tornado wind loads. One bundle of conductors for one span adjacent to the tower of interest, are removed. Such failure case is noticed by industry experts after tornado events.

2.2 Finite Element Modelling of Transmission Line Systems

Two guyed transmission line systems are used in the current study to assess the behaviour under F2 tornadoes. The two systems are modelled using nonlinear three dimensional finite element models developed by the commercial software SAP 2000. The first guyed transmission tower is labeled as T1 and has a line span of 480 m. The conductor and ground-wire sags are 20 m and 13 m, respectively. The second guyed transmission tower is labeled as T2. The tower height is 46.75 m and is supported by four supporting guys

with a line span of 460 m. The conductors and ground-wires sags are 16 m. Both towers are shown in Fig. 2-1.

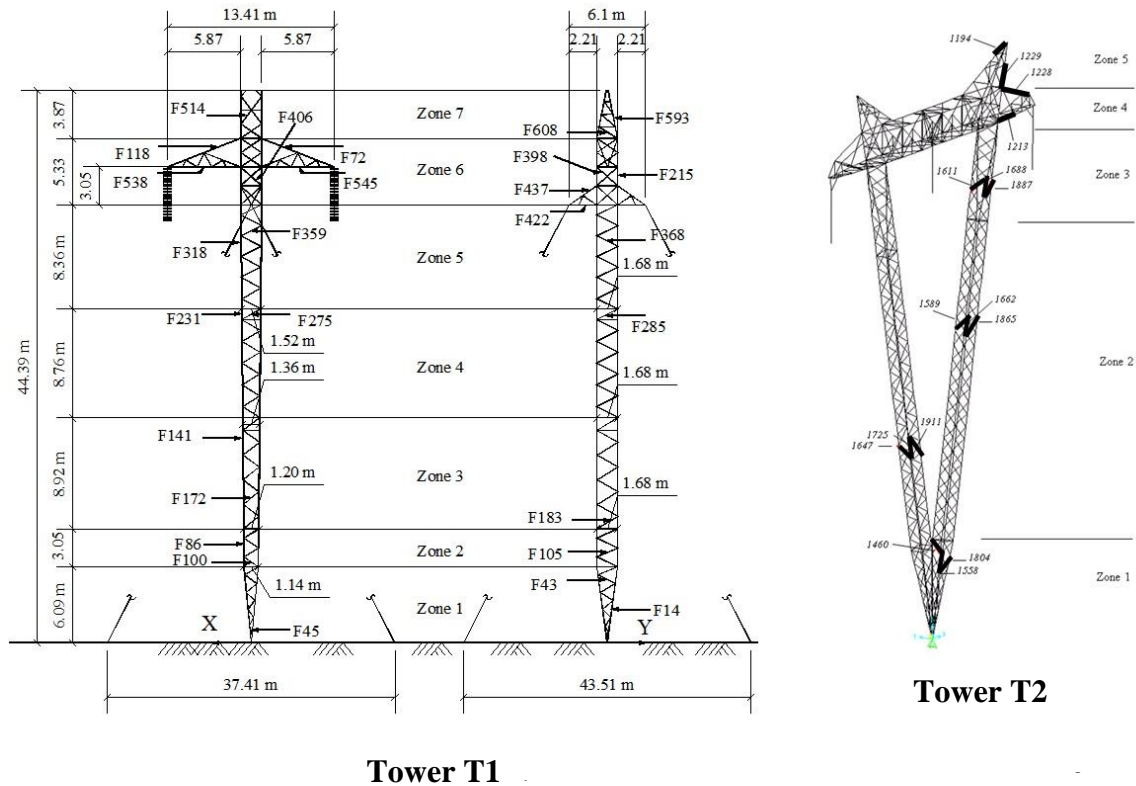


Fig. 2-1 Geometry of the Modelled Guyed Towers

The simulated transmission line system consists of the tower of interest and two towers from each side. As such, the three dimensional nonlinear finite element model includes five towers and six spans with hinged supports at the two far ends of the conductors. This number of spans was recommended by Shehata et al. (2005) and Hamada et al. (2010) to accurately account for the force transferred from both the conductors and the ground-wires to the tower of interest (middle tower). More details regarding the three dimensional nonlinear finite element model of the two transmission line systems are provided by Hamada et al. (2010) and Hamada and El Damatty (2011).

2.3 F2 Tornado

2.3.1 F2 Tornado Wind Field

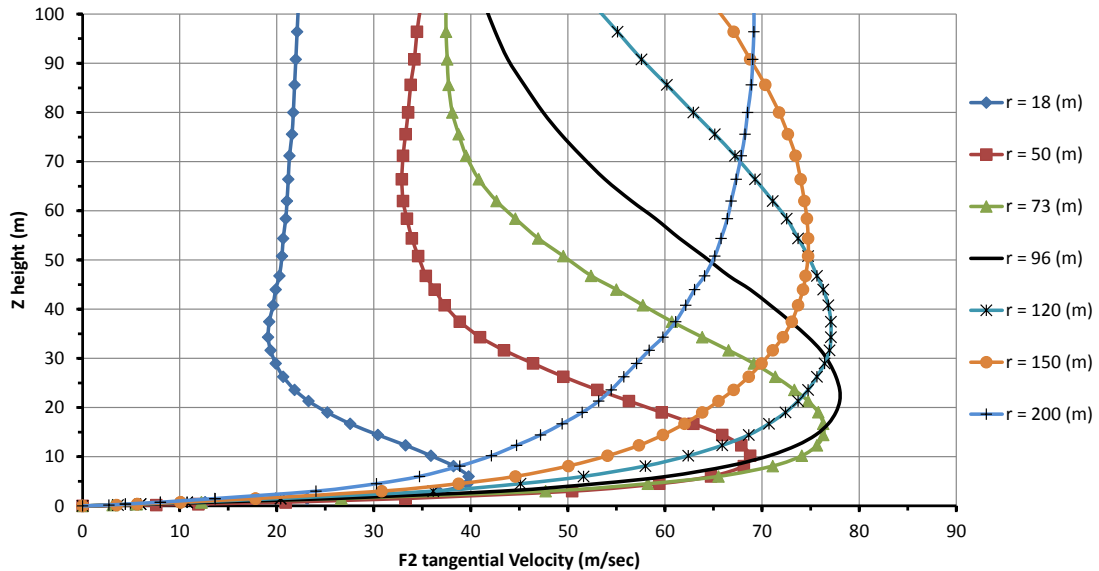


Fig. 2-2 Vertical Profile of Tangential Component for Different Radial Distances from Tornado Centre

The velocity wind field associated with F2 tornadoes is described in details in Hamada et al. (2010) and Hamada and El Damatty (2011). The tornado wind field is obtained from a three dimensional computational fluid dynamics (CFD) simulation conducted by Hangan and Kim (2008). The CFD analyses were conducted in a steady state manner with smooth surface. Accordingly, the F2 tornado wind field does not vary with time. The velocity field $V_m(r, \theta, z)$ has a three dimensional spatial variation and is given as a function of the cylindrical coordinates r , θ , and z . The velocity field $V_m(r, \theta, z)$ has three velocity components: the radial $V_{mr}(r, \theta, z)$, the tangential $V_{mt}(r, \theta, z)$, and the axial $V_{ma}(r, \theta, z)$. The maximum tangential velocity of the F2 tornado is 78 m/sec and occurs at a radius $r = 96$

m and a height $Z = 19$ m. The maximum radial velocity is 49 m/sec and corresponds to a radius $r = 146$ m and a height $Z = 6$ m. The maximum axial velocity is 37 m/sec and corresponds to a radius $r = 171$ m and a height $Z = 127$ m. The vertical profiles of the F2 tornado's tangential velocity component for different radial distances from the tornado centre are shown in Fig. 2-2.

2.3.2 Evaluation of the Tornado velocity Components at Various Locations of the Transmission Lines System

The horizontal projection of a transmission tower and an arbitrary location of F2 tornado are shown in Fig. 2-3. The following steps are followed to evaluate the tornado velocity components at the arbitrary point "a" shown in Fig. 2-3:

- 1- The centre of the studied transmission tower is considered as the origin of the set of axes used in the analysis.
- 2- The tornado centre relative to the centre of the tower is defined by the polar coordinates R and θ , as shown in Fig. 2-3.
- 3- Knowing R and θ and the coordinates of point "a", the coordinates R_{fa} and θ_{fa} , shown in Fig. 2-3, can be evaluated.
- 4- Knowing R_{fa} and θ_{fa} , and their equivalent R_{ma} , Z_{ma} and θ_{ma} in the CFD model scale, the 3-D set of F2 tornado data can be used to obtain the model radial velocity, tangential velocity, and axial velocity components of point "a". More details are provided by Hamada et al. (2010).

The values of R_{ma} , Z_{ma} and θ_{ma} might not coincide with any of the coordinate values at which the CFD data is provided. Accordingly, a three dimensional linear interpolation scheme is conducted between the CFD data points to obtain the three velocity components at point “a”. The three dimensional linear interpolation scheme has more stringent constraints in the Z-direction due to the significant variation of the wind profile along the height as shown in Fig. 2-2. The evaluation of the three velocity components for conductors, ground-wires, and supporting guys nodes is conducted in a similar way.

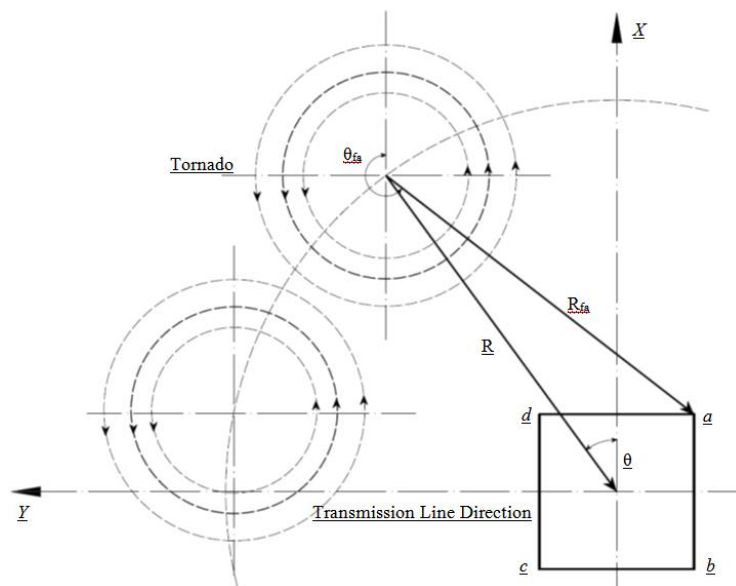


Fig. 2-3 Horizontal Projection of Transmission Tower and F2 Tornadoes

2.4 ASCE No. 74 Guidelines Wind Field

In the current section, the considered transmission line systems are analyzed using the recommended wind load procedures described in the ASCE (2010). Eq. (2-1) provided in the ASCE (2010) guidelines is used to calculate the wind forces acting on the tower and the conductors' nodes in a certain direction “i”. F_{wi} is the wind force in the “i” direction,

ρ_a is the air density = 1.226 kg/m³; K_{zt} is the topographic factor; V_i is the 10 m reference 3-sec wind speed in the “i” direction m/sec, A_i is the projected area of all the elements connected to the considered node and perpendicular to the “ i ” direction, G is the gust response factor, and C_f is the drag force coefficient . The values of K_{zt} are taken equal to 1, as also recommended by ASCE (2010). A value of force coefficient $C_f = 1$ is assumed for the conductors as recommended by ASCE (2010). As For the tower, the values of force coefficient C_f are obtained from Table 2-4 and Appendix G of the ASCE (2010). The wind velocity exposure coefficient, K_z , used in Eq. (2-1), modifies the wind speed to account for height and terrain effects. Exposure C, open terrain with scattered obstructions with heights less than 9 (m), is used in the current study. ASCE (2010) recommends Eq. (2-2) to calculate the exposure coefficient K_z .

$$F_{wi} = \frac{1}{2} \rho_a K_z K_{zt} (V_i)^2 G C_{fi} A_i \quad \text{Eq. 2-1}$$

$$K_z = 2.01 \left(\frac{Z_h}{Z_g} \right)^\alpha \quad \text{for } 10 \leq Z_h \leq Z_g \quad \text{Eq. 2-2}$$

Where Z_g is the gradient height (274.32 m for exposure C); α is the power law exponent (9.50 for exposure C); and Z_h is the effective height. The effective heights of the conductors and ground-wire are approximated as the height above ground of the conductors and ground-wire attachment points to the transmission tower. The gust response factor, G , used in the current study was introduced by Davenport (1980). ASCE (2010) modified Davenport (1980) equations to account for 3-sec gust wind speed, as the original equations were based on 10-min average wind speed. The gust responses

equations take into account the dynamic effect and lack of correlation of gusts on the wind response of transmission line components. Eq. (2-3) and (2-4) determine the transmission lines and transmission tower gust response factors, respectively.

$$G_w = \frac{1 + 2.7E\sqrt{B_w}}{Kv^2} \quad \text{Eq. 2-3}$$

$$G_t = \frac{1 + 2.7E\sqrt{B_t}}{Kv^2} \quad \text{Eq. 2-4}$$

Where,

$$E = 4.9\sqrt{k} \left(\frac{33}{Z_h} \right)^{\frac{1}{\alpha_{FM}}} \quad B_w = \frac{1}{1 + \frac{0.8S'}{L_s}} \quad B_t = \frac{1}{1 + \frac{0.56Z_h}{L_s}}$$

Where Z_h are the effective heights of the transmission lines for the calculation of G_w in ft, and the effective heights of transmission tower nodes for the calculation of G_t in ft, S' is the design wind span in ft. Kv is the ratio between 3-sec gust wind speed to the 10-min average wind speed and is equal to 1.43, α_{FM} , k , and L_s are wind parameters based on exposure category (Exposure C) and are equal to 7, 0.005, and 220, respectively.

2.5 CIGRE` Overhead Lines Design Guidelines Wind Field

The transmission line systems considered in this study, are also analyzed using HIW analysis procedures recommended by CIGRE`. The CIGRE` committee was developed in 2004 with a primary objective to identify the characteristics of severe windstorms and HIW impact on overhead lines (CIGRE` 2009). Wind speeds exceeding 45 m/sec are

defined as HIW and can take the form of Cyclones, Hurricanes, Typhoons, Tornadoes, Downbursts, and Microburst's. The CIGRE` guideline recommended an average F2 tornado wind speed of 60 m/sec. Transmission Lines facing higher intensity tornados, such as F3 and F4, are considered not economically or structurally adequate to be designed against failure. This recommended wind speed will lead to a design dynamic wind pressure of 2.2 kPa, using the recommended equations and factors of CIGRE` (2009). The wind pressure would be applied as a uniform pressure to the transmission tower. In addition, a torsional wind case, of the same wind pressure, should be applied to the transmission tower as shown Fig. 2-4. According to CIGRE` (2009), no wind loads are to be applied to the lines (conductors and ground-wires) in both cases.

2.6 Evaluation of Tornado and Wind Forces on Transmission Line Nodes

The ASCE (2010) is used in the current study to calculate the wind forces acting on the towers', conductors', ground-wires', and supporting guys' nodes. The shielding effects and factors for the vertical wind component of multiple lattice configurations in a row is a debatable issue in the literature and design codes. Georgiou and Vickery (1980) conducted a comprehensive study for up to 10 frames in any group with five different values of solidarity ratios and three aspect ratios. The study concluded that the multiple frame shielding coefficients that are present in codes of design (Canada, U.K., N.Z., Switzerland, Belgium, and Germany) are not conservative in most of the cases. Accordingly, the method described by ASCE (2010) to determine the wind force on each member independently (excluding shielding) is used to calculate the vertical forces on tower nodes. This method is based on geometry between the wind velocity vector and the

axis of the member to calculate the member's projected area. More details regarding the evaluation of tornado and wind forces on the transmission line components are provided by Hamada et al. (2010) and Hamada and El Damatty (2011).

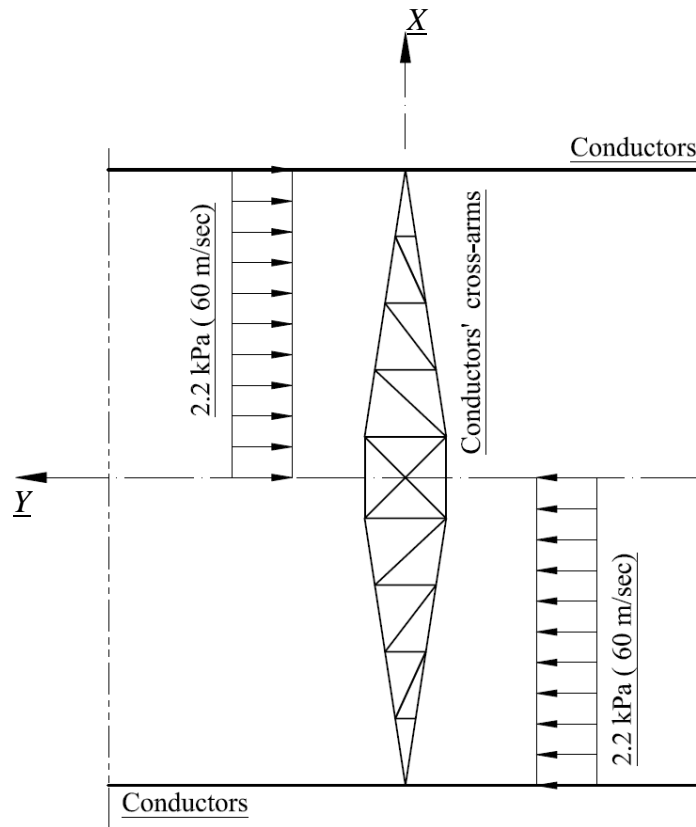


Fig. 2-4 Recommended Torsional Wind Load Case Recommended by CIGRE`

2.7 Parametric Study

An extensive parametric study is conducted to assess the behaviour of guyed transmission lines under F2 tornado wind loads. The study is conducted in a quasi-static manner. The self-weight of the towers, conductors, ground-wire, and insulators strings are included in the analyses. 240 analysis cases are considered for each guyed transmission line. Each analysis corresponds to a specific tornado location, defined by the polar coordinates R

and θ , as shown in Fig. 2-3. The parametric study is conducted for both transmission lines by covering the following values for $R = 0.0, 25, 50, 75, 90, 100, 125, 150, 200, 250, 300, 350, 400, 450,$ and 500 m. For each relative tornado distance R , 16 different values of θ are used.

2.7.1 Analysis of Transmission Line Type T1 under F2 Tornado, ASCE 2010, CIGRE`, and Downburst Wind Fields

The results of this extensive parametric study, in terms of peak internal forces for various members of tower T1 are provided in Table 2-1. Different zones at which the internal forces are reported are illustrated in Fig. 2-1 for towers T1 and T2. The terms diagonal (1) and Diagonal (2) denoted in Tables 2-1 and 2-2 represent diagonal members located in plans parallel and perpendicular to the lines, respectively. Zone 6 for tower T1 includes the guys and conductors' cross-arms and the internal forces are reported in an upper and a lower chord members for each cross-arm. Similarly, the conductors' cross-arms is located in Zone 4 for tower T2.

In Table 2-1, a comparison is carried out between the internal forces resulting from F2 tornado and those resulting from normal wind loads (ASCE 2010), CIGRE` (2009), and downburst loading. According to the electrical company, this particular tower was designed using a reference wind speed of 32.6 m/sec. Thus, the peak forces in the members are calculated under normal wind loads using the procedures explained in Section 4 with reference wind speed of 32.6 m/sec. The members' peak forces due to the two CIGRE` F2 recommended cases of loading are also provided in Table 2-1. The members' internal forces due to downburst wind loads, with a downburst jet velocity of

70 m/sec were provided by Shehata and El Damatty (2007). In the two last columns of the table, the strength capacity of the members, as well as, the design compression forces, as provided by the electrical company, are shown.

Table 2-1 Results of the Parametric Study due to F2 Tornado, Downburst, Conventional Wind, and CIGRE` Wind

	Member		F2 Tornado	Downburst Loading	ASCE (2010)	Cigre'		Electrical Company Forces		
	No.	Type	Parametric Study Axial (kN)	Jet Velocity 70 (m/sec) Axial* (kN)	V _{ref} (32.6 m/sec) Axial (kN)	60 (m/sec) Axial (kN)	Torsion Axial (kN)	Members Capacity Axial (kN)	Design Compression Force (kN)	
Zone 1	F14	Chord	-144	89	-59	-122	-39	-162	-154	
	F43	Diagonal (1)	2	2	1	2	2	58	-2	
	F45	Diagonal (2)	-11	10	-4	-11	-2	-9	-1	
Zone 4	F231	Chord	-244	175	-61	-151	-33	-209	-203	
	F285	Diagonal (1)	-8	7	-2	-5	-6	-12	-4	
	F275	Diagonal (2)	-17	23	-6	-11	-10	-21	-9	
Tower	F215	Chord	-78	57	-37	-31	-17	-302	-206	
	F398	Diagonal (1)	47	46	8	16	-7	116	-21	
	F406	Diagonal (2)	-37	54	-21	-14	-1	-46	-36	
Zone 6	Guy	F437	Upper Chord	227	143	54	104	24	192	0
		F422	Lower Chord	-134	127	-41	-56	-7	-172	-156
Conductor		F118	Upper Chord	40	99	28	28	26	203	0
		F538	Lower Chord	-47	128	-45	-41	-41	-149	-146

Axial* = Absolute members' peak force

2.7.2 Analysis of Transmission Line Typ2 T2 under F2 Tornado, ASCE 2010, and Downburst Wind Fields

In this section, the extensive parametric study is repeated for tower T2. The results in terms of peak internal forces for some selected members are shown in Table 2-2. In Table 2-2, a comparison is carried out between the internal forces resulting from F2 tornado and those resulting from normal wind loads and downburst loading. According to Electrical Company, this particular tower was designed using a reference wind speed of 40 m/sec. The internal forces due to downburst wind loads, with a downburst jet velocity of 70 m/sec are calculated and provided in Table 2-2. The peak forces in the members are calculated under normal wind loads with reference wind speed of 40 m/sec. The last four columns of the table, the design compression and tension forces, as calculated using ASCE 10-97, are provided.

2.7.3 Discussion

A comparison is carried out between the peak forces due to the F2 tornado to those resulting from normal wind load, downburst wind field, and CIGRE` recommended wind fields. The following observations can be drawn from the results shown in Tables 2-1 and 2-2:

- Members' force due to F2 tornado exceed the normal wind, downburst, CIGRE` forces.
- Members' force due to the two equivalent tornado loads recommended by C CIGRE` exceed the conventional wind forces.

- For the majority of members for tower T1, the F2 tornado forces are found to be less than the capacity of the members.
- For tower T2, specifically the chord members, the resulting peak internal forces of the F2 tornado and the downburst are found to be higher than the capacity of the members.

Table 2-2 Results of the Parametric Study due to F2 Tornado, Downburst, and Conventional Wind Fields (Tower T2)

	Member		F2 Tornado	Downburst Loading	ASCE (2010)	ASCE 10-97 Design of Latticed Steel Transmission Structures				
	No.	Type	Parametric Study Axial (kN)	Jet velocity 70 (m/sec) Axial (kN)	Vref (40 m/sec) Axial (kN)	Design Compression Force (kN)	Comp. Control Criteria	Design Tension Force (kN)	Tension Control Criteria	
Zone 1	F1558	Chord	-282	318	-100	-181	<i>L/r</i>	384	Net Section	
	F1460	Diagonal (1)	-9	1	-2	-11	<i>L/r</i>	31	Bearing	
	F1804	Diagonal (2)	-8	-1	-2	-8	<i>L/r</i>	31	Bearing	
Zone 2	F1725	Chord	-545	-438	-131	-222	<i>L/r</i>	384	Net Section	
	F1647	Diagonal (1)	-12	-7	-2	-12	<i>L/r</i>	31	Bearing	
	F1911	Diagonal (2)	-18	-2	-3	-9	<i>L/r</i>	31	Bearing	
	F1662	Chord	-495	-293	-131	-188	<i>L/r</i>	198	Shear	
	F1589	Diagonal (1)	-14	-1	-3	-8	<i>L/r</i>	31	Bearing	
	F1865	Diagonal (2)	12	8	3	-8	<i>L/r</i>	31	Bearing	
Zone 4	Conductor	F1228	Upper Chord	49	41	25	-13	<i>L/r</i>	186	Net Section
		F1213	Lower Chord	-58	-58	-37	-182	<i>L/r</i>	454	Net Section

2.8 Analysis of Transmission Line System – Broken Wire

This section assesses the behaviour of transmission line structures in the case of a broken wire under F2 tornado wind loads. For both transmission lines, the nonlinear staged-

construction analyses option provided by the commercial software SAP 2000 are conducted on three steps. Each stage starts with initial conditions, including previously defined loads, equal to the end of the previous stage. First, the analysis is conducted for the whole transmission line system to adjust the pretension force in the supporting guys, conductors, and ground-wire. The nonlinear stiffness matrix, which includes tension stiffening, is calculated. The displacements, stresses, and loads from the end of this case are carried forward to the second step. Then, the nonlinear analysis is conducted using the applied F2 tornado wind loads. The F2 tornado wind loads are applied on the whole transmission line system. Third, the specific conductors are removed from the model. In the current analysis, one bundle of conductors for one span adjacent to the tower of interest, are removed. Again, the nonlinear analysis is conducted and results are shown in the following sections.

2.8.1 Tower T1

Two cases are chosen to assess the behaviour of tower type T1 during the case of a broken wire. First, the tornado is assumed to be near the tower of interest where $R = 125$ m and $\theta = 90^\circ$. Second case, the tornado is assumed to be far from the tower of interest with $R = 450$ m and $\theta = 90^\circ$. These two cases are chosen to simulate the two extreme cases where the tornado is close and far from the tower of interest. These critical cases were recommended in previous studies conducted by Hamada et al. (2010) and Hamada and El Damatty (2011). The results of the broken-wire cases can be observed significantly in the conductors' and supporting guys' cross-arm zone. Thus, Table 2-3 shows the results of the two broken wire cases in the cross-arms zone only.

2.8.2 Tower T2

Two cases are chosen to assess the behaviour of guyed tower T2 during the case of a broken wire. Based on the same analogy used in Tower T1, the tornado relative location of the two cases are $R = 100$ m with $\theta = 90^\circ$, and $R = 400$ m with $\theta = 90^\circ$. These two critical cases are recommended by El Damatty and Hamada (2013) for transmission tower T2.

2.8.3 Broken Wire Discussion

The following observations can be drawn from the results shown in Tables 2-3 and 2-4:

- The members' peak forces resulting from the broken wire cases are significantly higher than the members' peak forces with all conductors attached to the tower of interest. For the supporting guys' cross-arm chord members, for tower T1, the peak internal forces due to the broken wire cases are approximately 300% higher than the normal tornado loading cases.
- Some members become subjected to compression force, such as conductors' cross-arm upper-chord members F72 and F1228. These upper chord members were originally designed for zero compression forces as shown in Tables 2-1 and 2-2, respectively.
- For the broken wire cases, the members' peak forces due to tornado configuration of $R = 450$ m and $\theta = 90^\circ$ and $R = 400$ m with $\theta = 90^\circ$ are higher than the members' peak force due to tornado configuration of $R = 125$ m and $\theta = 90^\circ$ and $R = 100$ m with $\theta = 90^\circ$. For cross-arms' zone, the far tornado location from the tower of interest is more critical than a closer tornado in the case of broken wire. This is due to:

- The fully loaded adjacent spans.
- The unbalanced loading of the adjacent spans of the tower of interest.
- The out-of-plane bending effect on line's cross-arms due to the broken wire.

Table 2-3 Results of Broken Wire Cases – Tower T1

		Member		R = 125 m $\theta = 90^\circ$		R = 450 m $\theta = 90^\circ$	
		No.	Type	Full Tower	Broken Wire	Full Tower	Broken Wire
				Axial (kN)	Axial (kN)	Axial (kN)	Axial (kN)
Zone 6	Tower	F215	Chord	-49	-58	-78	-89
		F398	Diagonal (1)	7	63	-6	55
		F406	Diagonal (2)	-26	-72	-28	-81
	Guy	F437	Upper Chord	75	237	98	278
		F422	Lower Chord	-90	-101	-36	-135
Conductor	F72	Upper Chord	20	-55	14	-65	
	F545	Lower Chord	-36	82	-32	87	

Table 2-4 Results of Broken Wire cases – Tower T2

Member		R = 100 m $\theta = 90^\circ$		R = 400 m $\theta = 90^\circ$		Member's Design Capacity	
No.	Type	Full Tower	Broken Wire	Full Tower	Broken Wire	Compression	Tension
		Axial (kN)	Axial (kN)	Axial (kN)	Axial (kN)	(kN)	(kN)
F1228	Upper Chord	26	-78	49	-89	-13	186
F1213	Lower Chord	-33	31	-58	32	-182	454

2.9 Conclusion

The following conclusions can be drawn from the study conducted:

- Comparing the internal forces due to F2 tornado to the those resulting from conventional wind load and the high intensity wind load cases recommended by CIGRE`, it is concluded that the F2 tornado forces exceed the peak forces resulting from these loading cases.
- Members' peak forces due to F2 tornado exceed the peak internal forces developed due to downburst wind having a jet velocity of 70 (m/sec).
- Despite the fact that the two-guyed towers were designed in nearly similar environmental conditions, there is a significant difference in terms of the peak internal forces due to F2 tornado wind loads and members resistances.
- For the supporting guys' and conductors cross-arms members, the peak internal forces due to the broken wire cases during F2 tornado can be up to 300% higher than the F2 tornado peak internal forces. Some of these cross-arms members become subjected to relatively high compression forces, while they were originally designed for zero compression forces.
- For the broken wire cases, the study reveals that a relatively far tornado location from the tower of interest is more critical than a relatively closer tornado, especially for guys' and conductors cross-arms members.

2.10 Acknowledgement

The authors gratefully acknowledge Hydro One Inc. for the in-kind support, the collaboration, and the financial support provided for this research. The first author is indebted to the Vanier Canada Graduate and NSERC for the financial support provided for this research.

2.11 Reference

American Society of Civil Engineers. 10 - 1997. Design of latticed steel transmission structures. *American Society of Civil Engineers*, New York, NY.

American Society of Civil Engineers. (2010). "Guidelines for electrical transmission line structural loading." ASCE manuals and reports on engineering practice, no. 74 (3rd ed.), *American Society of Civil Engineers*, New York, NY.

CIGRÉ (Conseil International des Grands Réseaux Électriques/ International Council on Large Electrical Systems) (2009). "Overhead line design guidelines for mitigation of severe wind storm damage." *Scientific Committee B2 on Overhead Lines*, B2. 06.09.

Davenport, A.G. 1980. Gust Response Factors for Transmission Line Loading. *Zement-Kalk-Gips*, 2: 899-909.

El Damatty, A. A., and Hamada, A. 2013. Behaviour of guyed transmission line structures under tornado wind loads - Case studies. *Electrical Transmission and Substation Structures 2012: Solutions to Building the Grid of Tomorrow, November 4, 2012 - November 8*, American Society of Civil Engineers (ASCE), Columbus, OH, United states, 193-204.

Georgiou, P.N., and Vickery, B.J. 1980. Wind Loads on Building Frames. *Zement-Kalk-Gips*, 1: 421-433.

Hamada, A., Damatty, A.A.E., Hangan, H., and Shehata, A.Y. 2010. Finite element modelling of transmission line structures under tornado wind loading. *Wind and Structures*, 13(5): 451-469.

Hamada, A., and El Damatty, A.A. 2011. Behaviour of guyed transmission line structures under tornado wind loading. *Computers and Structures*, 89(11-12): 986-1003.

Hangan, H., and Kim, J.-. 2008. Swirl ratio effects on tornado vortices in relation to the Fujita scale. *Wind and Structures*, 11(4): 291-302.

Ishac, M.F. and White, H.B. 1994. Effect of tornado loads on transmission lines. *In Proceedings of the 1994 IEEE Power Engineering Society Transmission and Distribution Conference*, April 10, 1994 - April 15, 1994. Publ by IEEE, Chicago, IL, USA, pp. 521-527.

Kim, J., and Hangan, H. 2007. Numerical simulations of impinging jets with application to downbursts. *Journal of Wind Engineering and Industrial Aerodynamics*, 95(4): 279-298.

Li, C.Q. 2000. Stochastic model of severe thunderstorms for transmission line design. *Probabilistic Engineering Mechanics*, 15(4): 359-364.

McCarthy, P and Melsness, M. 1996. Severe weather elements associated with September 5, 1996 hydro tower failures near Grosse Isle, Manitoba, Canada. *Manitoba Environmental Service Centre*, Environment Canada.

McClure, G., Langlois, S. and Rogier, J. 2008. Understanding how overhead lines respond to localized high intensity wind storms. *In 2008 Structures Congress - Structures Congress 2008: Crossing the Borders*, April 24, 2008 - April 26, 2008. American Society of Civil Engineers, Vancouver, BC, Canada.

Sarkar, P., Haan, F., Gallus, Jr., W., Le, K. and Wurman, J. 2005. Velocity measurements in a laboratory tornado simulator and their comparison with numerical and full-scale data. *In 37th Joint Meeting Panel on Wind and Seismic Effects*, Tsukuba, Japan, May 2005.

Savory, E., Parke, G.A.R., Zeinoddini, M., Toy, N., and Disney, P. 2001. Modelling of tornado and microburst-induced wind loading and failure of a lattice transmission tower. *Engineering Structures*, 23(4): 365-375.

Shehata, A.Y., El Damatty, A.A., and Savory, E. 2005. Finite element modeling of transmission line under downburst wind loading. *Finite Elements in Analysis and Design*, 42(1): 71-89.

Shehata, A.Y., and El Damatty, A.A. 2007. Behaviour of guyed transmission line structures under downburst wind loading. *Wind and Structures*, 10(3): 249-268.

Shehata, A.Y., and El Damatty, A.A. 2008. Failure analysis of a transmission tower during a microburst. *Wind and Structures*, 11(3): 193-208.

Wen, Y. 1975. Dynamic tornadic wind loads on tall buildings. *ASCE Structural Division*, 101(1): 169-185.

CHAPTER 3

NONLINEAR FORMULATION OF FOUR-NODED CABLE ELEMENT AND APPLICATION TO TRANSMISSION LINES UNDER TORNADOES

3.1 Introduction

Many Civil Engineering structures are supported by cables such as cable-stayed bridges, cable roofs, and suspension bridges. Guyed transmission towers are another examples of cable supported structures where the stability of the structures is provided through a pin support at the base and supporting guys attached to the top region of the towers. In addition, transmission line towers support the electrical conductors usually through cross-arms and insulators.

Cables are nonlinear structural elements as they are very flexible and can be subjected to large displacements that exceed significantly their cross-sectional dimensions. The behaviour of cables are affected by the magnitude of the initial prestressing forces that are necessary in order to remain stable under their own weights (Han and Lee 2003). The flexural stiffness of cable elements is usually neglected and those elements possess stiffness only in the axial direction. This axial stiffness depends on the initial prestressing force, the initial sagging and varies nonlinearly with the magnitude of the applied loads. The behaviour of cables becomes even more challenging when the cables have a curved shape similar to the case of electrical conductors (transmission wires) spanning between transmission towers.

An approach for modelling curved conductors involves using straight linear three dimensional truss elements. However, this approach would require employing a large number of elements to simulate the curved shape of the conductors. Thus, curved elements are best suited to simulate curved cables with large sag and a catenary shape as stated by Desai et al. (1988). Desai et al. (1988) also concluded that a fine mesh of two-noded curved elements might not be satisfactory to model cables even under uniform loading. Cables modeled by many standard two-noded elements have convergence difficulties because displacements may be in the same order of the structure dimensions (Cook 2002). Felippa (1974) found that a parabolic three-noded curved element would be too stiff axially and poorly approximates a catenary shape. Felippa (1974), Haase (1979), and Schrefler et al. (1983) concluded that a very fine mesh of two-noded elements is required for non-uniformly distributed loads.

The objective of this study is to develop a numerical model that can simulate the behaviour of transmission line conductors under tornado loading. Since such a loading is expected to be highly non-uniform, the use of high-order element is preferred for such a case. A four-noded three dimensional curved cable element that uses a cubic shape function to interpolate both the displacements and the geometry was introduced by Koziey (1993). However the formulation of this powerful cable element was limited to the linear range of behaviour. After describing the element and its linear formulation as outlined by Koziey (1993), the task is taken in this study to extend its formulation by including the geometric nonlinear effect. A validation for this development is then carried out. Details related to the specific modelling of transmission line conductors are then presented. In particular, the study discusses the formulation of a nonlinear spring system

simulating the rigidity of the transmission towers and the insulators that support the conductors. Using this development, a conductor system of a real transmission line is numerically simulated. The model is used to assess the performance of the conductor under F2 tornado simulated loads. The importance of accounting for the flexibility of the towers and the insulators is then quantified.

3.2 Cable Element Formulation

3.2.1 Four-Noded Cable Element and Linear Derivation

A sketch of the cable element introduced by Koziey (1993) is provided in Fig. 3-1. The element was used by Koziey (1993) to model steel reinforcement in concrete sections. The coordinate systems used in the element's formulation are shown in Fig. 3-1, and are defined as follows:

- Global Cartesian coordinate system x^r , y^r , and z^r corresponding to global displacements u^r , v^r , and w^r .
- Curvilinear coordinate ζ tangent to the element.
- Local dimensional coordinate ξ tangent to the element to define the local axial displacement d_{ξ}^r , the local strain ε_{ξ}^r , and the local stress σ_{ξ}^r .

A curvilinear transformation based on the curvilinear coordinate ζ is used for geometric distortion of the element. The location of any point along the element in the global coordinate system is given as

$$\begin{Bmatrix} x^r \\ y^r \\ z^r \end{Bmatrix} = \sum N_i^r \begin{Bmatrix} x_i^r \\ y_i^r \\ z_i^r \end{Bmatrix} \quad \text{Eq. 3-1}$$

Where the cubic interpolation functions N_i^r are given as

$$N_1^r(\zeta) = -\frac{9}{16} (1-\zeta)\left(\frac{1}{3}+\zeta\right)\left(\frac{1}{3}-\zeta\right) \quad \text{Eq. 3-2}$$

$$N_2^r(\zeta) = \frac{27}{16} (1+\zeta)(1-\zeta)\left(\frac{1}{3}-\zeta\right) \quad \text{Eq. 3-3}$$

$$N_3^r(\zeta) = \frac{27}{16} (1+\zeta)(1-\zeta)\left(\frac{1}{3}+\zeta\right) \quad \text{Eq. 3-4}$$

$$N_4^r(\zeta) = -\frac{9}{16} (1+\zeta)\left(\frac{1}{3}+\zeta\right)\left(\frac{1}{3}-\zeta\right) \quad \text{Eq. 3-5}$$

and x_i^r , y_i^r , and z_i^r are the global coordinates of the i^{th} node.

The global displacement u^r , v^r , and w^r are calculated using the nodal global displacement degrees of freedom u_i^r , v_i^r , and w_i^r at each of the four nodes. A total of twelve degrees of freedom exists per element. The axial displacement d_ξ^r at any point along the element can be written in terms of the nodal degrees of freedom as

$$d_\xi^r = \sum N_i^r \begin{bmatrix} \lambda_1^r & \lambda_2^r & \lambda_3^r \end{bmatrix} \begin{Bmatrix} u_i^r \\ v_i^r \\ w_i^r \end{Bmatrix} \quad \text{Eq. 3-6}$$

The direction cosines (λ_1^r , λ_2^r , λ_3^r) relate the local coordinate axis ξ to the global axes (x^r , y^r , z^r) at any point along the element where axial displacement d_ξ^r is to be calculated. The direction cosines are computed as follows:

$$\lambda_1^r = \frac{dx^r}{d\zeta} / \sqrt{\left[\frac{dx^r}{d\zeta}\right]^2 + \left[\frac{dy^r}{d\zeta}\right]^2 + \left[\frac{dz^r}{d\zeta}\right]^2} \quad \text{Eq. 3-7}$$

$$\lambda_2^r = \frac{dy^r}{d\zeta} / \sqrt{\left[\frac{dx^r}{d\zeta}\right]^2 + \left[\frac{dy^r}{d\zeta}\right]^2 + \left[\frac{dz^r}{d\zeta}\right]^2} \quad \text{Eq. 3-8}$$

$$\lambda_3^r = \frac{dz^r}{d\zeta} / \sqrt{\left[\frac{dx^r}{d\zeta}\right]^2 + \left[\frac{dy^r}{d\zeta}\right]^2 + \left[\frac{dz^r}{d\zeta}\right]^2} \quad \text{Eq. 3-9}$$

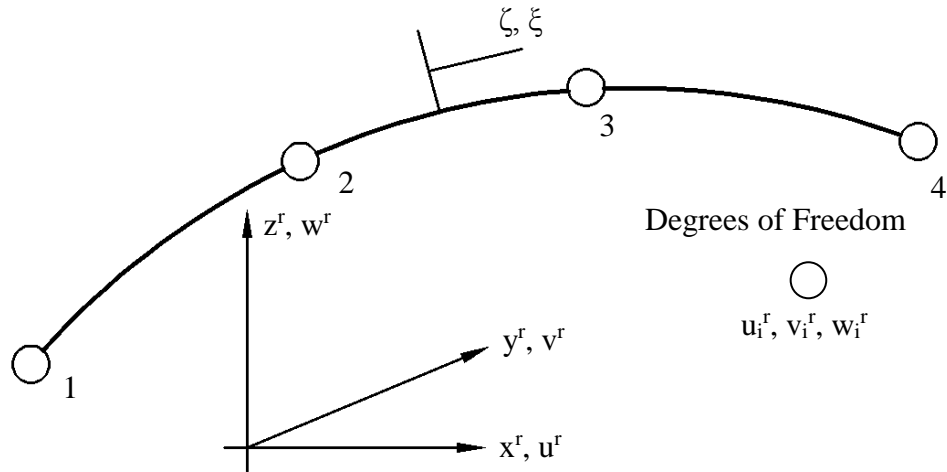


Fig. 3-1 Cable Element Coordinate and Systems and Nodal Degrees of Freedom

The local axial strain ε_{ξ}^r is given by

$$\varepsilon_{\xi}^r = \frac{d d_{\xi}^r}{d\xi} = \sum_1^4 \frac{dN_i^r}{d\xi} [\lambda_1^r \quad \lambda_2^r \quad \lambda_3^r] \begin{Bmatrix} u_i^r \\ v_i^r \\ w_i^r \end{Bmatrix} \quad \text{Eq. 3-10}$$

The local axial strain can also be calculated as $\varepsilon_{\xi}^r = [B^r] \{d^r\}$. $\{d^r\}$ is the vector of nodal degrees of freedom and B-matrix $[B^r]$, which is provided in Appendix I, is the strain-

displacement matrix. The B-matrix contains the derivatives of the shape functions N^r with respect to the local dimensional coordinate ξ . Differential $d\zeta$ in the non-dimensional coordinate system is related to differential $d\xi$ in the dimensional coordinate system through

$$d\xi = \sqrt{\left[\frac{dx^r}{d\zeta}\right]^2 + \left[\frac{dy^r}{d\zeta}\right]^2 + \left[\frac{dz^r}{d\zeta}\right]^2} d\zeta \quad \text{Eq. 3-11}$$

Using the chain rule, for derivatives of the shape function can be calculated as follows

$$\frac{dN_i}{d\xi} = \frac{dN_i}{d\zeta} \frac{d\zeta}{d\xi} = \frac{dN_i}{d\zeta} / \sqrt{\left[\frac{dx^r}{d\zeta}\right]^2 + \left[\frac{dy^r}{d\zeta}\right]^2 + \left[\frac{dz^r}{d\zeta}\right]^2} \quad \text{Eq. 3-12}$$

The axial stress σ_ξ^r can be calculated as follows

$$\sigma_\xi^r = E \varepsilon_\xi^r \quad \text{Eq. 3-13}$$

Where E is the elastic modulus. It should be noted that for cable elements, the axial strain is the most significant parameter and all other strains are neglected.

The element stiffness matrix $[k^r]$ is calculated as

$$[k^r]_{12 \times 12} = \int [B^r]^T_{12 \times 1} E [B^r]_{1 \times 12} dV \quad \text{Eq. 3-14}$$

And the load vector $\{P^r\}$ due to the internal pretension stress σ_ξ^r (due to sagging) is calculated as

$$\{P^r\} = \int [B^r]^T_{12 \times 1} \sigma_\xi^r dV \quad \text{Eq. 3-15}$$

Both $[k^r]$ and $\{P^r\}$ are integrated numerically using the Gaussian Quadrature method. Five integration points are used for the numerical integration. The element stiffness matrix $[k^r]$ and load vector $\{P^r\}$ can be written in non-dimensional coordinate system $d\zeta$ as follows

$$[k^r]_{12 \times 12} = \int_{-1}^{+1} [B^r]^T_{12 \times 1} E [B^r]_{1 \times 12} A^r \sqrt{\left[\frac{dx^r}{d\zeta}\right]^2 + \left[\frac{dy^r}{d\zeta}\right]^2 + \left[\frac{dz^r}{d\zeta}\right]^2} d\zeta \quad \text{Eq. 3-16}$$

$$\{P^r\} = \int_{-1}^{+1} [B^r]^T_{12 \times 1} \sigma_{\xi}^r A^r \sqrt{\left[\frac{dx^r}{d\zeta}\right]^2 + \left[\frac{dy^r}{d\zeta}\right]^2 + \left[\frac{dz^r}{d\zeta}\right]^2} d\zeta \quad \text{Eq. 3-17}$$

Where A^r is the cable element cross-section area.

3.2.2 Geometric Nonlinear Formulation of the Cable Element

The derivation of the finite element formulation is conducted based on the total Lagrangian approach. Using the virtual work approach described by Bathe (1996) and El Damatty et al. (1997), the finite element discretization expression, written in matrix form, at the k^{th} iteration of load increment t is given by:

$$\left[[K_{NL}]^{t(k-1)} + [K_S]^{t(k-1)} \right] \{\Delta u\} = \{R\}^t - \{F\}^{t(k-1)} \quad \text{Eq. 3-18}$$

Where nonlinear stiffness matrix $[K_{NL}]_{12 \times 12}^{t(k-1)}$ can be obtained as follow

$$[K_{NL}]_{12 \times 12}^{t(k-1)} = \int [B_{NL}^{t(k-1)}]^T_{12 \times 1} E [B_{NL}^{t(k-1)}]_{1 \times 12} dV$$

and the numerical integration can be used through the following equation

$$[K_{NL}]_{12 \times 12}^{t(k-1)} = \int_{-1}^1 [B_{NL}^{t(k-1)}]_{12 \times 1}^T E [B_{NL}^{t(k-1)}]_{1 \times 12} A^r \sqrt{\left[\frac{dx^r}{d\zeta}\right]^2 + \left[\frac{dy^r}{d\zeta}\right]^2 + \left[\frac{dz^r}{d\zeta}\right]^2} d\zeta \quad \text{Eq. 3-19}$$

El Damatty et al. (1997) developed an approach where the nonlinear B- Matrix can be evaluated using the linear B-Matrix and this leads to the following relation:

$$[B_{NL}^{t(k-1)}]_{1 \times 12} = [B^r]_{1 \times 12} + \varepsilon_{\zeta}^r [B^r]_{1 \times 12}$$

The stress stiffness matrix $[K_s]_{12 \times 12}^{t(k-1)}$, which contain the effect of tension stiffening and the initial pretension stress, can be obtained as follow

$$[K_s]_{12 \times 12}^{t(k-1)} = \int [S^{t(k-1)}] [\bar{N}]_{12 \times 12} dV$$

and the numerical integration can be applied through the following equation

$$[K_s]_{12 \times 12}^{t(k-1)} = \int_{-1}^1 \sigma_{\zeta}^r [\bar{N}]_{12 \times 12} A^r \sqrt{\left[\frac{dx^r}{d\zeta}\right]^2 + \left[\frac{dy^r}{d\zeta}\right]^2 + \left[\frac{dz^r}{d\zeta}\right]^2} d\zeta \quad \text{Eq. 3-20}$$

Where the matrix $[\bar{N}]_{12 \times 12}$ is provided in Appendix II.

The unbalanced load vector $\{R\}^t - \{F\}^{t(k-1)}$ represents the difference between the external forces load vector $\{R\}^t$ and the internal forces $\{F\}^{t(k-1)}$. The internal forces load vector is calculated in each iteration using the following equation:

$$\{F\}_{12 \times 1}^{t(k-1)} = \int [B_{NL}^{t(k-1)}]_{12 \times 1}^T [S^{t(k-1)}] dV$$

and the numerical integration can be conducted using the following equation

$$\{F\}_{12 \times 1}^{t(k-1)} = \int_{-1}^1 [B_{NL}^{t(k-1)}]_{1 \times 12} \sigma_{\xi}^r A^r \sqrt{\left[\frac{dx^r}{d\zeta}\right]^2 + \left[\frac{dy^r}{d\zeta}\right]^2 + \left[\frac{dz^r}{d\zeta}\right]^2} d\zeta \quad \text{Eq. 3-21}$$

The full element derivation is provided in Appendix III.

3.2.3 Steps of Nonlinear Analysis

The following steps are followed to perform the nonlinear analysis:

- 1- At the beginning of the analysis, the initial axial stress σ_{ξ}^r is equated to the pretension stress in the cables associated with its own weight and initial sagging.
- 2- The external Load is applied incrementally. At each increment (t), the external load vector $\{R\}^t$ is calculated.
- 3- Iterations are applied within each load increment (t) until convergence is reached. For an iteration (k) of a load increment (t), the components of the stiffness matrix $[K_{NL}]_{12 \times 12}^{t(k-1)}$, $[K_s]_{12 \times 12}^{t(k-1)}$, and the internal load vector $\{F\}_{12 \times 1}^{t(k-1)}$ at the previous iteration are calculated using Eqs. (3-19), (3-20), and (3-21), respectively. Gaussian Quadrature method is used with five integration points to perform the numerical integration.
- 4- Eq. (3-18) is solved to obtain the incremental displacement $\{\Delta u\}$, then the total displacement is updated.
- 5- The incremental strain and stress are then evaluated using the following equations

$$\{\Delta \mathcal{E}\} = [B_{NL}] \{\Delta u\} \quad \text{Eq. 3-22}$$

$$\{\Delta\sigma\} = E\{\Delta\varepsilon\} \quad \text{Eq. 3-23}$$

- 6- The convergence criterion is checked. If the convergence criterion is satisfied, the analysis proceeds to step 2 with an updated load increment. If convergence is not satisfied, further iterations are conducted as described in step 3.

A force convergence criterion is applied by calculating the ratio between the unbalance force and the total load applied in the considered increment. A fraction of 0.001 of the total load is set as a convergence tolerance as recommended by Cook (2002). It was recommended by Cook (2002) to use force convergence criterion in such nonlinear hardening problems.

3.3 Finite Element Modelling of Transmission Line's Cables

In the current study, the behaviour of a conductor of a generic guyed transmission line is assessed using the developed cable element. The purpose is to evaluate the reactions provided by the supporting towers under an F2 tornado wind load case. As shown in Fig. 3-2, the conductor has a span of 480 (m) with properties provided in Table 3-1. The numerical simulation of the conductor is provided in Fig. 3-2. Three conductor spans are simulated from each side of the tower of interest where the reactions are assessed. The three dimensional spring systems, shown in Fig. 3-2, represent the stiffness of the towers, which provide support to the conductor. This stiffness results from the combined rigidity of the towers and the attached insulators. Because of the large rotations experienced by the insulators during tornadoes, the spring system is expected to behave in a nonlinear manner. The derivation of this nonlinear spring system is provided below.

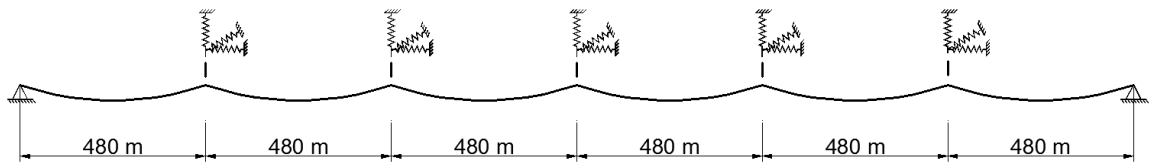


Fig. 3-2 Finite Element Model for Transmission Line Systems

Table 3-1 Physical Parameters Employed for Conductors and Ground-wires

Parameters		Transmission Line Conductor
Name		1843.2 MCM 72/7 Nelson ACSR
Wind Span	m	480
Diameter	mm	40.64
Weight	N/m	28.97
Modulus of Elasticity	N/m ²	6.23x10 ¹⁰
Sag	m	20

3.3.1 Derivation of Spring System

Fig. 3-3 shows an insulator attached to a cross arm and supporting a conductor. The objective of this sub-section is to derive the stiffness of a spring system simulating the stiffness at point “B”, where the conductor is attached. The derivation starts by evaluating the flexibility matrix at point “A” as follows:

$$[f_A] = \begin{pmatrix} f_{xxl} & 0 & f_{xzl} \\ 0 & f_{yyL} & 0 \\ f_{zxL} & 0 & f_{zzL} \end{pmatrix}$$

Where, f_{xxl} and f_{xzl} are the transverse and vertical displacement of point “A”, respectively, due to unit transverse load applied at point “A”. f_{yyL} is the longitudinal

displacement of point “A” due to unit longitudinal load applied at point “A”. Similarly, f_{zxI} and f_{zzI} are the transverse and vertical displacements of point “A”, respectively, due to unit vertical load applied at point “A”.

The insulators are considered to be rigid in the vertical direction and pin connected to the tower’s cross-arm and the conductors. They can be replaced by two perpendicular nonlinear springs K_{IY} and K_{IX} , in the Y and X direction, respectively. Y and X are the longitudinal and transverse directions, respectively. The linear expressions for the spring constants K_{IY} and K_{IX} are given by Desai et al. (1995). These are modified in the current study to account for the variation of stiffness with the rotation angles of the insulator θ_L and θ_T . This leads to the following expressions for K_{IY} and K_{IX} :

$$K_{IY} = \left(\frac{1}{L_I \cos(\theta_L)} \right) \left(P_y * L + \frac{W_I}{2} \right) \quad \text{Eq. 3-24}$$

$$K_{IX} = \left(\frac{1}{L_I \cos(\theta_T)} \right) \left(P_y * L + \frac{W_I}{2} \right) + \frac{2T}{L_x} \quad \text{Eq. 3-25}$$

Where, L_I and W_I are the length and weight of the insulators, respectively. L and L_x are the total and horizontal span lengths of the conductor at the adjacent towers, respectively. P_y is the weight per unit length of the adjacent conductors, the rotation angles θ_L and θ_T are as shown in Fig. 3-3, and T is the horizontal component of the conductor pretension force.

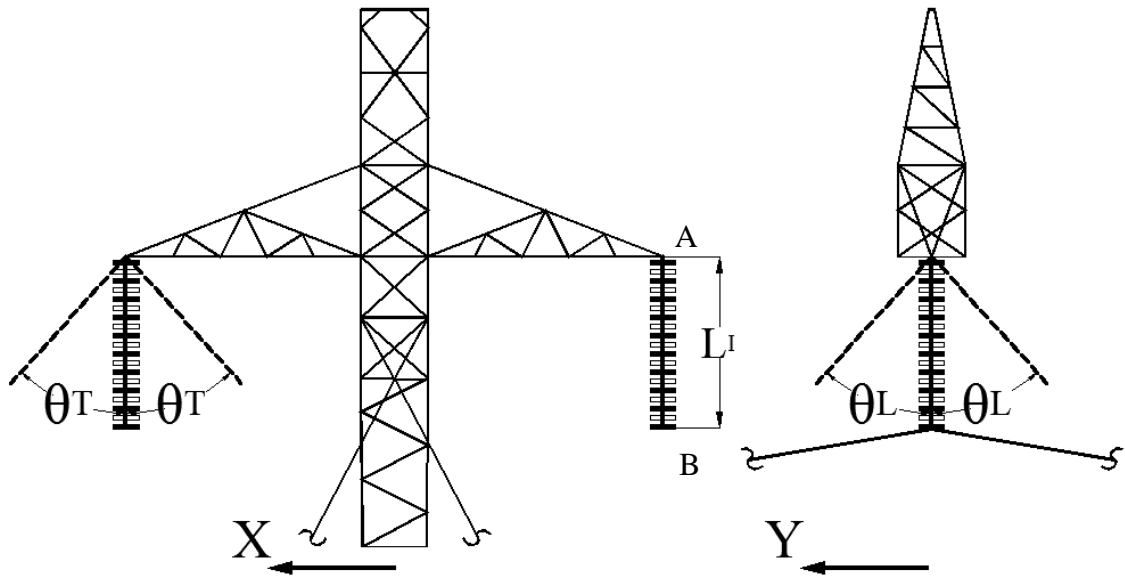


Fig. 3-3 Conductors' Cross-arms and Insulators Configurations

The flexibility matrix at point "B", shown in Fig. 3-3, can be evaluated by adding the flexibility of the insulator as follows;

$$[f_B] = \begin{pmatrix} \left(f_{xxt} + \frac{1}{K_{IX}} \right) & 0 & f_{xzt} \\ 0 & \left(f_{yyt} + \frac{1}{K_{IY}} \right) & 0 \\ f_{zxt} & 0 & f_{zzt} \end{pmatrix}$$

The stiffness matrix at point "B" can be then evaluated by inverting the flexibility matrix

$$[K_B] = \begin{pmatrix} K_{xx} & K_{xy} & K_{xz} \\ K_{yx} & K_{yy} & K_{yz} \\ K_{zx} & K_{zy} & K_{zz} \end{pmatrix} = [f_B]^{-1}$$

The rotation limits of the conductors in the longitudinal and the transverse direction are set to 90° ; rotations at which the insulators become locked to the tower. Once this limit is reached in the longitudinal direction, the insulator stiffness K_{IY} is assigned a value of infinity. Similarly, once the rotation limit is reached in the transverse direction, the insulator stiffness K_{IX} is assigned a value of infinity.

3.3.2 Cables Modelling

The three dimensional isoparametric cable element developed in Section 2 is used to model the considered transmission line conductor. Each cable span is divided into ten elements. The pretension force, T , is assumed to be constant over the entire length of the conductor and can be evaluated calculated using Eq. (3-26), in terms of the sag S , weight per unit length P_y , and the horizontal wind span of the cable L_x .

$$T = \frac{P_y L_x^2}{8S} \quad \text{Eq. 3-26}$$

3.4 Tornado Velocity Profile and Loading

The conductors described above is analyzed under F2 tornado loading. The F2 tornado wind field is obtained based on the procedures developed by Hamada et al. (2010) to estimate a velocity field for F2 tornadoes from the computational fluid dynamics (CFD) simulations conducted by Hangan and Kim (2008). The analyses are conducted under the tornado configuration of $R = 125$ (m) and $\theta = 180^\circ$, where R is the distance between the tornado center to the tower of interest, and θ is the angle shown in Fig. 3-4. The profile of the transverse velocity along the six spans conductors is shown in Fig. 3-5. Similar

profile for the vertical velocity component is shown in Fig. 3-6. The tornado loads acting on the conductors depends on the square of the velocity. Accordingly and in view of Figures 3-5 and 3-6, one can conclude that the tornado loads acting on the conductors are not uniform in both the transverse and vertical directions. Also, the loads acting on both sides of the tower of interest are unequal. This will result in difference in tension forces on the adjacent spans of this tower. An unbalanced load results from this difference in tension, which will be transferred as force acting along the longitudinal direction of the line.

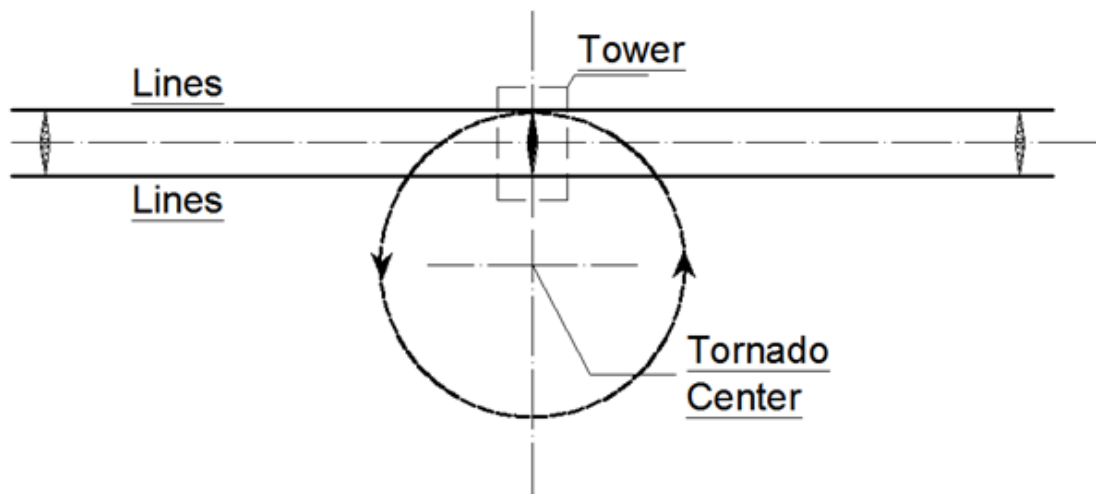


Fig. 3-4 Horizontal Projection of F2 Tornado Located at Relative Distance $R = 125$ (m) and $\theta = 180^\circ$

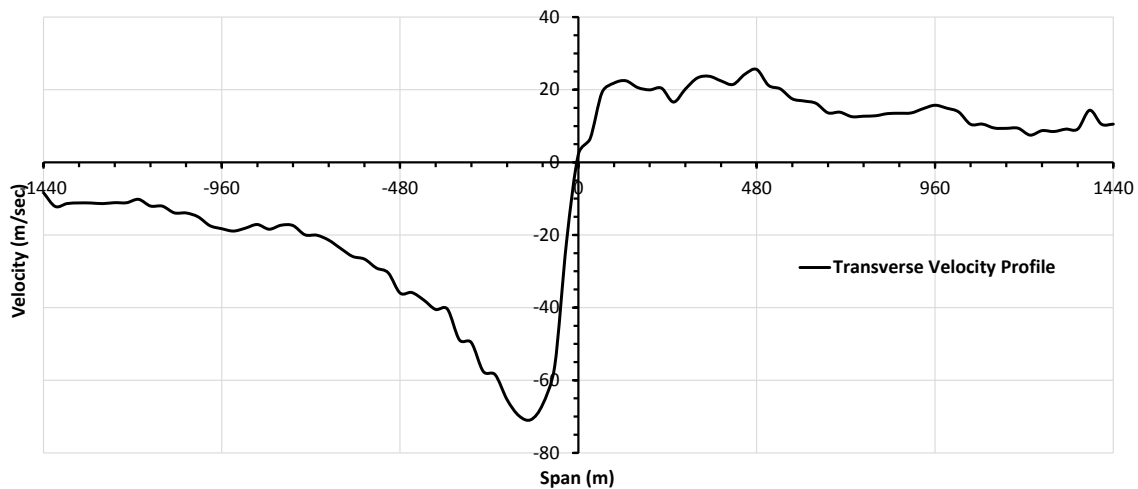


Fig. 3-5 Transverse Velocity Profile – Conductors ($R = 125$ (m), and $\theta = 180^\circ$)

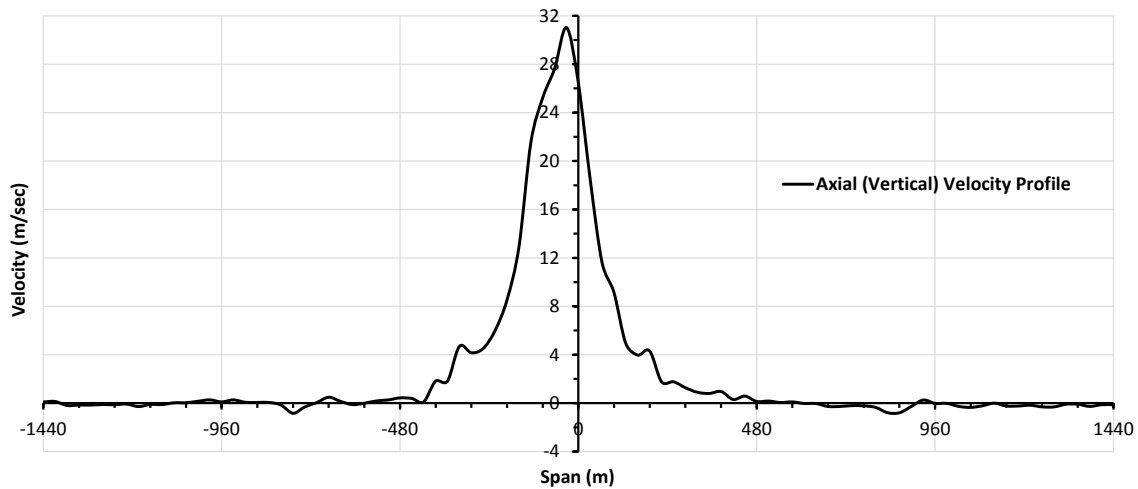


Fig. 3-6 Conductors Axial (Vertical) Velocity Profile ($R = 125$ (m), and $\theta = 180^\circ$)

3.5 Model Validation

A validation for the developed in-house numerical model is conducted by comparing its results to those obtained using the commercial finite element program SAP 2000 (CSI).

Inc. 2010). Each span is modelled using thirty two-noded cable element available in SAP 2000. The Insulators are modelled using a three dimensional truss element. The considered conductor is analyzed under the loading associated with the tornado configuration $R = 125$ (m) and $\theta = 180^\circ$, described above. The profiles of the deformed shape of the conductor obtained from both the SAP 2000 and the in-house numerical code are provided in Fig. 3-7. The profiles projected in both vertical and horizontal plans are provided in this figure. The figure shows a very good agreement in terms of deformed shapes for both models. The conductor longitudinal, transverse, and vertical reactions are evaluated at the support simulating the intermediate tower from both the SAP and the in-house numerical models, and are provided in Table 3-2. Again, the results obtained from the two sets of analyses indicate an excellent agreement, thus provide a validation for the developed numerical model.

Table 3-2 In-house and SAP 2000 Conductor's Reactions Comparison (F2 Tornado Configuration $R= 125$ and $\theta = 180^\circ$)

Conductor's Reactions	Direction	In-house Numerical Code			SAP 2000	
		Flexible Tower + Insulators	Rigid Tower + Insulators	Flexible Tower Only	Rigid	Flexible Tower + Insulators
Fx (N)	Transverse	15,422	15,557	16,122	15,775	15,571
Fy (N)	Longitudinal	6841	6067	25,113	45,876	6155
Fz (N)	Vertical	24,855	25,337	25,335	25,664	25,217

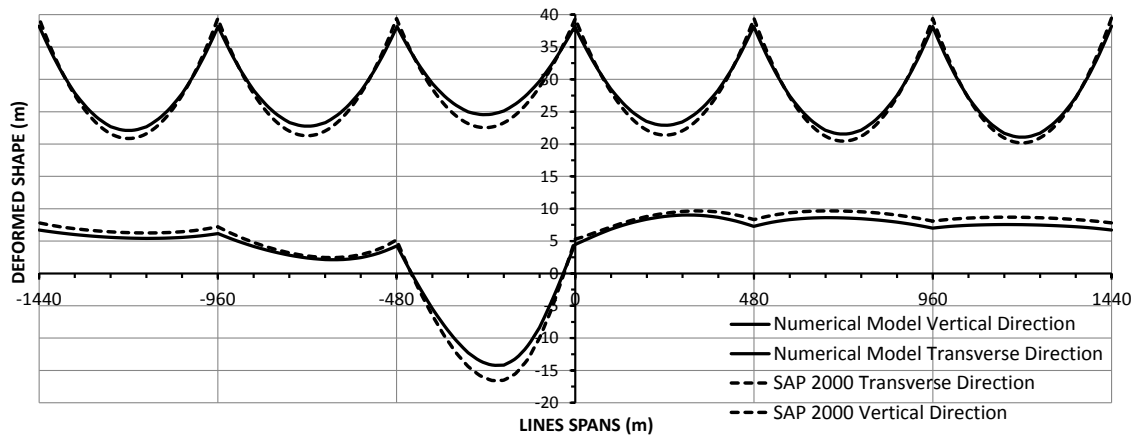


Fig. 3-7 Cable Displacements in Elevation and Plan View using SAP 2000 and Current Numerical Code (F2 Tornado $R= 125$ and $\theta = 180^\circ$)

3.6 Effect of Conductors' Supports on the Force Transmitted to Transmission Towers

Having validated the developed numerical model, the study proceeds by conducting a parametric study to assess the effect of flexibility of the conductors' supports on the forces transmitted to the towers from the conductors due to F2 tornado. The following four cases are considered in this parametric study:

- a) Case 1: the flexibility of both the towers and the insulators are included in the analyses. The springs' stiffness resulting for both the supporting tower and the insulators is calculated and updated at each nonlinear step.
- b) Case 2: the insulators are assumed to be flexible while the towers are assumed to be rigid. This represents an assumption that the towers are much rigid compared to the insulators.
- c) Case 3: the insulators' flexibility is neglected. The three dimensional springs simulates only the stiffness of the towers.

d) Case 4: the springs simulating the towers' and insulators' flexibility are replaced by hinged support. This case assumes that the tower and insulators are both rigid. The results shown in the table indicate that the four assumptions made regarding the supports' rigidity do not affect the values of the reactions in both the transverse and vertical directions. Meanwhile, those assumptions affect significantly the values of the longitudinal reactions. As shown in Table 3-2, the case involving neglecting the flexibility of the insulators leads to an increase in the longitudinal reaction from a value of 6841 (N) to 25,113 (N), i.e. about 3.50 times. The assumption of pin support increases the longitudinal reaction further to a value of 45,876 (N). Also the results indicate that neglecting the flexibility of the towers has a minor effect on the longitudinal reactions.

3.7 Conclusion

The formulation of a high order finite cable element is extended in this chapter to include the geometric nonlinear effect. The element has four nodes and, therefore, provides a cubic interpolation for both of geometry and displacements. Such a high order interpolation is quite beneficial in modelling curved cables such as electric conductors used in transmission line systems. The element is then used to model transmission line conductors under the combined effects of own weight, initial tension and forces associated with F2 tornadoes. In this simulation, the conductors' support are modelled using three dimensional nonlinear springs representing the combined stiffness of the insulators and the towers. The formulation of these nonlinear springs are derived in this chapter. This numerical development is used to assess the effect of boundary condition assumptions on the cable reactions, which in turn, are transferred to the transmission

towers under an F2 tornado. The results indicate that the boundary conditions have no effect on the transverse and vertical reactions while they affect significantly the longitudinal reactions. The results also show that it is very important to include the flexibility of the insulators and less important to include the flexibility of the towers when evaluating longitudinal reactions of the conductors.

3.8 Acknowledgement

The first author is indebted to the Vanier Canada Graduate and the Natural Science and Engineering Research Council of Canada (NSERC) for the financial support provided for this research.

3.9 Reference

Bathe, K., and Bathe, K. (1996). *Finite element procedures*. Prentice Hall, Englewood Cliffs, N.J.

Cook, R. D., and Cook, R. D. (2002). *Concepts and applications of finite element analysis*. Wiley, New York.

Desai, Y. M., Popplewell, N., Shah, A. H., and Buragohain, D. N. (1988). "Geometric nonlinear static analysis of cable supported structures." *Computers and Structures*, 29(6), 1001-1009.

Desai, Y. M., Yu, P., Popplewell, N., and Shah, A. H. (1995). "Finite element modelling of transmission line galloping." *Computers and Structures*, 57(3), 407-420.

El Damatty, A. A., and Hamada, A. (2013). "Behaviour of guyed transmission line structures under tornado wind loads - Case studies." *Electrical Transmission and Substation Structures 2012: Solutions to Building the Grid of Tomorrow*, November 4,

2012 - November 8, American Society of Civil Engineers (ASCE), Columbus, OH, United states, 193-204.

El Damatty, A. A., Korol, R. M., and Mirza, F. A. (1997). "Large displacement extension of consistent shell element for static and dynamic analysis." *Computers and Structures*, 62(6), 943-960.

Felippa, C. A. (1974). "Finite element analysis of three-dimensional cable structures." *Proceedings of International Conference of Computational Methods in Nonlinear Mechanics*. Austin, TX, 23-25 Sept., pp. 311-314

M. Haase (1979), Zur naturlichen formulierung von simplex elementen hoherer ordnung fur die berechnung elastischer membranschalen und seilkonstruktionen unter grossen verformungen. Doctoral dissertation, University of Stuttgart, Stuttgart (1979)

Hamada, A., Damatty, A. A. E., Hangan, H., and Shehata, A. Y. (2010). "Finite element modelling of transmission line structures under tornado wind loading." *Wind and Structures, an International Journal*, 13(5), 451-469.

Hamada, A., and El Damatty, A. A. (2011). "Behaviour of guyed transmission line structures under tornado wind loading." *Computers and Structures*, 89(11-12), 986-1003.

Han, S., and Lee, K. (2003). "A study of the stabilizing process of unstable structures by dynamic relaxation method." *Computers and Structures*, 81(17), 1677-1688.

Hangan, H., and Kim, J. -. (2008). "Swirl ratio effects on tornado vortices in relation to the Fujita scale." *Wind and Structures*, 11(4), 291-302.

Koziey, B. L. (1993). "Formulation and applications of consistent shell and beam elements". Ph.D. McMaster University (Canada), Canada.

Schrefler, B. A., Odorizzi, S., and Wood, R. D. (1983). "A total Lagrangian geometrically non-linear analysis of combined beam and cable structures." *Computers and Structures*, 17(1), 115-27.

3.10 Appendix

3.10.1 Appendix I

B-matrix $[B^r]$

$$[B^r]_{1 \times 12} = \left[\frac{dN_1^r}{d\xi} \lambda_1^r \frac{dN_1^r}{d\xi} \lambda_2^r \frac{dN_1^r}{d\xi} \lambda_3^r \frac{dN_2^r}{d\xi} \lambda_1^r \frac{dN_2^r}{d\xi} \lambda_2^r \frac{dN_2^r}{d\xi} \lambda_3^r \frac{dN_3^r}{d\xi} \lambda_1^r \frac{dN_3^r}{d\xi} \lambda_2^r \frac{dN_3^r}{d\xi} \lambda_3^r \frac{dN_4^r}{d\xi} \lambda_1^r \frac{dN_4^r}{d\xi} \lambda_2^r \frac{dN_4^r}{d\xi} \lambda_3^r \right]$$

3.10.2 Appendix II

$$[\bar{N}]_{12 \times 12} = \begin{pmatrix} \left(\frac{dN_1^r}{d\xi}\right)^2 & 0 & 0 & \left(\frac{dN_1^r}{d\xi} \frac{dN_2^r}{d\xi}\right) & 0 & 0 & \left(\frac{dN_1^r}{d\xi} \frac{dN_3^r}{d\xi}\right) & 0 & 0 & \left(\frac{dN_1^r}{d\xi} \frac{dN_4^r}{d\xi}\right) & 0 & 0 \\ \left(\frac{dN_1^r}{d\xi}\right)^2 & 0 & 0 & \left(\frac{dN_1^r}{d\xi} \frac{dN_2^r}{d\xi}\right) & 0 & 0 & \left(\frac{dN_1^r}{d\xi} \frac{dN_3^r}{d\xi}\right) & 0 & 0 & \left(\frac{dN_1^r}{d\xi} \frac{dN_4^r}{d\xi}\right) & 0 & 0 \\ \left(\frac{dN_1^r}{d\xi}\right)^2 & 0 & 0 & \left(\frac{dN_1^r}{d\xi} \frac{dN_2^r}{d\xi}\right) & 0 & 0 & \left(\frac{dN_1^r}{d\xi} \frac{dN_3^r}{d\xi}\right) & 0 & 0 & \left(\frac{dN_1^r}{d\xi} \frac{dN_4^r}{d\xi}\right) & 0 & 0 \\ \left(\frac{dN_2^r}{d\xi}\right)^2 & 0 & 0 & \left(\frac{dN_2^r}{d\xi} \frac{dN_3^r}{d\xi}\right) & 0 & 0 & \left(\frac{dN_2^r}{d\xi} \frac{dN_4^r}{d\xi}\right) & 0 & 0 & \left(\frac{dN_2^r}{d\xi} \frac{dN_4^r}{d\xi}\right) & 0 & 0 \\ \left(\frac{dN_2^r}{d\xi}\right)^2 & 0 & 0 & \left(\frac{dN_2^r}{d\xi} \frac{dN_3^r}{d\xi}\right) & 0 & 0 & \left(\frac{dN_2^r}{d\xi} \frac{dN_4^r}{d\xi}\right) & 0 & 0 & \left(\frac{dN_2^r}{d\xi} \frac{dN_4^r}{d\xi}\right) & 0 & 0 \\ \left(\frac{dN_2^r}{d\xi}\right)^2 & 0 & 0 & \left(\frac{dN_2^r}{d\xi} \frac{dN_3^r}{d\xi}\right) & 0 & 0 & \left(\frac{dN_2^r}{d\xi} \frac{dN_4^r}{d\xi}\right) & 0 & 0 & \left(\frac{dN_2^r}{d\xi} \frac{dN_4^r}{d\xi}\right) & 0 & 0 \\ \left(\frac{dN_3^r}{d\xi}\right)^2 & 0 & 0 & \left(\frac{dN_3^r}{d\xi} \frac{dN_4^r}{d\xi}\right) & 0 & 0 & \left(\frac{dN_3^r}{d\xi} \frac{dN_4^r}{d\xi}\right) & 0 & 0 & \left(\frac{dN_3^r}{d\xi} \frac{dN_4^r}{d\xi}\right) & 0 & 0 \\ \left(\frac{dN_3^r}{d\xi}\right)^2 & 0 & 0 & \left(\frac{dN_3^r}{d\xi} \frac{dN_4^r}{d\xi}\right) & 0 & 0 & \left(\frac{dN_3^r}{d\xi} \frac{dN_4^r}{d\xi}\right) & 0 & 0 & \left(\frac{dN_3^r}{d\xi} \frac{dN_4^r}{d\xi}\right) & 0 & 0 \\ \left(\frac{dN_3^r}{d\xi}\right)^2 & 0 & 0 & \left(\frac{dN_3^r}{d\xi} \frac{dN_4^r}{d\xi}\right) & 0 & 0 & \left(\frac{dN_3^r}{d\xi} \frac{dN_4^r}{d\xi}\right) & 0 & 0 & \left(\frac{dN_3^r}{d\xi} \frac{dN_4^r}{d\xi}\right) & 0 & 0 \\ \left(\frac{dN_4^r}{d\xi}\right)^2 & 0 & 0 & \left(\frac{dN_4^r}{d\xi}\right)^2 & 0 & 0 & \left(\frac{dN_4^r}{d\xi}\right)^2 & 0 & 0 & \left(\frac{dN_4^r}{d\xi}\right)^2 & 0 & 0 \\ \left(\frac{dN_4^r}{d\xi}\right)^2 & 0 & 0 & \left(\frac{dN_4^r}{d\xi}\right)^2 & 0 & 0 & \left(\frac{dN_4^r}{d\xi}\right)^2 & 0 & 0 & \left(\frac{dN_4^r}{d\xi}\right)^2 & 0 & 0 \\ \left(\frac{dN_4^r}{d\xi}\right)^2 & 0 & 0 & \left(\frac{dN_4^r}{d\xi}\right)^2 & 0 & 0 & \left(\frac{dN_4^r}{d\xi}\right)^2 & 0 & 0 & \left(\frac{dN_4^r}{d\xi}\right)^2 & 0 & 0 \end{pmatrix}$$

3.10.3 Appendix III

The derivation of the finite element formulation is based on the total Lagrangian approach. The virtual work approach described by Bathe (1996) and El Damatty et al. (1997) is used. Newton – Raphson (N-R) method is used to conduct the nonlinear

analysis. Cables have almost no flexural stiffness. Stress stiffening has to be accounted for to avoid singularity in the first cycle of the tangent-stiffness under lateral loading and accurately accounts for pretension force due to sagging (slacking) behavior. The solution is carried out incrementally. At each load increment, iterations are performed till convergence is achieved and the load (R) – displacement (u) curve, shown in Fig. 3-8 is established.

$$u_i^{t(k)} = u_i^{t(k-1)} + \Delta u_i^{(k)} \quad \text{Eq. 3-27}$$

Where, $u_i^{t(k)}$ is the total displacement value at the current step k , $\Delta u_i^{(k)}$ is the incremental displacement, t for static analysis represents the different intensities of the applied load as shown in Fig. 3-8, and k is the iteration number.

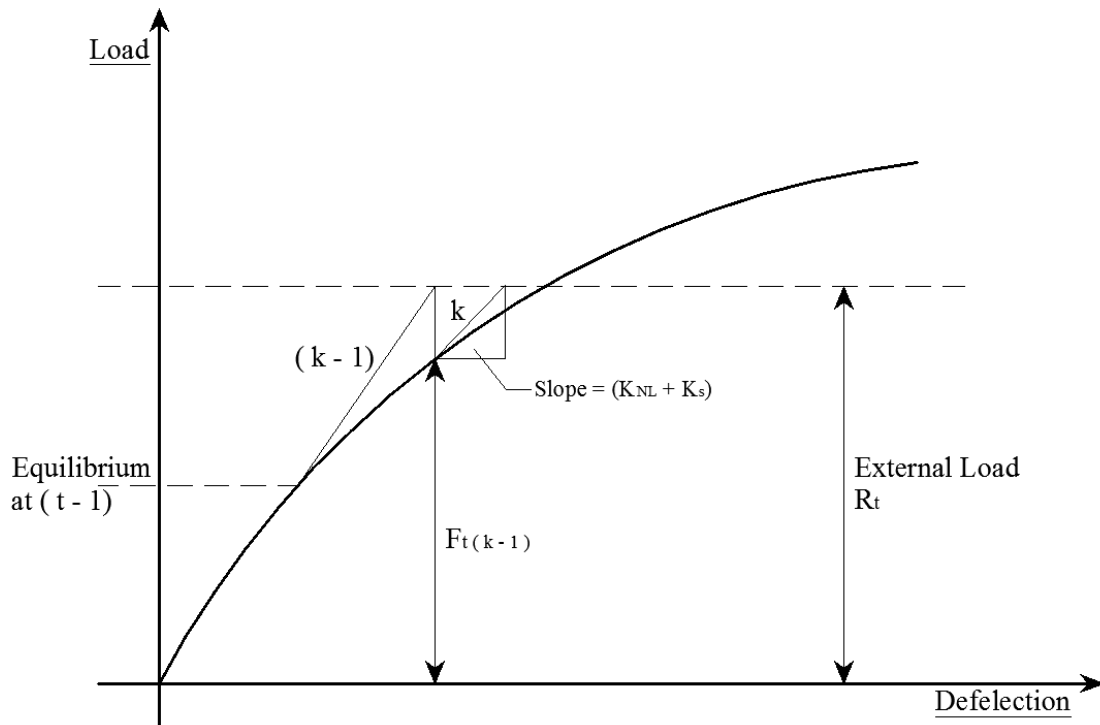


Fig. 3-8 Iterations to Convergence at Load Level R_t , Newton – Raphson Method

the virtual work expression at the k^{th} iteration of load increment t is given by:

$$\int S_{ij}^{t(k)} d(\Delta \epsilon_{ij}^{t(k)}) dV^O = Rt \quad \text{Eq. 3-28}$$

$$S_{ij}^{t(k)} = S_{ij}^{t(k-1)} + \Delta S_{ij} \quad \text{Eq. 3-29}$$

Where $S_{ij}^{t(k-1)}$ is known, and ΔS_{ij} is unknown

Using Green Lagrangian strain tensor Cook (2002) and Bathe (1996)

$$\epsilon_{ij} = \frac{1}{2} \left(\frac{\partial u_j}{\partial x_i} + \frac{\partial u_i}{\partial x_j} + \frac{\partial u_m}{\partial x_i} \frac{\partial u_m}{\partial x_j} \right) \quad \text{Eq. 3-30}$$

Using equations Eq. (3-27) and (3-30)

$$\epsilon_{ij}^{t(k)} = \frac{1}{2} \left[\begin{array}{l} \left(u_{i,j}^{t(k-1)} + \Delta u_{i,j} \right) + \left(u_{j,i}^{t(k-1)} + \Delta u_{j,i} \right) \\ + \left(u_{p,i}^{t(k-1)} + \Delta u_{p,i} \right) \left(u_{p,j}^{t(k-1)} + \Delta u_{p,j} \right) \end{array} \right] \quad \text{Eq. 3-31}$$

Eq. 3-31 can be written as

$$\epsilon_{ij}^{t(k)} = \epsilon_{ij}^{t(k-1)} + \Delta e_{ij} + \Delta \eta_{ij} \quad \text{Eq. 3-32}$$

Where:

$$\Delta e_{ij} = \frac{1}{2} \left(\Delta u_{i,j} + \Delta u_{j,i} + u_{p,i}^{t(k-1)} \Delta u_{p,j} + u_{p,j}^{t(k-1)} \Delta u_{p,i} \right) \quad \text{Eq. 3-33}$$

$$\Delta \eta_{ij} = \frac{1}{2} \Delta u_{p,i} \Delta u_{p,j} \quad \text{Eq. 3-34}$$

Substituting Eqs. 3-29 and 3-32 into Eq. 3-28 to get:

$$\int (Sij^{t(k-1)} + \Delta Sij) (d(\Delta e_{ij}) + d(\Delta \eta_{ij})) dV = Rt \quad \text{Eq. 3-35}$$

Expanding Eq. 3-35 to get:

$$\int (Sij^{t(k-1)}) (d(\Delta e_{ij})) dV + \int (\Delta Sij) (d(\Delta e_{ij})) dV + \int (Sij^{t(k-1)}) (d(\Delta \eta_{ij})) dV + \int (\Delta Sij) (d(\Delta \eta_{ij})) dV = Rt$$

Eq. 3-36

Neglect $\int (\Delta Sij) (d(\Delta \eta_{ij})) dV$ due to its small value

Substituting

$$\Delta Sij = C_{ijrs} \Delta e_{rs} \quad \text{Eq. 3-37}$$

Where C_{ijrs} is the constitutive matrix, which depends on the material behaviour

$$\int (Sij^{t(k-1)}) (d(\Delta e_{ij})) dV + \int (\Delta e_{rs}) C_{ijrs} (d(\Delta e_{ij})) dV + \int (Sij^{t(k-1)}) (d(\Delta \eta_{ij})) dV = Rt$$

Eq. 3-38

Eq. 3-38 is the basic equation to be used in the derivation of the finite element formulation for the cable element based on the total lagrangian approach. Using finite element discretization

$$\Delta u_i = \sum_{n=1}^4 N_n \Delta u_i^n \quad \text{Eq. 3-39}$$

Where N_n are the cubic interpolation functions, Δu_i^n is the incremental degree of freedom in the i^{th} direction (u, v, w) associate with the shape function n.

Substituting Eq. 3-39 into Eq. 3-33

$$\Delta e_{ij} = \frac{1}{2} \left[N_{n,j} \Delta u_i^n + N_{n,i} \Delta u_j^n + u_{p,i}^{t(k-1)} N_{n,j} \Delta u_p^n + u_{p,j}^{t(k-1)} N_{n,i} \Delta u_p^n \right] \quad \text{Eq. 3-40}$$

Since Eq. 3-38 represents a scalar equation and both e_{ij} and Sij are symmetric in i and j , it is to exchange i and j in any terms of Eq. 3-36 without affect the final value of Eq. 3-38. Thus, Δe_{ij} can be written as:

$$\Delta e_{ij} = N_{n,i} \Delta u_j^n + u_{p,j}^{t(k-1)} N_{n,i} \Delta u_p^n$$

$$\Delta e_{ij} = \Delta u_p^n \left[N_{n,i} \delta_{jp} + u_{p,j}^{t(k-1)} N_{n,i} \right]$$

$$\Delta e_{ij} = \Delta u_p^n \left[\delta_{jp} + u_{p,j}^{t(k-1)} \right] N_{n,i}$$

$$\partial(\Delta e_{ij}) = \partial(\Delta u_p^n) \left[\delta_{jp} + u_{p,j}^{t(k-1)} \right] N_{n,i} \quad \text{Eq. 3-41}$$

And

$$\Delta e_{rs} = \Delta u_p^n \left[\delta_{sp} + u_{p,s}^{t(k-1)} \right] N_{n,r} \quad \text{Eq. 3-42}$$

Change the dummy variable from p to q :

$$\Delta e_{rs} = \Delta u_q^n \left[\delta_{sq} + u_{q,s}^{t(k-1)} \right] N_{n,r} \quad \text{Eq. 3-43}$$

Substituting Eq. 3-41 and Eq. 3-43 into Eq. 3-38

$$\begin{aligned} & \int \left(\left[\delta_{sq} + u_{q,s}^{t(k-1)} \right] N_{n,r} \right) C_{ijrs} \left(\left[\delta_{jp} + u_{p,j}^{t(k-1)} \right] N_{n,i} \right) \Delta u_p^n \partial(\Delta u_p^n) dV + \int (Sij^{t(k-1)}) (d(\Delta \eta_{ij})) dV \\ & = Rt - \int (Sij^{t(k-1)}) \left(\left[\delta_{jp} + u_{p,j}^{t(k-1)} \right] N_{n,i} \right) \partial(\Delta u_p^n) dV \end{aligned}$$

$$\text{Eq. 3-44}$$

Eq. 3-44 leads to the following equations written in matrix form:

$$\left[[K_{NL}]^{t(k-1)} + [K_s]^{t(k-1)} \right] \{\Delta u\} = \{R\}^t - \{F\}^{t(k-1)} \quad \text{Eq. 3-45}$$

Where:

Nonlinear stiffness matrix $[K_{NL}]_{12 \times 12}^{t(k-1)}$ can be obtained as follow

$$[K_{NL}]_{12 \times 12}^{t(k-1)} = \int [B_{NL}^{t(k-1)}]_{12 \times 1}^T [D] [B_{NL}^{t(k-1)}]_{1 \times 12} dV$$

and the numerical integration can be used through the following equation

$$[K_{NL}]_{12 \times 12}^{t(k-1)} = \int_{-1}^1 [B_{NL}^{t(k-1)}]_{12 \times 1}^T E [B_{NL}^{t(k-1)}]_{1 \times 12} A^r \sqrt{\left[\frac{dx^r}{d\zeta} \right]^2 + \left[\frac{dy^r}{d\zeta} \right]^2 + \left[\frac{dz^r}{d\zeta} \right]^2} d\zeta \quad \text{Eq. 3-46}$$

Where

$$[B_{NL}^{t(k-1)}]_{1 \times 12} = [B^r] + \left[\varepsilon_{\xi}^r [B^r] \right]$$

Stress stiffness matrix $[K_s]_{12 \times 12}^{t(k-1)}$, which contain the effect of tension stiffening and the initial pretension stress, can be obtained as follow

$$[K_s]_{12 \times 12}^{t(k-1)} = \int [S^{t(k-1)}] [N_{n,i} N_{n,j}]_{12 \times 12} dV$$

and the numerical integration can be used through the following equation

$$[K_s]_{12 \times 12}^{t(k-1)} = \int_{-1}^1 \sigma_{\xi}^r [N_{n,i} N_{n,j}]_{12 \times 12} A^r \sqrt{\left[\frac{dx^r}{d\zeta} \right]^2 + \left[\frac{dy^r}{d\zeta} \right]^2 + \left[\frac{dz^r}{d\zeta} \right]^2} d\zeta \quad \text{Eq. 3-47}$$

The unbalanced load vector $\{R\}^t - \{F\}^{t(k-1)}$, as shown in Fig. 3-8, contains of the external forces load vector $\{R\}^t$ and the internal forces $\{F\}^{t(k-1)}$. The internal forces load vector is calculated in each iteration using the following equation:

$$\{F\}_{12 \times 1}^{t(k-1)} = \int [B_{NL}^{t(k-1)}]_{12 \times 1}^T [S^{t(k-1)}] dV$$

and the numerical integration can be used through the following equation

$$\{F\}_{12 \times 1}^{t(k-1)} = \int_{-1}^1 [B_{NL}^{t(k-1)}]_{1 \times 12} \sigma_{\xi}^r A^r \sqrt{\left[\frac{dx^r}{d\zeta}\right]^2 + \left[\frac{dy^r}{d\zeta}\right]^2 + \left[\frac{dz^r}{d\zeta}\right]^2} d\zeta \quad \text{Eq. 3-48}$$

CHAPTER 4

BEHAVIOUR OF TRANSMISSION LINE CONDUCTORS UNDER TORNADO WIND LOADS

4.1 Introduction

Tornadoes are high intensity wind (HIW) events that produce strong and damaging wind forces in various directions. Those events are localized and have a narrow width. Most structures are not designed to resist tornado loads since the probability of being exposed to a tornado is quite small. This is not the case of long span structures like transmission lines that extend for kilometers. When a tornado occurs at a transmission line location, the probability that it hits one of the towers is quite high. The failure of one tower can trigger a cascade failure because of the unbalanced loads resulting from the conductors' tension. Dempsey and White (1996) reported that 80% of all weather related transmission line failures worldwide are due to HIW events. Despite this fact, very little information about tornado loads is available in transmission line codes of practice and guidelines. The limited information available in some codes ASCE (2010) and CIGRE` (2009) states that the tornado forces acting on the conductors can be neglected. The reason behind that, as stated in those guidelines, is that the prediction of the conductor response to such loads is complicated. As such, the purpose of the current study is to assess the effect of tornado loads acting on conductors on the overall response of transmission towers. The study is conducted numerically using results of computational fluid dynamics (CFD) simulations for the tornado wind field and finite element modelling for the conductors. The CFD simulations were conducted by Hangan and Kim (2008) and validated using field

measurements reported by Sarkar et al. (2005) and Lee and Wurman (2005) for the 1998 Spencer South Dakota F4 tornado and the 1999 Mullhall F4 tornado, respectively. The CFD data was processed by Hamada et al. (2010) to simulate the wind field for F2 tornadoes. The finite element modelling of the conductors is based on the four-noded three dimensional curved cable element that was developed by Koziey (1993) and then extended in Chapter (3) to include the geometric nonlinear effect.

The chapter starts by describing the tornado wind field. It focuses on F2 tornadoes since the majority of tornadoes are within or less than this level, and it is not practical to design structures to resist higher levels of tornadoes (ASCE 2010 and CIGRE` 2009). Real transmission towers are numerically simulated and then analyzed with and without the inclusion of the lines (conductors and ground-wires). The results are used to assess the importance of including the lines in the analysis of transmission lines under tornado loads. The behaviour of the conductors under the most critical tornado configuration is described. Finally, the sensitivity of the conductors' behaviour to the magnitude of loading, the level of initial sag, the insulator string's length, and the lines self-weight is assessed.

4.2 F2 Tornado Wind Field on Tower and Conductors

The current study assess the forces transferred from the lines (line's reactions) to the supporting towers under F2 tornado wind loads. Two main components are essential to conduct the current study: a) the F2 tornado wind field, and b) the modelling of transmission line systems used to assess the effect of the conductors on the overall behaviour. The current section summarizes the tornado wind field and the following

section discusses the nonlinear three dimensional finite element model of the transmission line system. The wind field used in the current study is based on the procedures developed by Hamada et al. (2010) to estimate a velocity field for F2 tornadoes from the computational fluid dynamics (CFD) simulations conducted by Hangan and Kim (2008). The CFD analyses are conducted with smooth surface and the resulting tornado wind field represents the steady state, i.e. does not vary with time. The velocity field $V(r, \theta, z)$ has a three dimensional spatial variation and is given as a function of the cylindrical coordinates r , θ , and z . The tornado velocity field has three velocity components: the radial velocity $V_r(r, \theta, z)$, the tangential velocity $V_t(r, \theta, z)$, and the axial velocity $V_a(r, \theta, z)$. The maximum tangential velocity of F2 tornado is 78 (m/sec) and occurs at a radius $r = 96$ (m) and a height $z = 19$ (m). The maximum radial velocity is 49 m/sec and corresponds to a radius $r = 146$ m and a height $z = 6$ m. The maximum axial velocity is 37 m/sec and corresponds to a radius $r = 171$ m and a height $z = 127$ m.

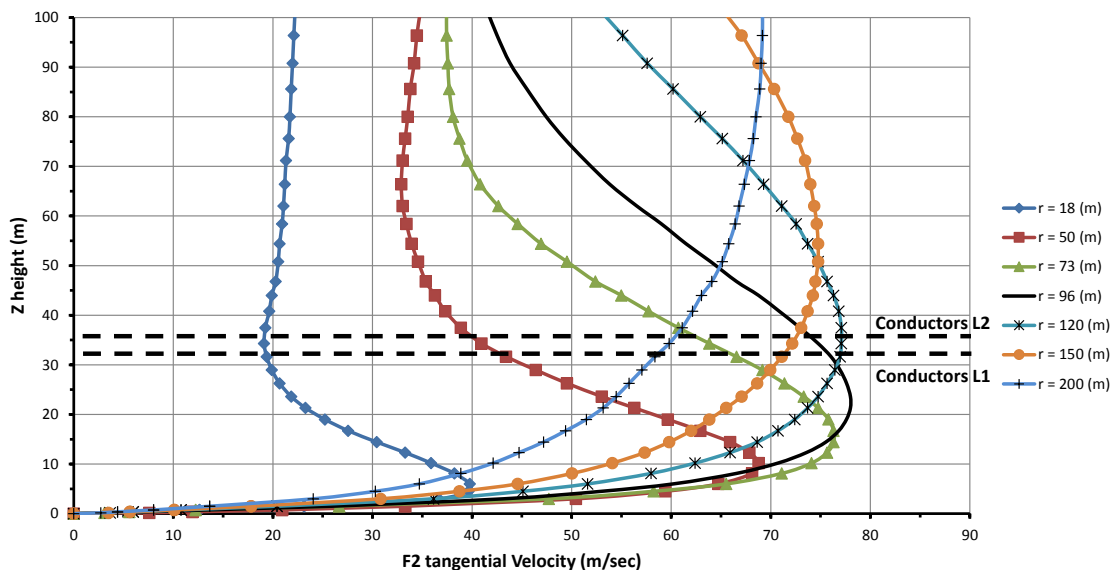


Fig. 4-1 Vertical Profile of Tangential Velocity Component for Different Radial Distances from Tornado Center (F2 Tornado)

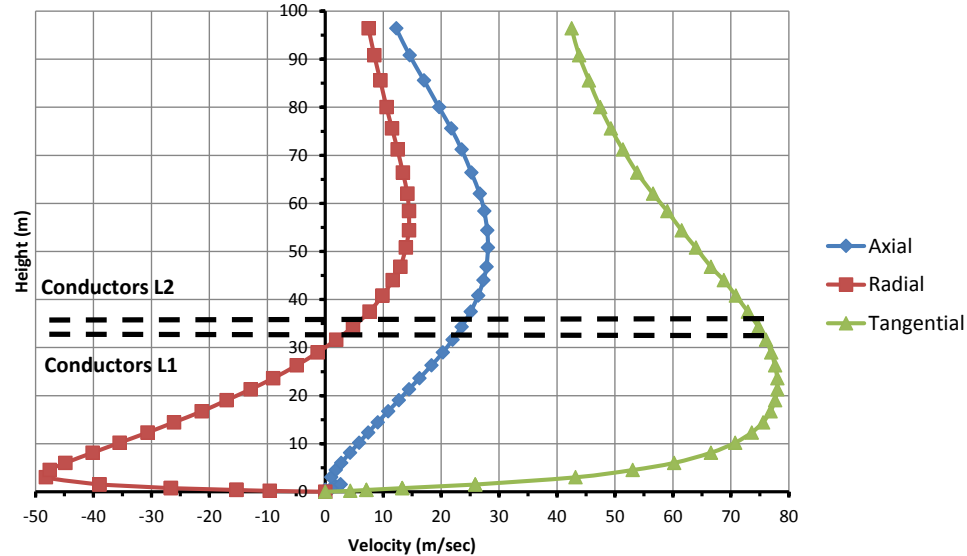


Fig. 4-2 Variation of the Three Velocity Components of F2 Tornado along the Height at Distance 100 (m) from Tornado Center

In order to gain an insight about the F2 tornado wind field, the profile of the tangential velocity component along the height is plotted in Fig. 4-1 for different values of r , where r is the distance from the tornado center. The near ground region, Z less than or equal 100 (m), is the main interest of transmission line design. In addition, the vertical profile of the three velocity components for radii $r = 100$ (m) and $r = 150$ (m) are provided in Fig. 4-2 and 4-3. The dotted lines shown in these figures indicate the location of the transmission lines (conductors) for the two transmission towers considered in the current study. As shown in the figures, the tornado wind profile is significantly different than the conventional boundary layer wind profile. The peak velocities are close to the ground and the velocities change direction with height. The tornado wind profiles in the tangential,

radial, and vertical directions are different for each distance r from the tornado center. The evaluation of the F2 tornado wind forces on the lines is described in detail by Hamada et al. (2010) and Hamada and El Damatty (2011).

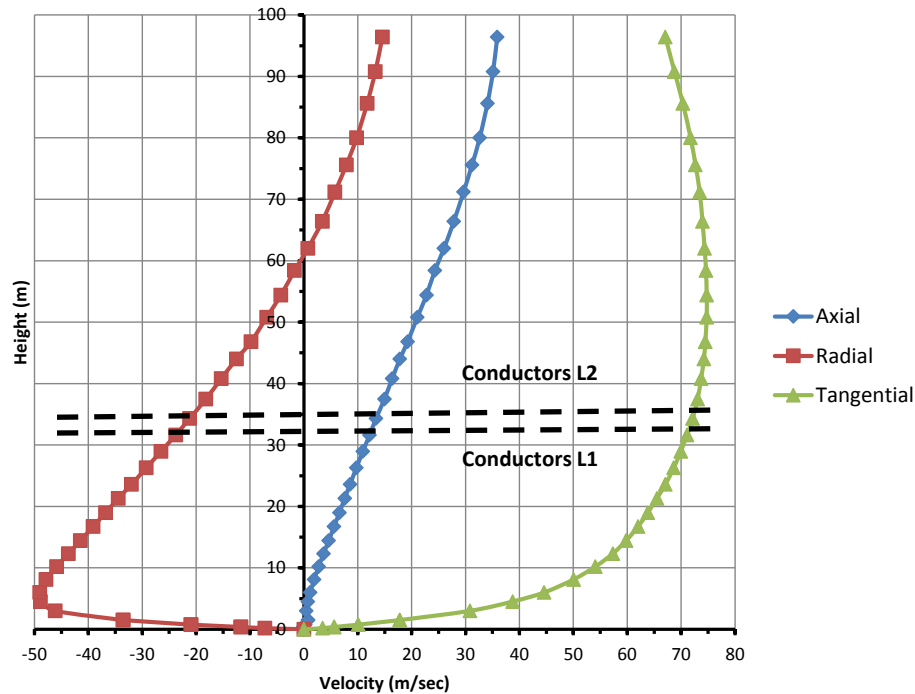


Fig. 4-3 Variation of the Three Velocity Component of F2 Tornado along the Height at Distance 150 (m) from Tornado Center

4.3 Description of Transmission Lines and Finite Element Model

Two different transmission lines are selected to assess the forces transferred from the lines to the supporting towers under F2 tornado wind loads. The first guyed transmission line is labeled as L1 and has a line span of 480 (m). Two conductors and one ground-wire are connected to the supporting guyed towers T1 as shown in Fig. 4-4. The tower height is 44.39 (m) and is supported by four guys attached to the tower guy's cross-arms at an

elevation of 38.23 (m). The geometric and material properties of the conductors and ground-wires are provided in Table 4-1. The second guyed transmission line is labeled as L2 and has a line span of 460 (m). The guyed tower height is 46.57 (m) and is supported by four guys attached to the tower bridge. Three conductors and two ground-wire are connected to tower T2 as shown in Fig. 4-4. The conductors in transmission lines L1 and L2 are connected to the tower cross-arms using a 4.27 (m) insulators. The geometric and material properties of the conductors and ground-wires are provided in Table 4-1.

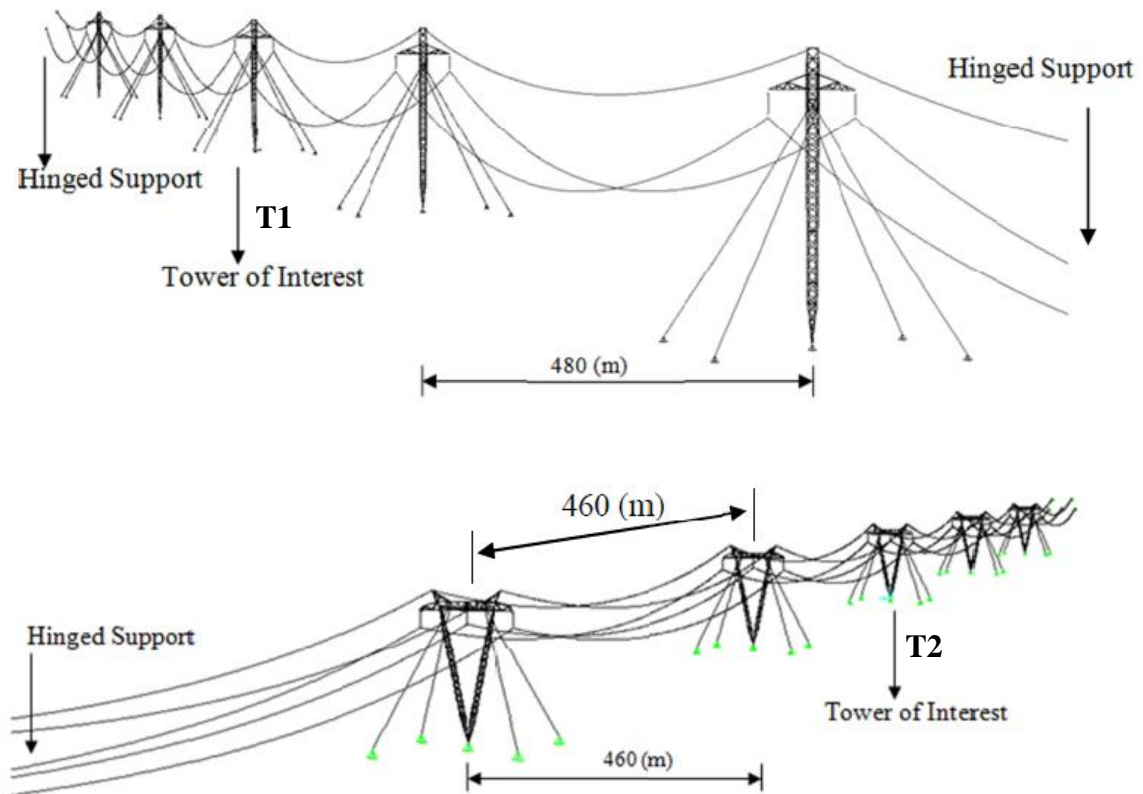


Fig. 4-4 Geometry of the Modelled Guyed Transmission Lines

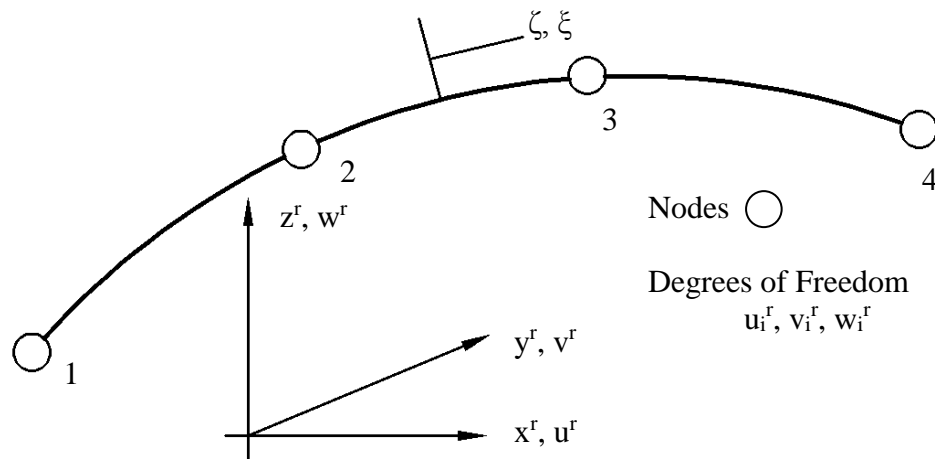


Fig. 4-5 Cable Element Coordinate and Systems and Nodal Degrees of Freedom

The tower of interest refers to the middle tower as shown in Fig. 4-4, where the conductors' forces transferred to the supporting tower are studied. The modelling of the conductors is based on the four-noded cable element developed in Chapter (3) and shown in Fig. 4-5. It follows the same procedures adopted in Chapter (3) where the stiffness of the towers and insulators are simulated using a three dimensional nonlinear spring system. Three spans from each side of the tower of interest are included in the analysis as suggested before by Shehata et al. (2005) and Hamada (2009). The forces in the intermediate spring obtained from the nonlinear analyses are evaluated and then reversed representing the effect of the conductors on the supporting towers when the system is subjected to an F2 tornado. These forces have three components: a) transverse component associated with drag loads, b) longitudinal component related to the nonlinear behaviour of the conductors and resulting from the differential tension between the two span adjacent to the tower, and c) vertical component associated with the lift loads. These forces are referred to as lines' (conductors) reactions in the rest of the study. The tower is analyzed under the combined effects of the conductors' forces and the tornado forces

acting on the main body of the tower. More details about the three dimensional nonlinear finite element model of the two transmission line systems are provided by Hamada et al. (2010) and Hamada and El Damatty (2011).

Table 4-1 Physical Parameters Employed for Conductors and Ground-wires

Parameters	L1 Lines		L2 Lines	
	Conductor	Ground-wire	Conductor	Ground-wire
Name	1843.2 MCM 72/7 Nelson ACSR	9 mm Grade 1300 Steel Skywire	1Kcmil 4x495 0.85" (22x7) ACSR	3/8" Steel (GR180)
Wind Span	m	480	460	460
Diameter	mm	40.64	21.59	9.53
Weight	N/m	28.97	35.83	3.9
Modulus of Elasticity	N/m ²	6.23x10 ¹⁰	5.177x10 ¹⁰	2x10 ¹¹
Sag	m	20	16	16

4.4 Effect of Conductors on the Transmission Towers Behaviour

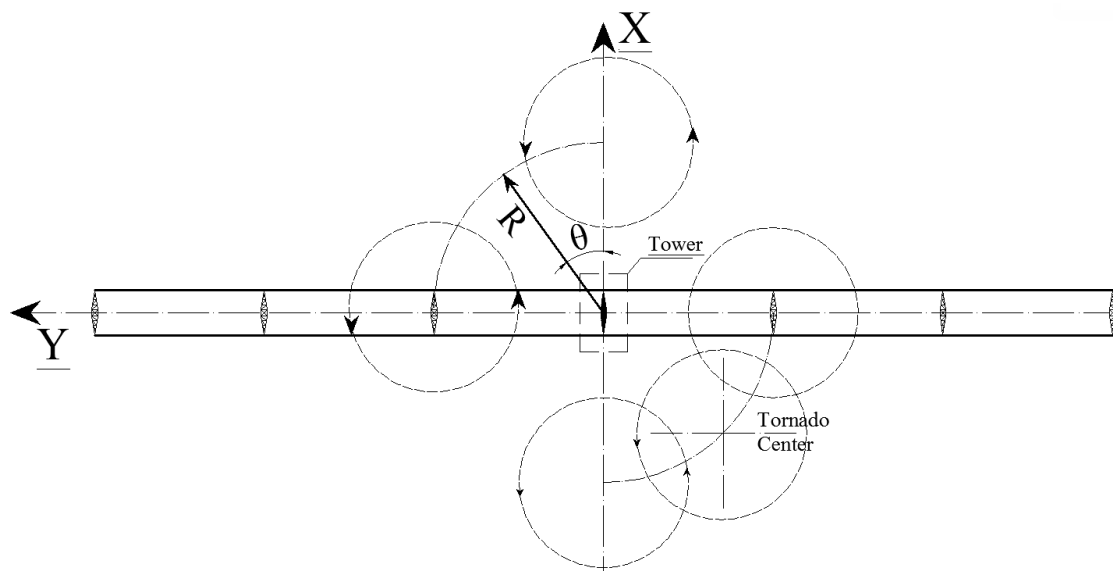


Fig. 4-6 Tornado Parameters (Configurations) R and θ

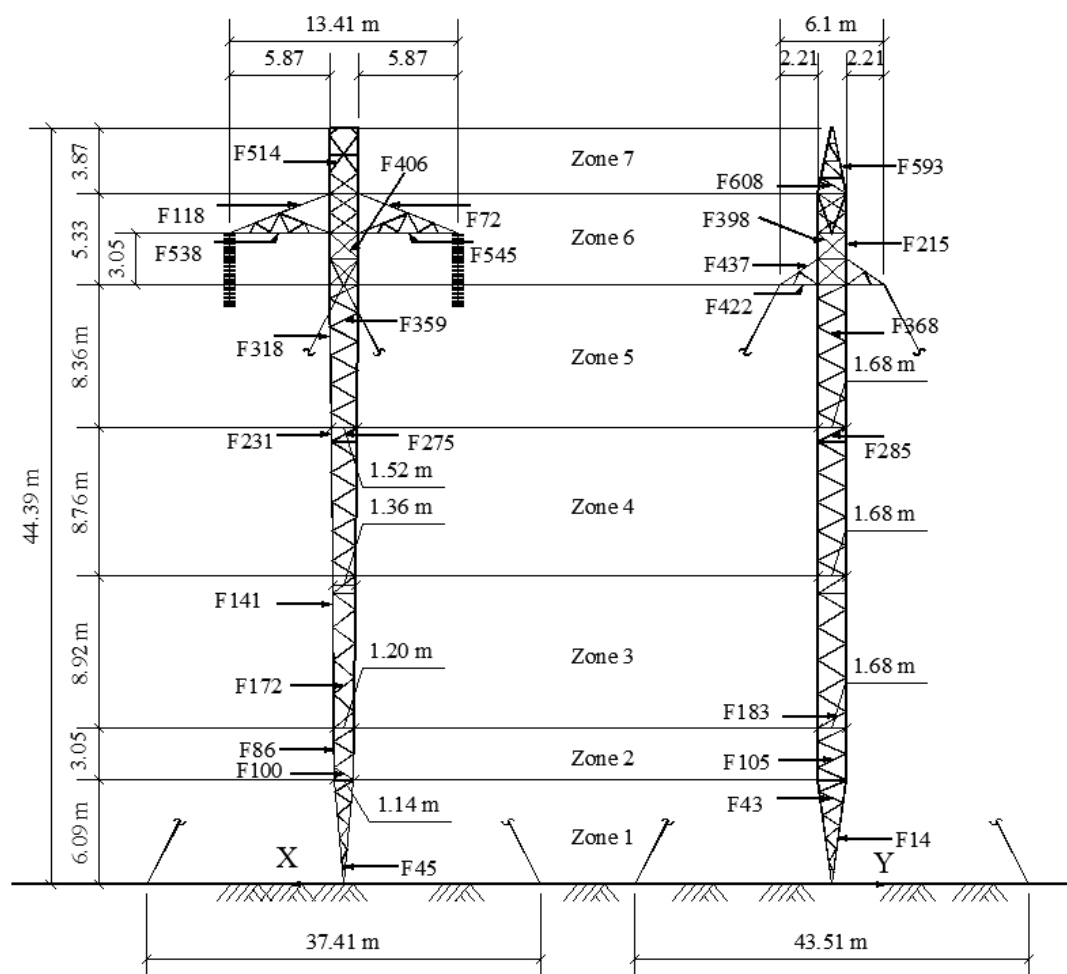


Fig. 4-7 Geometry of Guyed Tower T1 – Transmission Line L1

The importance of considering the conductors and ground-wires in the analysis of transmission line systems under tornado loading is assessed in this section. ASCE (2010) states that tornado loading applied to the lines can be neglected because of the small tornado path widths (150 m in the case of the F2 tornado) and the complexity of the wind force mechanism applied to the lines. Extensive parametric studies are conducted for transmission line systems L1 and L2. For each system, the parametric study is repeated twice; with and without considering the tornado loads acting on the lines (conductors and ground-wire). The difference between the two sets of analyses conducted for each system

represents the effect of the conductor forces. Such a study will assist in assessing the validity of the recommendation made in some codes of practice for neglecting such forces. Similar to the investigation done by Hamada et al. (2010) and Hamada and El Damatty (2011), the parametric study for each transmission line system involves a large number of quasi-static analyses by considering different values for the tornado configurations (R and θ) as shown in Fig. 4-6; R and θ define the tornado location relative to the tower of interest. Combinations of thirteen values for R and sixteen values for θ are considered in each parametric study. The considered values for R are 50, 75, 90, 100, 125, 150, 200, 250, 300, 350, 400, 450, and 500 (m) and for the angles θ are 0, 30, 45, 60, 90, 120, 135, 150, 180, 210, 225, 240, 270, 300, 315, and 330°.

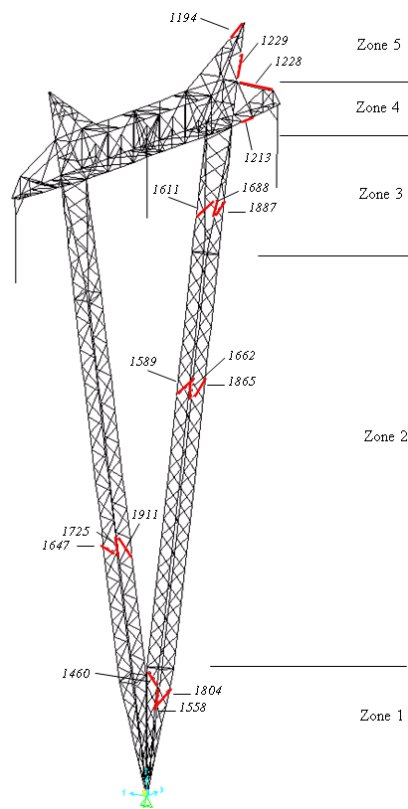


Fig. 4-8 Geometry of Guyed Tower T2 – Transmission Line 2

Table 4-2 Results of the Parametric Study Conducted for Transmission Tower T1

	Member		F2 Tornado				Percentage	
	No.	Type	Parametric Study with Lines (W.L.)		Parametric Study without Lines (WO.L.)		(W.L. - WO.L.)/W.L. %*	
			Axial (kN)	Tornado Configuration	Axial (kN)	Tornado Configuration		
Zone 1	F14	Chord	-144	$R = 125$ $\theta = 330$	-118	$R = 100$ $\theta = 270$	22	
	F43	Diagonal (1)	2	$R = 75$ $\theta = 150$	2	$R = 90$ $\theta = 330$	0	
	F45	Diagonal (2)	-11	$R = 125$ $\theta = 240$	-11	$R = 125$ $\theta = 240$	2	
Zone 3	F141	Chord	-225	$R = 125$ $\theta = 30$	-174	$R = 90$ $\theta = 330$	30	
	F183	Diagonal (1)	-16	$R = 100$ $\theta = 30$	-16	$R = 100$ $\theta = 0.0$	4	
	F172	Diagonal (2)	-5	$R = 90$ $\theta = 60$	-7	$R = 125$ $\theta = 60$	-23	
Zone 5	F318	Chord	-215	$R = 125$ $\theta = 30$	-150	$R = 125$ $\theta = 0.0$	44	
	F368	Diagonal (1)	15	$R = 150$ $\theta = 150$	14	$R = 100$ $\theta = 150$	5	
	F359	Diagonal (2)	-23	$R = 100$ $\theta = 240$	-22	$R = 100$ $\theta = 270$	4	
Tower	F215	Chord	-78	$R = 450$ $\theta = 90$	-33	$R = 125$ $\theta = 180$	140	
	F398	Diagonal (1)	47	$R = 125$ $\theta = 30$	26	$R = 125$ $\theta = 0.0$	81	
	F406	Diagonal (2)	-37	$R = 200$ $\theta = 60$	-13	$R = 125$ $\theta = 90$	198	
Zone 6	Guy	F437	Upper Chord	227	$R = 125$ $\theta = 180$	148	$R = 125$ $\theta = 180$	53
		F422	Lower Chord	-134	$R = 125$ $\theta = 210$	-82	$R = 125$ $\theta = 225$	62
Conductor		F118	Upper Chord	40	$R = 450$ $\theta = 90$	5	$R = 125$ $\theta = 180$	634
		F538	Lower Chord	-47	$R = 450$ $\theta = 90$	-8	$R = 125$ $\theta = 180$	510

* Negative values - peak forces due to exclusion of the lines are higher than with lines

The results of the parametric studies conducted for transmission line systems L1 and L2 are provided in

Table 4-2 and Table 4-3, respectively. Each table reports the peak forces in selected members of both towers that result from the entire parametric study. Those peak forces are given for the case of with and without lines. Different zones at which the internal forces are reported are illustrated in Fig. 4-7 and Fig. 4-8 for towers T1 and T2, respectively. The term diagonal (1) and diagonal (2) used in Table 4-2 and Table 4-3 represent diagonal members located in plans parallel and perpendicular to the lines, respectively. Zone 6 for tower T1 includes the guys and conductors' cross-arms and the internal forces are reported in an upper and a lower chord members for each cross-arm. Similarly, the conductors' cross-arms is located in Zone 4 for tower T2. In addition to the peak internal forces, the tables provide also the tornado configurations corresponding to those peak forces for each of the reported members. By comparing the results reported in Table 4-2 and Table 4-3, the following observations can be concluded:

- The chords' peak internal forces increase by 22% to 140% due to the inclusion of the lines (conductors and ground-wires) in the analysis of transmission towers under tornado wind loads.
- Some diagonal members experience higher internal forces when the conductors and ground-wires are excluded.
- The critical tornado configurations R and θ that lead to peak internal forces in both cases of with and without transmission lines generally coincides. The inclusion of the lines results in variation in the critical configurations for few members.
- The reduction in the cross-arms members' peak internal forces, due to the exclusion of the conductors and the ground-wires, is significant. This is expected,

as the cross-arms and the upper part of the towers (Zone 6 for tower T1 and Zone 4 for Tower T2) are mainly responsible of carrying the lines loads. The critical tornado configurations that lead to the peak internal forces in these two zones when the conductors are included are $R = 125$ and $\theta = 180^\circ$ and $R = 450$ and $\theta = 90^\circ$.

Table 4-3 Results of the Parametric Study Conducted for Transmission Tower T2

Member		F2 Tornado				Percentage		
No.	Type	Parametric Study with Lines (W.L.)		Parametric Study without Lines (WO.L.)		(W.L. - WO.L.)/W.L. %*		
		Axial (kN)	Tornado Configuration	Axial (kN)	Tornado Configuration			
Zone 1	F1558	Chord	-282	$R = 100$ $\theta = 180$	-290	$R = 75$ $\theta = 150$	-3	
	F1460	Diagonal (1)	-9	$R = 100$ $\theta = 180$	-10	$R = 75$ $\theta = 150$	-6	
	F1804	Diagonal (2)	-8	$R = 100$ $\theta = 180$	-3	$R = 150$ $\theta = 150$	138	
Zone 2	F1725	Chord	-545	$R = 90$ $\theta = 330$	-412	$R = 90$ $\theta = 330$	32	
	F1647	Diagonal (1)	-12	$R = 150$ $\theta = 45$	-17	$R = 100$ $\theta = 45$	-28	
	F1911	Diagonal (2)	-18	$R = 150$ $\theta = 330$	-17	$R = 125$ $\theta = 0.0$	5	
	F1662	Chord	-495	$R = 100$ $\theta = 180$	-469	$R = 125$ $\theta = 180$	6	
	F1589	Diagonal (1)	-14	$R = 90$ $\theta = 330$	-16	$R = 150$ $\theta = 330$	-14	
	F1865	Diagonal (2)	12	$R = 100$ $\theta = 225$	19	$R = 75$ $\theta = 225$	-35	
Zone 3	F1688	Chord	-257	$R = 100$ $\theta = 180$	-215	$R = 100$ $\theta = 180$	20	
	F1611	Diagonal (1)	53	$R = 100$ $\theta = 180$	52	$R = 125$ $\theta = 180$	2	
	F1887	Diagonal (2)	7	$R = 125$ $\theta = 180$	11	$R = 100$ $\theta = 150$	-35	
Zone 4	Conductor	F1228	Upper Chord	49	$R = 125$ $\theta = 180$	20	$R = 125$ $\theta = 135$	145
		F1213	Lower Chord	-58	$R = 400$ $\theta = 270$	-25	$R = 125$ $\theta = 0.0$	131
Zone 5		F1229	Upper Chord	47	$R = 100$ $\theta = 30$	59	$R = 125$ $\theta = 0.0$	-21
		F1194	Lower Chord	-81	$R = 125$ $\theta = 180$	-56	$R = 125$ $\theta = 0.0$	45

*% Negative values - Peak forces due to exclusion of the lines are higher than with lines

4.5 Effect of Various Parameters on Conductors' Longitudinal Reaction

Having recognized the importance of including the conductors in the analysis of transmission lines under tornadoes, the study proceeded by conducting a parametric study for the conductor reactions. The study focuses on the longitudinal reaction resulting from the unbalanced loads that might result from a tornado configuration. Such a reaction is not easy to evaluate and requires nonlinear analyses unlike the transverse and vertical reactions, which can be evaluated accurately enough based on tributary area. Also, the parametric study focuses mainly on one tornado configuration ($R=125$ (m) and $\theta = 180^\circ$), which is shown to be critical for many tower members. However, some other angles " θ " are considered in the parametric study for this critical value of R . A schematic showing the location of the tornado relative to the tower of interest for the configuration ($R=125$ (m) and $\theta = 180^\circ$) is shown in Fig. 4-9. The distribution of the transverse and vertical wind field velocity due to this configuration and along a distance of 1500 (m) from both side of the tower are provided in Fig. 4-10 and Fig. 4-11, respectively. Fig. 4-10 shows that the transverse velocity change directions along the opposite sides of the tower. The distribution is shown for values of $\theta = 30, 45, 60, 90, 180^\circ$. The longitudinal reaction result from the difference between the magnitudes of transverse velocities along the opposite spans. As shown in Fig. 4-10, the tornado configurations of $R = 125$ (m) with $\theta = 180^\circ$ leads to the maximum unbalanced load between the two adjacent spans. The vertical profile shown in Fig. 4-11 is almost symmetric, and it acts upward against the weight of the conductors. As shown in the Figure, the vertical velocity can reach up to 40% of the maximum transverse velocity.

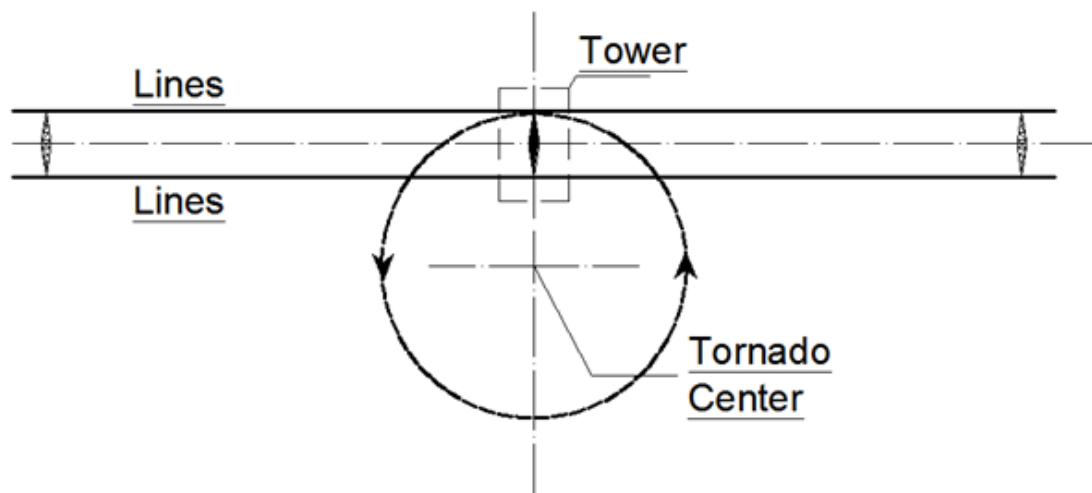


Fig. 4-9 Horizontal Projection of F2 Tornado Located at Relative Distance $R = 125$ (m) and $\theta = 180^\circ$

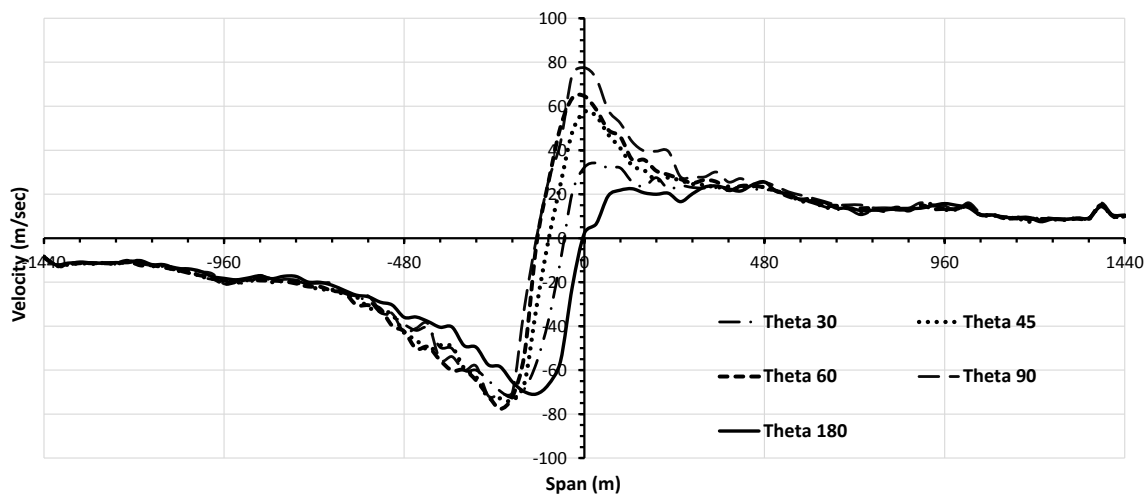


Fig. 4-10 Transverse Velocity Distribution along the Conductors – $R = 125$ (m) and $\theta = 30, 45, 60, 90, 180^\circ$

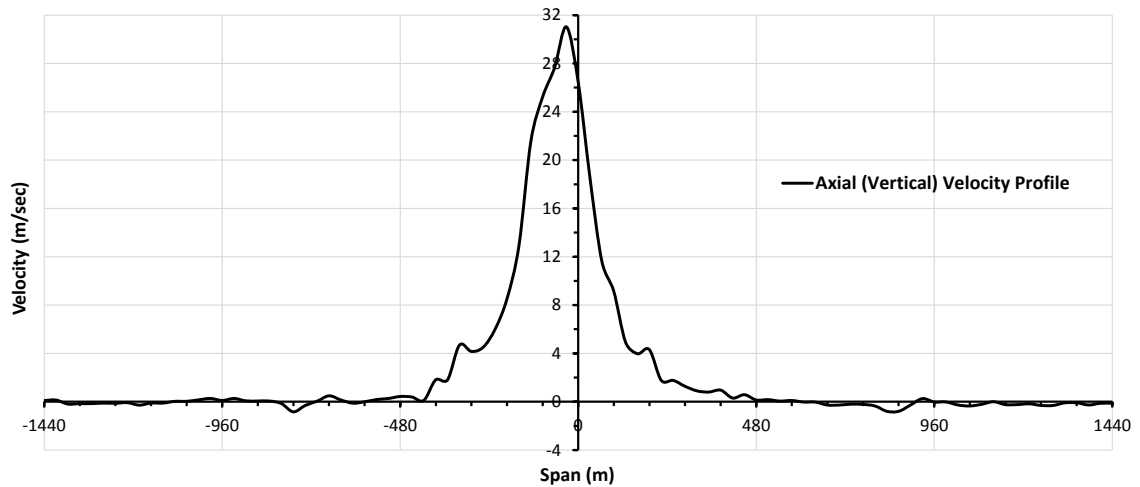


Fig. 4-11 Vertical Velocity Distribution along the Conductors – $R = 125$ (m) and $\theta = 180^\circ$

The deformation of the conductors due to this wind field, as obtained from the finite element analysis, are provided in Fig. 4-12 and Fig. 4-13 for the lines L1 and L2, respectively. In each figure, the projection of the deformed shape are provided in a vertical and horizontal plan reflecting the effects of the vertical and transverse velocities, respectively. For this tornado configuration, the longitudinal reaction obtained from the analysis is comparable to the transverse reaction. Longitudinal reaction of 9,006 (N) and 7,700 (N) are calculated for lines L1 and L2, respectively. The transverse reactions for the same lines are 15,422 (N) and 11,841 (N), respectively. The ratio between the longitudinal and transverse reactions is in the order of 65%.

Various parameters can affect the values of the longitudinal reactions. Those include the magnitude of loading, the pretension force, the insulator length, and the own weight of the conductor. The variation of the longitudinal reactions with those parameters is assessed in the following subsections.

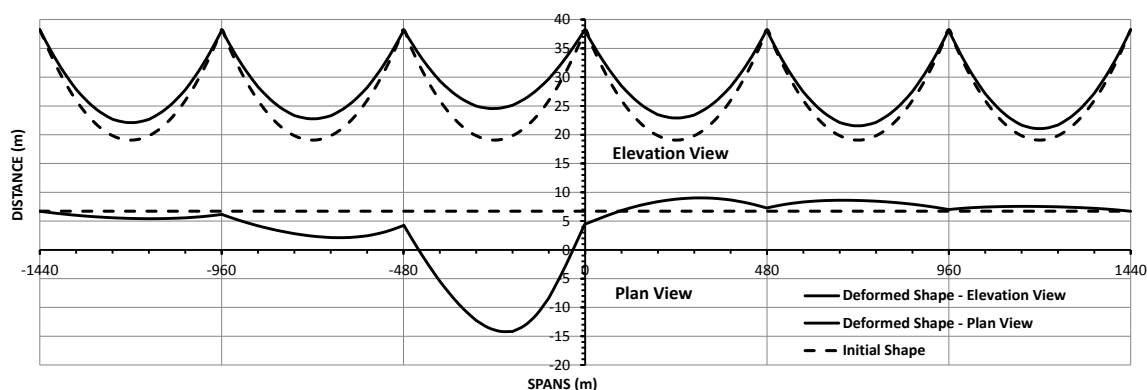


Fig. 4-12 Deformed Shape of Transmission Line L1 due to F2 Tornado
Configurations $R = 125$ (m) and $\theta = 180^\circ$

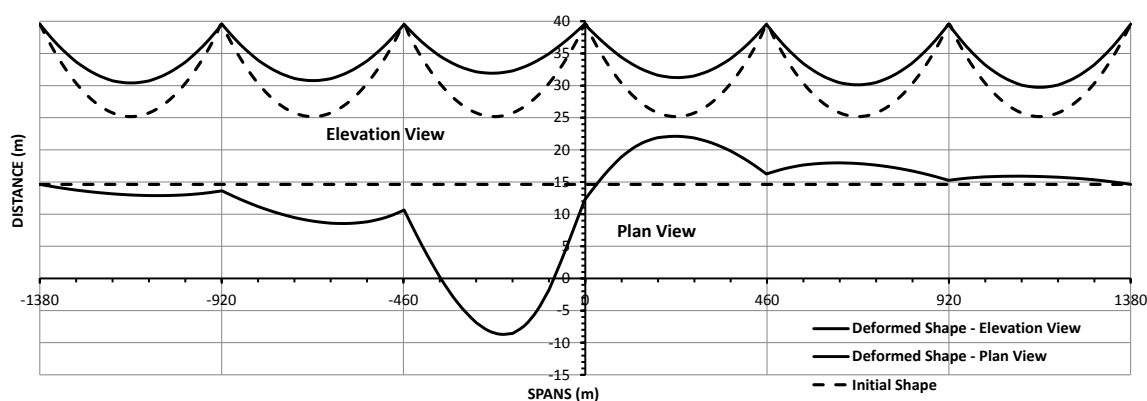


Fig. 4-13 Deformed Shape of Transmission Line L2 due to F2 Tornado
Configurations $R = 125$ (m) and $\theta = 180^\circ$

4.5.1 Effect of Magnitude of Load

The variation of the conductors' longitudinal reactions with the magnitude of F2 tornado loads is investigated in this part. The F2 tornado wind load is applied incrementally in a quasi-static manner using a load increment of 5%. The variation of the longitudinal reactions with the magnitude of F2 tornado loads is plotted for transmission line systems L1 and L2 in Fig. 4-14 and Fig. 4-15, respectively. The figures show the plots for the two

conductors belonging to line L1 and the three conductors belonging to line L2. For each line, the conductors are located at similar height while their locations vary along the transverse direction of the cross-arms as shown in Fig. 4-7 and Fig. 4-8. The variation in the reaction values between different conductors belonging to the same system is due to the difference in their horizontal location relative to the tornado. This difference is small for line L1, where the cross-arm is relatively narrow (13 m width). Meanwhile, a large difference is shown for line L2, where the cross-arm has a width of 29.3 m. All plots show a nonlinear variation of the longitudinal reactions with the magnitude of load, especially at the early stage of loading.

For illustration, the transverse and vertical reactions for the conductors of the two lines are plotted in Fig. 4-16 and Fig. 4-17 versus the magnitude of applied load. As shown in the figures, those reactions exhibit a linear behaviour with variation in magnitudes again due to the difference in the transverse location of the conductors. The 29.3 m distance between the two edge conductors in transmission line system L2 leads to significant change in the F2 tornado forces applied on the conductors. Consequently, a difference in the conductor's reactions of 25% occurs in the longitudinal direction, and 33% occurs in the transverse direction. The results conclude that the horizontal and vertical F2 tornado forces change significantly in space. In addition, this significant change in the lines' reactions leads to an additional torsional moment on the supporting towers and significant additional forces in some of the supporting guys.

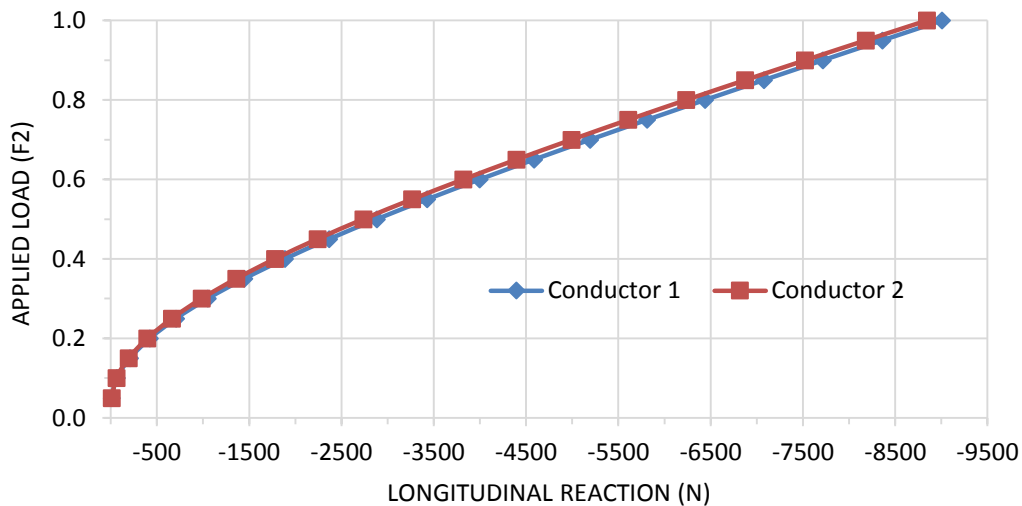


Fig. 4-14 Transmission Line System L1 Longitudinal Reactions due to the Variation of the Applied F2 Tornado Loads

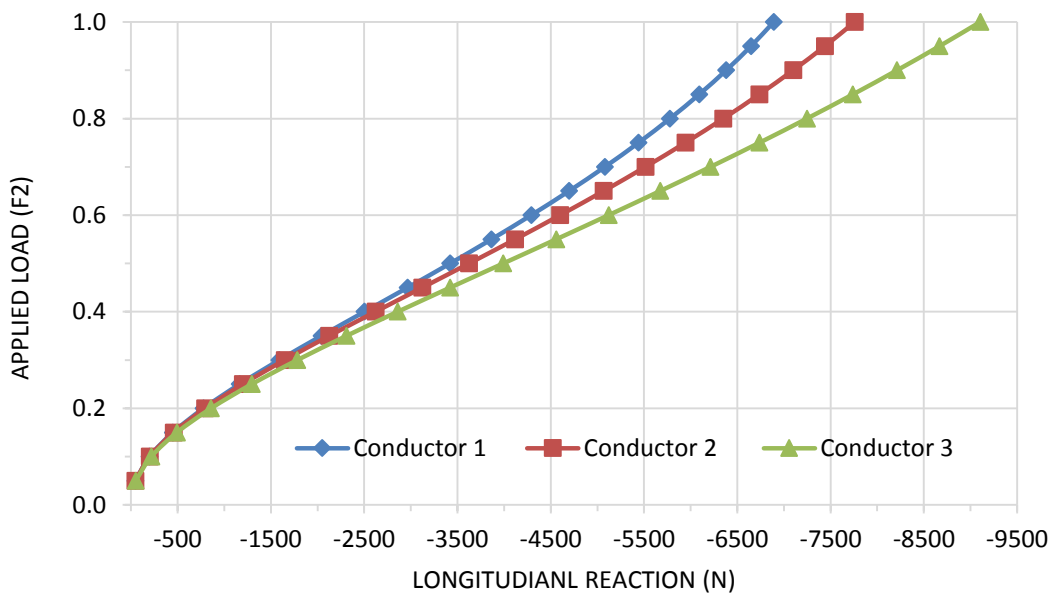


Fig. 4-15 Transmission Line System L2 Longitudinal Reactions due to the Variation of the Applied F2 Tornado Loads

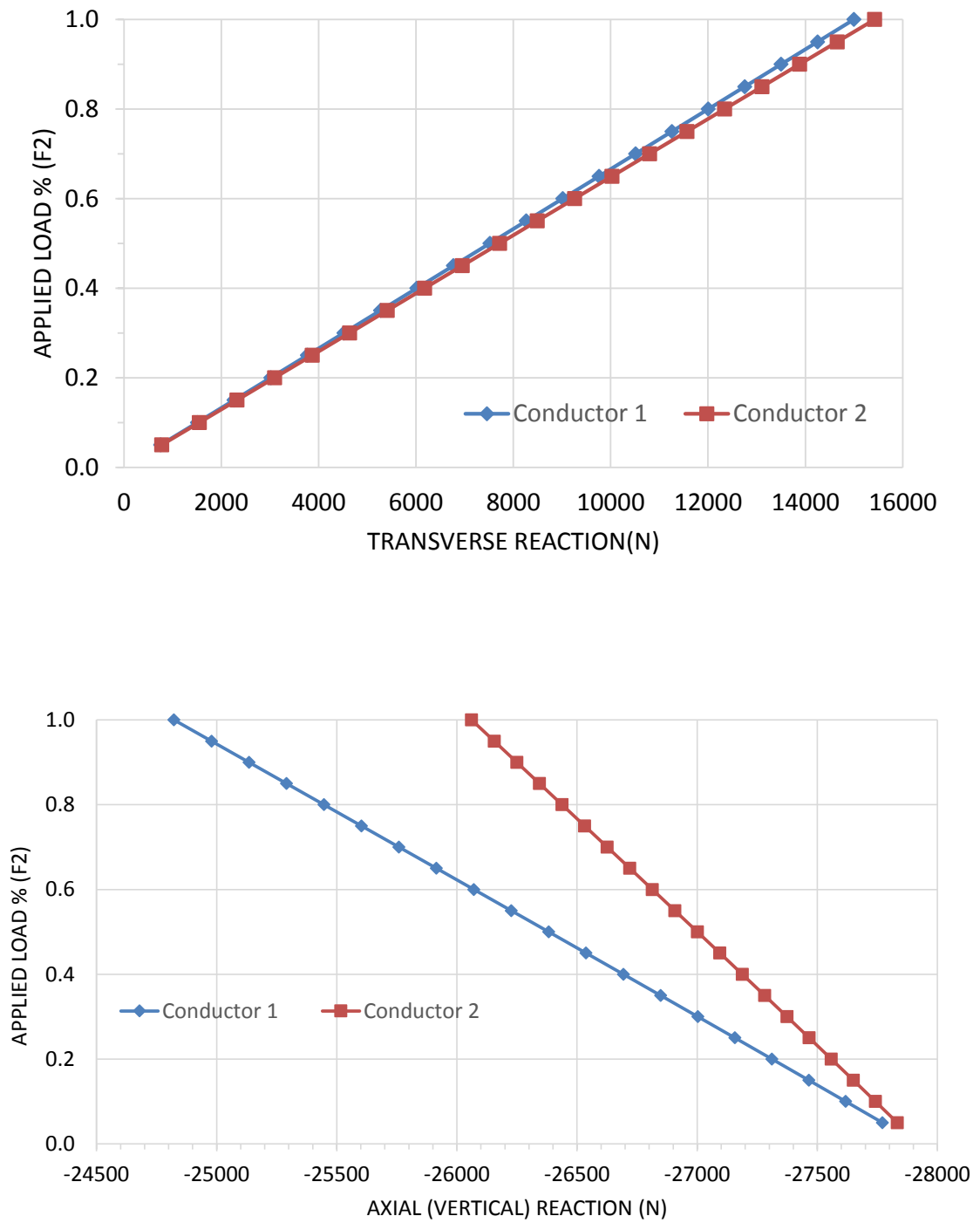


Fig. 4-16 Transmission Line System L1 Transverse and Vertical Reactions due to the Variation of the Applied F2 Tornado Loads

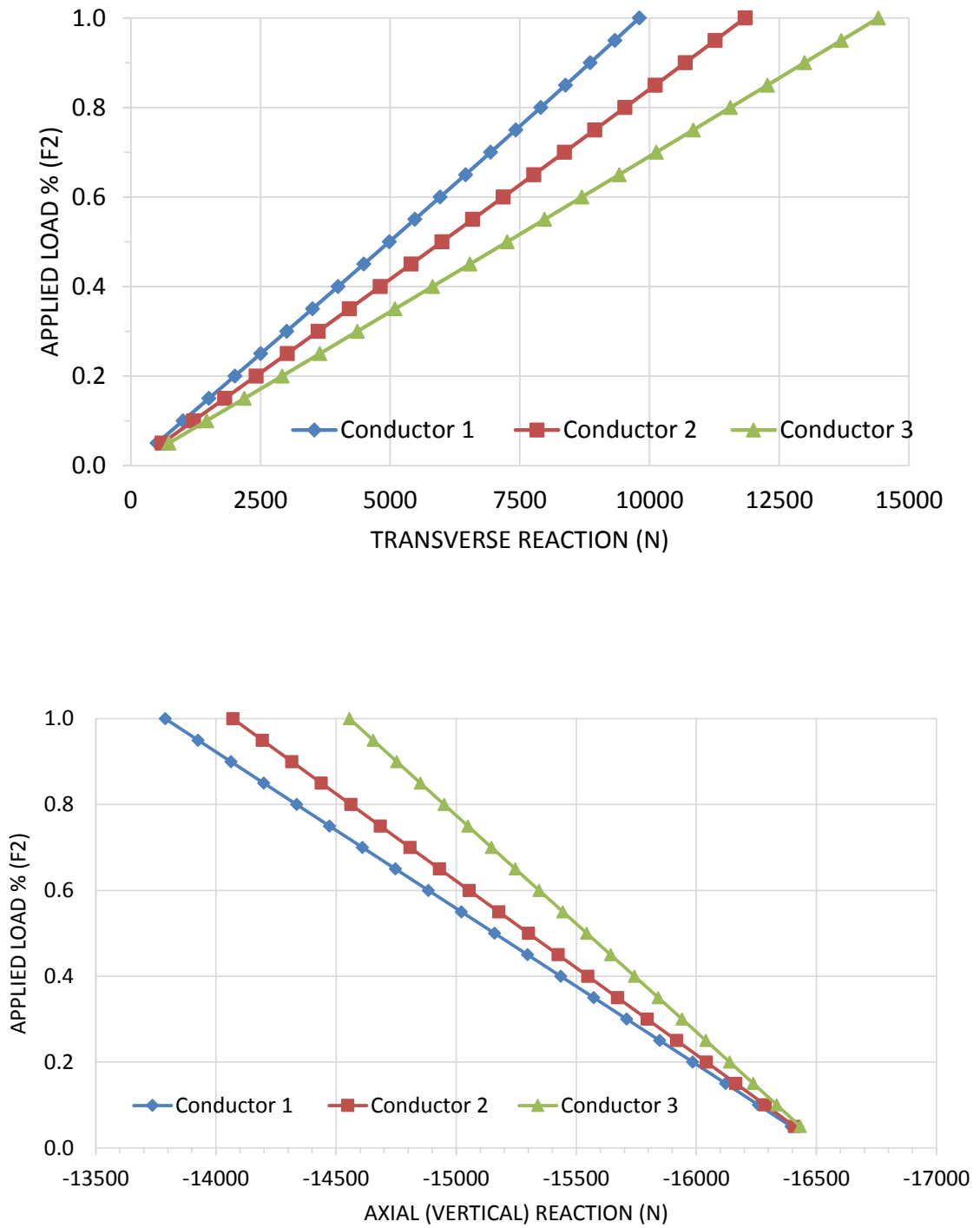


Fig. 4-17 Transmission Line System L2 Transverse and Vertical Reactions due to the Variation of the Applied F2 Tornado Loads

4.5.2 Effect of Conductors' Pretension and Sag

In this part of the parametric study, both the value of the pre-tension force and yaw angle θ are varied, while the tornado location distance R is kept constant at a value of 125 (m). Only one conductor of line L1 is shown in the results presented in the current study, with similar behaviour for all other conductors in this parametric study. The pretension force is varied from 60 (kN) to 200 (kN). Fig. 4-18 to Fig. 4-20 show that the three reaction components vary with angle θ , especially the transverse and longitudinal components. Regarding the effect of pretension force, negligible variation for the transverse and vertical reactions, and significant variation for the longitudinal reactions are exhibited. Fig. 4-20 shows that the maximum value for the longitudinal reaction occurs at $\theta = 180^\circ$. Fig. 4-21 indicates that the longitudinal reaction decreases nonlinearly with the increase of the pretension force.

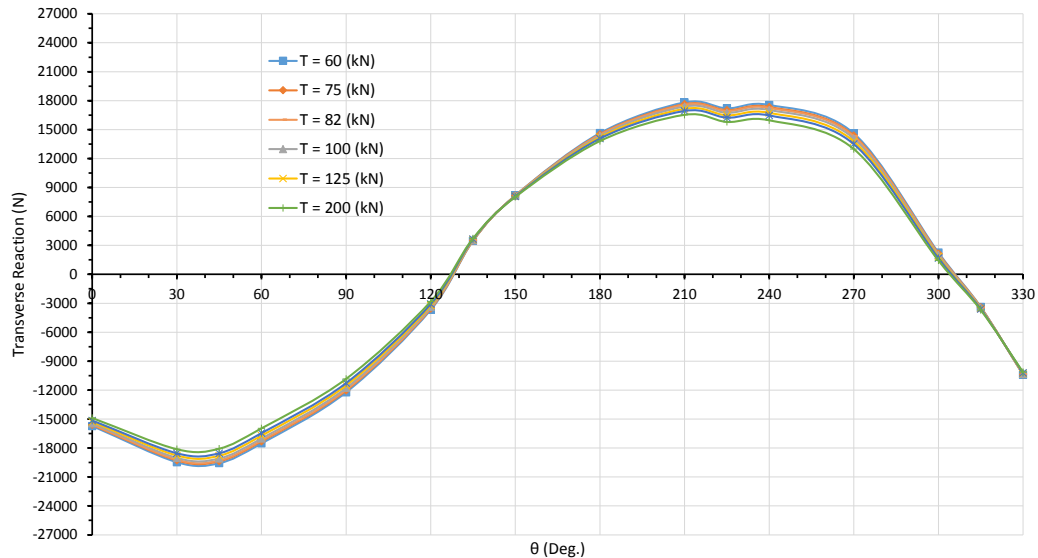


Fig. 4-18 Variation of Transmission Line's Transverse Reaction with Pretension Force and Sag – $R = 125$ (m) (Transmission Line System L1)

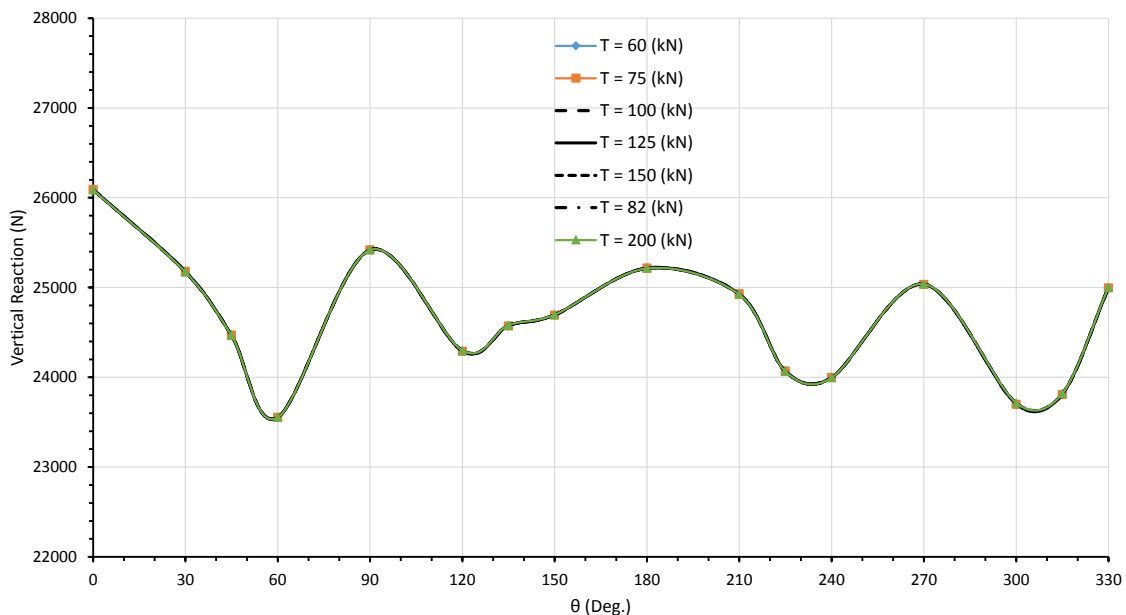


Fig. 4-19 Variation of Transmission Line’s Vertical Reaction with Pretension Force and Sag – $R = 125$ (m) (Transmission Line System L1)

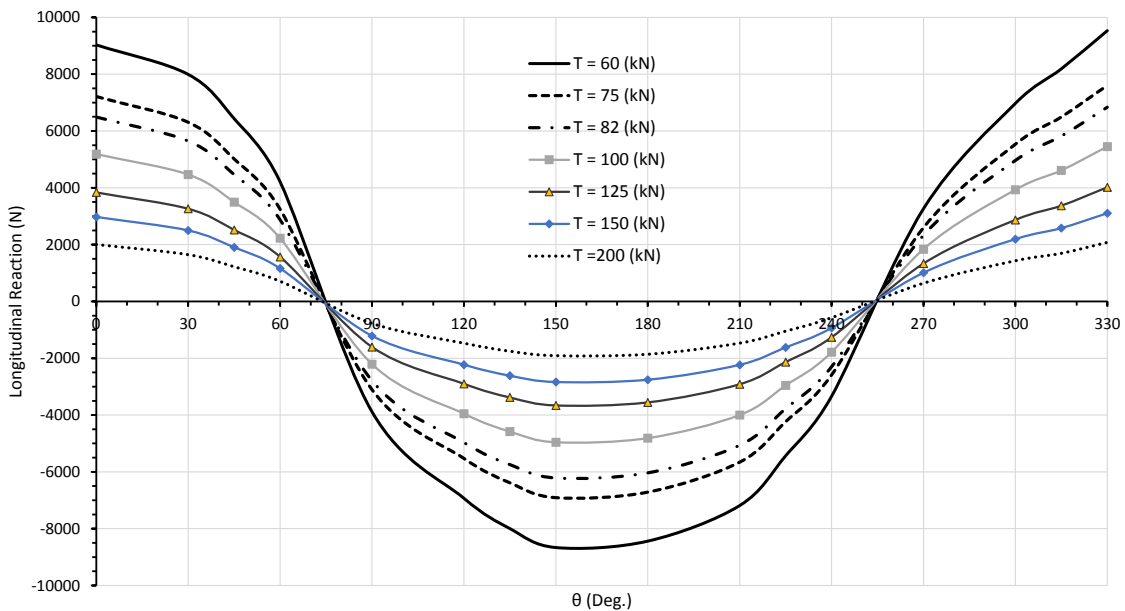


Fig. 4-20 Variation of Transmission Line’s Longitudinal Reaction with Pretension Force and Sag – $R = 125$ (m) (Transmission Line System L1)

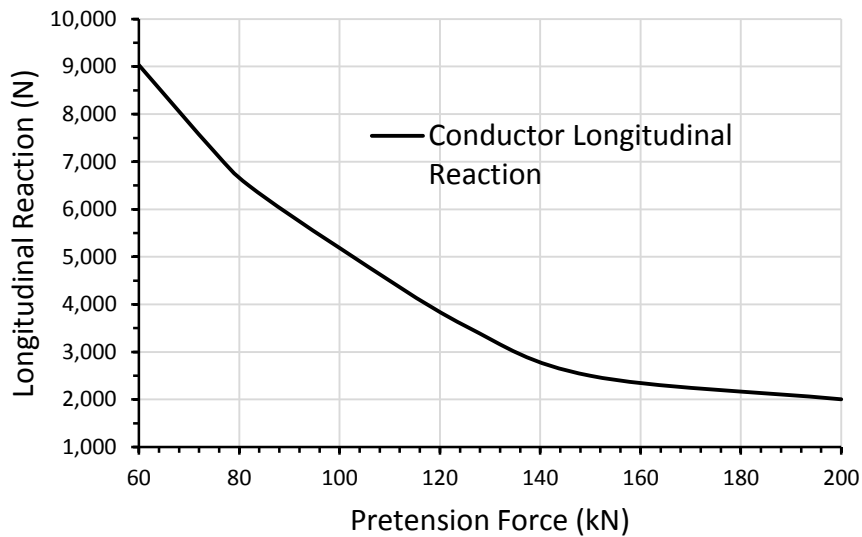


Fig. 4-21 Variation of Longitudinal Reaction with Pretension force

4.5.3 Effect of Insulator Length

Insulators are responsible of transferring the transmission line loads to the supporting towers. Insulators used in the industry can have different lengths. Based on industry recommendations, the range of insulator's length is 1 to 4.27 (m). In order to assess the effect of the insulators length on the longitudinal reaction of transmission lines during a tornado event, the analyses are repeated by varying the insulator length within this range. Both transmission line systems L1 and L2 are considered in this parametric study. The results of this parametric study are provided in Fig. 4-22, which illustrates that the longitudinal reaction changes significantly and in a nonlinear manner with the change of the insulator length. Shorter insulators lead to higher longitudinal reactions. The nonlinear behaviour is due to the nonlinear change of the insulators stiffness with movement as explained in detail in Chapter (3).

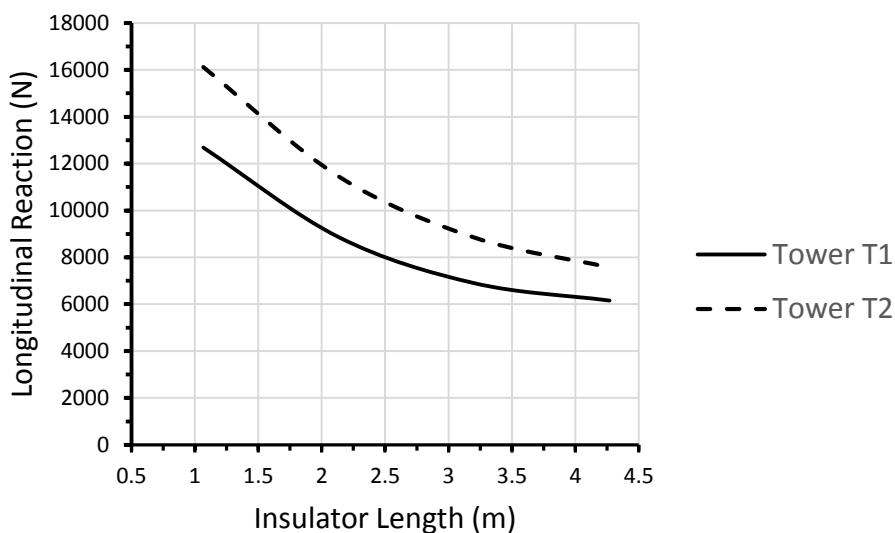


Fig. 4-22 Variation of Longitudinal Reaction with Insulator Lengths

4.5.4 Effect of Conductor Self-Weight

Transmission lines (conductors) are made of different composite materials. The selection of the lines material is based on different factors, such as the span, weather parameters, and method of installation. The self-weight of these lines varies from one hydro company to another and from country to another. Accordingly, the current section investigates the effect of the conductors self-weight on the longitudinal reactions. Both transmission line systems L1 and L2 are considered in this investigation. The results of this parametric study are shown in Fig. 4-23, which indicates that the longitudinal reaction change linearly with the variation of the conductor's self-weight.

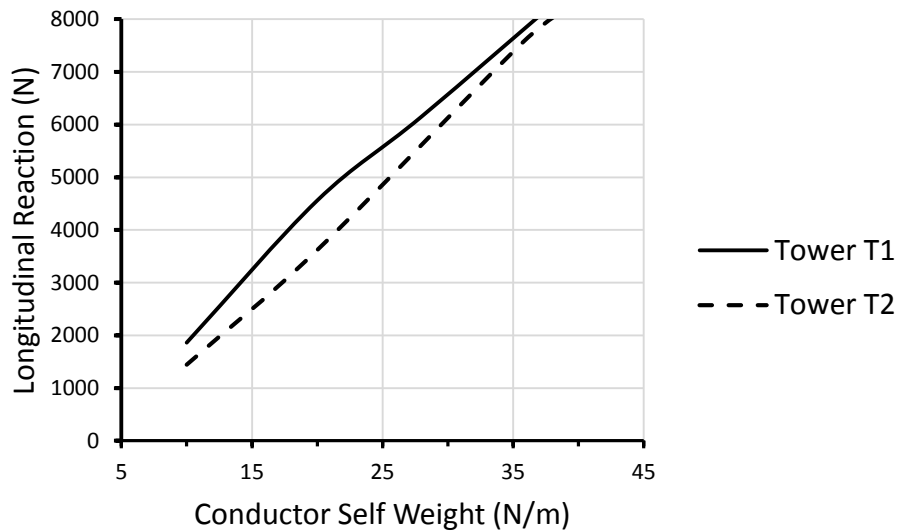


Fig. 4-23 Variation of Longitudinal Reaction with Conductor's self-weight

4.6 Conclusion

The following conclusions can be drawn from the conducted study:

- The F2 tornado force (velocity) distribution on transmission lines, such as conductors and ground-wires, is highly non-uniform and varies nonlinearly. In addition, the applied tornado velocities on transmission lines can change directions within one line span, which leads to a high nonlinear behaviour and a more complex behaviour.
- The vertical (uplift and downdraft) velocity component of F2 tornado is significant and can be up to 40% of the transverse velocity component. Accordingly, nonlinear three dimensional analysis, involving coupling between the transverse and the vertical responses, is recommended for the studying transmission lines under tornado wind loads.

- The study investigates the validity of the recommendation made in some codes of practice to neglect the tornado loads acting on the lines. The results show that chord's peak internal forces increase by 22 to 140 % due to the inclusion of the lines in the analysis under tornado loads.
- The length of transmission tower's cross-arms has a significant effect on the conductor's reactions associated with tornado loads. For the same tower, differences of 25% and 33% in the longitudinal and transverse reactions, respectively, are reported due to a horizontal distance between the two edge conductors of 29 (m). This difference in reactions leads to an additional torsional moment on the supporting towers.
- Significant longitudinal line's reaction leads to compression forces in tower's cross-arms that are not typically considered in the design of those cross-arm's members. Accordingly, the current study investigates the effect of different parameters on the longitudinal reactions of transmission lines. The study shows that the longitudinal reaction:
 - a) has a nonlinear variation with the magnitude of the applied F2 tornado wind loads.
 - b) changes significantly and in a nonlinear manner with both the value of the initial pretension force and sag, and the length of the insulator springs attached to the line.
 - c) varies linearly with the change of the conductor's self-weight

In view of these conclusions, transmission lines' conductors and ground-wires are recommended to be considered in the analysis and design of transmission towers subjected to tornado wind loads.

4.7 Acknowledgement

The authors gratefully acknowledge Hydro One Inc. for the in-kind support, the collaboration, and the financial support provided for this research. The first author is indebted to the Vanier Canada Graduate and the Natural Science and Engineering Research Council of Canada (NSERC) for the financial support provided for this research.

4.8 References

American Society of Civil Engineers (ASCE), 2010. Guidelines for Electrical Transmission Line Structural Loading, third edition. ASCE Manuals and Reports on Engineering Practice, vol. 74. Reston, VA, USA.

CIGRÉ (Conseil International des Grands Réseaux Électriques/ International Council on Large Electrical Systems) (2009). "Overhead line design guidelines for mitigation of severe wind storm damage." Scientific Committee B2 on Overhead Lines, B2. 06.09.

Dempsey, D., and White, H. B. (1996). "Winds wreak havoc on lines." *Transmission & Distribution World*, 48(6), 32 - 42.

El Damatty, A. A., and Hamada, A. (2013). "Behaviour of guyed transmission line structures under tornado wind loads - Case studies." *Electrical Transmission and Substation Structures 2012: Solutions to Building the Grid of Tomorrow*, November 4, 2012 - November 8, American Society of Civil Engineers (ASCE), Columbus, OH, United states, 193-204.

Hamada, A., (2009). *Analysis and behaviour of guyed transmission line structure under tornado wind loading*. School of Graduate and Postdoctoral Studies, University of Western Ontario, London, Ontario, Canada.

Hamada, A., Damatty, A. A. E., Hangan, H., and Shehata, A. Y. (2010). "Finite element modelling of transmission line structures under tornado wind loading." *Wind and Structures, an International Journal*, 13(5), 451-469.

Hamada, A., and El Damatty, A. A. (2011). "Behaviour of guyed transmission line structures under tornado wind loading." *Computers and Structures*, 89(11-12), 986-1003.

Hangan, H., and Kim, J. -. (2008). "Swirl ratio effects on tornado vortices in relation to the Fujita scale." *Wind and Structures*, 11(4), 291-302.

Koziey, B. L. (1993). "Formulation and applications of consistent shell and beam elements". Ph.D. McMaster University (Canada), Canada.

Sarkar, P., Haan, F., Gallus, Jr., W., Le, K. and Wurman, J. (2005). "Velocity measurements in a laboratory tornado simulator and their comparison with numerical and full-scale data." *37th Joint Meeting Panel on Wind and Seismic Effects*.

Shehata, A. Y., El Damatty, A. A., and Savory, E. (2005). "Finite element modeling of transmission line under downburst wind loading." *Finite Elements Anal.Des.*, 42(1), 71-89.

Wen-Chau Lee, and Wurman, J. (2005). "Diagnosed three-dimensional axisymmetric structure of the Mulhall tornado on 3 May 1999." *J.Atmos.Sci.*, 62(7), 2373-93.

CHAPTER 5

FAILURE ANALYSIS OF GUYED TRANSMISSION LINES DURING F2 TORNADO EVENT

5.1 Introduction

Electricity plays a vital and essential role in our daily lives. Almost all businesses and activities depend on having a reliable continuous source of electricity. Transmission lines are responsible for delivering electricity by carrying it from the source of production to the distribution systems. Failure of transmission lines can have devastating social and economical consequences, so it is imperative to understand how failure occurs, and how to prevent it. As stated by Dempsey and White (1996), more than 80% of weather-related transmission line failures world-wide are found to be attributed to high intensity wind (HIW) events in the form of downbursts, and tornadoes.

In Canada, tornadoes occur in almost all the southern regions of the country, such as in southern Alberta, Manitoba, Saskatchewan, Ontario, and Quebec. Ishac and White (1994) reported that of all the populated areas in Canada, southwestern Ontario experiences the highest rate of tornado incidences; about two tornadoes per 10,000 (km²) every year, and most of the transmission line failures in this area are caused by tornadoes. 92% of these tornadoes were F2 or less on the Fujita scale. Newark (1984) concluded that, on average, a F3 tornado occurs in southwestern Ontario every five years. Despite these facts, the codes of practice, design guidelines, and utility companies' design methodologies are based on the loads resulting from large-scale synoptic events with conventional boundary

layer wind profiles. Conventional wind profiles are characterized by a monotonic increase in velocity with height, which is different than wind profiles attributed to tornadoes where the maximum wind speed occurs near the ground (Kareem 2010). In addition, tornadoes are localized events with relatively narrow path widths. Also, a significant vertical wind component (uplift) exists in the tornado wind profile, which does not exist for synoptic winds.

Although it has been well reported that high intensity wind (HIW) events are responsible for most weather-related transmission line failures, very few studies were done to assess these failures. Shehata and El Damatty (2008) assessed the failure of one of the transmission towers that collapsed in 1996 during a microburst event in Winnipeg, Canada. Their developed in-house numerical model was able to predict failure modes and progression of failure compatible with the post event field observations. The study predicted three possible failure scenarios and the progression of failure of each case was described in details. Savory et al. (2001) conducted a research study on a self-supported transmission tower under both microburst and tornado wind loadings. The study investigated the tower behaviour and failure modes under specific microburst and tornado parameters. The loading on the conductors and ground-wires was not considered in this study. In addition, only the effects of radial velocity component of the microburst and tangential velocity component of the tornado were considered on the transmission tower. The predicted failure mode showed that the horizontal shear force was the main reason for the collapse of the tower. In addition, no significant dynamic effect was found due to the translational movement of the tornado. Ladubec et al. (2012) studied the effect of secondary moment (P-delta) on the response of transmission towers under a downburst

wind field. The analysis used nonlinear space frame elements to simulate the tower members. The study showed an increase of 20% compared to the linear analysis in the peak axial forces in the tower main legs' chord members. The study is considered an improvement to the linear analysis of transmission towers that was performed by Shehata and El Damatty (2008).

Hamada et al. (2010) and Hamada and El Damatty (2011) developed numerical models to investigate the behaviour of transmission line structures under different tornado wind fields. One of the challenges in assessing the behaviour of transmission lines under tornado loads is that the peak forces vary with the location of the center of the tornado relative to the center of the tower of interest, which is defined by the angle of attack as well as the relative distance between the tornado and the structure. Accordingly, the investigations conducted by Hamada et al. (2010) and Hamada and El Damatty (2011) involved large parametric studies by varying those two geometric parameters in order to determine the critical tornado locations leading to peak internal forces in various members of the towers. In the current study, the numerical model is extended in order to predict the tornado velocities at which failure might initiate and to describe the progress of collapse under this type of loading. Two guyed transmission line systems are considered in this chapter as case studies. Using the developed numerical model, failure studies are conducted for each system. For each system, the failure studies included two critical tornado configurations, selected in view of the parametric studies conducted by Hamada et al. (2010) and Hamada and El Damatty (2011). In addition, each failure study case was repeated twice using different two material models describing the post yield behaviour of tensions members. The objectives of this study are to gain an insight about

the resilience of lattice transmission towers against failures when experiencing an F2 tornado, to describe the failure modes under such events, to assess the effect of different assumptions regarding post yield tension behaviour, and to quantify the effect of inclusion of geometric nonlinearities in this type of analysis.

5.2 F2 Tornado Wind Fields

A computational fluid dynamics (CFD) model for a small-scale tornado model was developed by Hangan and Kim (2008). Firstly, the CFD analysis was conducted using a swirl ratio S of 0.28, where S is the ratio between the tangential and radial velocities at the inlet boundary. The wind field produced by this CFD analysis was compared to the experimental data presented by Baker (1981), which was produced using a Ward-type vortex chamber. These experimental results were used to validate the CFD model. The numerical model was then extended for values of $S = 0.1, 0.4, 0.7, 0.8, 1.0,$ and 2.0 . By comparing the numerical results to field measurements, Hangan and Kim (2008) found a good agreement between the CFD predicted field with swirl ratio $S = 2.0$ and the F4 tornado field measurements provided by Sarkar et al. (2005). Hamada et al. (2010) concluded that a swirl ratio $S = 1.0$ provides a good simulation for the F2 tornado wind field. The F4 and F2 tornado velocity wind profiles produced using the CFD simulations vary in space in a three dimensional manner, and are presented as functions of the cylindrical coordinates' $r, \theta,$ and z measured from the tornado center. The wind fields represent steady-state conditions for the tornadoes and, therefore, do not vary with time. The tornado wind field has three velocity components; the tangential velocity component $V_{\theta}(r,\theta,z)$, the radial velocity component $V_{r}(r,\theta,z)$, and the axial (vertical) velocity

component $V_{ma}(r, \theta, z)$. More details regarding the F4 and F2 tornado wind fields are provided by Hamada et al. (2010) and Hangan and Kim (2008).

5.3 Description of the Two Considered Guyed Transmission Line Systems

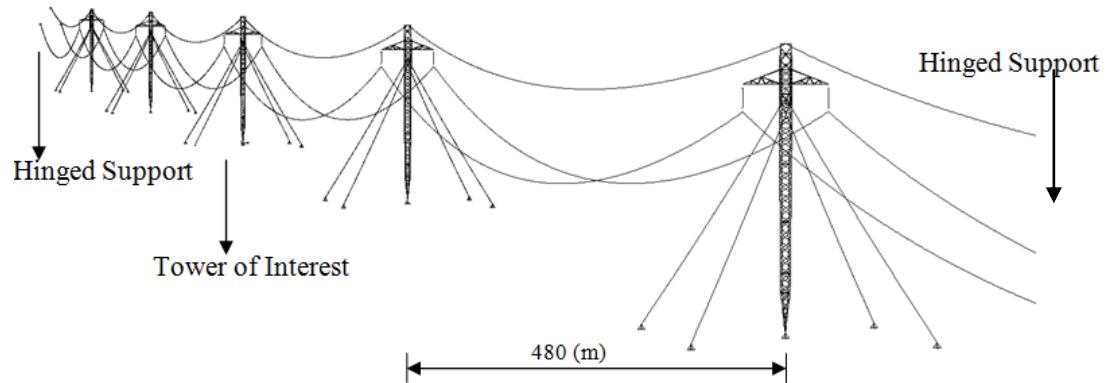


Fig. 5-1 Transmission line system (L1) – Tower Type (T1)

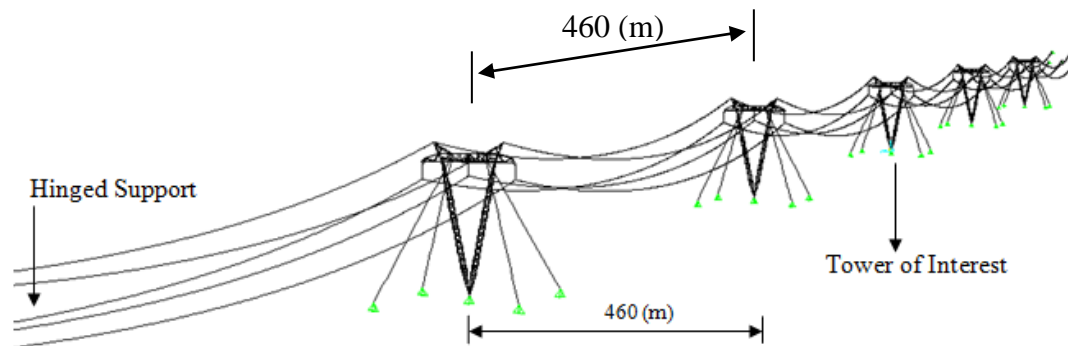


Fig. 5-2 Transmission line system (L2) – Tower Type (T2)

In the current study, two guyed transmission line systems are investigated to assess the structural behaviour and progressive failure mechanism under F2 tornado wind field. The first guyed transmission line system is labeled as L1 and the corresponding supporting

towers are labeled as T1, as shown in Fig. 5-1. Each guyed tower (T1) has a height of 44.39 (m) and is supported by four guys attached to two cross-arms at an elevation of 38.23 (m). Two conductor bundles are attached to the towers' cross-arms using 4.27 (m) insulators. One ground-wire is connected to the top of the towers. The conductors' span is 480 (m). The conductors and ground-wire initial sags are 20 (m) and 13 (m), respectively. The second guyed tower is labeled as T2 and the transmission line system is labeled as L2, as shown in Fig. 5-2. The towers' height is 46.57 (m) and are supported by four guys. Three conductor bundles are connected to the towers' cross-arms using 4.27 (m) insulators. Two ground-wires are attached to the top of the towers. The conductors and ground-wires have a span of 460 (m) and they both have an initial sag of 16 (m).

The numerical simulation of the transmission line systems consists of the tower of interest and two adjacent towers from each side, which are included to properly simulate the stiffness of the system. As shown in Fig. 5-1 and 5-2, the models include five towers and six spans with hinged supports at the two ends. Such a number of spans was recommended by Shehata et al. (2005) and Hamada (2009) to accurately account for the forces transferred from the conductors and ground wire to the tower of interest. More details regarding the two transmission line systems are provided by Hamada et al. (2010) and Hamada and El Damatty (2011).

5.4 Components and Validation of the Numerical Model

The numerical simulation reported in the current study is conducted using a finite element code, called “*FTTHIW*”, developed in-house. *FTTHIW* stands for Failure of Transmission Towers under High Intensity Wind. In *FTTHIW*, the transmission lines, the

insulators, the tower members, and the guys are simulated using different elements. The numerical code is an extension to the models developed and validated previously by Shehata and El Damatty (2008), Ladubec et al. (2012), Shehata et al. (2005), Shehata and El Damatty (2007) and Shehata et al. (2008). Shehata et al. (2005) modeled the conductors using two-dimensional nonlinear curved frame elements, the tower members using three dimensional linear frame elements, and the insulators using linear spring elements. In addition to the inclusion of the nonlinear geometric effects and a material model for the tower members, an improvement in the simulation of the behaviour of the conductors is conducted in this study. While using two-dimensional modeling and decoupling the analysis of the conductors vertically and transversally were accepted for the downburst applications considered by Ladubec et al. (2012) and Shehata et al. (2005), this might not be adequate for tornado analysis. For downbursts, the vertical forces are quite small compared to the transverse forces and thus decoupling the two effects or even neglecting the vertical forces can be acceptable. In contrast for tornadoes, the vertical and transverse forces are of same order of magnitude and, therefore, they should be coupled together in a three dimensional analysis.

The nonlinear analyses of the transmission line systems are divided into two main steps. Firstly, the six spans of conductors and ground wires, including the insulator springs, are modeled separately as shown in Fig. 5-3. In this model, the combined flexibility of the towers and the insulators are simulated using three dimensional springs as shown in the figure. The model is analyzed nonlinearly under tornado forces and the spring reactions are evaluated. In the second step, the lines' reactions are reversed and applied as forces

acting on the tower's cross-arms. The tower is analyzed under those forces as well as under the loads resulting from the F2 tornado acting on the lattice members.

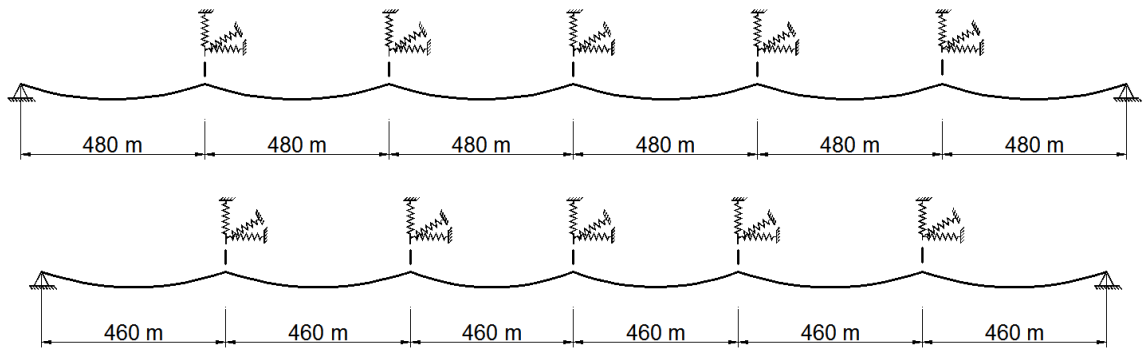


Fig. 5-3 Finite Element Model for L1 and L2 Transmission Lines (Conductors and Ground wires)

5.4.1 Modeling of Conductors and Ground-wires

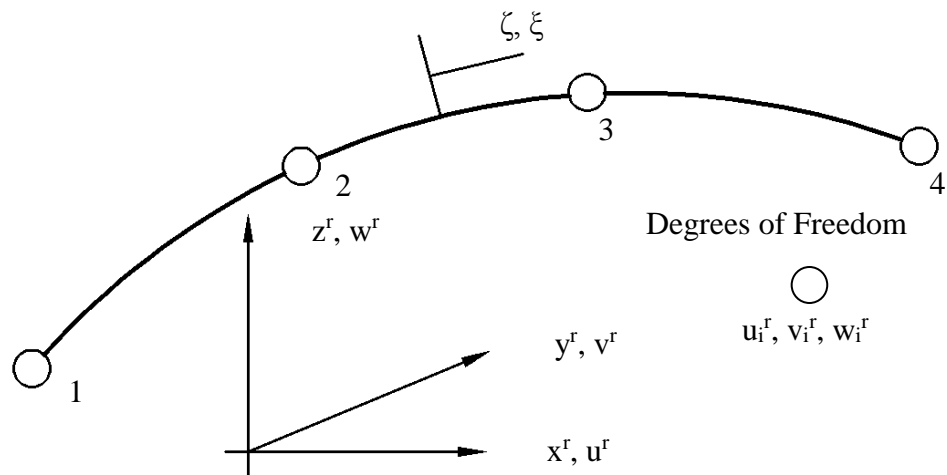


Fig. 5-4 Cable Element Coordinate System and Nodal Degrees of Freedom

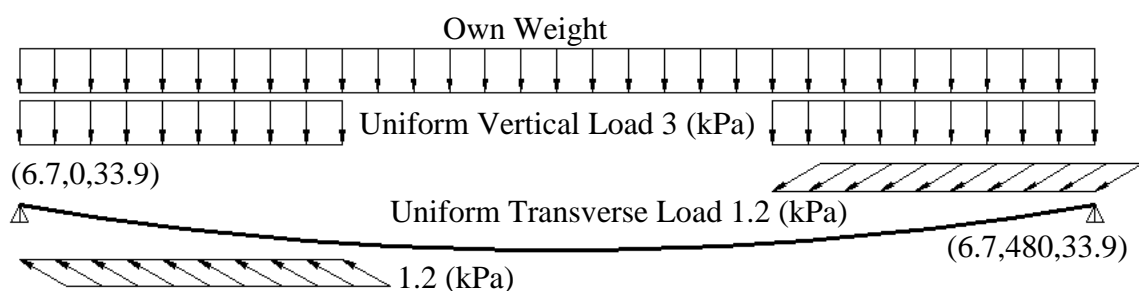


Fig. 5-5 Cable Geometry and Loading

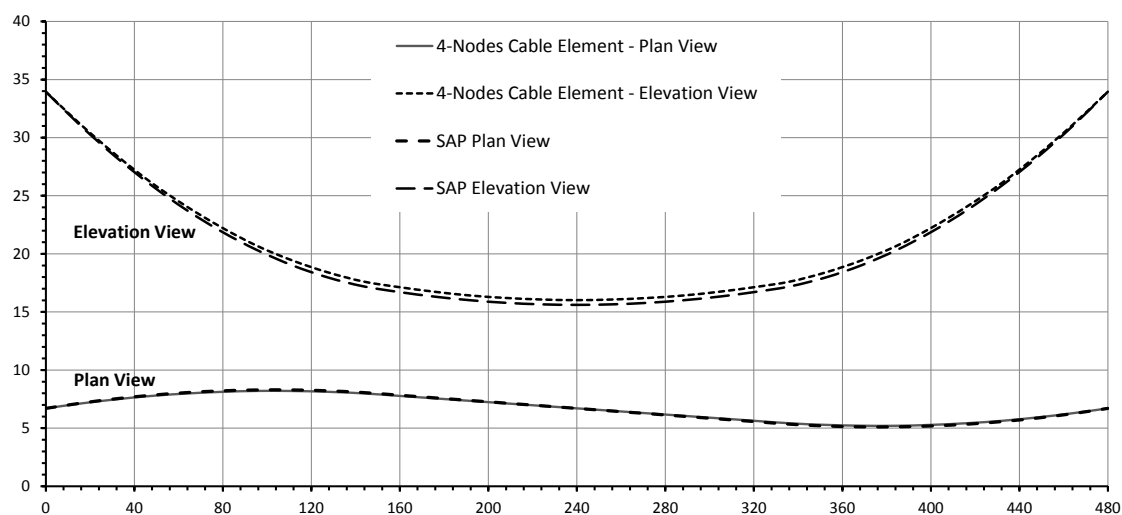


Fig. 5-6 Cable Displacements in Elevation and Plan View using SAP 2000 and Current 4-Nodes Cable Element

The conductors and ground-wires are modeled using a three dimensional four-noded nonlinear cable element developed in-house and discussed in detail in Chapters (3) and (4). As shown in Fig. 5-4, the element has 4 nodes allowing a cubic simulation for the three displacement components at any points within its length. The accuracy of the cable element is verified in the current study using the commercial software package SAP 2000 (CSI Inc. 2010). The cable geometry and properties shown in Fig. 5-5 and Table 5-1 are

used for this validation purpose. The cable is modeled using 10 four-noded elements. The cable is analyzed under the combined effect of its own weight and distributed vertical and transverse loads applied on a portion of the cable as shown in Fig. 5-5. An initial prestressing force of 86 (kN) is applied to the cable and the initial sag under the combined effect of own weight and initial prestressing force is assumed to be 20 (m). The same cable is modeled using the nonlinear two-noded cable element included in SAP 2000, when 30 elements are used to simulate the same problem. The two analyses assume a linear elastic material behaviour for the cable while the nonlinearity results from the inclusion of the large displacement and the $P-\delta$ effects. The material nonlinearity is not included in the current study, as the cable material model behaves linearly till failure. In addition, field observations of most of transmission lines failures did not report lines or insulators ruptures. This was confirmed in discussions carried out with engineers from various utility companies. The profiles of the deformed shape projected along vertical and horizontal plans, as obtained from the analyses, are provided in Fig. 5-6. The figure shows the profiles obtained from both the *FTTHIW* code and the commercial program, indicating an excellent agreement. The final axial forces in the cable obtained from the two sets of analysis are provided in Table 5-1 indicating also an excellent agreement.

Table 5-1 Cable Properties and Axial Forces

Length (m)	Sag (m)	E (N/m ²)	Weight per Unit volume (N/m ³)	Initial Pretension (N)	SAP 2000 Axial Force (kN)	Numerical Code Axial Force (kN)
480	20	6.23E+10	22333	86715	172	174

5.4.2 Simulation of Insulators

As shown in Fig. 5-3 the simulation of the lines incorporates a number of springs, which represent the combined stiffness of the towers and insulators. At each tower location, the equivalent spring system is three dimensional and behaves nonlinearly. The derivation of the stiffness of this nonlinear spring system is provided in this section. In this derivation, X is the direction perpendicular to the line, Y is parallel to the line, and Z is the vertical direction. The flexibility matrix of the transmission tower at point “A” shown in Fig. 5-7 is first evaluated. It is expressed as follows:

$$[f_A] = \begin{pmatrix} f_{xxl} & 0 & f_{xzl} \\ 0 & f_{yyl} & 0 \\ f_{zxl} & 0 & f_{zzl} \end{pmatrix}$$

Where, f_{xxl} and f_{xzl} are the transverse and vertical displacement of point “A”, respectively, due to unit transverse load applied at this location. f_{yyl} is the longitudinal displacement of point “A” due to unit longitudinal load applied at this point. Similarly, f_{zxl} and f_{zzl} are the transverse and vertical displacements of point “A”, respectively, due to unit vertical load at this location. The insulators are considered to be rigid in the vertical direction and pin connected to the tower’s cross-arm and the conductors. The insulators can be replaced by two perpendicular nonlinear springs K_{IY} and K_{IX} , in the Y and X direction, respectively. An expression for K_{IX} and K_{IY} assuming a linear behaviour is provided by Desai et al. (1995). This expression is valid for small values of the rotation angles θ_L and θ_T , of the insulators, shown in Fig. 5-7. This expression is modified here to account for finite values for θ_L and θ_T as follows

$$K_{iy} = \left(\frac{1}{L_l \cos(\theta_L)} \right) \left(P_y * L + \frac{W_l}{2} \right)$$

$$K_{ix} = \left(\frac{1}{L_l \cos(\theta_T)} \right) \left(P_y * L + \frac{W_l}{2} \right) + \frac{2T}{L_x}$$

Where, L_l and W_l are the length and weight of the insulators, respectively. L and L_x are the total and horizontal span lengths of the conductor, respectively. P_y is the weight per unit length of the conductors, the angles θ_L and θ_T are shown in Fig. 5-7, and T is the horizontal component of the conductor pretension force.

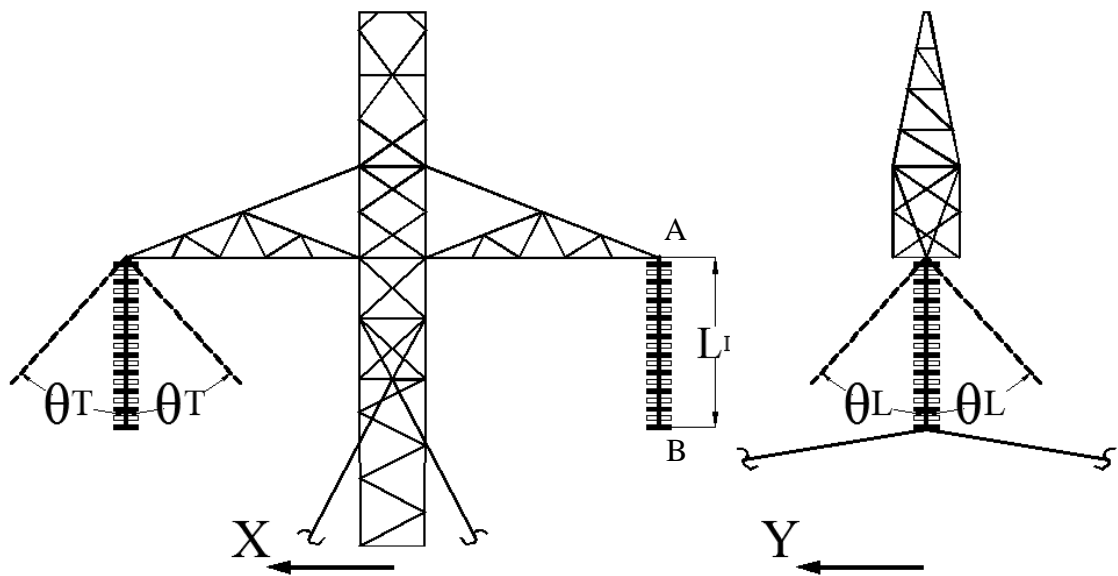


Fig. 5-7 Conductors' Cross-arms and Insulators Configurations of Tower T1

Accounting for the deformation of the tower and insulator, the flexibility matrix at point "B" shown in Fig. 5-7, is given by:

$$[f_B] = \begin{pmatrix} \left(f_{xxI} + \frac{1}{K_{IX}} \right) & 0 & f_{xzI} \\ 0 & \left(f_{yyI} + \frac{1}{K_{IY}} \right) & 0 \\ f_{zxI} & 0 & f_{zzI} \end{pmatrix}$$

This flexibility matrix is inverted to obtain the stiffness matrix of the three dimensional spring system supporting the lines.

5.4.3 Simulation of Guys

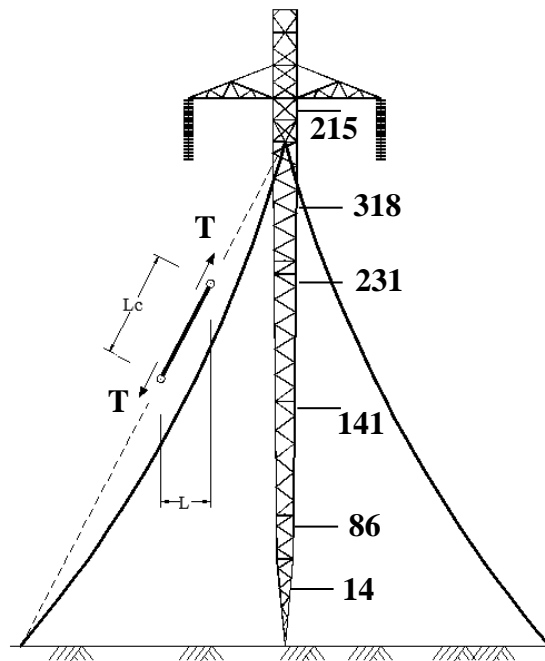


Fig. 5-8 Equivalent Cable Element

The initial conditions of the supporting guys, in terms of sag and applied pretension force, have a significant effect on the tower overall stiffness. An increase in the guys' pretension force leads to a decrease in sag and an increase in the axial stiffness of the

guys. To account for this variation in the cable's axial stiffness, an equivalent straight bar members with an equivalent modulus of elasticity, which combines the effect of both material and geometric deformations, are used to model the supporting guys, as shown in Fig. 5-8. The equivalent modulus of elasticity is calculated such that the stiffness of the straight bar is equal to the stiffness of the curved cable. This approach was described by Tung and Kudder (1968), Nazmy and Abdel-Ghaffar (1990) and is summarized in Appendix A. Each supporting guy is modeled using one equivalent straight bar element.

5.4.4 Simulation of Tower Members

Tower members are modeled using two-noded three dimensional frame elements with six degrees of freedom per node (three translations and three rotations). The primary leg members have multi-bolted connections that can resist moments, thus, a fixed connection assumption between the chord members is used. Meanwhile, a hinged assumption is employed for the connection of diagonal members with chord members since such connections are done using single bolts. The elastic stiffness matrix of a three dimensional frame element is available in many references, such as Przemieniecki (2012) and William and Gere (1990). The geometric nonlinear stiffness matrix for 3-D beam element can be obtained using the large deflection theory and nonlinear strain-displacement relationships discussed in detail by Przemieniecki (2012). The geometric nonlinear stiffness of the three dimensional frame element that represents the effect of large displacement is given in Appendix B. The coupling between axial and flexural stiffness can be considered in the nonlinear analysis using the concept of stability functions (William and Gere 1990). These functions are used to modify both the bending

and axial stiffness of the tower's members. The three dimensional linear frame element stiffness matrix, including the stability functions, is given in Appendix C. The axial forces in the members are related to the joint displacements and must be calculated in an iterative way within each load increment.

5.4.5 Numerical Model Validation

The transmission line L1 is modeled using *FTTHIW*. The same system is simulated using the commercial software SAP 2000 (CSI. Inc. 2012). A critical tornado configuration of $R = 125$ (m) and $\theta = 0.0$, shown in Fig. 5-9, is considered in this validation example, where R is the distance between the tornado center to the tower of interest, and θ is the angle shown in Fig. 5-9. This tornado configuration was found to be critical in the extensive parametric studies conducted by Hamada and El Damatty (2011). Analysis under wind loads associated with this tornado location that takes into account the geometric nonlinear effects, is conducted using both *FTTHIW* and the commercial code. The internal forces in the intermediate tower, as well as the transmission line reactions are recorded for the two analyses. The peak forces obtained from both analyses are presented in Table 5-2 for selected chord members shown in Fig. 5-8. Conductor's reactions at the intermediate tower are also evaluated for both analyses and are presented in Table 5-3. As shown in the two tables, an excellent agreement, in terms of internal forces and conductor reactions, is shown between the two simulations. This provides confidence in the accuracy of the developed numerical code within the elastic range of behaviour.

Table 5-2 FTTHIW and SAP 2000 Transmission Tower (T1) Peak Internal forces of Selected Members ($R = 125$ (m) and $\theta = 0$)

Selected Chord Members	<i>FTTHIW</i>	SAP 2000	Differnece
	(kN)	(kN)	%
14	12621	12859	2
86	11761	11988	2
141	10621	10851	2
231	9113	9354	3
318	8407	8628	3
215	2608	2603	1

Table 5-3 FTTHIW and SAP 2000 Conductor's Reactions ($R = 125$ (m) and $\theta = 0$)

Transmission lines Transferred Forces to the Tower	Forces Direction with Respect to Lines	<i>FTTHIW</i>	SAP 2000	Differnece
		(kN)	(kN)	%
Fx	Perpendicular	15422	15567	1
Fy	Parallel	6841	6401	6
Fz	Verical	26061	26122	1

5.5 Failure Analysis

The current section reports the progressive failure analysis of the two considered guyed towers under critical tornado cases chosen based on the extensive parametric study conducted in previous investigation by Hamada et al. (2010) and Hamada and El Damatty (2011). Most design codes and guidelines such as ASCE MOP. 74 recommend using only F2 tornado for the design and analysis of transmission lines. A similar recommendation was concluded by Hamada et al. (2010) and Hamada and El Damatty (2011).

Accordingly, only F2 tornado is considered in the current failure study. The analysis is conducted in a quasi-static manner despite the time variation of the wind load resulting from the convective velocity of tornadoes. Hamada and El Damatty (2011) concluded that the dynamic effect can be neglected due the following two reasons:

- a) The significant difference between the fundamental period of the towers and the period of loading associated with the convective component of the tornado.
- b) The large aerodynamic damping of the conductors and ground-wires.

It should be mentioned that the magnitude of the F2 tornado velocity used in the simulation coincides with the maximum value specified in the Fujita scale, which is based on field measurements that include both the local and convective portions.

Extensive parametric studies were previously conducted on the two considered line systems by varying the location of the tornadoes in space as shown in Fig. 5-9. The results of those parametric studies were reported by Hamada et al. (2010) and Hamada and El Damatty (2011), where the internal forces in all members of the tower were evaluated for various tornado configurations defined by the parameters “R” and “ θ ” shown in Fig. 5-9. The peak internal forces in all members of the tower obtained from the entire parametric studies are recorded. In the current study, the members’ capacities are evaluated using the ASCE (1997). The peak forces are divided by the members’ capacity to obtain a strength factor “ α ” for each member. The higher the value of “ α ”, the more critical is the member and the structure with respect to the tornado loading. The tornado configurations leading to large values of “ α ” for a significant number of tower members

are identified. The two most critical tornado configurations are considered in the failure study of each system.

For each critical tornado configuration, progressive failure analysis is carried out. The tower members are assumed to totally fail once the member capacity is reached. This assumption implies that the failure happens in the members' connection. In the incremental analysis, a member reaching this stage at a certain increment is eliminated from the structure, i.e. does not contribute to the stiffness or strength of the structure in the subsequent increments. This material model is referred to "No post yield".

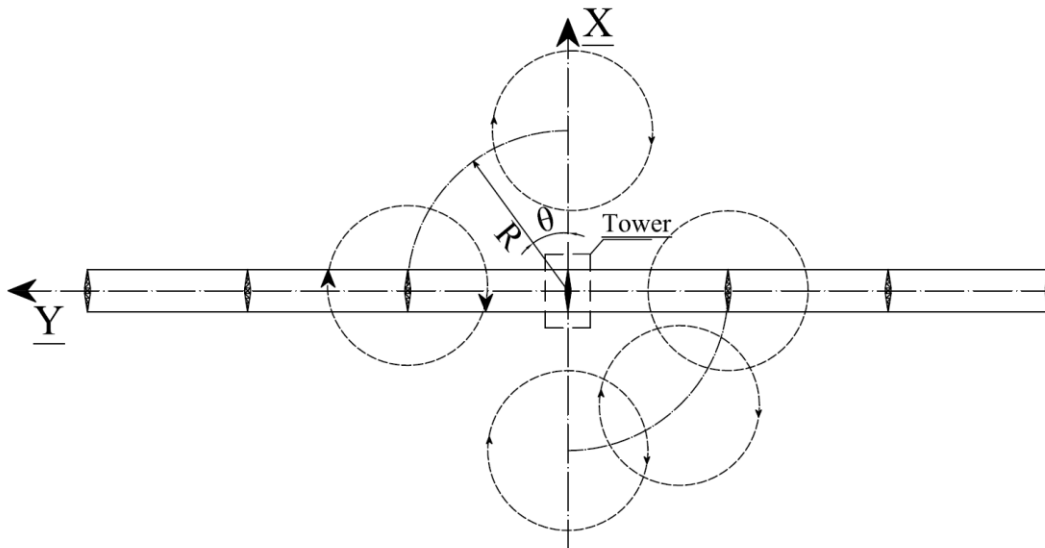


Fig. 5-9 Tornado Configurations R and θ Relative to the Tower of Interest

For each critical configuration, the following steps are conducted in the progressive failure analyses:

- 1- Using the upper limit of the velocity of the F2 tornadoes, given in Section 2, the maximum external loads acting on the conductors and the tower are calculated.
- 2- The tornado loads are applied incrementally by gradually increasing the loads. It was decided to use an increment of 1% of the maximum load. As such, the total load is divided to 100 increments.
- 3- A nonlinear analysis is conducted during each increment as described before. The internal forces are calculated for all members of the tower.
- 4- The ratio between the acting internal forces and the ultimate capacity of each member is calculated and denoted as “ λ ”. A value of $\lambda = 1$ (either in tension or compression) means that the member has reached its ultimate capacity and is eliminated from the model in the subsequent increments.
- 5- A state of collapse is assumed when no convergence in the numerical solution is reached at a certain increment implying that the structure has lost its overall stability.

The value of the tangential velocity at which failure occurs and its ratio relative to the maximum velocity of F2 tornadoes is recorded. In addition, the progression failure of the tower is described.

5.5.1 Failure Analysis – No Post Yield Strength

5.5.1.1 Failure Analysis of Transmission Line System L1 and Tower Type

T1 – No Post Yield Strength

In order to explain the sequence of failure and the failure mode of the tower T1, a description of the structure system and the forces acting on the tower is first provided. A sketch of the tower is given in Fig. 5-12 together with a simulation of the tower's structure system as an overhanging beam with pin support at the base and flexible support at the supporting guys' cross-arms location. The distributed forces shown in Fig. 5-12 represent the tornado loading acting on the tower. The concentrated forces shown at the cantilever portion at the top represent the forces transferred from the conductors and ground-wire to the tower through the insulators.

5.5.1.1.1 Failure Mode 1 – Critical Tornado Configuration $R = 125$ (m) and $\theta = 180^\circ$

The location of the F2 tornado relative to the tower and the line is shown in Fig. 5-10. A schematic of the directions of the radial and tangential components acting on the tower are shown in the figure. Also the resultant of those two components is illustrated. This value of R leads to large values for both tangential and the radial components as indicated by Hamada and El Damatty (2011). Due to this resultant force, supporting guy 1 is expected to slack while guy 3 is expected to be subjected to a large tensile force. This configuration, in which the line connecting the center of the tornado and the tower is perpendicular to the conductors, leads to approximately opposite forces on the conductors located on the adjacent spans of the tower. This will result in a relatively small transverse

force transmitted from the conductors to the tower as depicted from Fig. 5-11, where the transverse F2 tornado velocity acting on the conductors is illustrated. In view of the above discussion, and referring to Fig. 5-10, this tornado configuration will lead to large forces between the supports and minimum forces at the cantilever portion. This will tend to maximize the bending moment at the region between the two supports. Thus, the failure of the tower is expected to be triggered by two effects: a) large forces transmitted to the members attached to the supporting guy 3, b) large forces on chord members due to the significant bending effect.

The progression of failure resulting from this analysis is shown in Fig. 5-12. Seven sequences of members' failure (denoted as stage I to VII) are shown in the figure, each representing a specific load increment. The failure is initiated at stage I at the guys' cross-arms level as a result of the large force developing in guy # 3 as explained above. As a result of the double moment resulting from the tangential and radial components, one chord member will be subjected to compression forces from both bending moments. Total collapse occurs when this chord member buckles in load stage VII as shown in Fig. 5-12. This happens at a tornado velocity of 65 (m/sec), which corresponds to 84% of the maximum wind speed of F2 tornadoes.

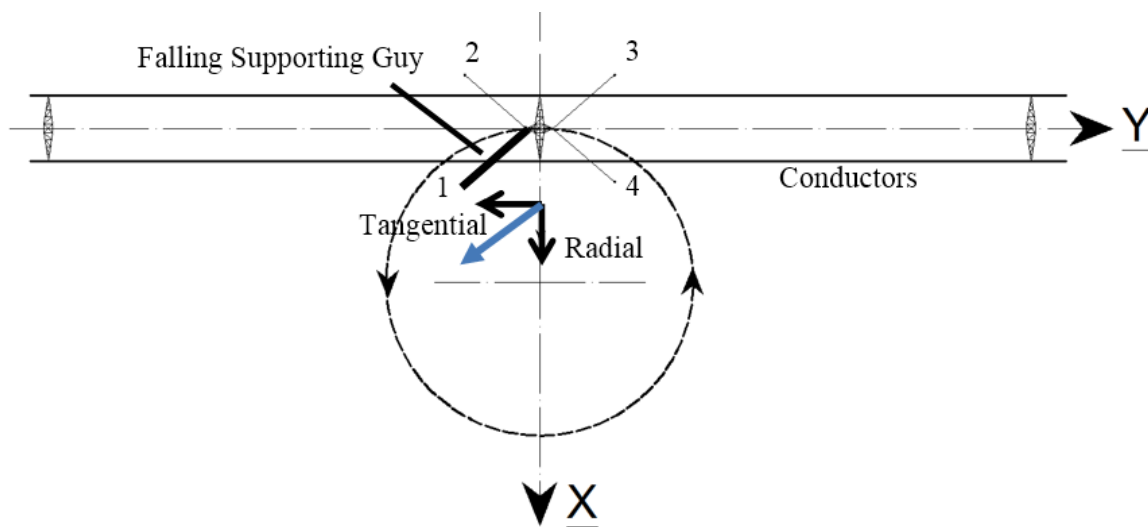


Fig. 5-10 Failure Analysis (First Method) L1 – T1, Analysis Case $R = 125$ (m) and $\theta = 180^\circ$

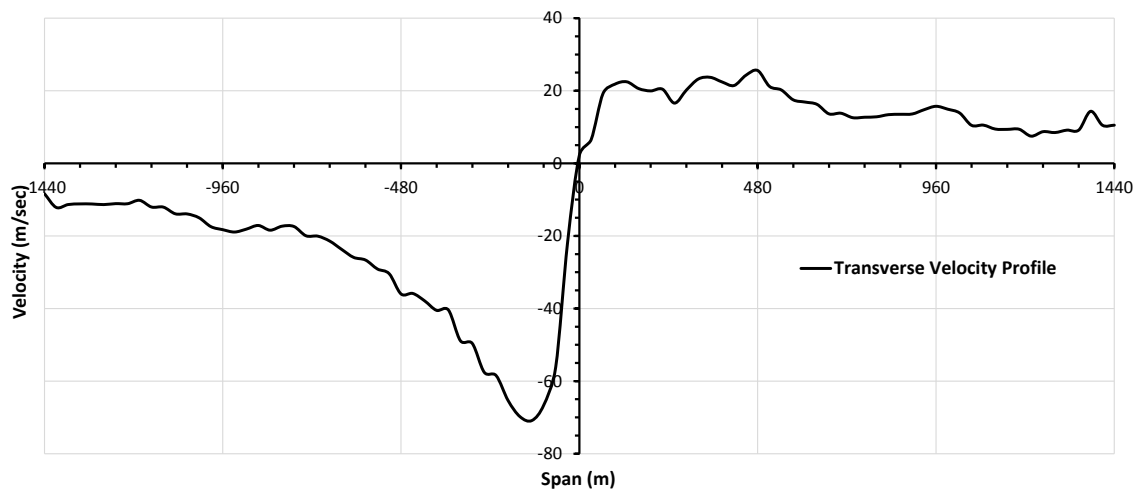


Fig. 5-11 Transverse Velocity Profile – Conductors

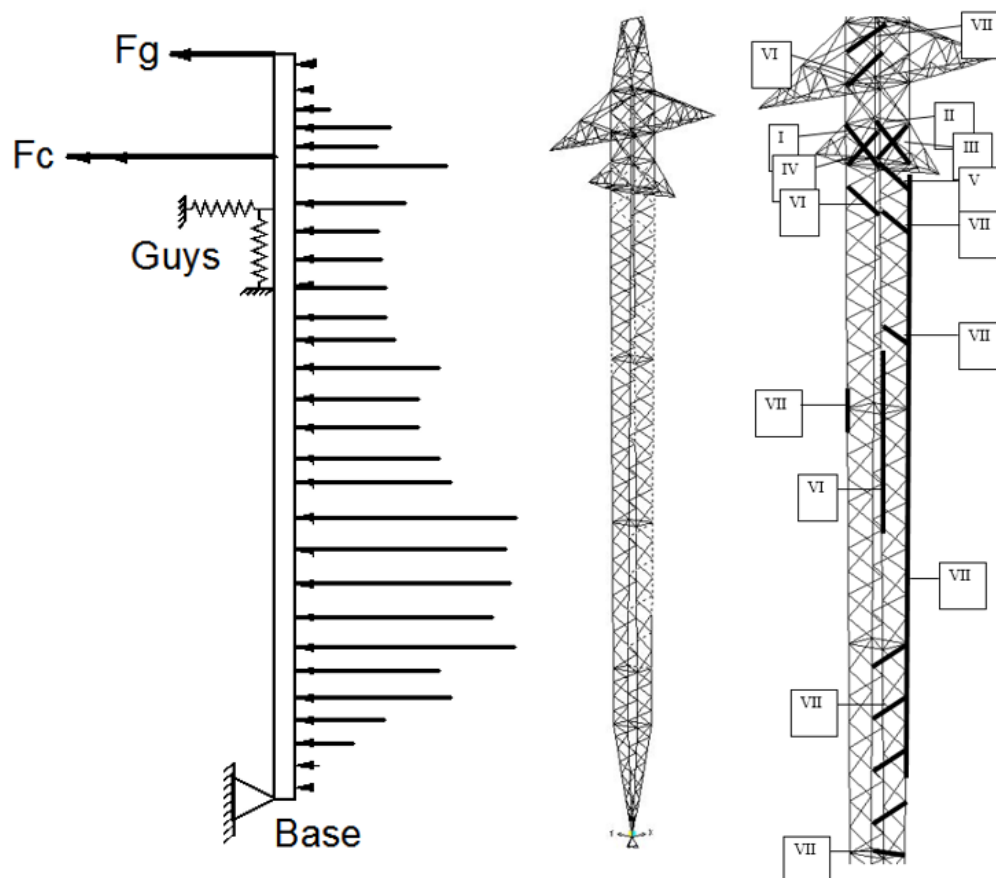


Fig. 5-12 Simulation of the Tower as an Over-hanging Beam - Failed Members L1 – T1, Analysis Case $R = 125$ (m) and $\theta = 180^\circ$

5.5.1.1.2 Failure Mode 2 – Critical Tornado Configuration $R = 125$ (m) and $\theta = 30^\circ$

Fig. 5-13 shows the location of the tornado relative to the tower and the line. The direction of the tangential and radial components acting on the tower due to this configuration is shown in the figure. Guy # 3 is expected to slack due to this loading configuration. The main difference between this loading configuration and the previous one is in the behaviour of the conductors. Fig. 5-14 shows the transverse velocity profile on the conductors. Unlike the previous load case, a significant transverse force will be transferred in this case from the conductors to the towers. This force acting on the

cantilever portion of the tower (see Fig. 5-12), results in reducing the bending moment acting on the region of the tower between the two supports. The sequence of failure due to this configuration is shown in Fig. 5-15. Failure initiates at the diagonal members at the guys' cross-arm region (stage I and II). Buckling of main chord members occur at subsequent load increments (stages III and IV). The tension force in guy # 4 becomes so large at this stage such that this guy fails by tension. This results in a change in the supporting system of the structure and a redistribution of the internal forces as shown in stage V. Other chord members start to fail and an overall collapse then occurs. This happens at a tornado velocity of 74 (m/sec), representing about 95% of the maximum F2 tornado velocity.

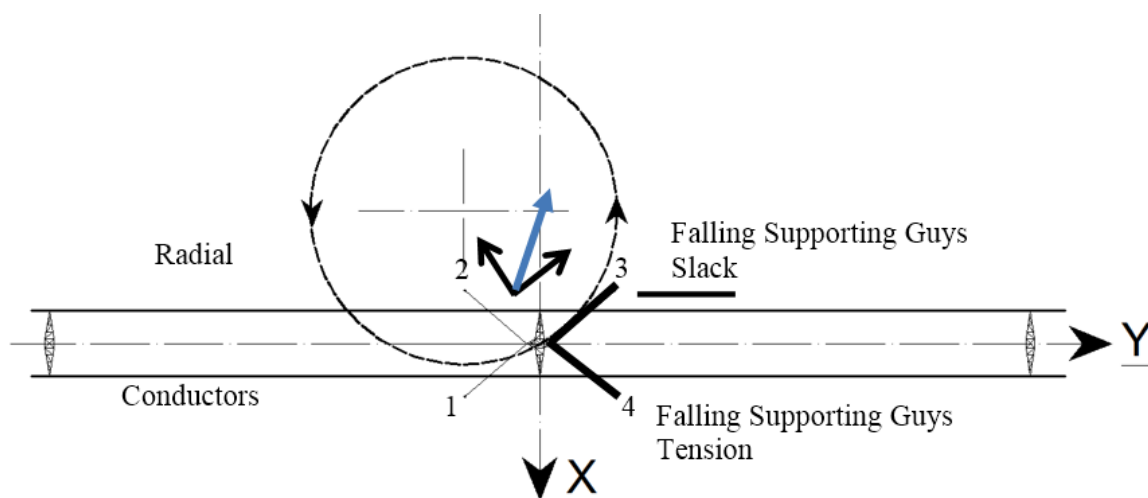


Fig. 5-13 Failure Analysis (First Method) L1 – T1, Analysis Case $R = 125$ (m) and $\theta = 30^\circ$

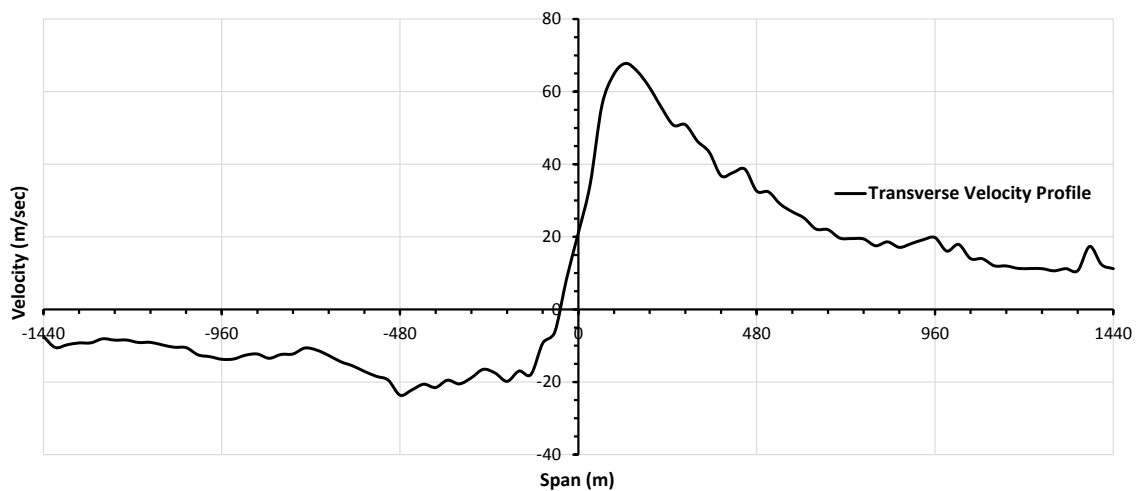


Fig. 5-14 Transverse Velocity profile – Conductors

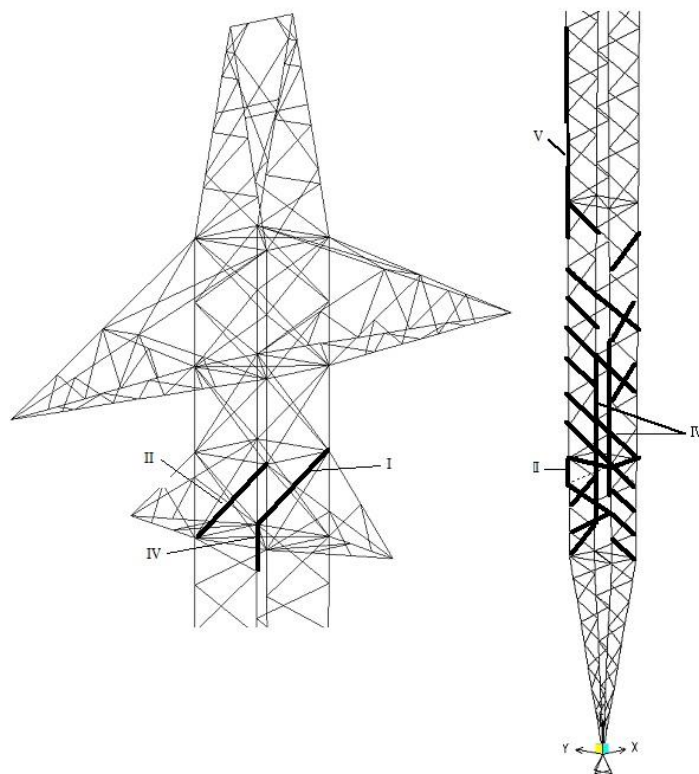


Fig. 5-15 Failed Members L1 – T1, Analysis Case $R = 125$ (m) and $\theta = 30^\circ$

5.5.1.2 Failure Analysis of Transmission Line System L2 and Tower Type T2 – No Post Yield Strength

In order to explain the failure modes and the sequence of failure of tower T2, the same description of the structure system provided for tower T1 (Section 5.1.1) can be used. The tower can be simulated as an overhanging beam with a pin support at the base and flexible supports at the guys' location. A major difference between towers T1 and T2 is that for tower T2, the conductors and supporting guys are both attached to the same cross-arms.

5.5.1.2.1 Failure Mode 1 – Critical Tornado Configuration $R = 125$ (m) and $\theta = 330^\circ$

The location of the tornado relative to the tower and the lines is shown in Fig. 5-16. The direction of the radial and tangential components acting on the tower is shown in the figure. This value of R leads to large values for both the tangential and the radial velocity components. The resultant of those two components acts almost along the lines directions. Thus, supporting guys # 3 and # 4 are expected to slack while guys # 1 and # 2 are expected to be subjected to a large tension force. A significant difference between tower T2 and tower T1 is in the effect of the conductors on the overall behaviour of the tower. The transverse and longitudinal forces transmitted from the conductors are in the same level of the supporting guys. As such, those forces will be transmitted directly to the supporting guys. This will tend to maximize the equivalent shear force near the guys supporting point. Thus the failure of the tower is expected to be triggered by a) the large forces transmitted to the members attached to guys # 1 and # 2, b) large forces on diagonal members due to the significant shear force near the cross-arm zone.

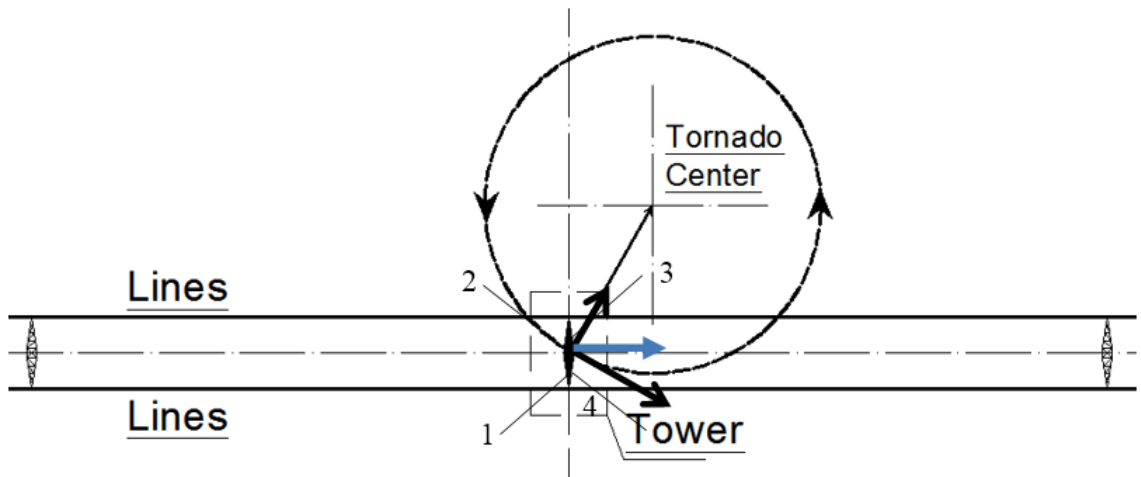


Fig. 5-16 Failure Analysis L2 – T2, Analysis Case $R = 125$ (m) and $\theta = 330^\circ$

The progression of failure resulting from this analysis is shown in Fig. 5-17. Seven sequences of member failures (denoted as stages I to VII) are shown in the figure. The failure initiates in stages I, II, and III at the guys location as a result of the large force developing in the supporting guys # 1 and # 2. As a result of shear force resulting from the tangential and radial components, diagonal members will be subjected to significant compression forces. Total collapse occurs when all diagonal members buckle in one region, and this happens gradually in stages IV, V, VI, and VII, as shown in Fig. 5-17. The total collapse occurs at a tornado velocity of 42 (m/sec), which corresponds to 54% of the maximum wind speed of F2 tornadoes.

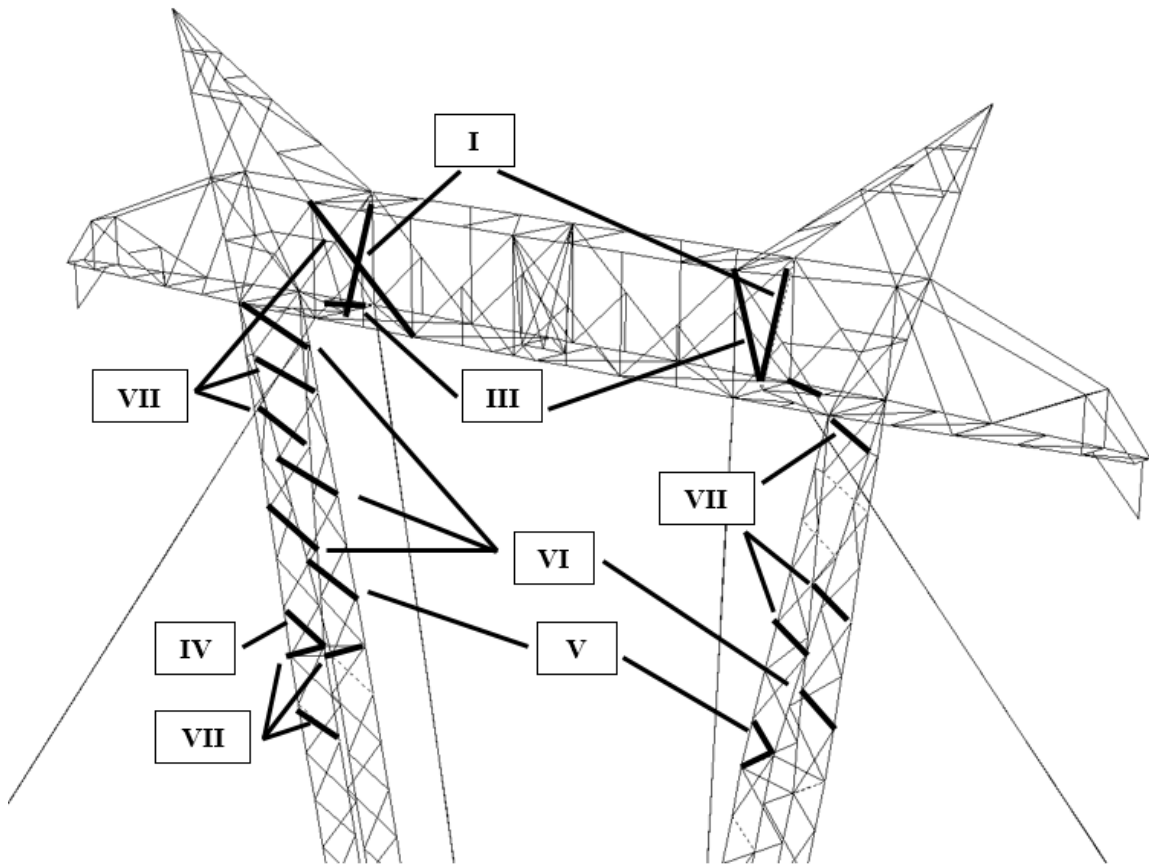


Fig. 5-17 Failed Members L2 – T2, Analysis Case $R = 125$ (m) and $\theta = 330^\circ$

5.5.1.2.2 Failure Mode 2 – Critical Tornado Configuration $R = 100$ (m) and $\theta = 180^\circ$

Fig. 5-18 shows the location of the tornado relative to the tower and the lines. The directions of the tangential and radial components acting on the tower due to this configuration are also shown in the figure. Supporting guys # 1 and # 2 are expected to slack due to this tornado configuration. The main difference between this loading configuration and the previous one is in the behaviour of the conductors. Unlike the previous configuration, a negligible transverse force will be transmitted from the conductors to the tower. In addition, the tangential and radial velocity profiles provided

in Fig. 5-19 show that the tower zone beneath the cross-arms is subjected to negligible radial forces, and large tangential forces. For this tornado configuration, the tangential force act along the direction longitudinal direction of the line.

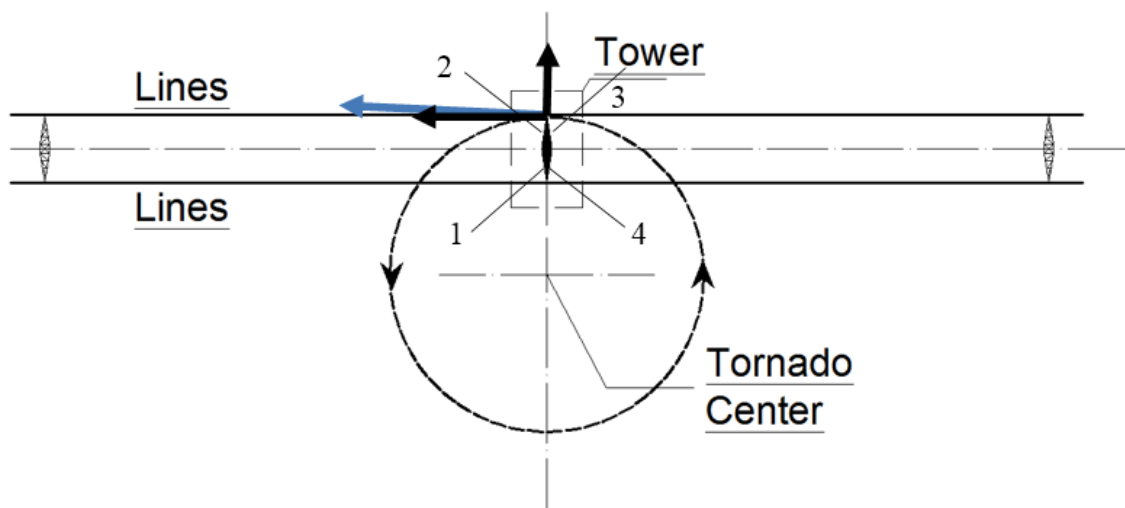


Fig. 5-18 Failure Analysis L2 – T2, Analysis Case $R = 125$ (m) and $\theta = 180^\circ$

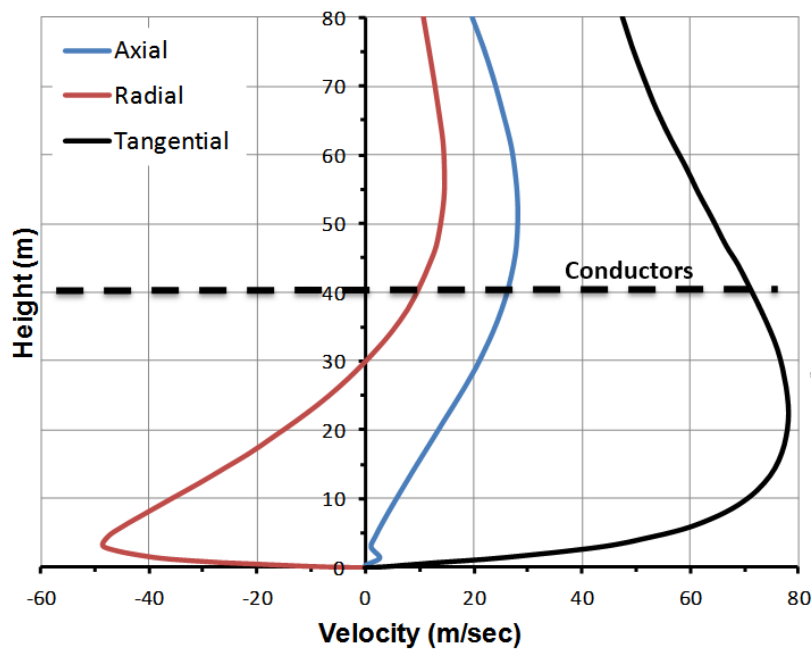


Fig. 5-19 Vertical Profile of F2 Tornado Three Velocity Components at $R = 100$ (m)

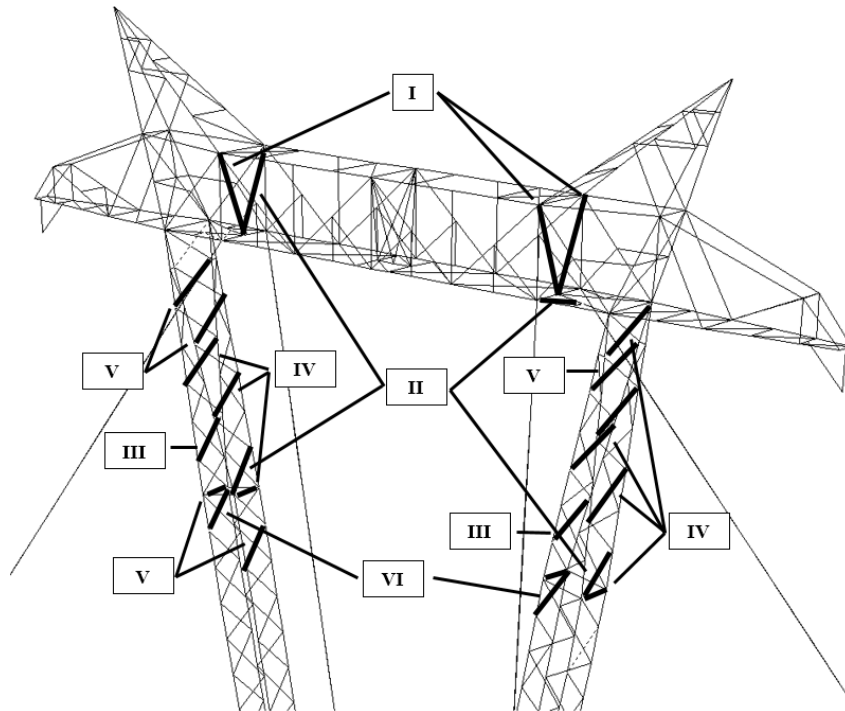


Fig. 5-20 Failed Members L2 – T2, Analysis Case $R = 125$ (m) and $\theta = 180^\circ$

The sequence of failure due to this configuration is shown in Fig. 5-20. Failure initiates at the diagonal members at the supporting guys region (stage I). Buckling of diagonal members' progresses gradually at subsequent load increments until an overall collapse occurs. This happens at a tornado velocity of 43 (m/sec), representing about 55% of the maximum F2 tornado velocity.

5.6 Effect of Material Model

The assumption used regarding the post yielding behaviour of the tension members is assessed in the current section. This is done by repeating the four reported failure analyses while assuming that tension members maintain their strength (but lose their stiffness) in the post yielding stages. This will represent the behaviour of ductile steel

members where no connection premature failure occurs. The sequence of failure obtained from this set of analysis and the previous set (with no post yielding tension strength) is shown to be almost the same for the two considered towers and the two analyzed load cases. The overall collapse is generally delayed and the structures are able to resist higher proportions of the F2 tornado. A major difference is shown in the behaviour of the diagonal members. In the first set of analysis, diagonal members in tension reaching their yielding capacity lose their strength and, consequently, transfer the forces to the adjacent compression diagonal members that eventually fail by buckling. This effect is delayed in the second set of analysis as tension members are able to withstand a level of tension force up to their yield capacities. A summary for the failure velocities predicted for each load case of the two towers and using the two assumption regarding post yielding behaviour of tension members is provided in Table 5-4.

Table 5-4 Summary of Failure Velocities Predicted by Both Material Models

		No Post Yield Strength	Post Yield Strength
	Critical Tornado Configurations	F2 tornado Wind Speed %	F2 tornado Wind Speed %
Transmission Line L1 (Tower T1)	Tornado Config. 1	84	92
	Tornado Config. 2	95	102
Transmission Line L2 (Tower T2)	Tornado Config. 1	54	59
	Tornado Config. 2	55	62

5.7 Comparison between Failure Studies of the two Lines

Despite the fact that the two studied transmission line systems L1 and L2 were designed under nearly similar environmental conditions, there is a significant difference in the

results of their failure studies under F2 tornadoes. The main difference between the results of the two systems can be stated as follows:

- 1- Tower T2 is predicted to fail under a significant lower level of tornado loads. This is clear from the values for maximum tornado velocities that the towers can sustain as summarized in Table 5-4.
- 2- The progressive failure mode is different between the two towers. For tower T1, failure is initiated by buckling of chord members. Meanwhile, for tower T2, it is initiated by buckling of diagonal members. As such, one can say that tower T1 fails by bending while tower T2 fails by shear. Those two modes of failure under tornadoes were also reported by Behncke and White (2006) and Ishac and White (1994) based on field observations.
- 3- Transmission tower T1 are most sensitive to the assumption used regarding the post yielding tension behaviour as around 8% difference in the failure velocities is obtained from the analyses conducted using the two different material models. This difference is reduced to around 6% for tower T2.
- 4- While a number of guys of the two towers slack during the analysis, only one guy for tower T1 has failed in tension. In comparison, none of the supporting guys fails under the critical tornado cases of tower T2.

These differences in behaviour can be attributed to the geometric configurations of the two towers. Tower T2 has two separate legs and a relatively wide cross-arm. The spatial variation in the location of the two parallel lines, resulting from the wide cross-arm, can lead to variation in the tornado loads on the two parallel transmission lines. As such, different values for unbalanced longitudinal forces acting on the cross-arms will develop

at those two parallel lines. This can lead to a net torsion effect on the tower. Another difference in the structure behaviour between the two towers results from the location of the guys which are connected to the conductors' cross-arms for the case of tower T2. It should be mentioned that although the two lines have almost equal spans, transmission line system L2 has three conductor bundles while transmission line system L1 has only two conductor bundles.

5.8 Effect of Geometric Nonlinearities

In order to assess the importance of considering the geometric nonlinear effect in the analysis, the progressive failure analyses for transmission line L1 is repeated while deactivating the geometric nonlinear feature. This means that the analyses assume a linear geometric behaviour and take into account only the material failure described as “No post yield strength”. Comparison between the wind failure velocities obtained with and without the inclusion of the geometric nonlinear effect is provided in Table 5-5. The results show that the difference between the nonlinear analyses and the linear analyses is about 8% in terms of failure velocities. A higher difference between the nonlinear and linear analyses is expected in the case of transmission tower T2 as the tower is more flexible and a higher nonlinear effect is therefore expected. Using linear analysis, tower T2 fails due to 71 % of F2 tornado wind velocity. This reflects a 17 % difference between the linear and nonlinear failure analyses for tower T2. In general, the results indicate that it is important to consider the geometric nonlinear effect in the analysis of transmission towers under tornado wind loads.

Table 5-5 Comparison between Linear and Nonlinear Analyses of Tower T1 under F2 Tornado Wind Loads

		% of F2 Tornado Velocity	
		Linear Analysis	Geometric Nonlinearity (Large deflections P- Δ) + (Bending P- δ)
Tower T1	Tornado Configuration 1	92	84
	Tornado Configuration 2	103	95

5.9 Conclusion

The following conclusions can be drawn from the failure studies conducted using the numerical code (*FTTHIW*) developed and validated in the current study:

The numerical model predicts that two considered guyed transmission tower systems cannot withstand the maximum velocity of an F2 tornado. However a significant difference in the tornado capacity is shown between the two systems. While system L1 is predicted to fail at 84% of the maximum tornado velocity, system L2 is predicted to fail at only 54%. Also, the failure modes predicted for the two systems are different; system L1 fails by bending while system L2 fails by shear. Despite the fact that the two systems have almost equal conductors' span and they were initially designed under similar environmental loads (without considering tornadoes), significant difference in tornado capacity and failure modes is observed. The main reason affecting the failure mode, whether it is bending and shear, is the location of the guys relative to the conductors as explained in the chapter. This difference in tornado behaviour between the two systems can be attributed to the difference in the geometric configuration of the

towers, in the number of conductor bundles and in the width of the conductors' cross-arm. As a result of the localized nature of tornadoes, a system with wide cross arms will have different forces acting on the parallel conductor lines. This can lead to a torsion effect on the tower. This is observed for system L2, which has wider cross arms compared to system L1.

The assumption made regarding the post yield tension behaviour has no significant effect on the failure velocity. Assuming that the tension members maintain their post yield strength compared to losing their strength has increased the failure velocity by about 8% and 10% for systems L1 and L2, respectively.

Due to the localized nature of tornadoes, the forces acting on a transmission tower depend on the location of the tornado relative to tower. Thus, the failure velocity of the same tower can vary based on the location of the tornado. For the two considered critical tornado locations, a difference of 11% is observed in the failure velocities for system L1. This is reduced to only 3% for system L2.

The inclusion of geometric nonlinearities is shown to alter the failure velocity of systems L1 and L2 by 8% and 17%, respectively. Because of the larger flexibility of system L2, the geometric nonlinear effect is shown to have a more pronounced effect for this system.

Although the conductors are not fully loaded during tornadoes, the failure studies conducted on the two systems give an indication that transmission lines are vulnerable to failure when they experience an F2 tornado. This is despite the many load cases that account for ice, wind, wind-on-ice, and broken wires forces and are typically considered in design. As such, studies are needed to develop load cases simulating critical tornado

configurations on generic transmission line systems. It should be noted that the results presented in this chapter do not include failures attributed to damage caused by debris during tornado events.

5.10 Acknowledgement

The first author is indebted to the Vanier Canada Graduate and the Natural Science and Engineering Research Council of Canada (NSERC) for the financial support provided for this research. The authors also gratefully acknowledge Hydro One Inc., Ontario, Canada for its support to this research project.

5.11 References

Kareem, A. (2010). "Bluff body aerodynamics and aeroelasticity: A wind Effects Perspective." *Journal of Wind Engineering*, 7, 30-74.

American Society of Civil Engineers. (1997). *Design of latticed steel transmission structures*. American Society of Civil Engineers, New York, NY.

Baker, D. E. (1981). "Boundary layers in laminar vortex flows". Ph.D. thesis. Purdue University.

Dempsey, D., and White, H. B. (1996). "Winds wreak havoc on lines." *Transmission & Distribution World*, 48(6), 32-42.

Desai, Y. M., Yu, P., Popplewell, N., and Shah, A. H. (1995). "Finite element modelling of transmission line galloping." *Computers and Structures*, 57(3), 407-420.

Hamada, A. (2009). *Analysis and behaviour of guyed transmission line structure under tornado wind loading*. School of Graduate and Postdoctoral Studies, University of Western Ontario, London, Ont.

Hamada, A., Damatty, A. A. E., Hangan, H., and Shehata, A. Y. (2010). "Finite element modelling of transmission line structures under tornado wind loading." *Wind and Structures, an International Journal*, 13(5), 451-469.

Hamada, A., and El Damatty, A. A. (2011). "Behaviour of guyed transmission line structures under tornado wind loading." *Computers and Structures*, 89(11-12), 986-1003.

Hangan, H., and Kim, J. (2008). "Swirl ratio effects on tornado vortices in relation to the Fujita scale." *Wind and Structures*, 11(4), 291-302.

Ishac, M. F., and White, H. B. (1994). "Effect of tornado loads on transmission lines." *Proceedings of the 1994 IEEE Power Engineering Society Transmission and Distribution Conference, April 10, 1994 - April 15, 1994*, Publ by IEEE, Chicago, IL, USA, 521-527.

Ladubec, C., El Damatty, A. E., and El Ansary, A. E. (2012). "Effect of geometric nonlinear behaviour of a guyed transmission tower under downburst loading." *2012 International Conference on Vibration, Structural Engineering and Measurement, ICVSEM 2012, October 19, 2012 - October 21, 2012*, Trans Tech Publications, Shanghai, China, 1240-1249.

Nazmy, A. S., and Abdel-Ghaffar, A. (1990). "Three-dimensional nonlinear static analysis of cable-stayed bridges." *Computers and Structures*, 34(2), 257-271.

Newark, M. J. (1984). "Canadian tornadoes, 1950-1979." *Atmospheric Ocean*, 22, 243-253.

Przemieniecki, J. S. (2012). *Theory of matrix structural analysis*. McGrawHill, New York; Toronto.

Sarkar, P., Haan, F., Gallus, Jr., W., Le, K. and Wurman, J. (2005). "Velocity measurements in a laboratory tornado simulator and their comparison with numerical and full-scale data." *37th Joint Meeting Panel on Wind and Seismic Effects*.

Savory, E., Parke, G. A. R., Zeinoddini, M., Toy, N., and Disney, P. (2001). "Modelling of tornado and microburst-induced wind loading and failure of a lattice transmission tower." *Eng.Struct.*, 23(4), 365-375.

Shehata, A. Y., and El Damatty, A. A. (2008). "Failure analysis of a transmission tower during a microburst." *Wind and Structures*, 11(3), 193-208.

Shehata, A. Y., and El Damatty, A. A. (2007). "Behaviour of guyed transmission line structures under downburst wind loading." *Wind and Structures, an International Journal*, 10(3), 249-268.

Shehata, A. Y., El Damatty, A. A., and Savory, E. (2005). "Finite element modeling of transmission line under downburst wind loading." *Finite Elements Anal.Des.*, 42(1), 71-89.

Shehata, A. Y., Nassef, A. O., and El Damatty, A. A. (2008). "A coupled finite element-optimization technique to determine critical microburst parameters for transmission towers." *Finite Elements Anal.Des.*, 45(1), 1-12.

Tung, D. H. H., and Kudder, R. J. (1968). "Analysis of cables as equivalent two-force members." *American Institute of Steel Construction - Engineering Journal*, 5(1), 12-19.

William, W., and Gere, J. M. (1990). *Matrix analysis of framed structures*. Van Nostrand Reinhold, New York.

5.12 Appendices

5.12.1 Appendix A

The Equivalent cable modulus of elasticity is given by

$$E_{eq} = \frac{E}{1 + \left[\frac{(wL)^2 AE}{12T^3} \right]} \quad \mathbf{Eq. 5-1}$$

in which E_{eq} = equivalent modulus of elasticity; E = cable material effective modulus of elasticity; L = horizontal projected length of the cable; W = weight per unit length of the cable; A = cross-sectional area of the cable; and T = cable tension. Eq. (5-1) calculates the tangential value of the equivalent modulus of elasticity when the tension in the cables equals T . If the tension in the cables changes due to the nonlinear iteration steps from T_i to T_{i+1} , the secant value of E_{eq} for each load iteration is given by

$$E_{eq} = \frac{E}{1 + \left[\frac{(wl)^2 (T_i + T_{i+1}) AE}{24T_i^2 T_{i+1}^2} \right]} \quad \mathbf{Eq. 5-2}$$

The stiffness matrix of an inclined cable of length L_c and cross section A , during a pretension T is simply similar to the elastic stiffness matrix of a bar element with an equivalent elastic modulus given by Eq. (5-1) or Eq. (5-2). The elastic stiffness matrix in local coordinates for the cable element shown in Fig. 5-21 is given by

$$K_E = \frac{AE_{eq}}{L_c} \begin{pmatrix} 1 & -1 \\ -1 & 1 \end{pmatrix} \quad \mathbf{Eq. 5-3}$$

Stiffness matrix of truss element using large deflection theory was given by Przemieniecki (2012). Local stiffness matrix including geometric nonlinearity is given as

$$[K_T] = [K_E] + [K_G] \quad \text{Eq. 5-4}$$

where $[K_T]$ is the element stiffness matrix in local coordinates, $[K_E]$ is the elastic stiffness matrix as given in Eq. (5-3), and $[K_G]$ is the geometric stiffness matrix of the equivalent cable element, and is given by

$$[K_G] = \begin{bmatrix} [G] & -[G] \\ -[G] & [G] \end{bmatrix}_{6 \times 6} \quad \text{Eq. 5-5}$$

in which the sub-matrix $[G]$ is given by

$$[G] = \frac{T}{L_c} \begin{bmatrix} 0 & 0 & 0 \\ 0 & 1 & 0 \\ 0 & 0 & 1 \end{bmatrix} \quad \text{Eq. 5-6}$$

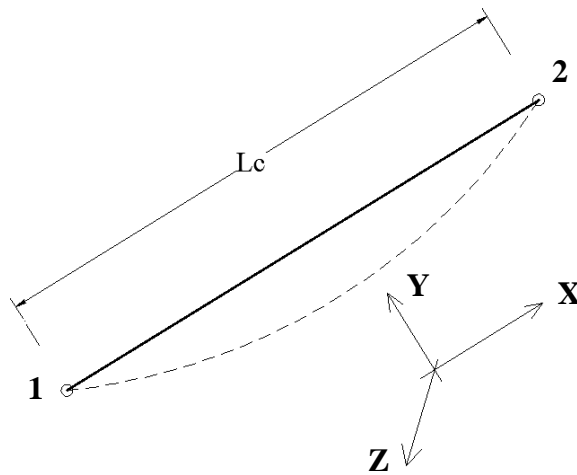


Fig. 5-21 Equivalent Cable Element in Local Coordinates

$$k(3,3) = k(9,9) = -k(3,9) = -k(9,3) = (12EI_y/L^3)S1_y \quad \text{Eq. 5-9}$$

$$\begin{aligned} k(2,6) &= k(6,2) = k(2,12) = k(12,2) = -k(6,8) \\ &= -k(8,6) = -k(8,12) = -k(12,8) = (6EI_z/L^2)S2_z \end{aligned} \quad \text{Eq. 5-10}$$

$$\begin{aligned} k(3,5) &= k(5,3) = k(3,11) = k(11,3) = -k(5,9) \\ &= -k(9,5) = -k(9,11) = -k(11,9) = (-6EI_y/L^2)S2_y \end{aligned} \quad \text{Eq. 5-11}$$

$$k(4,4) = k(10,10) = -k(4,10) = -k(10,4) = GI_x/L \quad \text{Eq. 5-12}$$

$$k(5,5) = k(11,11) = (4EI_y/L)S3_y \quad \text{Eq. 5-13}$$

$$k(6,6) = k(12,12) = (4EI_z/L)S3_z \quad \text{Eq. 5-14}$$

$$k(5,11) = k(11,5) = (2EI_y/L)S4_y \quad \text{Eq. 5-15}$$

$$k(6,12) = k(12,6) = (2EI_z/L)S4_z \quad \text{Eq. 5-16}$$

where E is the tower's members material modulus of elasticity; A is the cross-sectional area; L is the member length; I_y and I_z are the moments of inertia of the cross-section about the local principle y and z axes, respectively; I_x is the torsional moment of inertia of the cross-section; G is the member material shear modulus; and S are the stability functions. $S1$ through $S4$ modify the bending stiffness; while $S5$ modifies the axial stiffness. In the case of axial force P is zero; all stability functions take the value of 1. Stability functions are expressed in the members' axial force P , and the member end moments $M1$ and $M2$, about the member local y and z axes, as shown in Fig. 5-22.

For tension member (P is positive), the stability functions $S1_z$ through $S4_z$ are

$$S1_z = \omega^3 \sinh(\omega)/12R_t \quad \text{Eq. 5-17}$$

$$S2_z = \omega^2 (\cosh(\omega) - 1) / 6R_t \quad \text{Eq. 5-18}$$

$$S3_z = \omega(\omega \cosh(\omega) - \sinh(\omega)) / 4R_t \quad \text{Eq. 5-19}$$

$$S4_z = \omega(\sinh(\omega) - \omega) / 2R_t \quad \text{Eq. 5-20}$$

where

$$\omega = \mu L \quad \text{Eq. 5-21}$$

$$\mu^2 = P/EI_z \quad \text{Eq. 5-22}$$

$$R_t = 2 - 2 \cosh(\omega) + \omega \sinh(\omega) \quad \text{Eq. 5-23}$$

While for a compression member (P is negative),

$$S1_z = \omega^3 \sin(\omega) / 12R_c \quad \text{Eq. 5-24}$$

$$S2_z = \omega^2 (1 - \cos(\omega)) / 6R_c \quad \text{Eq. 5-25}$$

$$S3_z = \omega(\sin(\omega) - \omega \cos(\omega)) / 4R_c \quad \text{Eq. 5-26}$$

$$S4_z = \omega(\omega - \sin(\omega)) / 2R_c \quad \text{Eq. 5-27}$$

where

$$\omega = \mu L \quad \text{Eq. 5-28}$$

$$\mu^2 = P/EI_z \quad \text{Eq. 5-29}$$

$$R_c = 2 - 2 \cos(\omega) - \omega \sin(\omega) \quad \text{Eq. 5-30}$$

The stability functions $S1_y$ through $S4_y$ can be calculated by replacing I_z by I_y in Eq. (5-17) through Eq. (5-30).

The stability function $S5$ can be calculated as follow:

For tension members (P is positive)

$$S5 = 1/\left[1 - EA(R_{iy} + R_{iz})/4P^3L^2\right] \quad \text{Eq. 5-31}$$

where

$$\begin{aligned} R_{iy} &= \omega_y (M1_y^2 + M2_y^2)(\coth(\omega_y) + \omega_y \cos ech^2(\omega_y)) \\ &- 2(M1_y + M2_y)^2 + (M1_y M2_y)(1 + \omega_y \coth(\omega_y))(2\omega_y \cos ech(\omega_y)) \end{aligned} \quad \text{Eq. 5-32}$$

$$\omega_y = \mu_y L \quad \text{Eq. 5-33}$$

$$\mu_y^2 = P/EI_y \quad \text{Eq. 5-34}$$

$$\begin{aligned} R_{iz} &= \omega_z (M1_z^2 + M2_z^2)(\coth(\omega_z) + \omega_z \cos ech^2(\omega_z)) \\ &- 2(M1_z + M2_z)^2 + (M1_z M2_z)(1 + \omega_z \coth(\omega_z))(2\omega_z \cos ech(\omega_z)) \end{aligned} \quad \text{Eq. 5-35}$$

$$\omega_z = \mu_z L \quad \text{Eq. 5-36}$$

$$\mu_z^2 = P/EI_z \quad \text{Eq. 5-37}$$

For a compression member (P is negative),

$$S5 = 1/\left[1 - EA(R_{cy} + R_{cz})/4P^3L^2\right] \quad \text{Eq. 5-38}$$

where

$$R_{cy} = \omega_y (M1_y^2 + M2_y^2) (\cot(\omega_y) + \omega_y \operatorname{cosec}^2(\omega_y)) - 2(M1_y + M2_y)^2 + (M1_y M2_y) (1 + \omega_y \cot(\omega_y)) (2\omega_y \operatorname{cosec}(\omega_y)) \quad \text{Eq. 5-39}$$

$$\omega_y = \mu_y L \quad \text{Eq. 5-40}$$

$$\mu_y^2 = P/EI_y \quad \text{Eq. 5-41}$$

$$R_{cz} = \omega_z (M1_z^2 + M2_z^2) (\cot(\omega_z) + \omega_z \operatorname{cosec}^2(\omega_z)) - 2(M1_z + M2_z)^2 + (M1_z M2_z) (1 + \omega_z \cot(\omega_z)) (2\omega_z \operatorname{cosec}(\omega_z)) \quad \text{Eq. 5-42}$$

$$\omega_z = \mu_z L \quad \text{Eq. 5-43}$$

$$\mu_z^2 = P/EI_z \quad \text{Eq. 5-44}$$

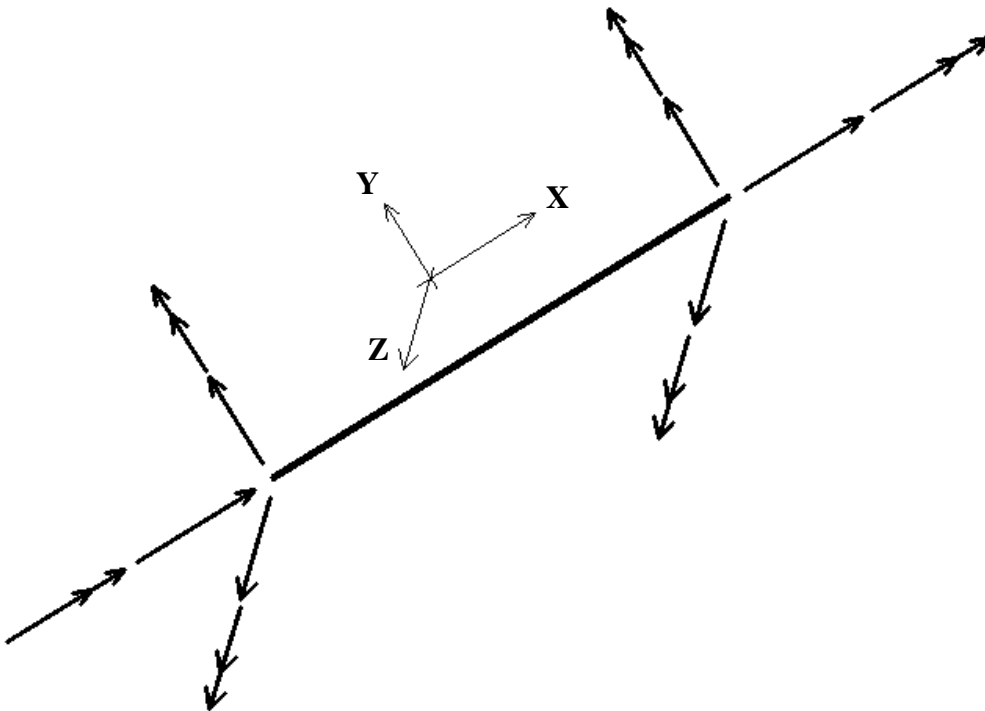


Fig. 5-22 Degrees of Freedom on Three Dimensional Frame Element in Local Coordinates

CHAPTER 6

DEVELOPMENT AND TESTING OF AN AEROELASTIC MODEL OF A GUYED TRANSMISSION LINE SYSTEM

6.1 Introduction

Transmission lines systems are responsible of transferring electricity from the source to the end users. Large transmission line systems such as the 500 (kv) are responsible for transferring electricity from generation stations to cities and counties, then distribution systems deliver the electricity inside cities. Transmission line systems travel for thousands of kilometers through different topographies and weather conditions. Failure of transmission lines can have significant social and economic impacts. A fact has proven during the 1998 Montreal snow storm and the 2003 northeast black out. The electrical company Ontario Hydro reported that five out of six weather-related line failures in their territory are due to high intensity wind (HIW), such as tornadoes and downbursts (Behncke and White 2006). In the United States, 800 to 1,000 high intensity wind storms occur each year causing extensive damages on transmission structures (Behncke and White 2006). The CIGRÉ (2006), a multinational committee, questionnaire on line failures indicated that 65% of weather-related events on transmission lines were caused by tornadoes. The structural components of a transmission line system are the towers, the conductors, the ground-wires, and the insulator strings. Although the tower's lattice form is favorable, the slenderness and flexibility of the system makes them vulnerable to strong wind loads. The transmission line system's response to wind load is nonlinear and complex due to both the large displacements of the towers and the significant movement

of the lines which can reach to same order of magnitude of the line's sag, as discussed in detail in Chapters 3, 4 and 5. In addition, the vertical conductor bundle deflects on an inclined plane under strong wind loads, different from the sagging observed under gravity on vertical planes. This deflection on inclined planes couples the in-plane and out-of-plane lines oscillations (Gattulli et al. 2007). Design codes and manuals of practice also recommend gust response factors to account for load amplification from dynamic response of structural components of a transmission line systems, e.g. towers and lines, to wind gusts. The recommendations include drag coefficients for various solidity ratios and shielding factors (ASCE 2010 and CIGRE` 2009). Although very useful and pragmatic, these recommendations are primarily derived from two dimensional and three dimensional lattice structure section tests and assume, uniformity of solidity ratio with in the section and do not consider among other things the following: (i) three dimensionality effects such as end effects, (ii) complex geometric variations with height (tapered towers, variable spacing of members along height and near the cross arms), and (iii) aeroelastic effects. Such complexity in the response of transmission line systems to normal wind requires the use of sophisticated numerical models or aeroelastic testing as performed in the current study.

There are various experimental, numerical and field studies reported in literature. Momomura et al. (1997) reported full-scale measurements of wind-induced vibration of a transmission line system in a mountainous area. The data was collected over a two year period, between 1991 and 1993. It was reported that the vibration characteristics and the total damping of the supporting towers are strongly influenced by the behaviour and the aerodynamic damping (measured up to 8% critical damping) of the conductors. The study

also concluded that the vibration mode shapes of the tower with conductors are similar to the mode shape of the tower without conductors. Loredou-Souza and Davenport (1998) investigated the effect of wind speeds and line's mass on the aerodynamic damping values of different lines in a boundary layer wind tunnel. The study concluded that the background response was the predominant contribution to the total fluctuation. The resonant component became more significant in the case of low wind speeds and heavier conductors, e.g. higher line mass. Loredou-Souza and Davenport (2001) also reported that it is very difficult to verify and measure full-scale aerodynamic behavior of transmission lines, and wind tunnel testing can be an acceptable alternative. Lin et al. (2012) studied a small scale aeroelastic model of a single transmission line span and a guyed transmission tower under boundary layer and downdraft wind. The study was conducted at a length scale of 1:100. The study concluded that the single span transmission line system has a quasi-static response to both boundary layer and downdraft wind. In addition, the resonant dynamic response was found to be less significant in the case of downdraft wind than boundary layer wind.

Extensive numerical studies were performed for transmission line system by (Shehata et al. 2005, Shehata and El Damatty 2007, Shehata and El Damatty 2008, Hamada 2009, Hamada et al. 2010, Hamada and El Damatty 2011, El Damatty and Hamada 2013) to assess the structural behaviour under computer simulated wind and HIW events such as downburst and tornadoes. The modelling and assessment of the behaviour of transmission lines under downburst loading was conducted by Shehata et al. (2005) and Shehata and El Damatty (2007). In these studies, a three dimensional finite element model simulating the towers and a two-dimensional model simulating the conductors were developed to

assess the structural performance of transmission towers under downburst loading. An extensive parametric study was conducted in the same investigations to evaluate the critical downburst loading cases. The studies carried out by Shehata et al. (2005) and Shehata and El Damatty (2007) was extended by Shehata and El Damatty (2008) to investigate the structural performance of the tower under these critical downburst loading cases. In the same study, the failure of a transmission tower during a downburst event, which occurred in Manitoba, Canada in 1996, was assessed. Hamada (2009), Hamada et al. (2010) and Hamada and El Damatty (2011) conducted a comprehensive study to assess the performance of transmission line structures under tornado loading. They investigated the variation of the tower members' internal forces with the tornado locations relative to the transmission line system. Their studies provided an insight into the structural response of the towers under tornado wind loads. For example, the dynamic effect associated with the translation motion of the tornado was assessed and the results of the parametric study were used to assess the sensitivity of the members' peak forces with the parameters defining the location of the tornado relative to the transmission line. Altalmas et al. (2012) and El Damatty and Hamada (2013) assessed the transmission lines' failure mechanisms under critical tornado configurations. In addition, the study predicted the maximum tornado velocity that various lines can withstand before experiencing global failure. Their studies also predicted the main type of failure experienced as well as the path of members susceptible to failure. Hamada and El Damatty (2013) assessed the behaviour of two guyed transmission line structures under F2 tornado wind field, boundary layer wind, electrical companies' recommended wind field, and CIGRE` recommended tornado loading cases.

The main objective of the current study is to investigate the aeroelastic characteristics of guyed lattice transmission line system, through a simultaneous testing of four aeroelastic guyed lattice towers and conductors. The transmission line system simulated in the current study is generic guyed transmission tower used by different hydro companies in North America and in different parts of the world. The aeroelastic model is designed for a geometry scale of 1:50 and tested in the Boundary Layer Wind Tunnel Laboratory (BLWTL) at the University of Western Ontario, Canada. The model is tested using an open exposure wind profile. The test is performed for three different wind directions and for two configurations, with and without the transmission lines (conductors and ground-wires). Such aeroelastic model of guyed transmission line system with multiple spans is not reported in literature. This represent a new contribution to the existing literature of the aeroelastic behavior of transmission lines under wind actions. The sub-objectives of the current study can be summarized as follow:

- Estimate accurately the overall wind load on transmission line system through a more accurate aeroelastic boundary layer wind tunnel testing
- Investigate the dynamic response of guyed transmission towers under fluctuating wind, and for different wind speeds
- Assess the effect of the conductors on the dynamic response of guyed transmission towers
- Assess the effect of the conductors on the overall structural response of the system.
- Assess the effect of the supporting guy's pretension on the natural frequency and mode shapes of the structure

- Validate the numerical model force calculations, drag, shielding by matching the overall reactions of the supporting guys and force balance
- Validate the finite element model of the transmission line system by matching the straining actions in the spine with the full tower numerical model results

6.2 Description of the Aeroelastic Model of Transmission Line System

6.2.1 Description of Transmission Line System

The guyed lattice transmission tower used in the present study is shown in Fig. 6-1. It has a total height of 44.39 (m) at full-scale. The tower is supported using four guys, which are connected to the tower using two guy's cross-arms, located at an elevation of 35.18 (m) from the ground level. Two conductor bundles are connected to the tower cross-arms using a 4.27 (m) insulator. The conductors are attached at an elevation of 38.23 (m). One ground-wire is connected to the top of the tower. The conductors and ground-wire spans used in the current study are 110 (m). The conductors and ground-wire sags are 5 (m). The supporting guys' cross-arms are orthogonal to the conductors' cross-arms. Steel angle members, L-shaped in cross-section, are used for all the transmission tower members. The transmission tower has an almost square plan view with a pinned base that allow rotation degrees of freedom and restrain translational and torsional ones.

The supporting guy system for the transmission tower consists of four guys with each guy cable consist of 11.68 (mm) diameter grade 225 galvanized steel wire. The presence of the supporting guys allow the use of narrow cross-section near the bottom of the transmission tower, as shown in Fig. 6-1. Two different initial pretension force of 7 and

10 (kN) are used. This pretension forces introduce an initial compression force to the vertical legs of the transmission tower beneath the guys' cross-arms. More details regarding the material and geometric properties of the conductors and ground-wire are provided by Shehata et al. (2005) and Hamada et al. (2010).

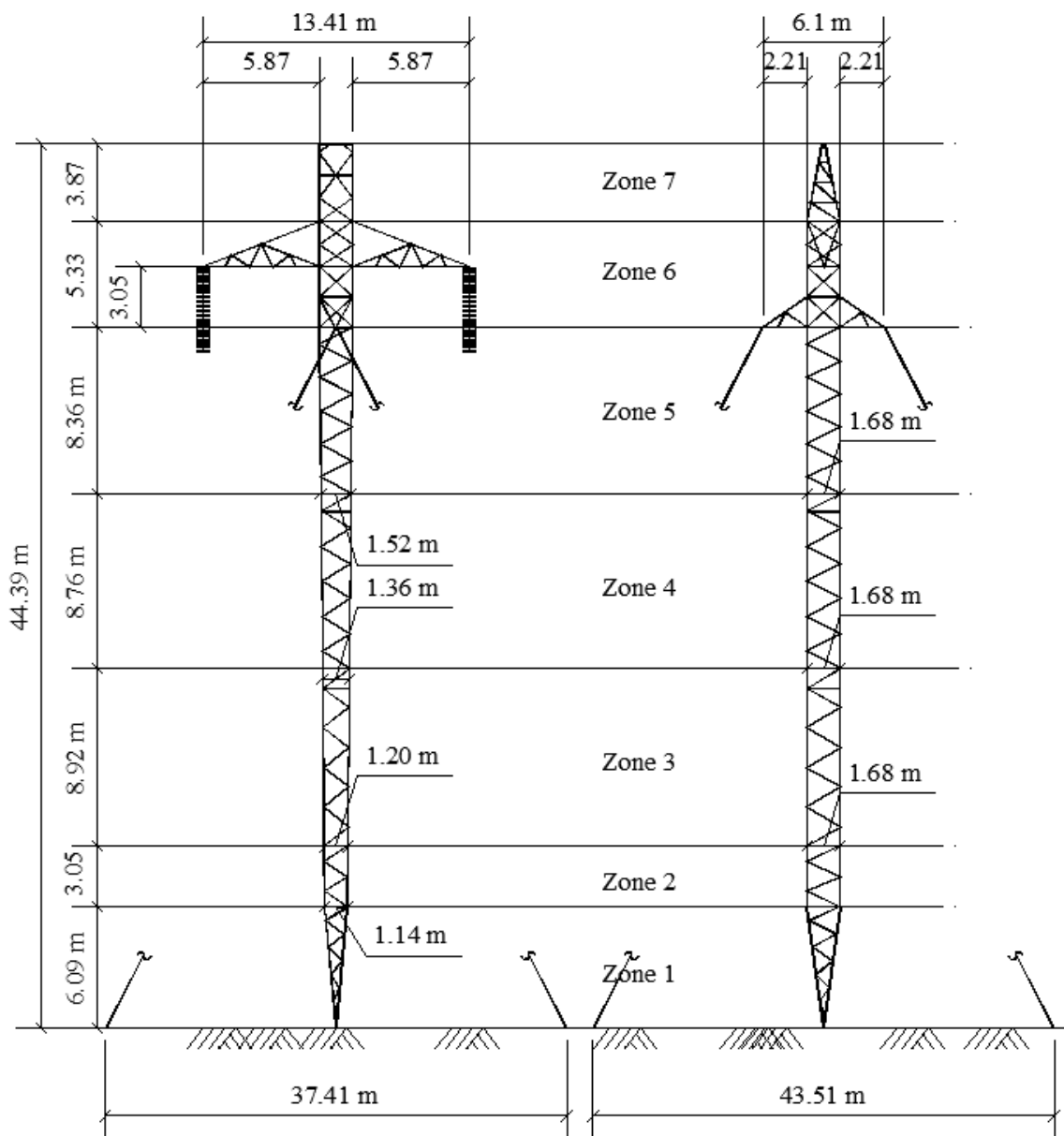


Fig. 6-1 Schematic of the Full-scale Guyed Transmission Tower

6.2.2 Dynamic Properties of Full-scale Transmission Line System

A schematic view of the developed nonlinear three dimensional finite element model of the full-scale transmission line system is shown in Fig. 6-2. As shown in the figure, the numerical simulation includes the tower of interest along with three conductor's spans along each side of the tower of interest. Simply supported conditions are assumed at the two far ends of the last conductors' span. Therefore, the numerical simulation includes five transmission towers with six bays of transmission lines (conductors and groundwires).

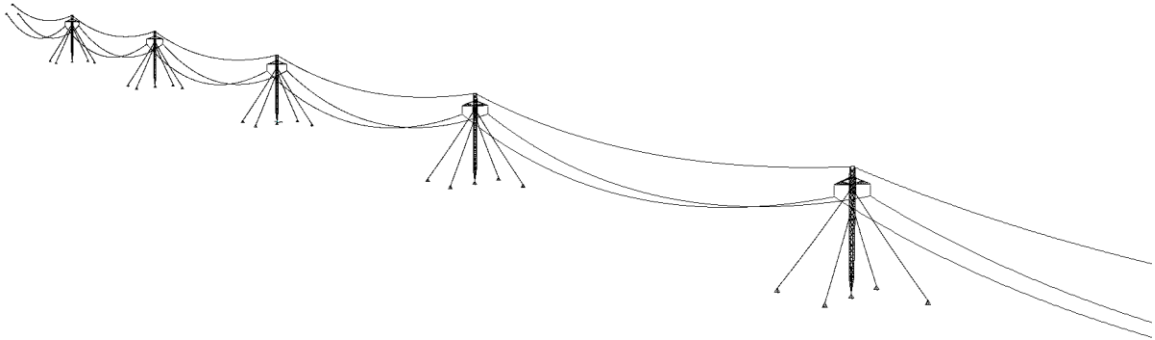


Fig. 6-2 Schematic View of the Three Dimensional Finite Element Model

6.2.2.1 Description of Transmission Line In-house Finite Element Model

The guyed transmission line system shown in Fig. 6-2 is modelled using the in-house nonlinear three dimensional finite element model that is developed in the previous Chapters. In summary, the transmission tower members are modelled using two-noded, three dimensional frame elements that takes into account the geometric nonlinear effect. Four-noded, nonlinear, three dimensional cable element is used to model the transmission

lines. The cable element has three translational degrees of freedom at each node. The cable element nonlinear formulation account for tension stiffness and geometric nonlinearities resulting from large displacements and the P-delta effect. Two-noded equivalent cable element is used to model the supporting guys. The equivalent cable elements accounts for the initial and variation of the pretension force and the tension stiffening of the supporting guys. More details regarding the finite element model are provided in Chapters 3 and 5.

6.2.2.2 Natural Frequency and Mode Shapes of the Transmission Line System

A free vibration analysis is conducted to estimate the natural frequency and mode shapes of the full-scale and the aeroelastic model of the transmission line systems. The free vibration analysis takes into account the tension stiffening resulting from the pretension force applied to the conductors, ground-wire and supporting guys. The free vibration analysis is calculated for the tower with and without the conductors and ground-wires. As concluded by Hamada and El Damatty (2011), the natural frequency and mode shapes of the towers are affected by the value of the initial pretension force applied to the supporting guys. The first two natural periods and frequencies of the tower together with the corresponding mode shapes are provided in Table 6-1 and Fig. 6-3, respectively. The results are presented for two cases representing different values for the guys pretension force. The first value of pretension force of 10 (kN) represents the recommended value by the Hydro Company. The second value of pretension force of 7 (kN) represents the slack case, which is affected by different parameters such as temperature change and

relaxation. It should be noted that the first vibration mode for the case of pretension force of 10 (kN) is along the conductors' direction (the Y-direction), and the second mode is along a perpendicular direction (the X-direction). For the case of pretension force of 7 (kN), the first vibration mode is perpendicular to the conductor's direction, and the second mode is along the conductors' direction.

Table 6-1 Frequencies and Damping of Full-scale Tower

Pretension Force (kN)	Full Transmission Tower				ASCE MOP. 74 (2010)		Normalized Aeroelastic Model		
	Mode	Direction	Period (sec)	Frequency (Hz)	Frequency (Hz)	Damping %	Direction	Frequency (Hz)	Damping %
10	1	X-Direction	0.685	1.46	2.0	4.0	X-Direction	1.55	2.65
	2	Y-Direction	0.709	1.41			Y-Direction	1.32	
7	1	Y-direction	0.826	1.21			Y-direction	1.30	3.2
	2	X-Direction	0.870	1.15			X-Direction	1.07	

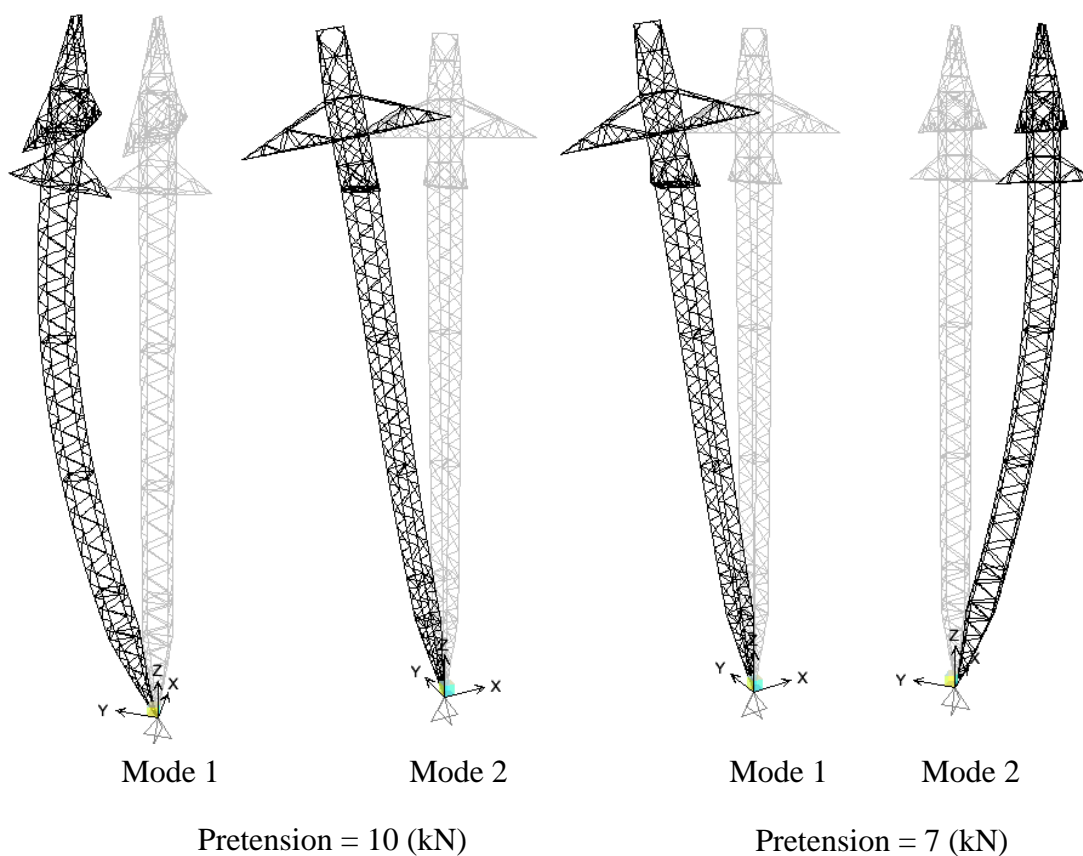


Fig. 6-3 First Two Mode Shapes of the Transmission Tower – (Pretension Force 10 and 7 (kN))

6.2.3 Aeroelastic Model and Testing Plan

The full aeroelastic model of the guyed transmission line system, shown in Fig. 6-4, was designed and constructed at a geometric scale of 1:50 relative to the full-scale. The aeroelastic model was designed to reproduce the structural and dynamic characteristics of the full-scale transmission line system. The Aeroelastic model of the guyed towers has the capability of changing the supporting guys pretension force that contribute to the overall stiffness of the tower and change the structural response. Three angles of attack (AOA), Yaw Ψ angles, are tested (i.e. AOA = 90, 75, and 30°). Fig. 6-4 shows the Ψ angle of 30°. Open terrain exposure with turbulence intensities of 17% is used. Thirty seven test wind speeds are used, ranging from 1.1 to 40.7 (m/sec) with an increment of 1.1 (m/sec) at full-scale. For each wind speed, the testing time is 2 min (14 minutes full-scale), followed by a 1 min of constant speed in order to give time to the wind flow to stabilize. The approach taken for the full aeroelastic model study is explained in detail by the Wind Tunnel Testing: A General Outline (2007) and Irwin (1982). The full aeroelastic model is studied in the 5 (m) wide low speed test section of the BLWTL II.

The aeroelastic model requires equality of the following non-dimensional quantities, between the model and full-scale, such as Froude Number, Cauchy Number, Density Ratio, Damping Ratio, and Reynolds Number. In addition, a geometric similarity is required. Since the lines and supporting guys both tension and sag under gravitational loads are important consideration in the dynamic response of transmission line structures,

hence the Froude Number scaling has to be considered. Froude Number is the ratio of the gravitational to inertia forces. Accordingly, the velocity scale is equal to the square root of the length scale, and time scale is equal to 1/velocity scale. The ratio of the elastic forces to the inertia force are represented through the non-dimensional Cauchy Number. This can be represented by the frequency ratio (frequency/time scale), which is maintained as a constant in both the model and full-scale for the modes of vibration. The Density Ratio is represented through the relation between the inertia forces of the structure to that of the flow. This ratio relates the aeroelastic model mass to the air flow in the wind tunnel. Since the air density of the test is assumed the same as that of the full-scale, the density ratio is taken equal to 1. The damping ratio is very critical for the dynamic response and the resonant motions of the structure. The model is designed to have as low a value of structural damping as possible to conservatively estimate the dynamic response and the magnitudes of the damping ratios are provided in Table 6-1. For sharp edged bluff structures, such as the angle members of the tower of interest, changes in Reynolds number of several orders of magnitude have negligible effect on wind forces (Irwin 1982). For circular members, such as the supporting guys and the conductors, the separation points of the wind around these members depend on Reynolds number. The Reynolds number for supporting guys and conductors are calculated for both the full-scale and the model. The variation of drag coefficient with Reynolds numbers graphs recommended by Holmes (2007), Vakil and Green (2009), and ASCE (2010) are used to check the variation in drag values.



Fig. 6-4 Assembled Aeroelastic Transmission Line Model ($\Psi = 30^\circ$)

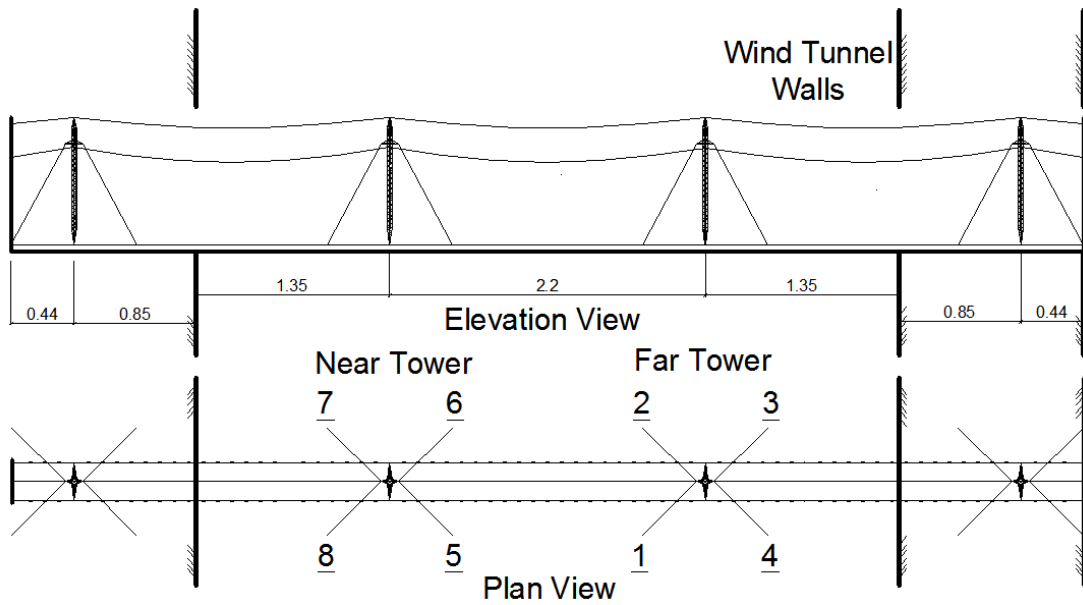


Fig. 6-5 Schematic of the Transmission line Full Aeroelastic Model

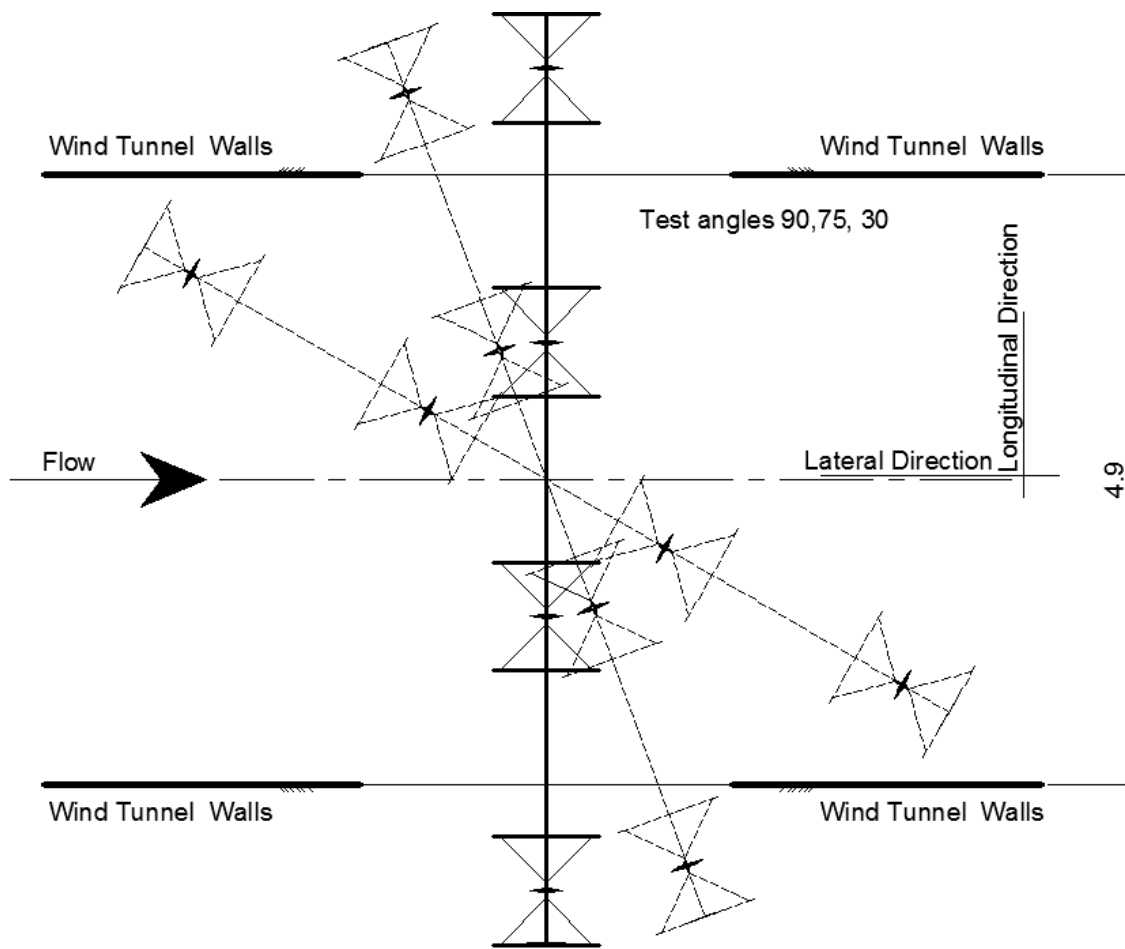


Fig. 6-6 Aeroelastic model Yaw angle ($\Psi = 90, 75, \text{ and } 30^\circ$)

Three full spans and four towers full aeroelastic model with different yaw angles Ψ of 90, 75, and 30° are tested, as shown in Fig. 6-5 and Fig. 6-6. The yaw (Ψ) angles are chosen based on the geometric scale and the BLWTL II width. The aeroelastic model is divided into four components: 1) transmission towers with supporting spines, 2) four supporting guys for each transmission tower, 3) two conductors and ground-wire, and 4) the bearings. Table 6-2 shows the scaling ratios of the physical parameters used in the current aeroelastic model.

Table 6-2 Scaling Ratio of Physical Parameters of the Aeroelastic Model

Parameters	Similitude Requirements	Scaling Ratio
Length	$\lambda_L = L_m / L_f$	1 : 50
Velocity	$\lambda_V = \lambda_L^{0.5}$	1 : 7.07
Time	$\lambda_T = \lambda_L / \lambda_V$	1 : 7.07
Density	$\lambda_\rho = \rho_m / \rho_f$	1 : 1
Mass	$\lambda_M = \lambda_\rho \lambda_L^3$	1 : 125,000
Mass Moment of Inertia	$\lambda_i = \lambda_M \lambda_L^2$	1 : 312,500,000
Acceleration	$\lambda_a = \lambda_V / \lambda_T$	1 : 1
Damping	$\lambda_\zeta = \zeta_m / \zeta_f$	1 : 1
Axial Stiffness	$\lambda_{EA} = \lambda_V^2 \lambda_L^2$	1 : 125,000
Bending Stiffness	$\lambda_{EI} = \lambda_V^2 \lambda_L^4$	1 : 312,500,000
Force	$\lambda_F = \lambda_V^2 \lambda_L^2$	1 : 125,000
Force / m'	$\lambda_f = \lambda_V^2 \lambda_L$	1 : 2,500
Bending and Torsional Moment	$\lambda_{BM-TM} = \lambda_V^2 \lambda_L^3$	1 : 6,250,000
Warping Stiffness	$\lambda_{CW} = \lambda_V^2 \lambda_L^6$	1 : 781,250,000,000

6.2.3.1 Transmission Tower and Spine

The elastic properties of the guyed lattice transmission tower are modelled by a central spine providing the adequate bending and torsional stiffness of the tower, as shown in Fig. 6-7 and Fig. 6-8. The spine is made of aluminum bar with different circular cross sections along the height as shown in Fig. 6-7. The choice of a circular spine is the most appropriate for wind tunnel tests with multiple angles of attacks. Both the flexural and torsional rigidity of the transmission tower components such as the vertical shaft, conductors' cross-arms, and guys' cross-arms are calculated and incorporated in the single spine and the equivalent conductor's and supporting guys' cross-arms. The conductors and guys' cross-arms are modelled as solid cylinder and rectangular sections,

respectively. Aluminum is used in order to achieve a light weight model to meet the mass scaling requirements, including the cladding mass, as shown in Table 6-3. In this table, a comparison between the full-scale and both the aeroelastic model and cladding is provided for the different tower sections.

The tower cladding is segmented into parts to allow wind induced tower movement during the wind tunnel test. However it is installed continuously along the tower height and fixed at a single point to the central spine which has negligible effect on the stiffness of the spine. The cladding is made of plastic materials and provides proper mass and geometric shape to simulate the aerodynamic forces. The cladding segments are affixed to the central spine through a plastic clamp located at the middle of the cladding sections. In order to assess the effect of the central spine on the aerodynamic characteristics of the transmission tower, the results recommended by Kong, et al. (2009) are used. Kong, et al. (2009) studied the wind action on a four-sided 102 (m) high guyed mast which was constructed primarily of angle section for the chord and diagonal members. Kong, et al. (2009) aeroelastic model was developed similar to the current model, with an aluminum circular central spine. Several aerodynamic section-models were constructed and tested to assess the effect of this central spine on the overall aerodynamic forces. The aerodynamic models were geometrically scaled from the full-scale tower, the first model with a 15% reduction of the member widths, the second model with a 20% reduction of the widths, and the third model with 30% reduction of the member widths. The study concluded that a 15% reduction of member areas leads to drag forces on the combined spine and cladding are closest to the target values for angles of attack 0 and 90°. In addition, the

study done by kong et al. (2009) concluded that it would be highly unlikely that the tower would experience aerodynamic instability, even with very small damping of 0.1%.

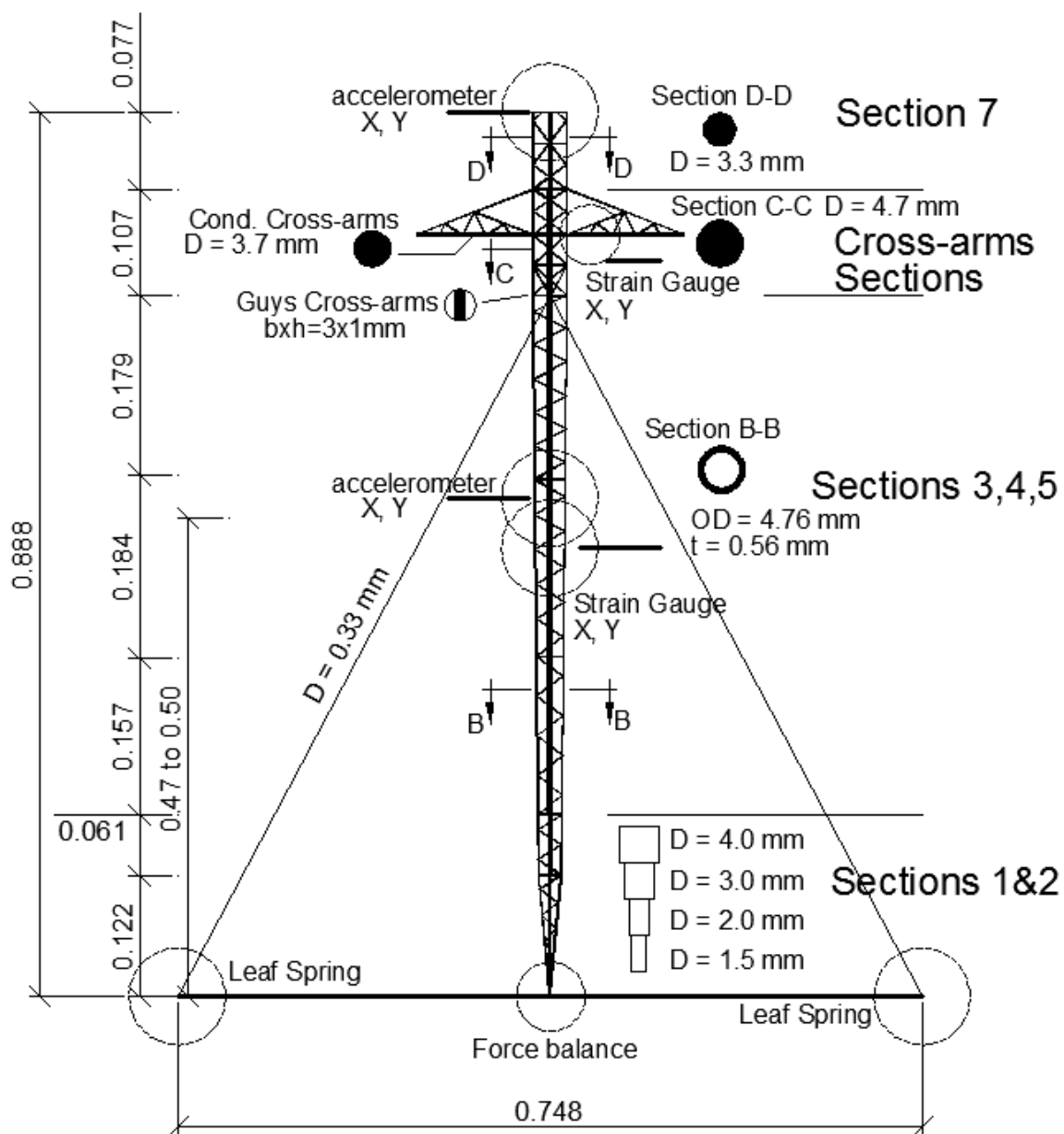


Fig. 6-7 The 1:50 Scale of Transmission Tower Aeroelastic Model



Fig. 6-8 Assembled Transmission Tower Aeroelastic Model

Table 6-3 Matching Tower Mass to Spine Mass

Tower Section	Tower Mass (kg)	Spine Mass (kg)	Cladding Mass (kg)	%
Sections 1 and 2	0.0368	0.0309	0.0055	99
Sections 3, 4, and 5	0.1260	0.1023	0.0189	96
Cross-arms	0.1040	0.0910	0.0156	103
Section 7	0.0200	0.0175	0.0030	103

6.2.3.2 Supporting Guys and Insulators

The four supporting guys are modelled by 0.33 (mm) diameter aircraft cables. This diameter is chosen to provide the appropriate scaled mass and wind-induced drag force. The aerodynamic drag is calculated by accounting the difference in Reynolds number between the full-scale and modelled wire using the value of an infinitely long cylinder. For the two middle towers, the equivalent axial stiffness of each supporting guy is provided by a calibrated leaf spring attached to the end of each supporting guy, as shown in Fig. 6-9. Strain gauges are fixed to each leaf spring in order to permit the adjustment of the supporting guys' pre-tension force to the desired values. As for the two edge towers, the axial stiffness is simulated using stainless steel coiled extensional springs.

The insulators strings are modelled with wood cylinders, as shown in Fig. 6-8. Wood is used to simulate the exact scaled mass and drag of the insulator springs. The insulators

are attached to the conductors' cross-arms by a very small diameter wire (0.18 mm). The conductors are attached to stainless steel coiled extensional springs that are hooked to end of the insulator spring. Accordingly, the insulators are allowed to swing freely under the actions of the wind on the conductors and the insulators.



Fig. 6-9 Supporting Guys Anchorage and Pretension Adjustment and Measurements

6.2.3.3 Conductors and Ground-wire

Each conductor bundle is modelled as a single steel cable with a diameter of 0.61 (mm) to match the conductors bundle mass. Foam cylinders, shown in Fig. 6-8, are added to the cables to match the scaled drag that is corrected for the difference in Reynolds numbers between the full-scale and modelled conductors. The conductor's end is connected with

stainless steel coiled extensional springs that can be moved as needed. The extension spring are chosen to simulate the axial stiffness of the scaled conductors.

The ground-wire is modelled as a single steel cable with a diameter of 0.18 (mm) to match the ground-wire mass and axial stiffness. The scaled ground-wire drag matches the target value within a 10% difference than the desired aerodynamic drag.

6.2.3.4 Bearings



Fig. 6-10 2-DOF Universal Base Support

The four spines are mounted on two degrees of freedom universal support systems shown in Fig. 6-10. The torsional motion is completely restrained, as well as all translations degree of freedom, while allowing base rotations. As for the two central spines, the universal supports are mounted on force balance shown in Fig. 6-10 that can measure the tower base reactions. The four supporting guys of each tower ends with a leaf spring that simulates the axial stiffness.

6.2.3.5 Model Instrumentation

Strain gauges are mounted at two locations on the two central transmission tower's spines as shown in Fig. 6-7. The first location is at almost the mid-height of the spine, where the maximum bending is expected and based on the transmission tower mode shapes shown in Fig. 6-3. The second location is at the conductors cross-arms to assess the contribution of the transmission lines on the overall forces in the supporting towers. The gauges are arranged in pairs, with each gauge attached to the opposing spine face as its partner. Two pairs are aligned to the longitudinal direction of the transmission line system, and the other two pairs are in the transverse direction. The strain gauges are calibrated prior the assembly process by clamping the spine as a cantilever beam subjected to incrementally increasing loads. For each strain gauges pair, the relation between the voltage output and the applied force is determined. The estimated bending moment uncertainty is less than $\pm 7\%$

Strain gauges are mounted on the leaf springs for both the central towers' supporting guys. Similar to the strain gauges on the spines, the strain gauges on leaf springs are calibrated. The estimated strain measurements uncertainty is $\pm 5\%$. In addition, the leaf

springs and extensional coil springs stiffness are calibrated by incrementally applying loads and measuring displacements.

Accelerometers are mounted at two locations on the two central transmission towers' spines as shown in Fig. 6-7. At each location, the accelerometers are placed in the X and Y (longitudinal and transverse) directions. Measurements are taken in the longitudinal and transverse directions for both locations. The first location is at mid-height of the spine, while the second location is at the top of the spine. These two locations are chosen based on the expected mode shapes of the transmission tower that are shown in Fig. 6-3.

6.2.3.6 Wind Profile

The full aeroelastic model is tested with class 3 flat open terrain (Exposure C) that is described by the ASCE (2012) as $Z_0 = 0.03$ (m) and $Z_g = 275$ (m). The wind speed scale is 1:7.07 based on the geometric scale and Froude number relation. A reference velocity profile is performed at the center location, location 1 shown in Fig. 6-12. The vertical profile of the normalized mean wind speed and the longitudinal turbulence (I_{uu}) at the center location are shown in Fig. 6-11. A reference height of 37.5 (m) is chosen, where the conductors' cross-arms are located. The profile measurements are done using Cobra probs, where the mean velocity and turbulent intensities on the three main axes are measured. The sampling time is 180 sec (20 minutes at full-scale). Such a long aeroelastic model requires different locations for profile measurements. Six velocity measurement locations, shown in Fig. 6-12, are chosen based on the length and width of the aeroelastic model of the transmission line system. The other profile measurements' locations are referenced to the center profile Table 6-4 shows both the normalized mean

wind speed at reference height and the longitudinal turbulence (I_{uu}) at the seven velocity measurement locations. The results presented in the table show negligible differences in the mean wind speed and turbulence intensities between the all seven locations of velocity measurements. The mean velocity and turbulence intensity profiles are matched to an Engineering Sciences Data Unit (ESDU) profile for open terrain by setting the height of roughness elements along the test section fetch to three urban sheets and eight suburban sheets followed by installing a barrier of 0.38 (m) height and installing four spires at the test section inlet, as shown in Fig. 6-4. The turbulence intensity in the flow direction is approximately 17% at the reference height, as shown in Fig. 6-11.

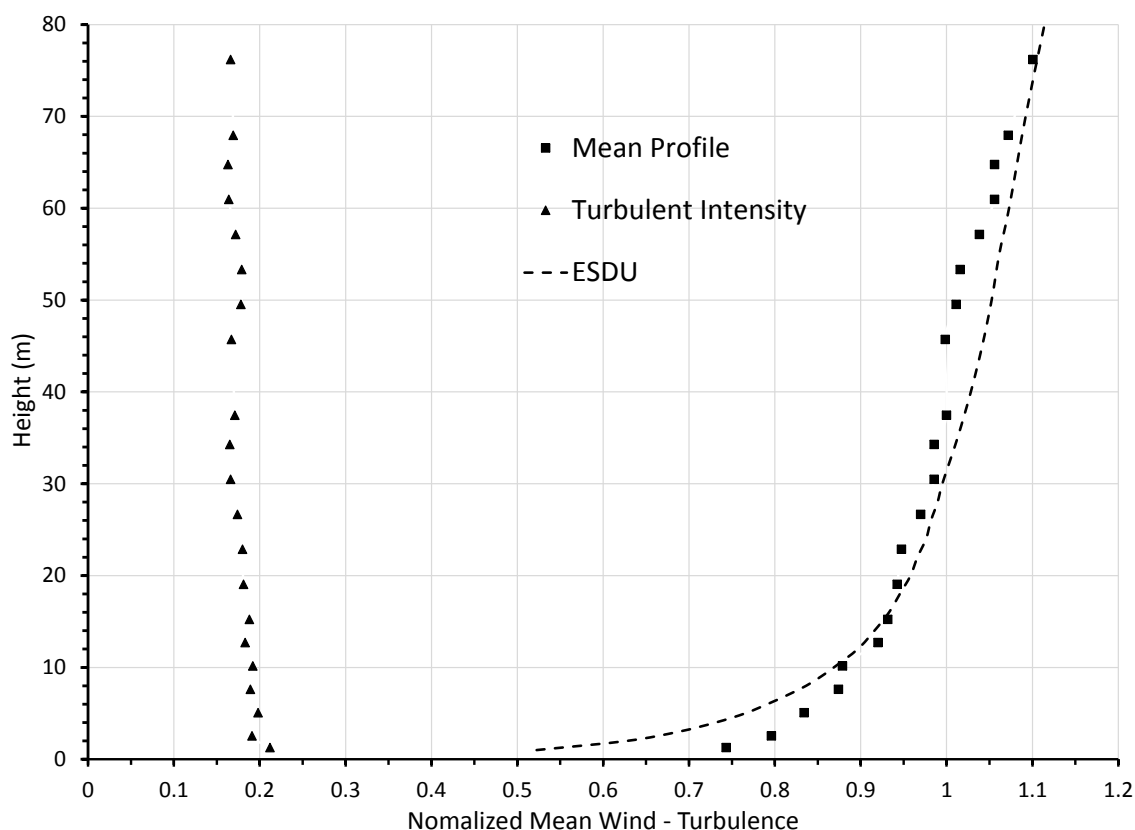


Fig. 6-11 Vertical Profile of Mean Wind Speed and Longitudinal Turbulence Intensity Measured at the Center Location, (Reference Wind 46.7 m/sec)

Table 6-4 Normalized Mean Wind Speed at Reference Height and the Longitudinal Turbulence at the Different Velocity Measurement Locations

Locations (ref. height 37.5 m)	Normalized Full Scale Mean Wind Speed	Turbulence Intensity Iuu %
1	1	17.1
2	1.01	17.8
3	0.99	17.3
4	1.01	17.2
5	1.005	17.3
6	0.95	16.7
7	0.95	17.1

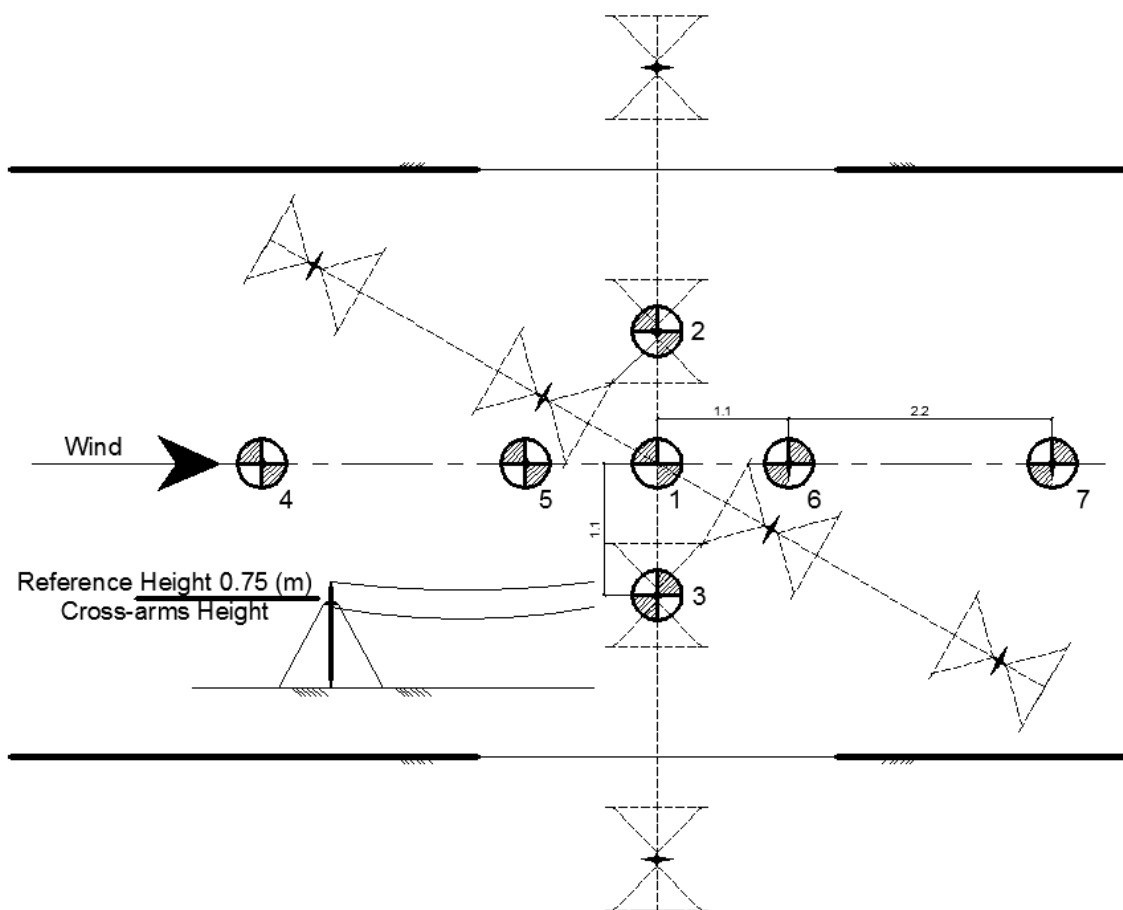


Fig. 6-12 Wind Profile Test Locations

6.3 Results and Discussion

The results presented in the current Chapter is only for the test with yaw (Ψ) angle equal to 90° , as shown in Fig. 6-13. This case is chosen to assess the objectives of the current chapter as discussed in detail in the following sections.



Fig. 6-13 Assembled Aeroelastic Transmission Line Model ($\Psi = 90^\circ$)

6.3.1 Mode Shapes Frequencies and Damping

A free vibration analysis is conducted to estimate the natural frequency and damping of the aeroelastic model of the transmission line system. The analysis is performed twice with an equivalent full-scale pretension force of 10 and 7 (kN). The measured first two

mode shapes' frequency of both cases are presented in Table 6-1. The aeroelastic model frequencies are in good agreement with both the results predicted by the developed in-house finite element model and the values recommended for lattice transmission lines by the ASCE (2010). The measured damping ratios from the aeroelastic model, shown in Table 6-1, are lower than the values recommended by the ASCE (2010), and matches the Momomura et al. (1997) measurements of full-scale transmission tower damping of 1.7 to 3.3% critical damping ratios. The low damping ratios of the aeroelastic model enables the identification of possible instabilities under the action of wind.

6.3.2 Accelerometer Results

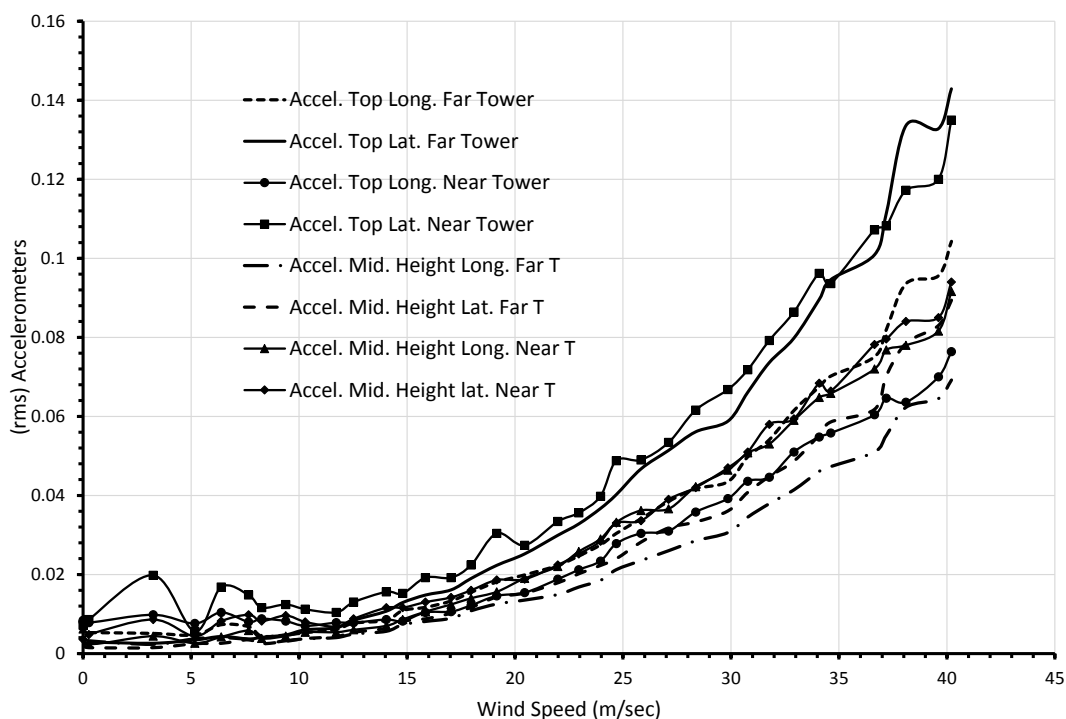


Fig. 6-14 Relation between Accelerometers rms and Wind Speeds (m/sec) for Both Towers – Case of Towers only

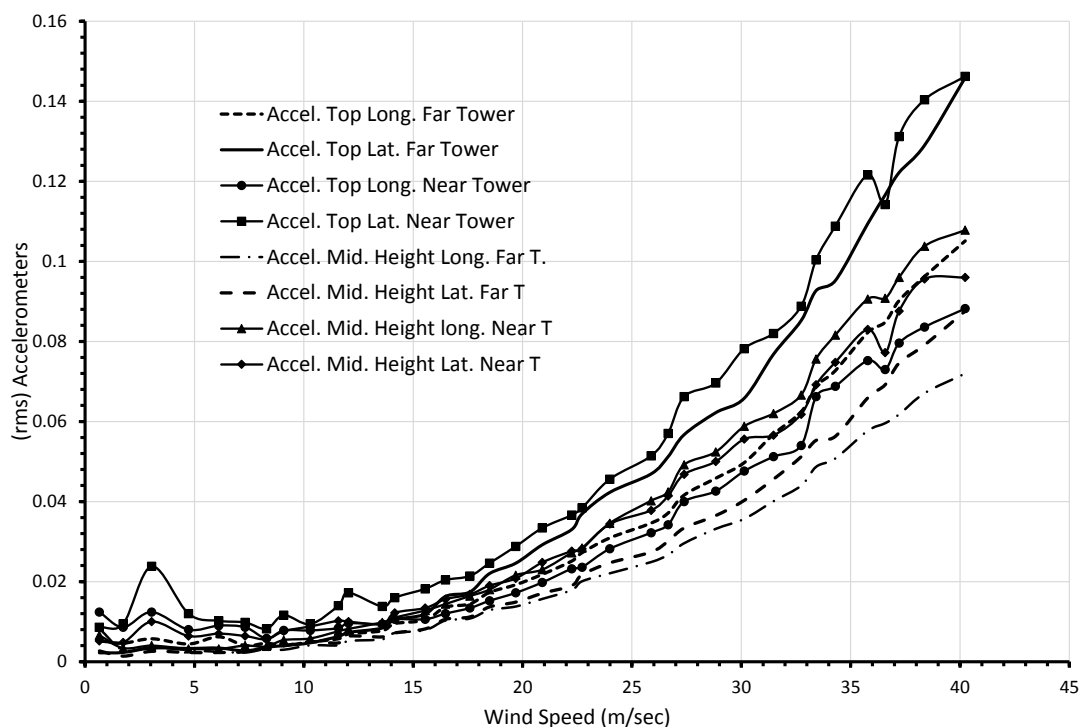


Fig. 6-15 Relation between Accelerometers rms values and Wind Speeds (m/sec) for Both Towers – Case of Towers with Conductors

Based on visual observations of the aeroelastic model under all test wind speeds, no instabilities are observed. In order to verify that, the relation between the root mean square (rms) of the four accelerometers and the different wind speeds of both towers is shown in Fig. 6-14 and Fig. 6-15 for the far and near towers. Fig. 6-14 shows the results for the tower with no conductors attached, and Fig. 6-15 shows the results with the conductors attached to the tower. As shown in the figure, the accelerometers rms values at different wind speeds are following an exponential curve, similar to the variation of the applied force with velocity square. This behaviour matches the response values for acceleration that was measured from a full-scale transmission line system by Momomura

et al. (1997). Momomura et al. (1997) concluded that the acceleration response increases in proportion to the power of the wind speed, with a power index generally less than 2. The acceleration values at the top of the tower in the same direction of the wind flow (lateral direction) are found to be the maximum. Some minor instabilities are observed for the top accelerometer in the lateral direction at low speeds, as shown in Fig. 6-14 and Fig. 6-15. By investigating the results, the vibration frequency leading to these instabilities is found to be 34 Hz. This is due to vortex shedding or instabilities caused at the insulator springs.

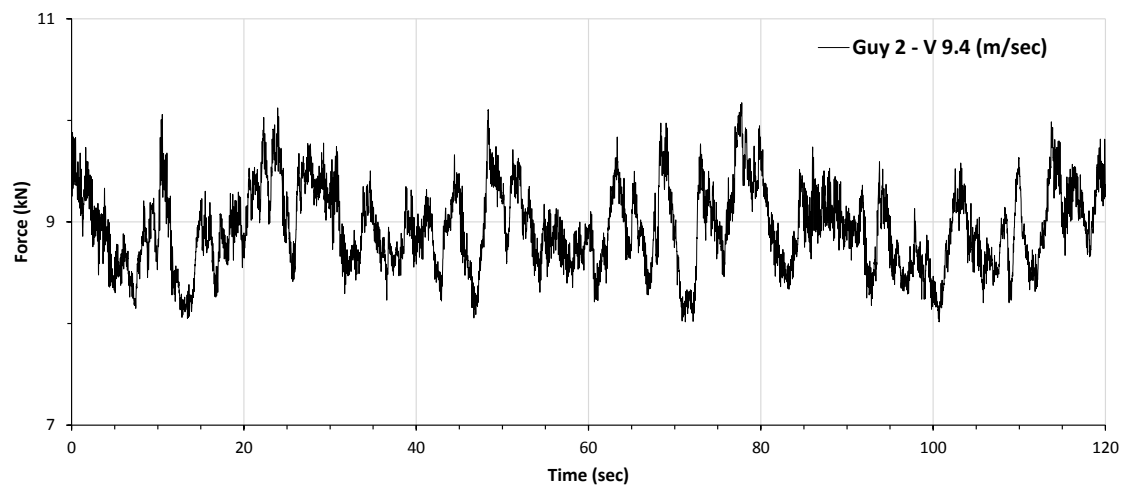
6.3.3 Tower Supporting Guy Forces

Guyed towers are challenging to analyze in comparison to self-supported towers, as the supporting guys' location, guys' pretension force, and response to wind loads affect the overall structural response and load path of the transmission tower. A clear evidence is noticed in the variation of the tower modes shapes and frequencies based on the value of the pretension force of the towers. In the following sections, the response of supporting guys of transmission towers for yaw (Ψ) angle of 90° of both with and without conductors are investigated.

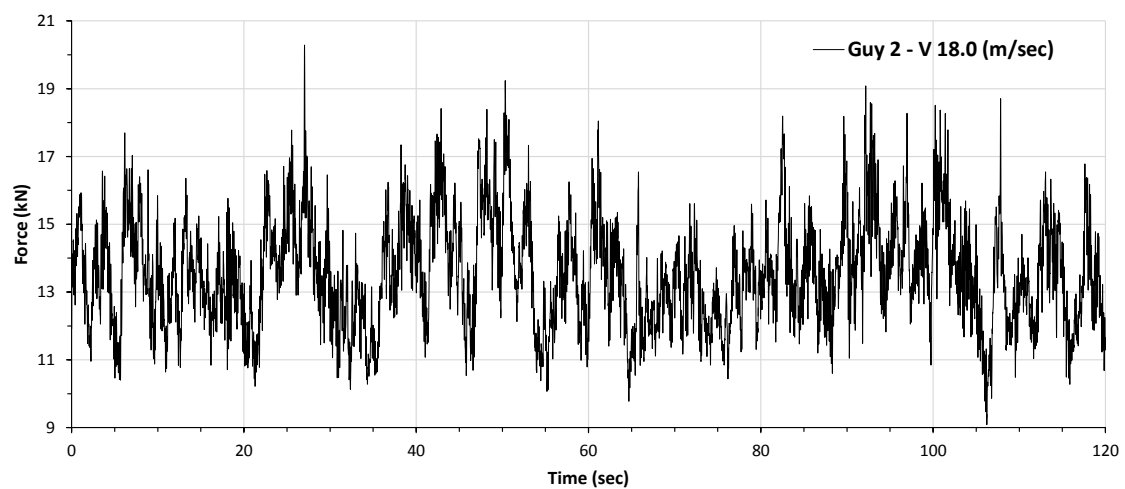
6.3.3.1 Tower Supporting Guys Forces without Conductors

The time history response of each of the four supporting guys of each tower are measured for each of the 37 wind speeds over 2 mins (14 minutes full-scale). The response time histories for the supporting guy number 2 for 9.4, 18.0, 27.0, and 36.6 (m/sec) reference

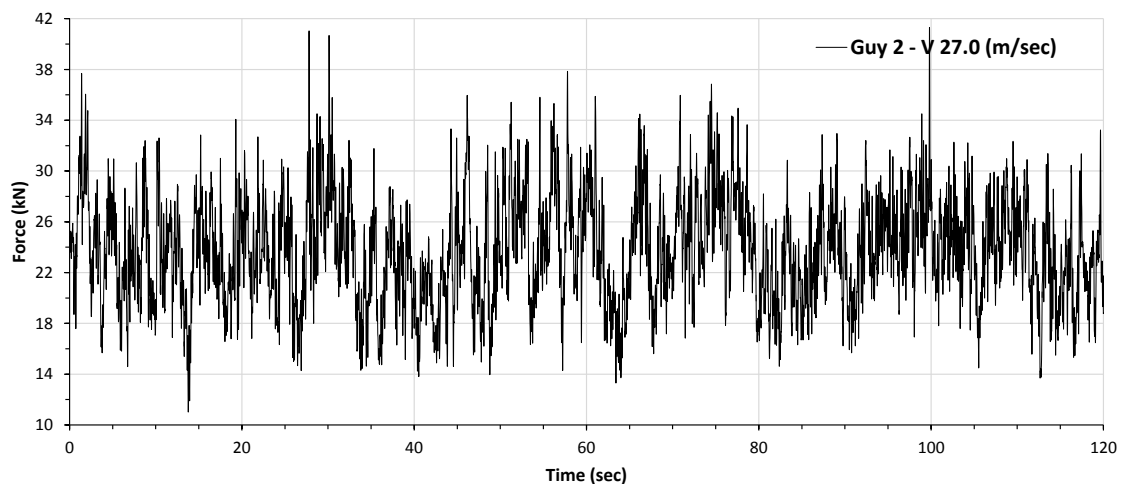
wind speeds as shown in Fig. 6-16. These wind speeds are measured at the reference height, which coincides with the cross-arms height.



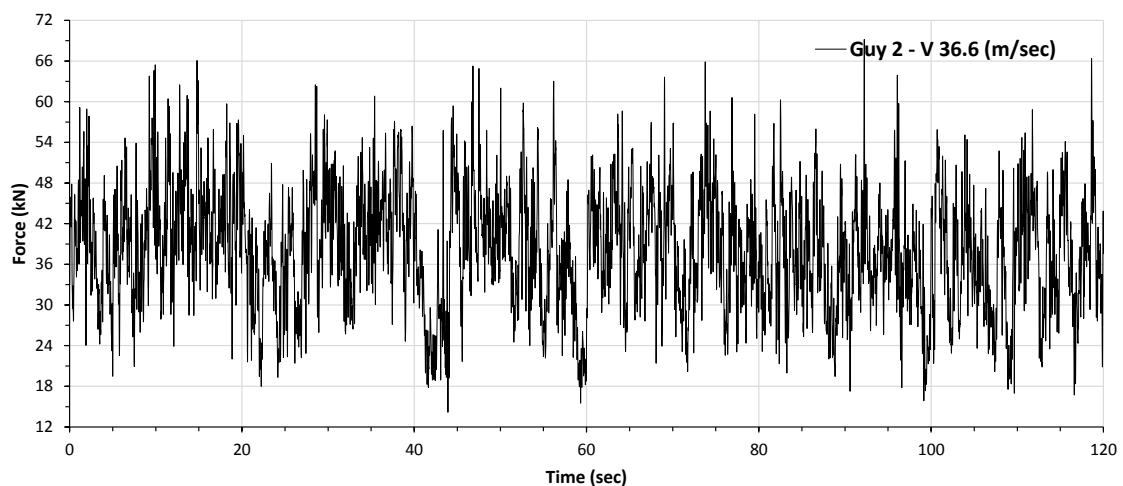
a) Reference Wind Speed = 9.4 (m/sec)



b) Reference Wind Speed = 18.0 (m/sec)



c) Reference Wind Speed = 27.0 (m/sec)

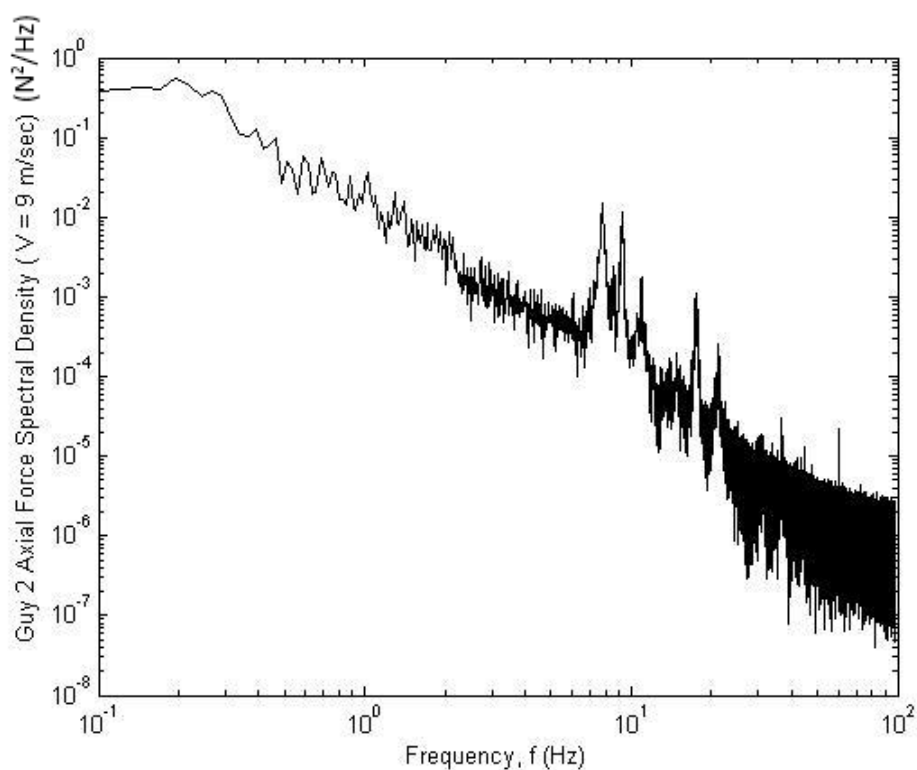


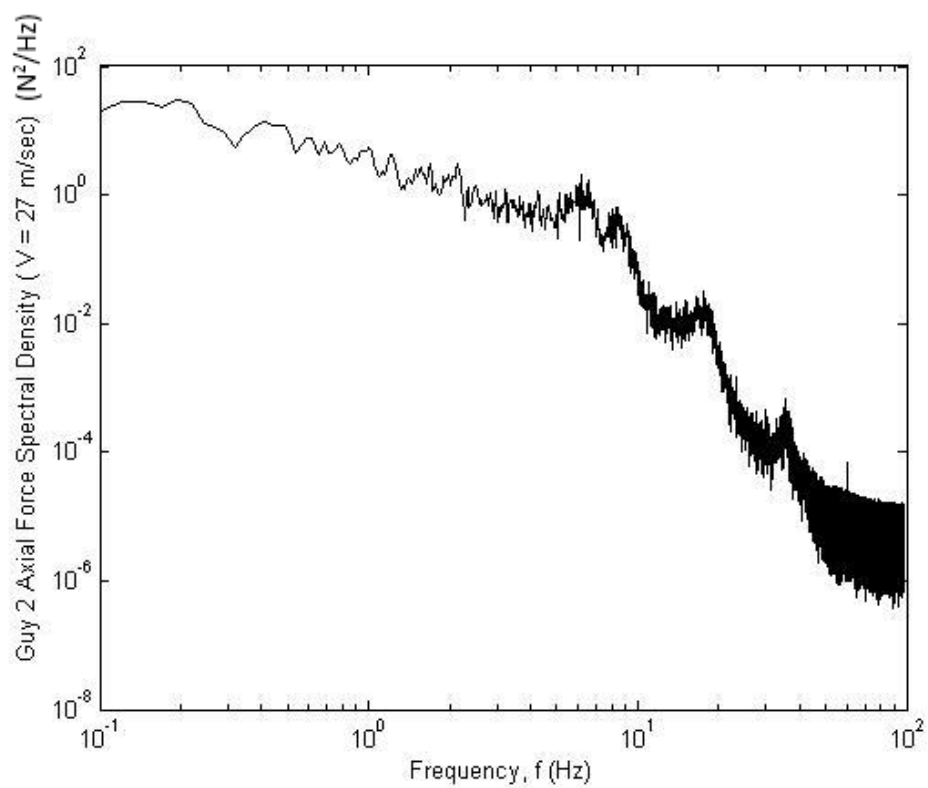
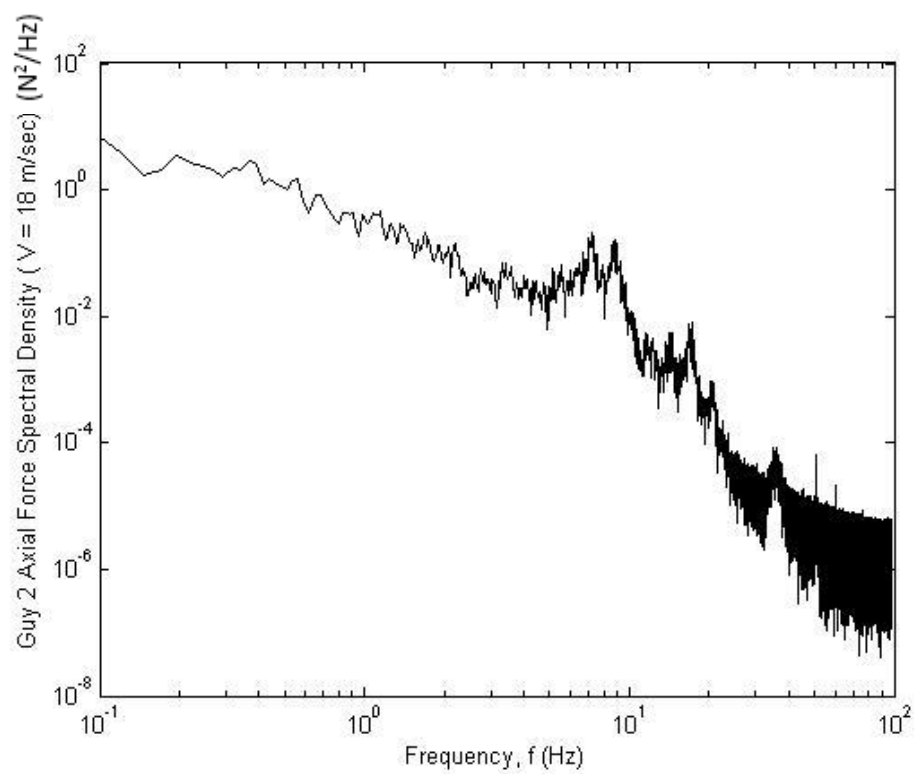
d) Reference Wind Speed = 36.6 (m/sec)

Fig. 6-16 Time Histories of Measured Supporting Guy 2 Axial Force for Different Wind Speeds – without Conductors Case

Fig. 6-17 shows the far tower supporting guy 2 response spectral density determined by spectral estimation from the fluctuating component of the axial force in guy 2 shown in Fig. 6-16. Resonant dynamic response can be distinguished from the background

response especially in low wind speeds. For low wind speeds (9 m/sec), the first resonant mode is centered a frequency of 8.0 Hz. With increasing the wind speed, the resonant peak is shifted slightly to 7 Hz, but with a widened band width and becomes less distinguished. A second peak is noticed at a frequency of 9.5 Hz, and is decreased until vanished by the increase of the wind speed. With time scaling of 1:7.07, the aeroelastic model, without conductors, predicted a fundamental frequency of 1.15 Hz for the full-scale transmission tower. This matches the results shown in Table 6-1.





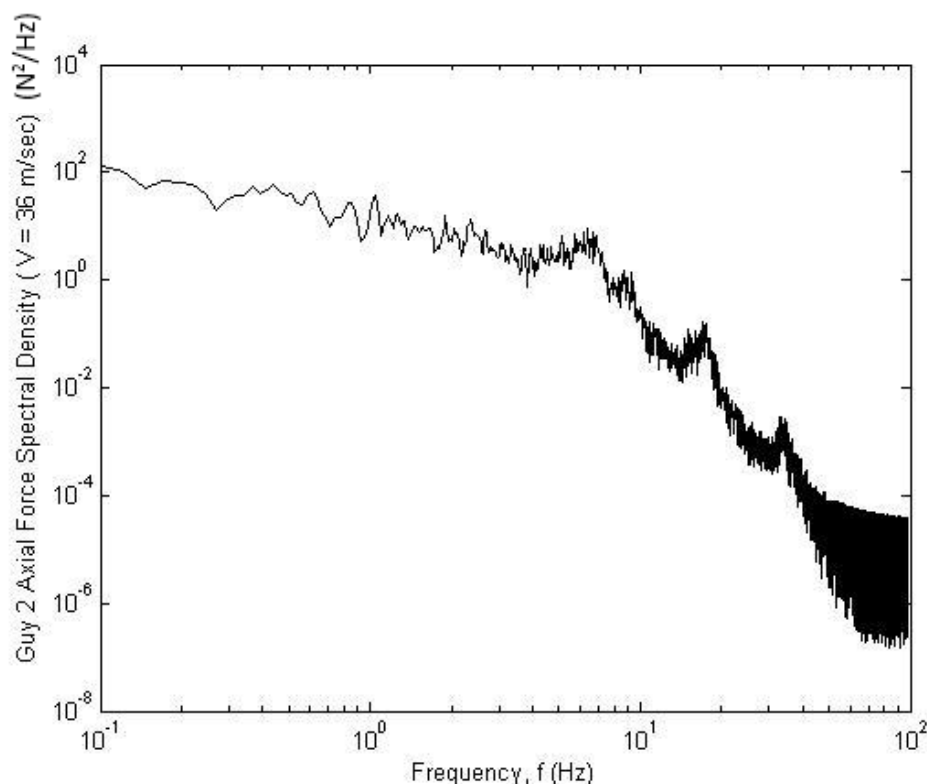


Fig. 6-17 Boundary Layer Supporting Guy 2 Response Spectra due to Reference Mean Wind Speed of 9.4, 18.0, 27.0, and 36.6 (m/sec), Respectively

The variation of the axial force of the supporting guy number 2 with different wind speed is shown in Fig. 6-18. As shown in the figure, the structural response of the supporting guy is following an exponential curve, similar to the variation of the applied force with velocity square. Similar results was concluded by Momomura et al. (1997) based on a full-scale measurements of transmission line system. Momomura et al. (1997) results shows increase in the tower response proportion to the power of the wind speed, with a power index generally less than 2.

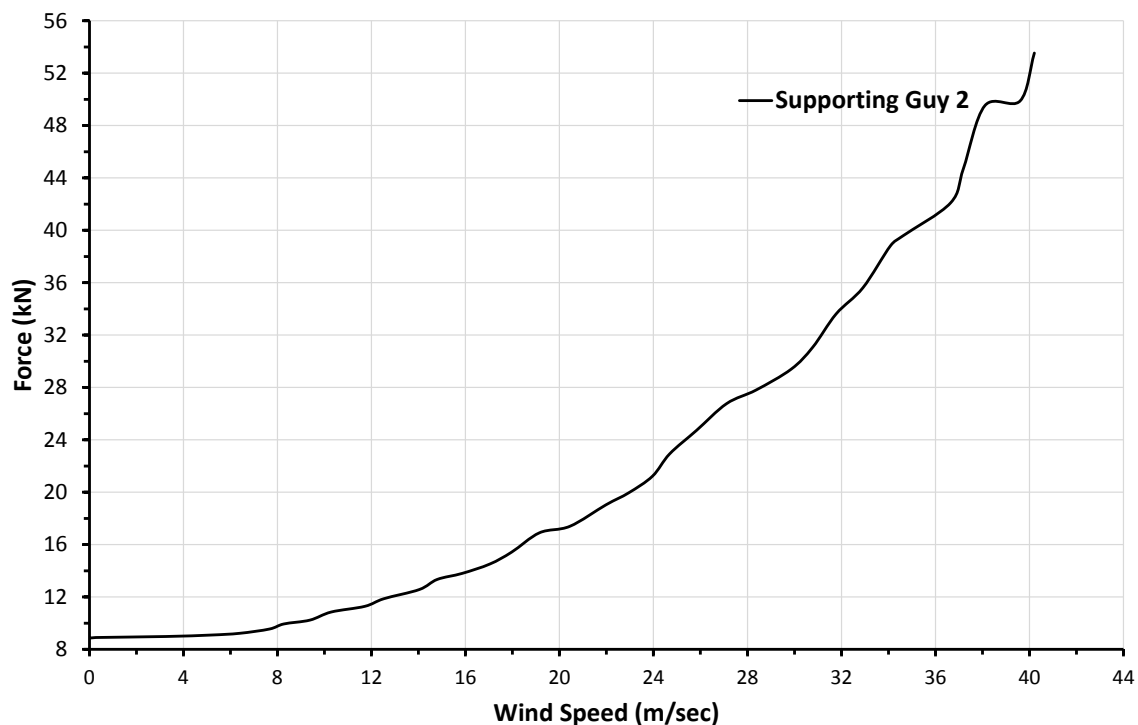
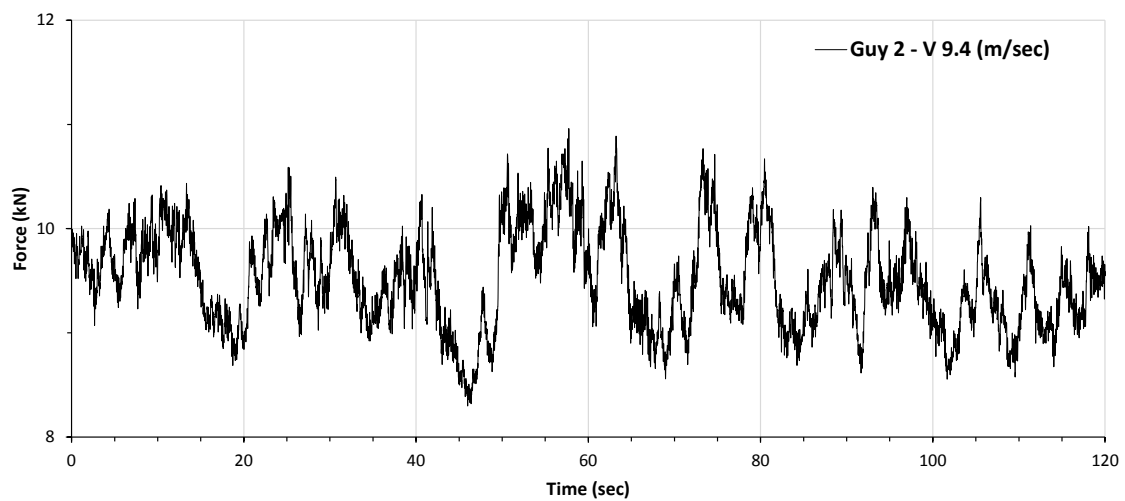
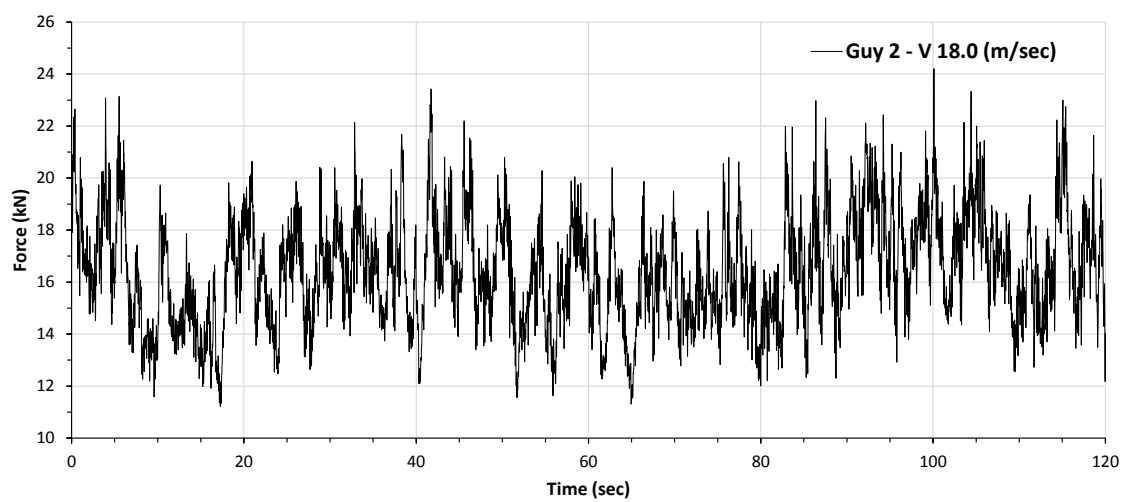
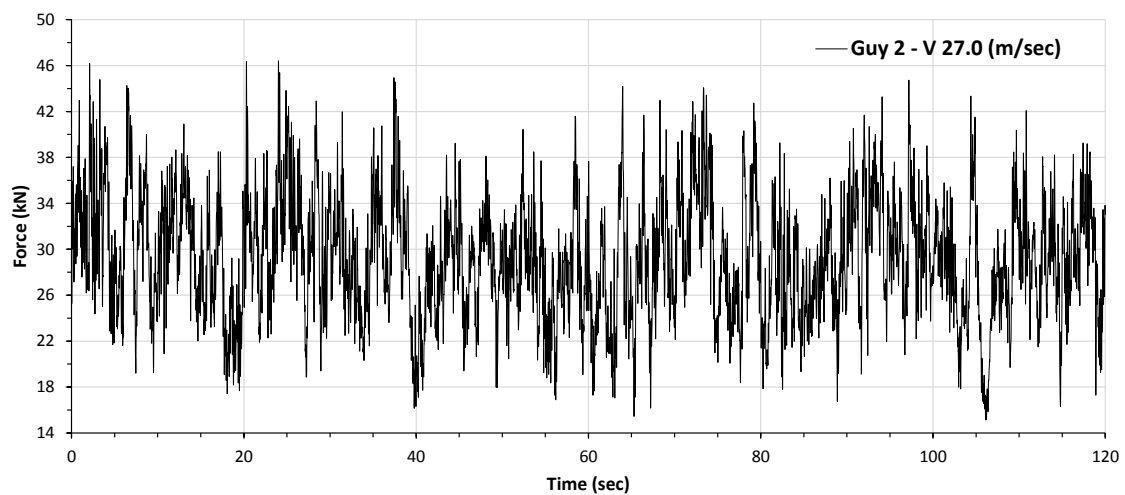


Fig. 6-18 Variation of the Internal Force of the Supporting Guy 2 with Different Wind Speeds

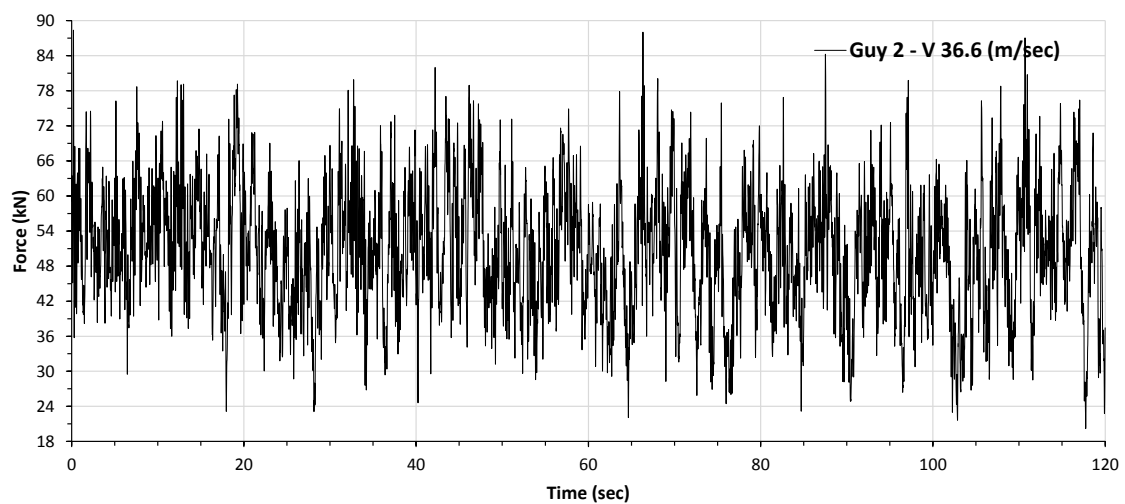
6.3.3.2 Tower Supporting Guys Forces with Conductors

The time history responses shown in the previous sections are presented in the current section but for the configuration where conductors are attached to the transmission towers. The response time histories are presented for the same supporting guy, guy 2, and at the same selected test wind speeds. These time histories are shown in Fig. 6-19. These wind speeds are selected as a representation of the results.

a) Reference Wind Speed $V = 9.40$ (m/sec)b) Reference Wind Speed $V = 18.0$ (m/sec)



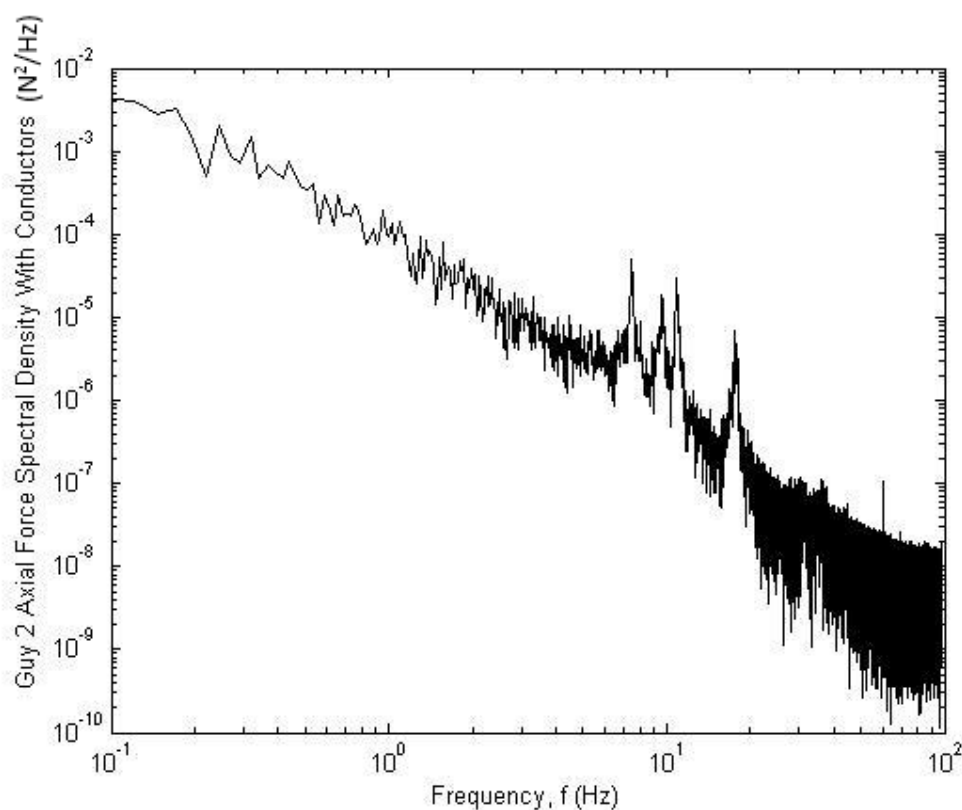
c) Reference Wind Speed $V = 27.0$ (m/sec)

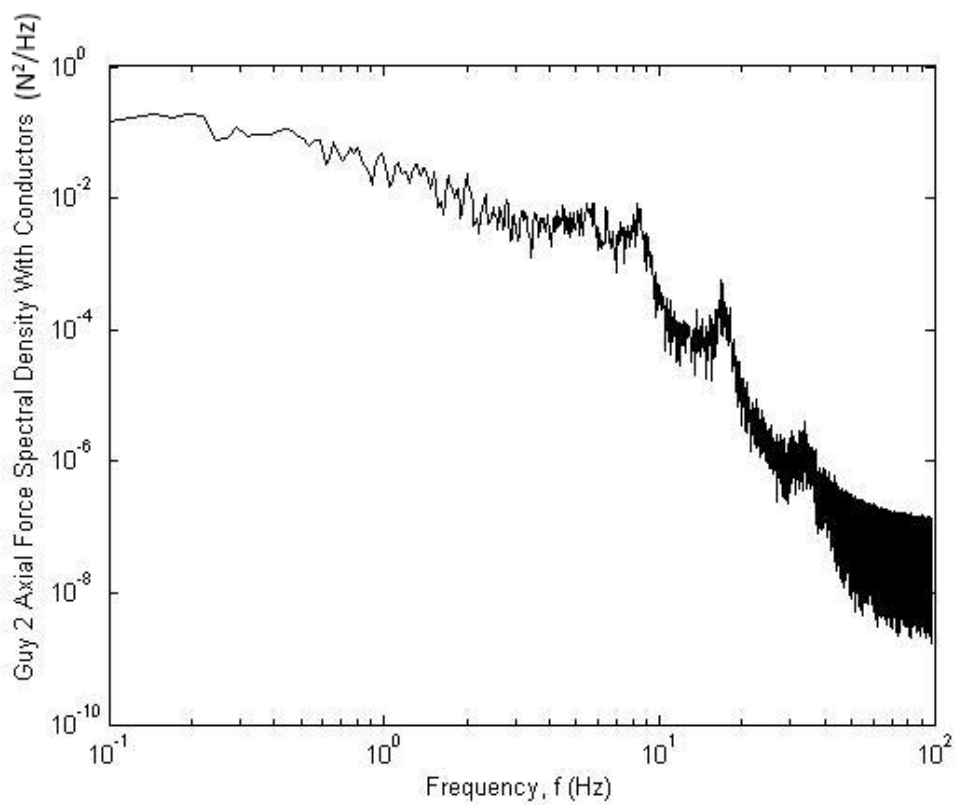
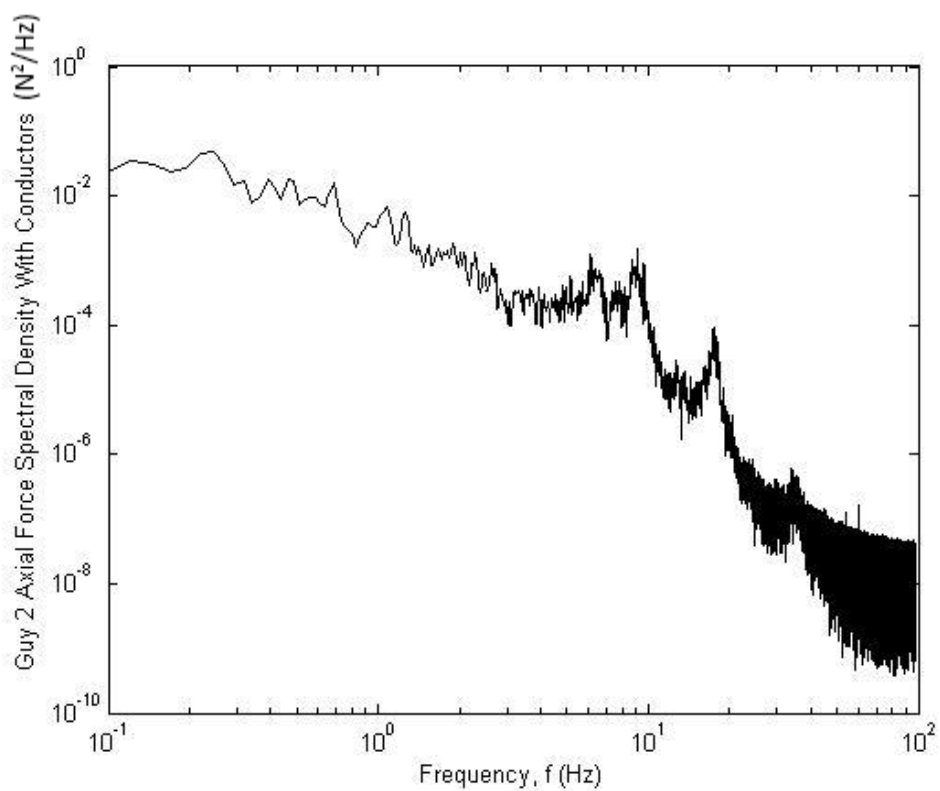


d) Reference Wind Speed $V = 36.6$ (m/sec)

Fig. 6-19 Time Histories of Measured Supporting Guy 2 Axial Force for Different Wind Speeds – with Conductors Case

For the case of testing with the conductors, Fig. 6-20 shows the far tower supporting guy 2 response spectral density determined by spectral estimation from the fluctuating component of the axial force in guy 2. Resonant dynamic response can be distinguished from the background response especially in low wind speeds. For low wind speeds (9 m/sec), the first resonant mode is centered a frequency of 7.5 Hz. With increasing the wind speed, the resonant peak was shifted slightly to 7 Hz, but with a widened band width and becomes less distinguished. Several peaks are noticed at frequencies of 9.5, 11, and 17 Hz, and are decreased until almost vanished by the increase of the wind speed.





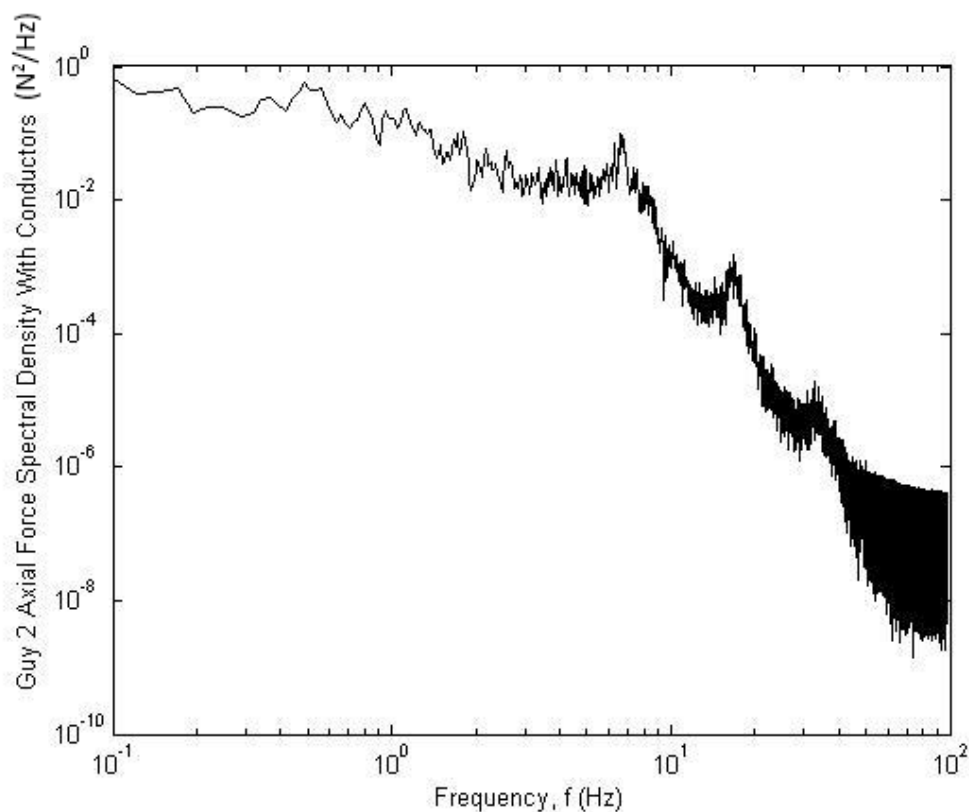


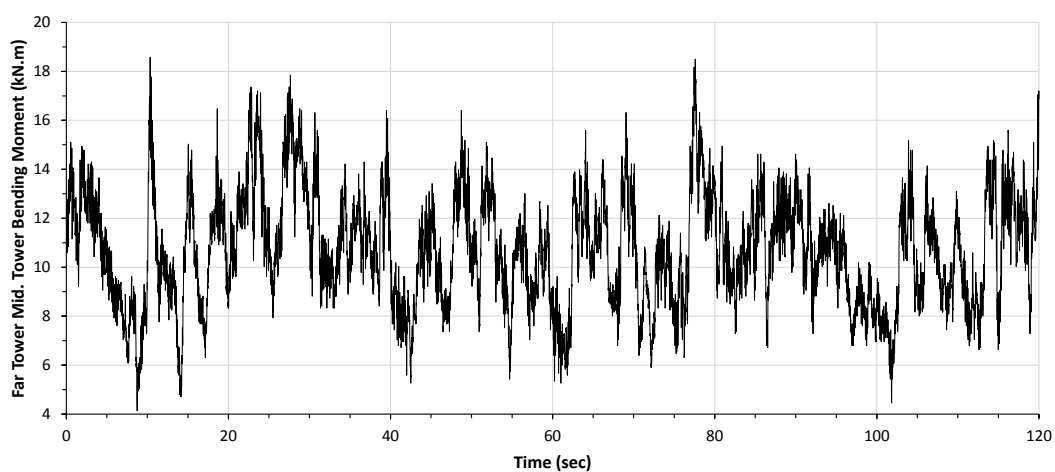
Fig. 6-20 Boundary Layer Supporting Guy 2 Response, with Conductors Case, Spectra due to Reference Mean Wind Speed of 9.4, 18.0, 27.0, and 36.6 (m/sec), Respectively

6.3.4 Bending Moments

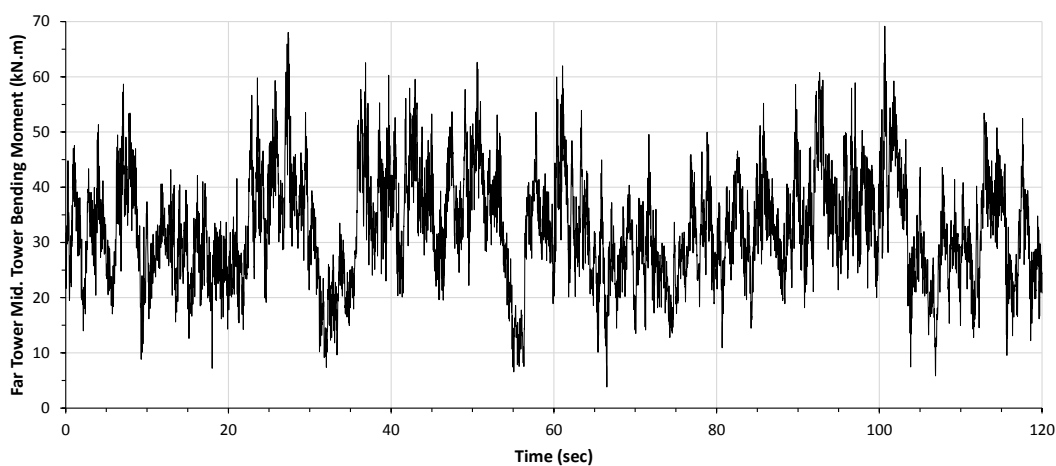
The bending moment at almost the mid-tower height is measured using strain gauges. This location is chosen based on the mode shapes shown in Fig. 6-3, to better represent the behaviour of the central spine which simulates the tower main body. In the following sections, the response of bending moment at mid-height for both cases with and without conductors are assessed and investigated.

6.3.4.1 Mid. Tower Bending Moment without Conductors

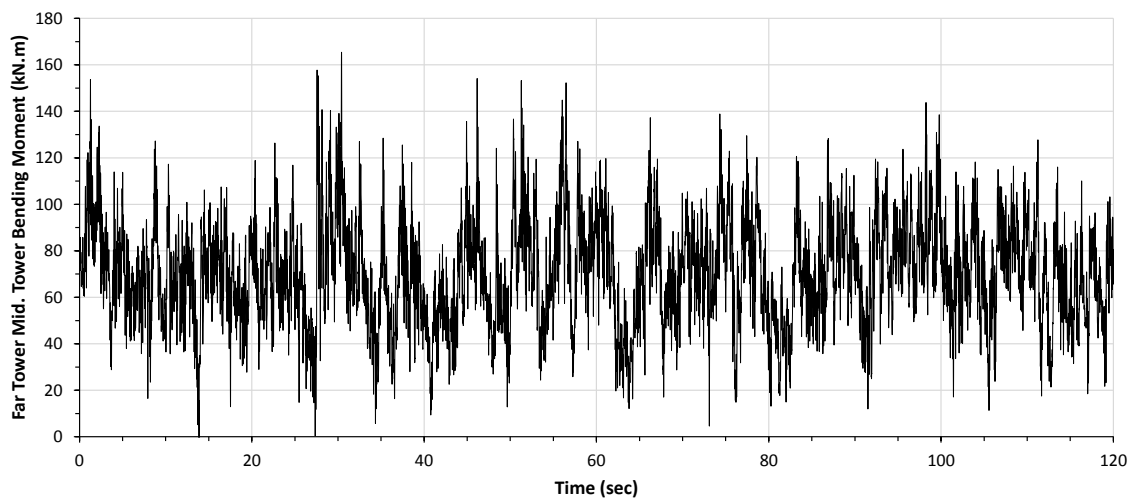
The time history response of the mid-height bending moment of both central towers are measured for each of the 37 wind speeds over 2 mins (equivalent to 14 mins at full-scale). The response time histories for the far tower mid-height bending moment for 9.4, 18.0, 27.0, and 36.6 (m/sec) reference wind speeds are shown in Fig. 6-21.



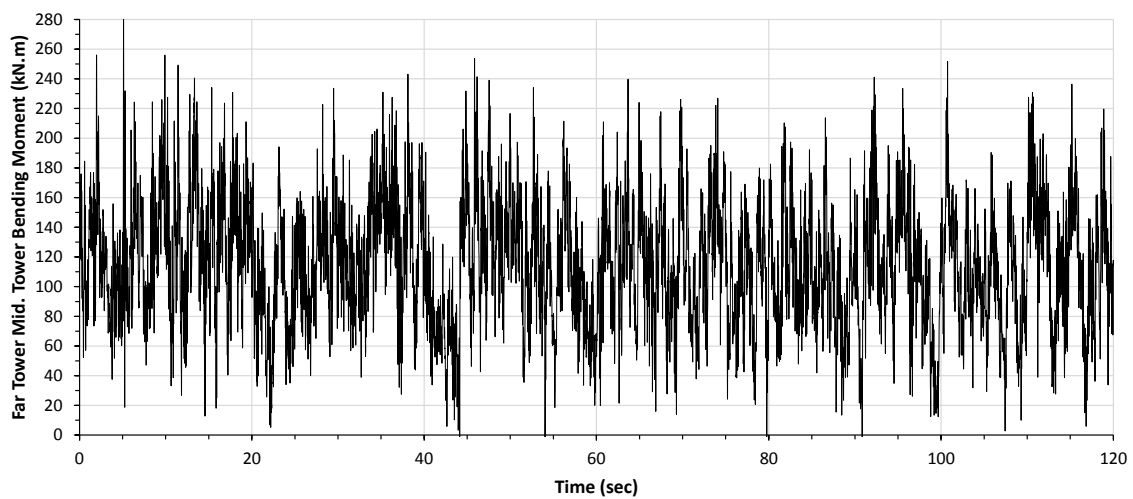
a) Reference Wind Speed (9.4 m/sec)



b) Reference Wind Speed (18.0 m/sec)



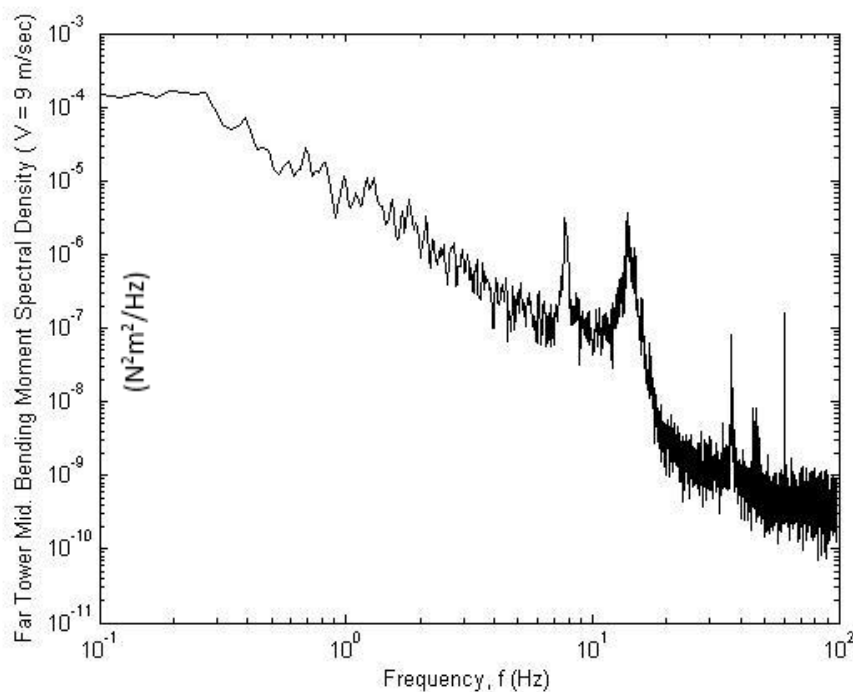
c) Reference Wind Speed (27.0 m/sec)

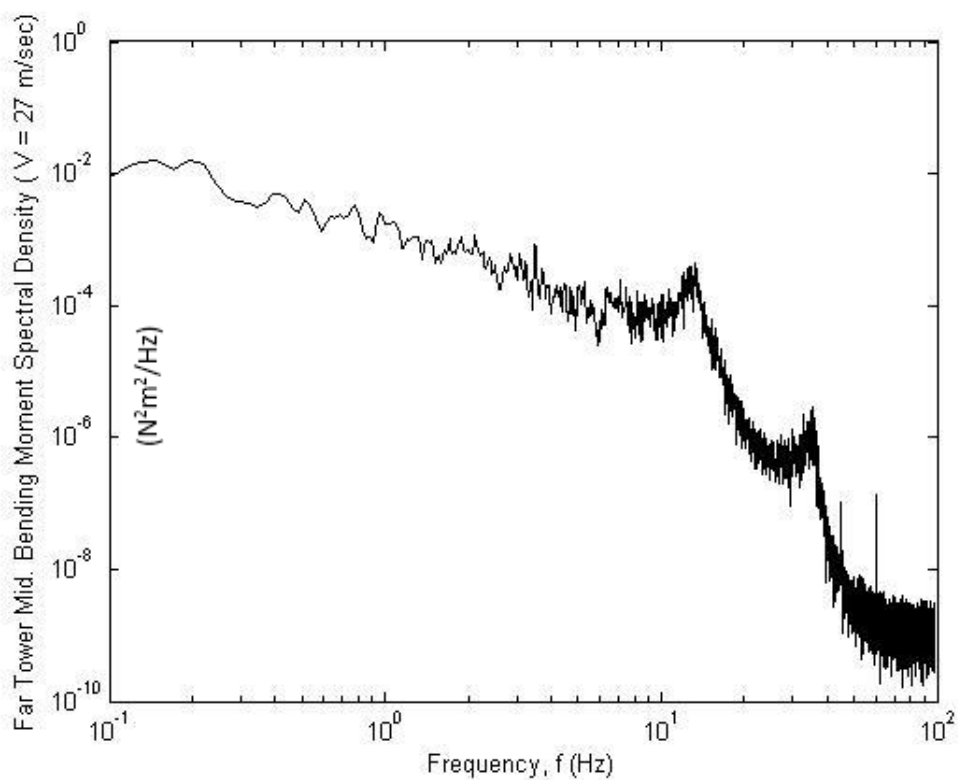
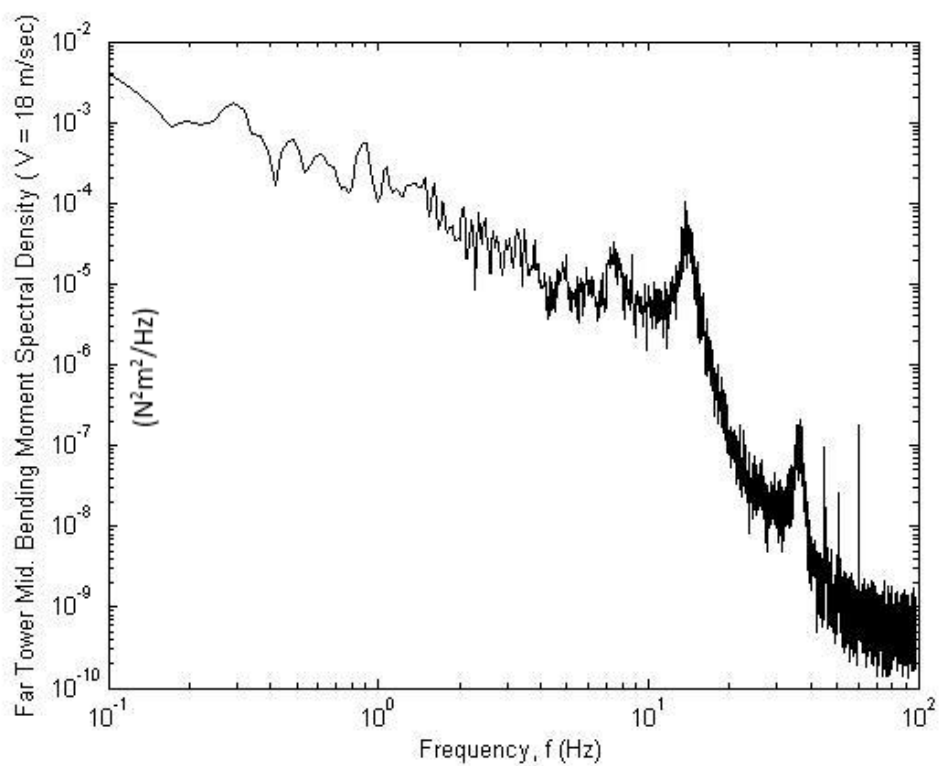


d) Reference Wind Speed (36.65 m/sec)

Fig. 6-21 Time Histories of Measured Mid. Far Tower Bending Moment for Different Wind Speeds – without Conductors Case

Fig. 6-22 shows the far tower mid-height bending moment response spectral density determined by spectral estimation from the fluctuating component of the bending moment at mid-height of the far tower shown in Fig. 6-21. Resonant dynamic response can be distinguished from the background response especially in low wind speeds. For low wind speeds (9 m/sec), two peaks can be distinguished and centered at frequencies of 8.0 and 13.5 Hz. With increasing the wind speed, the 8 Hz resonant peak becomes less distinguished and vanish at higher wind speed. The 13.5 Hz resonant peak shifted to 12 Hz, but with a widened band width and becomes less distinguished. With time scaling of 1:7.07, the aeroelastic model, without conductors, predicted at almost mid-height of the towers fundamental frequencies between 1.1 to 1.7 Hz for the full-scale transmission tower. This matches the results shown in Table 6-1.





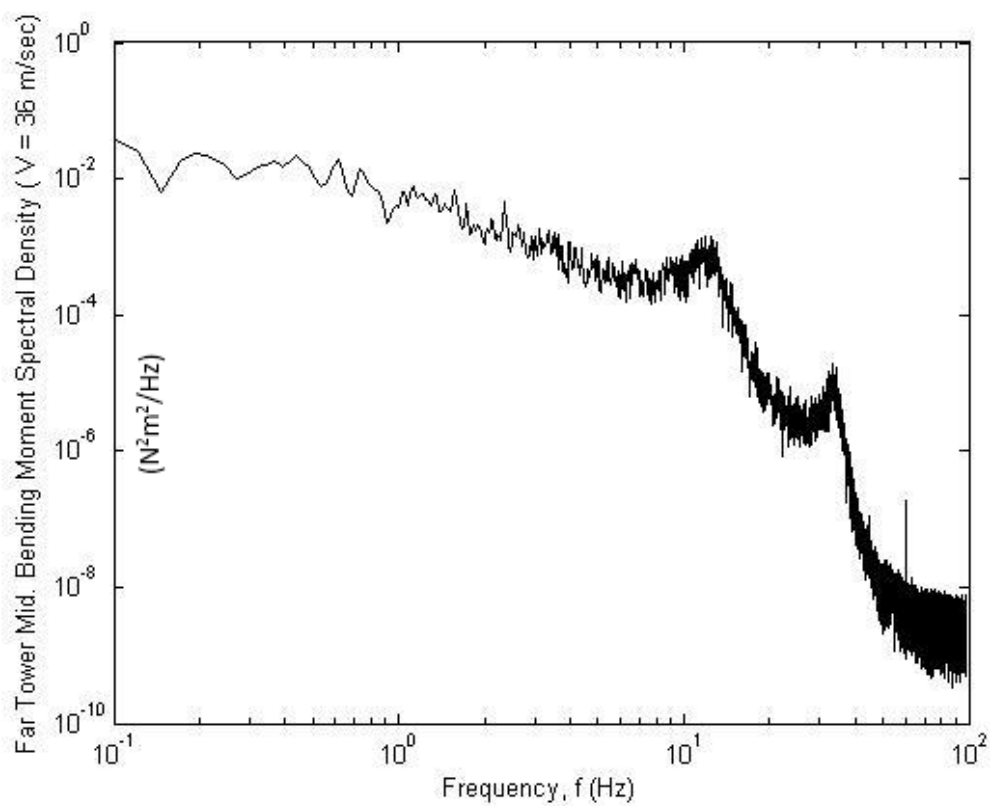
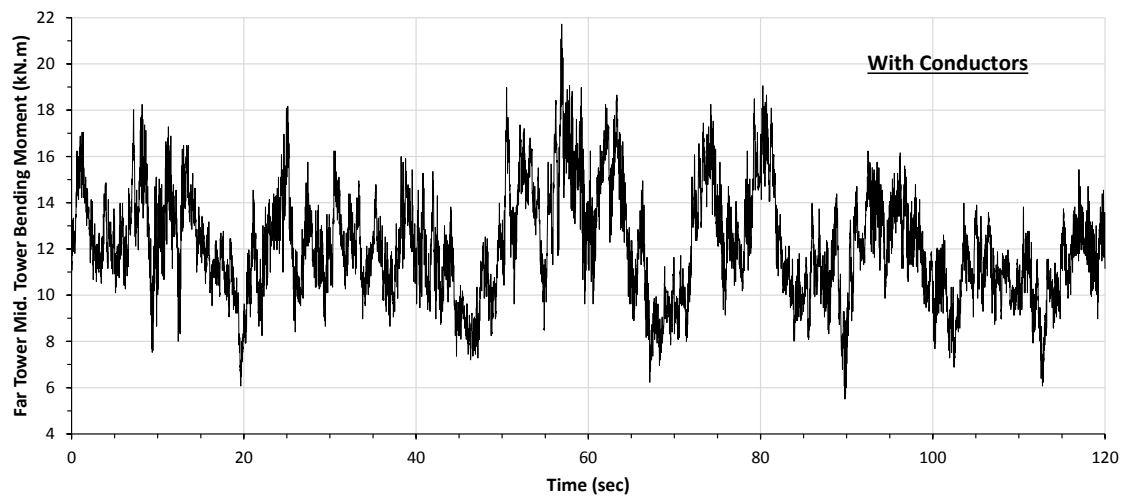
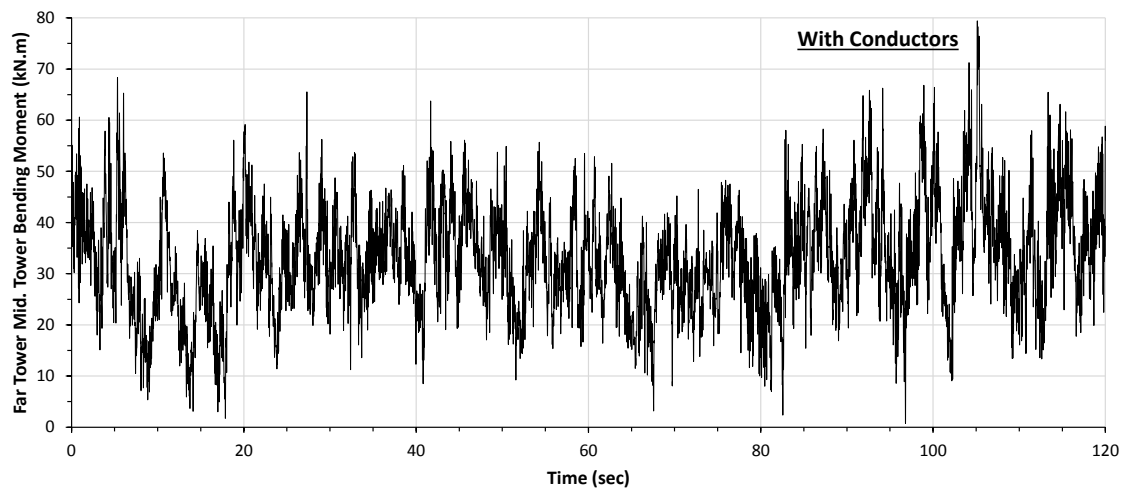
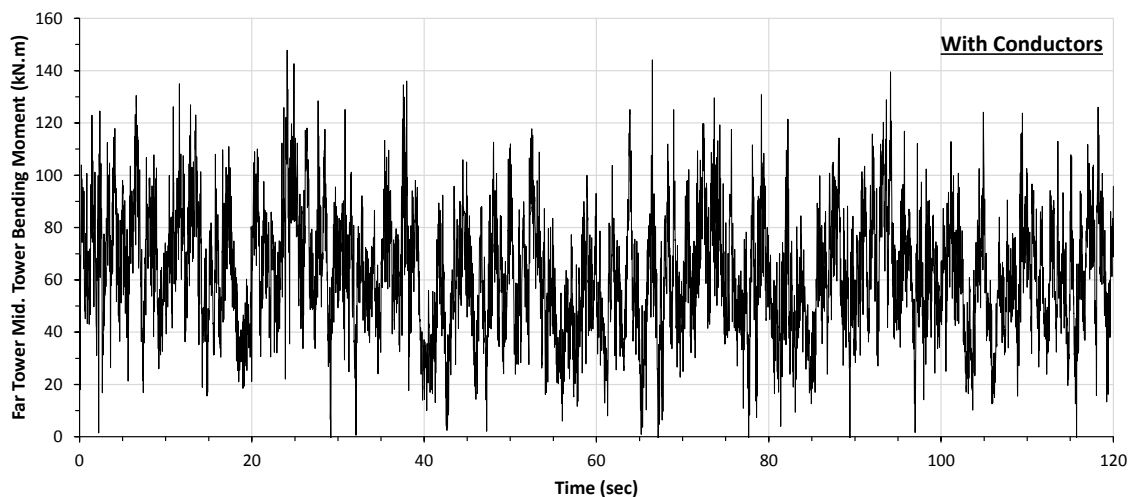


Fig. 6-22 Boundary Layer Far Tower Mid. Bending Moment Response Spectra due to Reference Mean Wind Speed of 9.4, 18.0, 27.0, and 36.6 (m/sec), Respectively

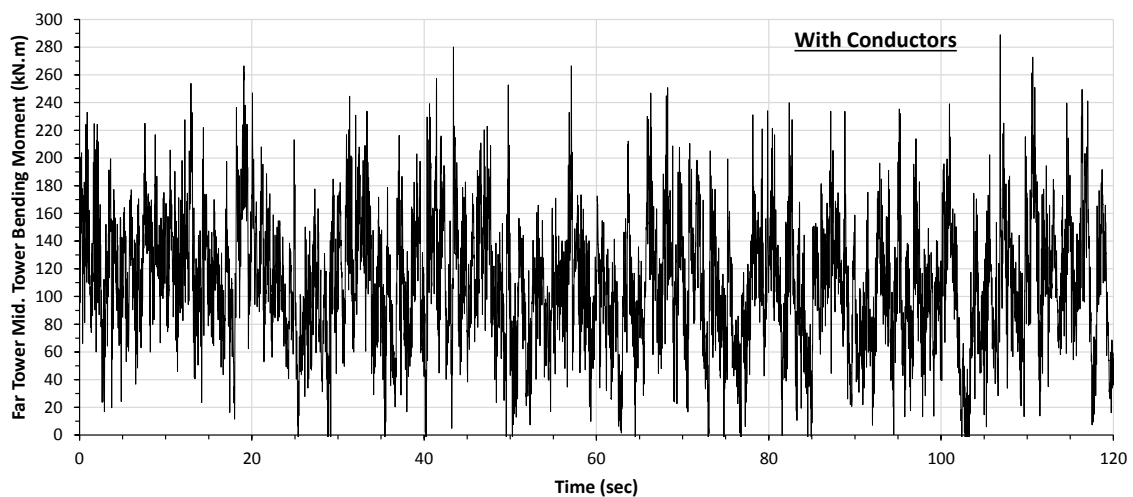
6.3.4.2 Mid. Tower Bending Moment with Conductors

The same time history response shown in the previous section are presented in the current section but for the test configuration where conductors are attached to the transmission towers. The response time histories are presented for the mid-height bending moment of the far tower and for the same selected wind speeds. These time histories are shown in Fig. 6-23. These wind speeds are selected as a representation of the results.

a) Reference Wind Speed $V = 9.4$ (m/sec)b) Reference Wind Speed $V = 18.0$ (m/sec)



c) Reference Wind Speed $V = 27.0$ (m/sec)

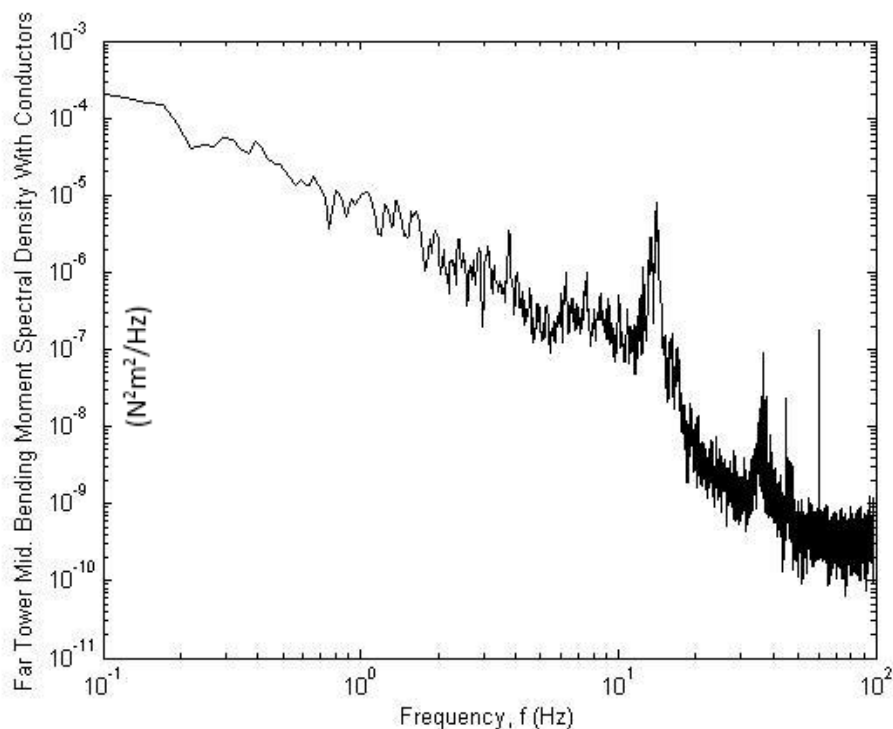


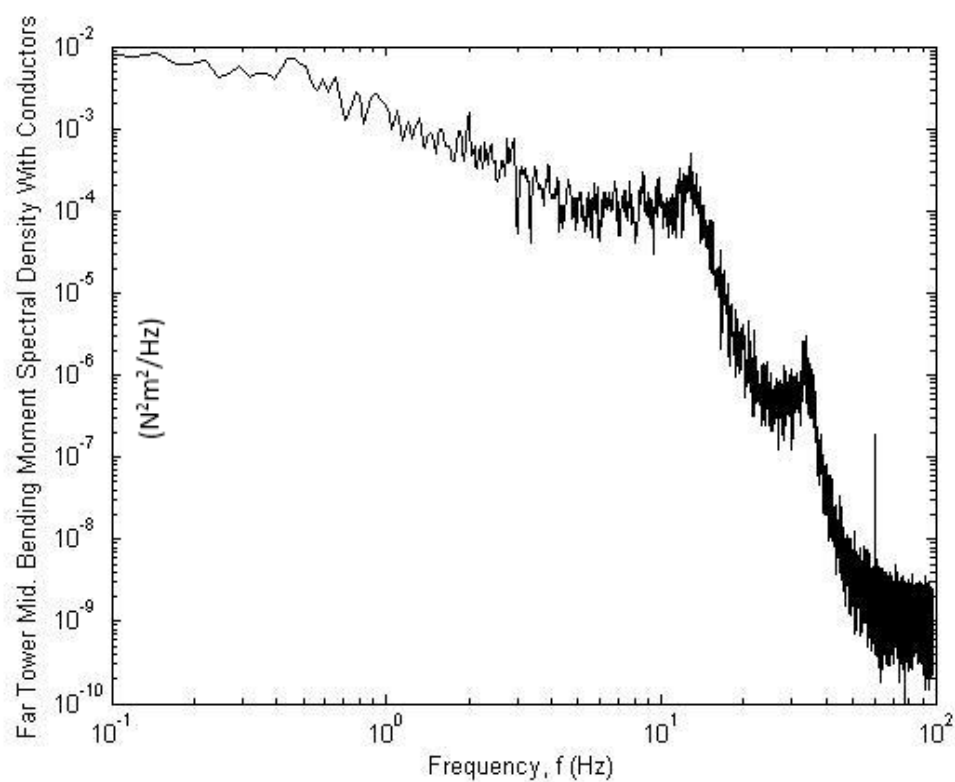
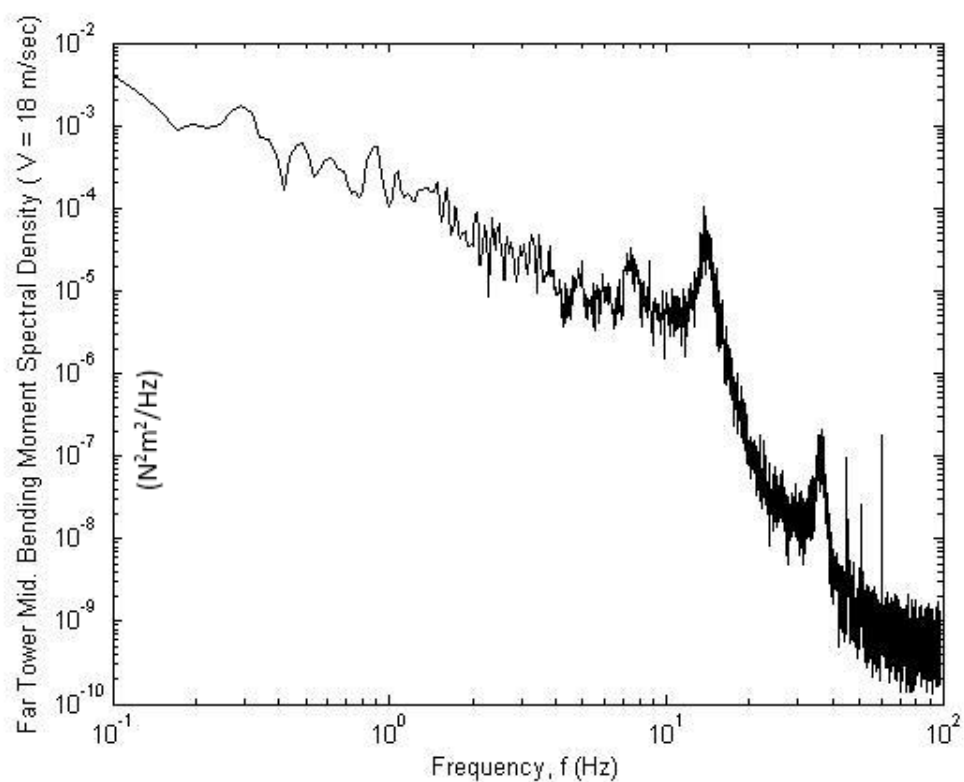
d) Reference Wind Speed $V = 36.6$ (m/sec)

Fig. 6-23 Time Histories of Measured Mid. Far Tower Bending Moment for Different Wind Speeds – with Conductors Case

For the configuration where the conductors are attached to the transmission towers, Fig. 6-24 shows the far tower mid-height bending moment response spectral density

determined by spectral estimation from the fluctuating component of the bending moment at mid-height of the far tower shown in Fig. 6-23. Resonant dynamic response can be distinguished from the background response especially in low wind speeds. For low wind speeds (9 m/sec), several peaks can be distinguished and centered at frequencies of 4, 6, 8, and 14 Hz. With increasing the wind speed, the 4, 6, and 8 Hz resonant peaks become less distinguished and vanish at higher wind speed. The 14 Hz resonant peak shifted to 11.5 Hz, but with a widened band width and becomes less distinguished. With time scaling of 1:7.07, the aeroelastic model, without conductors, predicted at almost mid-height of the towers fundamental frequencies between 0.5 to 1.63 Hz for the full-scale transmission tower. This matches the results shown in Table 6-1 for the high frequency. The low frequency peaks are due to the effect of the conductors' oscillation as discussed later.





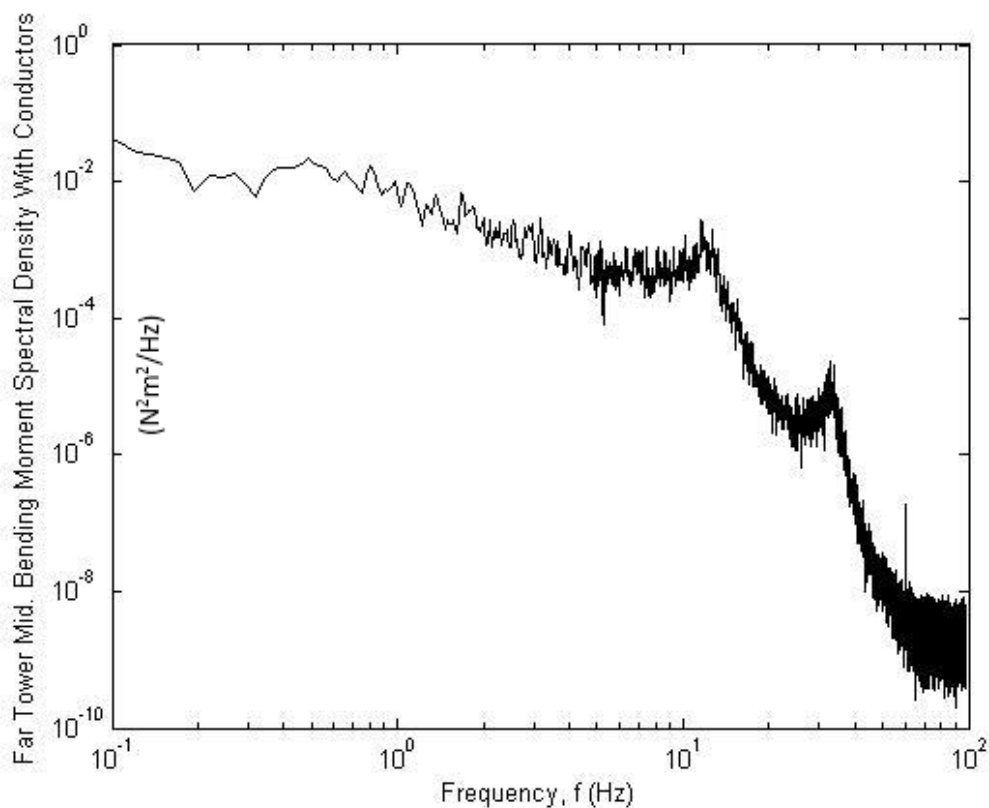


Fig. 6-24 Boundary Layer Far Tower Mid. Bending Moment, with Conductors Case, Response Spectra due to Reference Mean Wind Speed of 9.4, 18.0, 27.0, and 36.6 (m/sec), Respectively

6.4 Validation of an In-house Three Dimensional Finite Element Model of Transmission Line System

The current section compare the aeroelastic model results with the in-house nonlinear three dimensional finite element model that was developed by the author in the previous chapters. The main objectives are to validate a) the wind force calculations, including the drag coefficients and shielding effect, b) the structural response calculated by the in-house numerical model. The aeroelastic model results for the A.O.A. of 90° are used in the current section. The objective is to evaluate the wind forces without considering the

effect of the yaw angle on the applied wind forces on the transmission towers and lines. The wind speed of 36.6 (m/sec) is used for the validation of the numerical model. This wind speed is measured at the reference height, which is the cross-arms height. The equivalent 10 (m) wind speed is 32.18 (m/sec) that is used originally to design the transmission line system by the Hydro Company. The wind loads on the transmission towers and lines are calculated using the equations provided by the ASCE (2010). The mean wind speed is used for the validation purpose. The nonlinear three dimensional finite element model of the transmission line system is solved initially to adjust the pretension force of the supporting guys and conductors. The stiffness matrix that accounts for tension stiffening is formulated. The calculated wind loads are applied to the numerical model and the nonlinear analysis is performed. The analyses are repeated twice, with and without the conductors. A comparison between the aeroelastic model and the numerical model is discussed in the following sections.

6.4.1 Validation of the Numerical Model without Conductors

Table 6-5 Supporting Guys Forces, Tower Base Reactions, and Tower's Bending Moments of the Aeroelastic and the Numerical Models – without Conductors Case

	Supporting Guys				Tower Base Support				Bending Moment	Bending Moment
	Far Tower		Near Tower		Far Tower		Near Tower		Mid. Height	Mid. Height
	Guy 2 (kN)	Guy 3 (kN)	Guy 6 (kN)	Guy 7 (kN)	Lateral (kN)	Vertical (kN)	Lateral (kN)	Vertical (kN)	Far Tower (kN.m)	Near Tower (kN.m)
Aeroelastic Model	42	44	42	41	13	60	11	61	115	101
In-house Finite Element Model			41		11	50	11	50	110	110

In this section the wind loads are applied only to the transmission towers. As shown in previous sections, the aeroelastic model responses are recorded. The mean responses are

used for the validation. In order to satisfy the two main objectives of the validation, the comparison focuses on the mean response of the supporting guys' forces, tower base reactions, and the bending moments of the transmission tower main body. Table 6-5 shows the results of both the aeroelastic model and the numerical model. The results are shown for both the far and near towers. The forces of the upstream supporting guys' are shown. These supporting guys are identified as guy 2, 3, 6, and 7, as shown in Fig. 6-5, while the other supporting guys are slacking for the A.O.A. (Yaw angle) of 90° . As shown in Table 6-5, a good agreement between the aeroelastic and the numerical model results is indicated, with a maximum difference in the supporting guys' axial force of 7%. Each of the middle towers has a force balance attached to its bases that calculates the tower's reactions in the lateral, longitudinal, and vertical reactions. The lateral and vertical reactions of both towers are compared with the numerical model reactions. The values reported in Table 6-5 do not include the own weight of the tower and the effect of the supporting guys pretension force. These values represent the effect of the applied wind load on the transmission towers. As shown in the table, the difference in the lateral and vertical reaction between the aeroelastic and numerical model are 14 and 18%, respectively. The higher difference can be interpreted as a consequence of the higher wind effect at the near ground region in the wind tunnel while the numerical model assumes a zero wind at ground level. Each of the equivalent spines have a pair of strain gauges at the mid-height of the tower body to measure the bending moment at the mid-height. The results provided in Table 6-5 show a good agreement in terms of the bending moment at mid-height of the tower for both the aeroelastic and numerical models. The

maximum difference in the mid-height bending moment between the physical and the numerical model is 8%.

6.4.2 Validation of the Numerical Model with Conductors

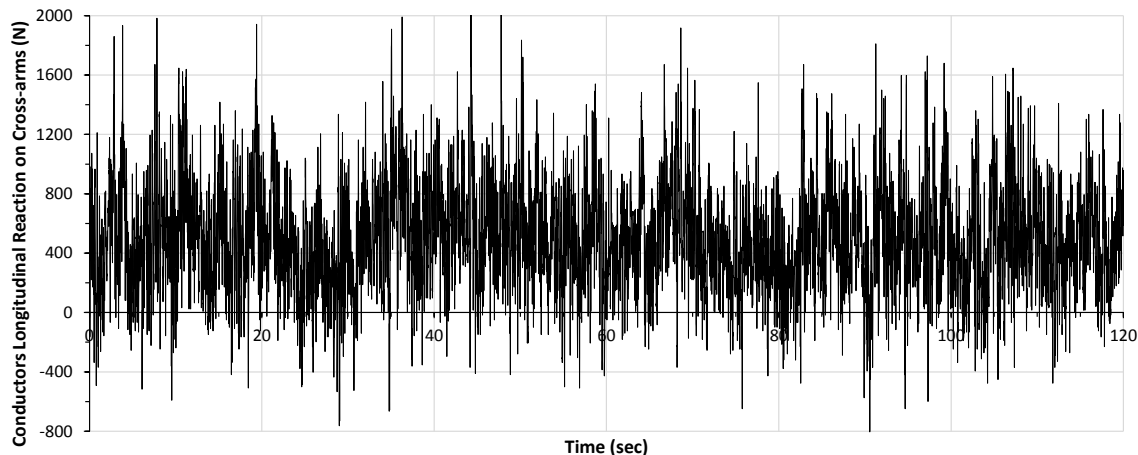


Fig. 6-25 Time History of Measured Conductor's Longitudinal Reaction on Tower's Cross-arm (N) – Near Tower

In this section the wind loads are applied on both the transmission towers and the conductors. The case of Yaw angle of 90° is used where only the middle span and two-third of the two adjacent spans are loaded with wind, as shown in Fig. 6-13. The remainder of the conductors' spans and the two edge towers are located outside the wind tunnel walls and are not subjected to wind loads, as shown in Fig. 6-5. The longitudinal forces in the conductors are reversed on the towers and called in the current study as the longitudinal reaction of the conductors. The bending moment response of the conductor cross-arms can be used to understand the behaviour of the conductors under fluctuating wind. The time history response of the conductor cross-arm out-of-plane moment are

measured for each of the 37 wind speeds over 2 mins (14 minutes full-scale). The response time history for the out-of-plane moment on the conductor cross-arm of the far tower for the 36.6 (m/sec) wind speed is shown in Fig. 6-25. Fig. 6-26 shows the far tower conductors' cross-arms out-of-plane bending moment response spectral density determined by spectral estimation from the fluctuating component shown in Fig. 6-25. Resonant dynamic response can be distinguished from the background response. Several peaks can be distinguished and centered at frequencies of 1.4, 3.5, 7, and 12 Hz. With time scaling of 1:7.07, the aeroelastic model predicted, at the conductors' cross-arms location, frequencies between 0.2 to 1.7 Hz for the full-scale transmission tower. This matches the results shown in Table 6-1 for the high frequency. The low frequency peaks are due to the effect of the conductors' oscillation, which is function of mass, length, sag, and pretension force. The results match the typical conductors' natural frequencies of 0.1 to 1.0 Hz that are reported in the literature by Hamada and El Damatty (2011), ASCE (2010), and Momomura et al. (1997). Table 6-6 shows the mean response of the supporting guys' forces, tower's mid-height bending moments, and conductor's longitudinal reactions of both the aeroelastic and the numerical models. The forces of the upstream supporting guys are reported for both models. The results shown in Table 6-6 indicate a good agreement between the aeroelastic and numerical models in terms of the axial force of the upstream supporting guys of both towers. A maximum difference of 13% between the aeroelastic and numerical models is reported. The bending moment at the mid-height of both the far and near tower are shown in Table 6-6. The maximum difference of the mid-height bending moment for the aeroelastic and numerical models of both towers is 11%. Due to the unbalanced wind loading on the conductors, the

conductors exhibit a longitudinal force on the supporting towers' cross-arms. These conductor's longitudinal reactions are reported in Table 6-6, with a 13% difference between the aeroelastic and the numerical model. This longitudinal force increase nonlinearly with the conductor's span length and other parameters such as insulators length, conductor's pretension force, sag, and own weight, till reach up to 60 % of the transverse reactions of the conductors. In the current analysis and due to the short conductor's span, the longitudinal force is only 10% of the transverse reaction of the conductors. More details regarding the longitudinal force and parameters affecting the magnitude of this force are provided in Chapters 3 and 4.

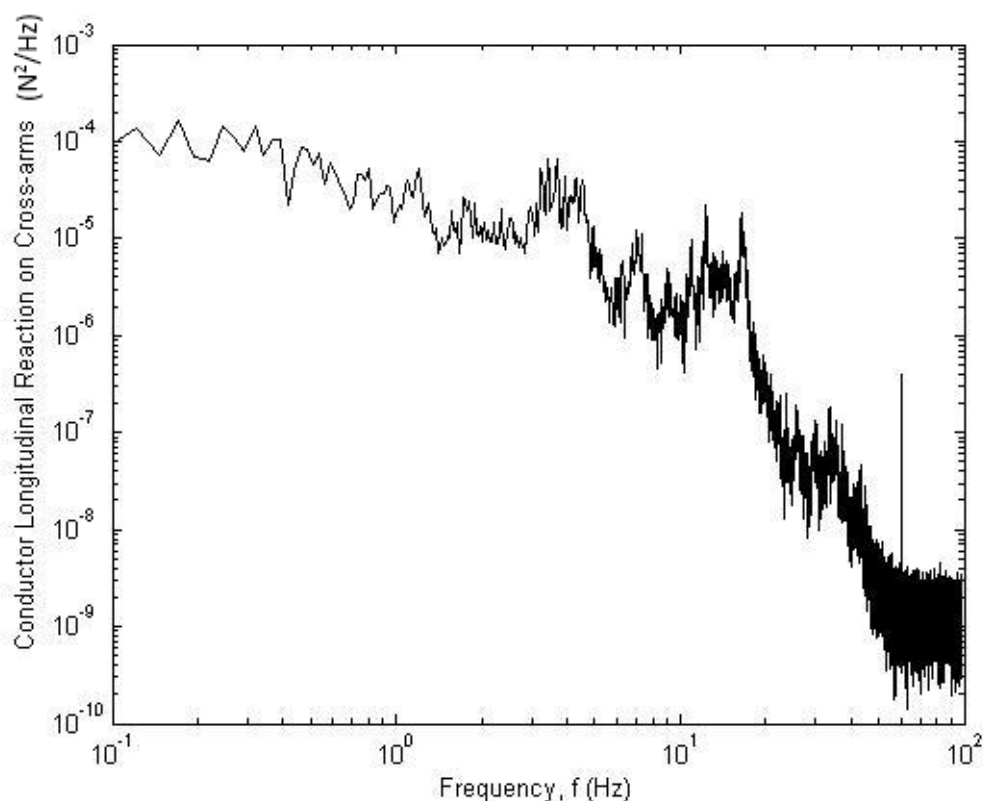


Fig. 6-26 Boundary Layer Conductor's Longitudinal Reaction on Tower Cross-arms Response Spectra due to Reference Mean Wind Speed of 36.6 (m/sec)

Table 6-6 Supporting Guys Forces, Tower's Bending Moments, Conductor's Longitudinal Reaction of the Aeroelastic and Numerical Model – with Conductors

	Supporting Guys				Bending Moment	Bending Moment	Conductor
	Far Tower		Near Tower		Mid. Height	Mid. Height	Longitudinal Reaction
	Guy 2 (kN)	Guy 3 (kN)	Guy 6 (kN)	Guy 7 (kN)	Far Tower (kN.m)	Near Tower (kN.m)	Far Tower (N)
Aeroelastic Model	53	56	52	59	106	86	425
In-house Finite Element Model	60	63	60	63	97	97	370

6.5 Effect of Conductors on the Structural Response of the Transmission Line System

The purpose of this section is to understand the effect of the conductors on the structural behaviour of the guyed tower in view of the results of Sections 6.4.1 and 6.4.2. The results in Section 6.4.1 represent the transmission tower response without the conductors. Section 6.4.2 discusses the aeroelastic model results for the test configuration where the conductors are attached. The choice of the A.O.A. of 90°, where parts of the adjacent spans are not fully loaded with wind load, is to assess the effect of the unbalanced wind loads on the transmission lines on the structural response of the supporting towers. The following discussion touches only the effect of the transmission line conductors on the structural response of the transmission towers, specifically the effect on the internal forces of both the supporting guys and the tower.

6.5.1 Transmission Tower's Supporting Guys

Based on the results shown in Table 6-5 and Table 6-6, 30 to 50% increase in the supporting guys' axial forces as a result of conductors' forces for such a short span. The

conductor span used in the current study is 110 (m), while for the same tower, the span can reach up to 500 (m). Accordingly, at the same wind speed and for the same number of the conductor bundle, the supporting guys' internal forces can reach up to 250% of the internal forces without including the conductor's wind loads. As shown in Table 6-6, the supporting guys' forces are not similar. For the same tower, both the supporting guys internal force are different, despite the fact that the wind flow is perpendicular to the transmission line system. The difference in the guys internal forces of the same tower can reach up to 12% of the higher internal force. This can be explained in view of the longitudinal reaction of the conductors due to the unbalance wind loads applied on the lines. This 12% difference increases by the increase of the longitudinal reaction of the conductors. It should be noted that the difference in results between the numerical and the aeroelastic model increases from 7 to 13% due to inclusion of the conductors, as the lines' behavior and longitudinal reactions are highly nonlinear and very complex to predict.

6.5.2 Transmission Tower's Internal Forces

The objective of this section is to assess the effect of the conductors on the internal forces of the transmission tower main body and cross-arms. A schematic representing the structural system of the guyed tower is shown in Fig. 6-27. In this figure, the tower is represented as an overhanging beam supported by a hinge support at its base and by a spring system, simulating the stiffness of the guys. The distributed load, P (force/length) shown in Fig. 6-27, results from the boundary layer wind acting on the tower. The concentrated force F_c result from the wind loads on the conductors. For the tower main

body, located between the supporting guys and base, the distributed wind load P and the concentrated reaction F_c tend to have opposite effects on the straining actions that develop in this part of the tower. The mid-height bending moment measurements of the central spine is considered as a good indication for the variation of the straining actions of the tower main body. As shown in the results presented in Table 6-5 and Table 6-6 for the mid-height bending moment, the bending moment increases for the case with no conductors attached and decreases significantly for the case with the conductors. Such structural response benefits from the use of the guyed support and the conductors load in the overhang to decrease the amount of internal forces in the tower chord members. An opposite structural response is expected for the case of self-supported towers, as they can be represented as a cantilever.

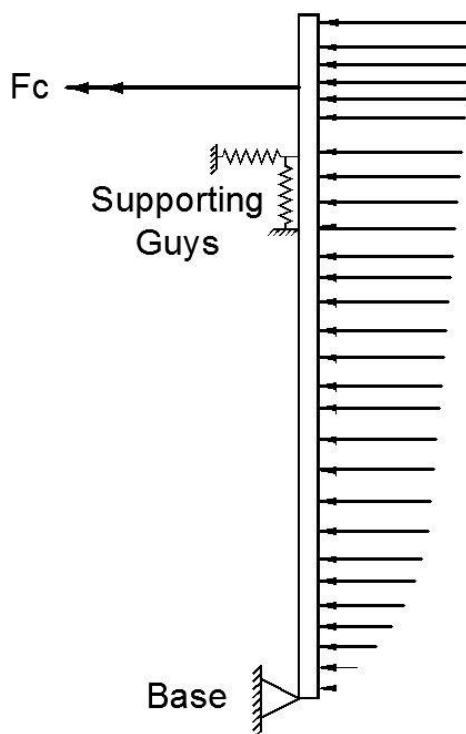


Fig. 6-27 Simulation of the Guyed Tower as an Overhanging Beam

The conductor's cross-arms are shown in Fig. 6-28. The internal forces in this area of the tower is mainly affected by the reaction provided by the conductors to the cross-arms. The unbalanced loads acting on the two spans adjacent to the middle two towers lead to a resultant forces acting on the conductor cross-arms along the longitudinal direction of the conductors as shown in Fig. 6-28. This leads to an out-of-plane bending moment, causing compression force in the upper members of the conductor cross-arms as shown in Fig. 6-28. These members are typically designed as tension only members, as the various load cases considered in the design of this tower do not predict any compression force in this member. Similar conclusion was reported by (Shehata and El Damatty 2007) for the behaviour of transmission towers under downburst wind loads, and by (Hamada and El Damatty 2011) for the behaviour of transmission towers under tornado wind loads.

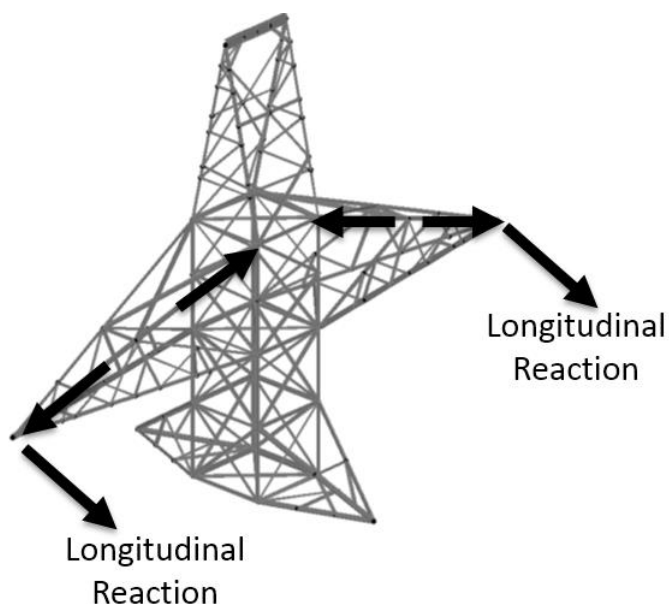


Fig. 6-28 Conductor's Cross-arms Orientation and Longitudinal Reaction

6.6 Conclusions

The following conclusions can be drawn from the current aeroelastic investigation of the transmission line system:

- For the thirty seven test wind speeds used in the current aeroelastic test, no instabilities are found for the tested transmission towers or lines. The general dynamic response of the tower follows an exponential curve, similar to the variation in the applied wind load.
- The resonant components of the dynamic response are more significant and noticeable in the low wind speeds. With increasing the wind speeds, these resonant components become less distinguished and in some cases vanishes.
- The measured resonant frequencies of the aeroelastic model match those calculated by the numerical model of the full tower.
- In terms of the resonant peaks of the tower's dynamic response and their correspondent frequencies, no significant differences are for the case with and without conductors. The resonant peaks almost have the same frequencies for both cases. The magnitude of the dynamic response is different due to the conductor's loads. This can be explained in view of both the high aerodynamic damping of the conductors and the significant difference in the natural frequencies between the conductors and the supporting towers. In addition, most of the conductor's load path is transferred by the supporting guys to ground supports.
- The conductors' oscillations under fluctuating wind affect the resonant component of the conductors' cross-arms. Such effect is noticed in the mid-tower

response at low wind speeds, and become less distinguished with the increase of the wind speed.

- The variation of the transmission tower straining actions with the increase of the wind speed follows an exponential curve, similar to the applied wind load.
- For the case of towers only (no conductors attached), a good agreement is found between the measured straining actions of the aeroelastic model and the calculated values using the in-house numerical model, with a maximum difference in the:
 - supporting guys axial force of 7%
 - lateral base reaction of 14%
 - mid-height bending moment of 8%.
- For the case of towers with conductors, a good agreement is found between the measured straining actions of the aeroelastic model and the calculated values using the in-house numerical model, with a maximum difference in the:
 - supporting guys axial force of 13%
 - mid-height bending moment of 11%.
- The effect of the conductors on the overall structural response of the transmission towers is investigated in the current study. The inclusion of the conductors changes the transmission towers response under wind loads, with increase or decrease of the internal forces of the tower. As shown in the current study, the conductors reaction decrease the internal forces in the towers main body, while increase the supporting guys and conductor's cross-arms straining actions. In addition, the conductors exhibit a longitudinal force on the supporting towers'

cross-arms due to the unbalanced wind loading on the conductors. This longitudinal reactions change the structural response and force distribution in different components of the guyed transmission tower.

6.7 Acknowledgement

The authors gratefully acknowledge Hydro One Inc. for the in-kind support, the collaboration, and the financial support provided for this research. The first author is indebted to the Vanier Canada Graduate and the Natural Science and Engineering Research Council of Canada (NSERC) for the financial support provided for this research. The first author gratefully acknowledge Mr. G. Dafoe for his continuous assistance with the model gauging, set-up, and testing.

6.8 References

American Society of Civil Engineers (ASCE). (1997). *Design of Latticed Steel Transmission Structures*. American Society of Civil Engineers, ASCE Standard ANSI/ASCE 10-90, New York, NY, USA.

American Society of Civil Engineers (ASCE). (2010). *Guidelines for electrical transmission line structural loading*. American Society of Civil Engineers, ASCE Manuals and Reports on Engineering Practice, vol. 74. Reston, VA, USA.

American Society of Civil Engineers (ASCE). (2012). *Wind Tunnel Testing for Buildings and Other Structures*. American Society of Civil Engineers, ASCE Standard ASCE/SEI 49-12, New York, NY, USA.

Behncke, R.H., and White, H. B. (2006). "Applying Gust Loadings to Your Lines." *Proceedings of the 9th International Conference on Overhead Lines*, American Society of Civil Engineers (ASCE), Fort Collins, Colorado

Boundary Layer Wind Tunnel Laboratory (BLWTL II). (2007). *Wind Tunnel Testing: A General Outline*. The University of Western Ontario, Boundary Layer Wind Tunnel Laboratory General Outline Report.

CIGRÉ (Conseil International des Grands Réseaux Électriques/ International Council on Large Electrical Systems) SC-22 WG22-06 (2006). "Review of IEC 826: Loading and Strength of Overhead Lines. Part 3: Analysis of Recent Transmission Line Failures." Scientific Committee B2 on Overhead Lines.

CIGRÉ (Conseil International des Grands Réseaux Électriques/ International Council on Large Electrical Systems) (2009). "Overhead line design guidelines for mitigation of severe wind storm damage." Scientific Committee B2 on Overhead Lines, B2. 06.09.

El Damatty, A. A., and Hamada, A. (2013). "Behaviour of guyed transmission line structures under tornado wind loads - Case studies." *Electrical Transmission and Substation Structures 2012: Solutions to Building the Grid of Tomorrow, November 4, 2012 - November 8*, American Society of Civil Engineers (ASCE), Columbus, OH, United states, 193-204.

Gattulli, V., Martinelli, L., Perotti, F., and Vestroni, F. (2007). "Dynamics of suspended cables under turbulence loading: Reduced models of wind field and mechanical system." *J.Wind Eng.Ind.Aerodyn.*, 95(3), 183-207.

Hamada, A. (2009). *Analysis and behaviour of guyed transmission line structure under tornado wind loading*. M.E.Sc. Thesis, School of Graduate and Postdoctoral Studies, University of Western Ontario, London, Ont., Canada.

Hamada, A., Damatty, A. A. E., Hangan, H., and Shehata, A. Y. (2010). "Finite element modelling of transmission line structures under tornado wind loading." *Wind and Structures, an International Journal*, 13(5), 451-469.

Hamada, A., and El Damatty, A. A. (2011). "Behaviour of guyed transmission line structures under tornado wind loading." *Computers and Structures*, 89(11-12), 986-1003.

Hamada, A., and El Damatty, A. A. (2013). "Analysis and Behaviour of Guyed Transmission Lines under Tornado Wind Loads – Case Studies." *Annual Conference of the Canadian Society for Civil Engineering 2013: General Conference, CSCE 2013, May 29, 2013 - June 1, Canadian Society for Civil Engineering, Montreal, QC, Canada.*

Holmes, J. D. (2007). *Wind loading of structures*. Taylor & Francis, London; New York.

Irwin, P. A. (1982). "MODEL STUDIES OF THE DYNAMIC RESPONSE OF TALL BUILDINGS TO WIND." *Volume 3: Hydrotechnical, Municipal Environment*, Canadian Society for Civil Engineering, Edmonton, Alberta, Can, 285-302.

Kong, L. Jeong, U.Y., EDEY, R.T., and King, J.P.C. (2009). *A study of wind effects for the Hoover Dam bypass Project – full aeroelastic model study*. The University of Western Ontario, Faculty of Engineering, Research Report, Boundary Layer Wind Tunnel Laboratory (BLWTL) SS11-2009

Kong, L. Jeong, U.Y., and King, J.P.C. (2009). *The Hoover Dam bypass project, section model and analysis of equivalent static loads*. The University of Western Ontario, Faculty of Engineering, Research Report, Boundary Layer Wind Tunnel Laboratory (BLWTL) SS15-2009

Lin, W. E., Savory, E., McIntyre, R. P., Vandelaar, C. S., and King, J. P. C. (2012). "The response of an overhead electrical power transmission line to two types of wind forcing." *J.Wind Eng.Ind.Aerodyn.*, 100(1), 58-69.

Loredo-Souza, A., and Davenport, A. G. (2001). "A novel approach for wind tunnel modelling of transmission lines." *J.Wind Eng.Ind.Aerodyn.*, 89(11-12), 1017-1029.

- Loredo-Souza, A., and Davenport, A. G. (1998). "The effects of high winds on transmission lines." *J. Wind Eng. Ind. Aerodyn.*, (74-76) 987-994.
- Momomura, Y., Marukawa, H., Okamura, T., Hongo, E., and Ohkuma, T. (1997). "Full-scale measurements of wind-induced vibration of a transmission line system in a mountainous area." *J. Wind Eng. Ind. Aerodyn.*, 72(1-3), 241-252.
- Shehata, A. Y., El Damatty, A. A., and Savory, E. (2005). "Finite element modeling of transmission line under downburst wind loading." *Finite Elements Anal. Des.*, 42(1), 71-89.
- Shehata, A. Y., and El Damatty, A. A. (2007). "Behaviour of guyed transmission line structures under downburst wind loading." *Wind and Structures, an International Journal*, 10(3), 249-268.
- Shehata, A. Y., and El Damatty, A. A. (2008). "Failure analysis of a transmission tower during a microburst." *Wind and Structures*, 11(3), 193-208.
- Vakil, A., and Green, S. I. (2009). "Drag and lift coefficients of inclined finite circular cylinders at moderate Reynolds numbers." *Computers and Fluids*, 38(9), 1771-1781.

CHAPTER 7

EQUIVALENT F2 TORNADO LOADING ON LATTICE TRANSMISSION LINE SYSTEMS

7.1 Introduction

Electricity plays a vital and essential role in our daily life. Almost all business and activities depend on having a reliable source of electricity. Transmission lines are responsible of carrying electricity from the source of production to the end users. Failure of transmission lines can have devastating social and economical consequences, so it is imperative to understand how failures occur and how to prevent them. It has been reported that 80% of weather-related transmission line failures are attributed to high intensity wind (HIW) events in the form of tornados and downbursts (ASCE 2010 and Dempsey and White 1996). Ishac and White (1994) reported that within populated areas in Canada, Southwestern Ontario experiences the highest rate of tornado incidence (about two tornadoes per 10,000 km² every year) and most transmission line failures in this area are caused by tornadoes. 92% of these tornadoes were F2 or less on the Fujita scale. Ontario Hydro has reported that five out of six weather-related line failures in their territory are due to tornadoes (Behncke and White 2006). Newark (1984) concluded that, on average, a F3 tornado occurs in Southwestern Ontario every five years. In the United States, 800 to 1,000 HIW storms occur each year leading to many transmission structures' damages or failures (Behncke and White 2006). CIGRE` (2006) questionnaire on line failures in different countries indicated that 65% of weather-related events on transmission lines were caused by HIW events such as tornadoes. Accordingly, an

extensive research program was initiated by a research group at Western University (formally The University of Western Ontario), Canada, six years ago to study the behaviour of transmission line structures under tornado wind loads. The research involved computational fluid dynamics (CFD) simulations of different tornado intensities and nonlinear three dimensional finite element modelling of transmission line systems. In addition to providing an insight about the behaviour of transmission line systems under tornadoes and the modes of failures, an approach for estimating critical tornado loads cases simulating the effect of tornadoes on transmission line structures resulted from this extensive research.

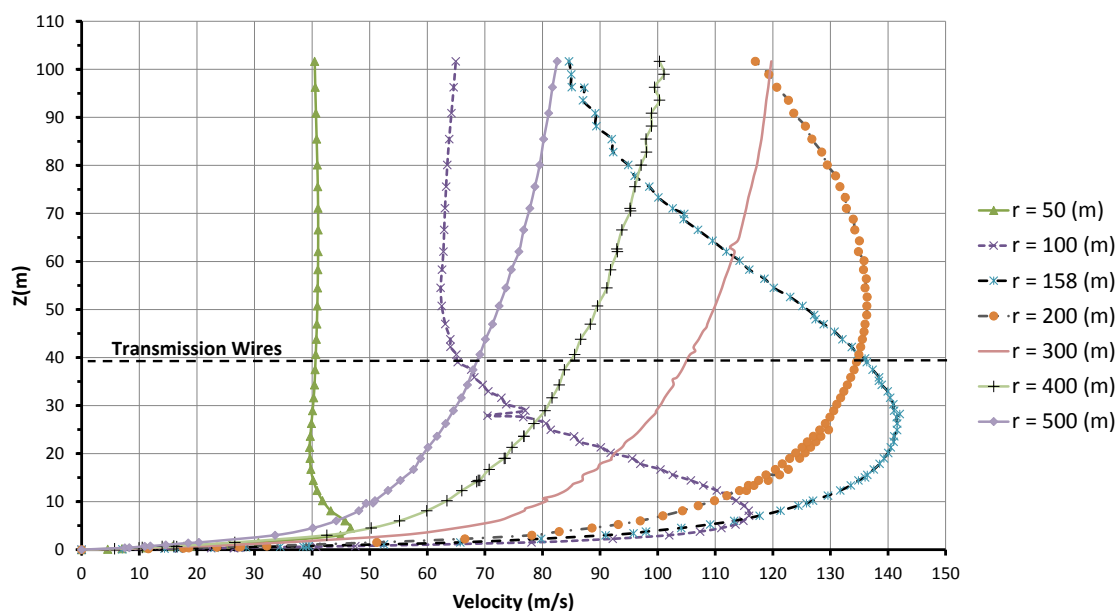


Fig. 7-1 Vertical profile of tangential velocity component for different radial distances from F4 tornado center

Tornadoes are categorized by the damage-based Fujita scale (Fujita and Pearson 1973), or the modified Enhanced Fujita scale (EF-scale). Both have six categories, 0 to 5 which

represent the damage level and take into account tornado characteristics such as path width, length, and wind speed. Due to the complexity and difficulty of obtaining full-scale data, especially for the near ground region, laboratory simulations such as Tornado Vortex Chambers (TVC) are used in which tornadoes are represented as vortices (Wan and Chang 1972, Ward 1972, Davies-Jones 1973, Church et al. 1977, Baker and Church 1979, Church et al. 1979, Rotunno 1979, Lund and Snow 1993, Wang et al. 2001, and Sarkar et al. 2005). The TVCs provide a good simulation of the flow characteristics inside a tornado, but the results are quite sensitive and are affected by the applied boundary conditions and the experimental limitations. For the near ground region, numerical analysis can be done using CFD simulations, which can provide a good description for the flow in this region. The field data for the 1998 Spencer South Dakota F4 tornado and for the 1999 Mulhal F4 tornado were used to validate the numerical (CFD) simulations of F4 and F2 tornadoes conducted by (Hangan and Kim 2008 and Hamada et al. 2010).

The complexity in analyzing transmission line structures under tornadoes arises from the following facts:

- 1- Tornadoes are localized events with complex wind profiles. The tornado wind profile has three velocity components. These are the tangential, radial, and vertical components. The forces acting on a tower and its attached conductors vary based on the location of the event relative to the tower (Hamada et al. 2010 and Hamada and El Damatty 2011). In fact, some incidences of transmission line

failures were attributed with tornadoes' centers located far from the transmission line as reported by ASCE (2010) and Hamada and El Damatty (2011).

- 2- The conventional wind profiles are characterized by a monotonic increase in velocity with height, which is different than wind profiles attributed to tornadoes where the maximum wind speed occurs near the ground (Holmes and Oliver 2000, Letchford and Chay 2002, Hamada et al. 2010, Kareem 2010, and Hamada and El Damatty 2011) as shown in Fig. 7-1. In this figure the vertical profiles of the tangential velocity component of an F4 tornado wind field are plotted at different radial distances from tornado center " r ".
- 3- The prediction of the structural performance of the conductors is challenging due to their expected highly nonlinear behaviour under tornadoes. As a result, the ASCE (2010) and CIGRE` (2009) recommend that the tornado loads on the lines should be neglected because of such complexity.

Despite the significance of tornado events on transmission towers as manifested by the many failures, the codes of practice, design guidelines, and utilities' design methodologies are based solely on the wind loads resulting from large-scale synoptic events with conventional boundary layer wind profiles.

Few studies related to the behaviour of transmission line systems under tornado wind loads are available in the literature. The failure of a self-supported lattice tower under tornado and microburst wind profiles was investigated by Savory et al. (2001). The analysis was done for the transmission tower, without modelling the lines, and without considering the vertical velocity component of the tornado. Hamada (2009) and Hamada

et al. (2010) studied the behaviour of guyed transmission line systems under both F4 and F2 tornado wind fields. A procedure to estimate the velocity field for F2 tornadoes relying on both CFD data and the parameters of F2 tornadoes defined in the Fujita scale was developed in this study. Hamada and El Damatty (2011) conducted a comprehensive study to assess and understand the performance of transmission line structures under tornado loading. The study investigated the variation of the tower members' internal forces with the location of the tornado relative to the transmission line system. The dynamic effect associated with the translation motion of the tornado was assessed and the results of the parametric study were used to determine the sensitivity of the members' peak forces with the parameters defining the location of the tornado relative to the transmission line. Altalmas et al. (2012) and El Damatty and Hamada (2013) assessed the transmission lines' failure mechanisms under critical tornado configurations. In addition, the studies predicted the maximum tornado velocity that various lines can withstand before experiencing global failure. The study also described the modes of failure and its progression for a number of transmission towers. Hamada and El Damatty (2013) assessed the behaviour of two guyed transmission line structures under F2 tornado wind field, boundary layer wind, electrical companies' recommended wind field, and CIGRE' (2009) recommended tornado loading cases. In addition, a comparison was carried out between the forces in the transmission tower members resulting from the tornado, and those obtained for the case of broken wires.

It is evident that the state-of-the-art literature for transmission line-related tornado studies includes only characterization of the wind field as well assessment for the behaviour and failure modes of the transmission towers. No study is available yet in the literature

guiding structural/line engineers to estimate the forces on transmission towers and lines due to such tornado events. This becomes very important for tangent towers since the risk of tornadoes to cross transmission lines is quite high for tangent towers. As such, the objective of the current study is to develop equivalent set of load cases that simulate and provide an envelope for the effect of tornadoes on tangent transmission line structures, and can be applied by a structural engineer designing such structures. Since F2 tornadoes have a cumulative frequency of occurrence of 86% (ASCE 2010), the current study focuses on providing equivalent load cases for this magnitude of tornadoes. The study also focuses on lattice steel towers. The developed load cases are based on extensive parametric studies conducted on four different transmission lines that cover a broad spectrum of the transmission line systems commonly used in the industry. The chapter starts with a description of the F2 tornado wind profile and the nonlinear three dimensional finite element modelling of transmission line systems. The results of the extensive parametric studies of the four transmission line systems are used to identify the critical tornado locations that lead to the peak internal forces in the studied systems. Then, equivalent loading cases with components in the three orthogonal directions are developed. Two different transmission line systems, one guyed and one self-supported, are finally used to verify the recommended tornado loading cases.

7.2 Description of the Transmission Line Systems Used to Develop Critical Load Cases

The transmission line systems simulated in the current study are generic guyed and self-supported tower systems used by different hydro companies. The structural layout of the

four transmission line system used for the development of the critical load cases is provided in Fig. 7-2 and 3. Towers T1 and T2 are guyed towers, while towers T3 and T4 are self-supported towers. Only tangent lattice structures are used in the current study. As shown in the figures, the considered systems cover single leg, as well as V-shaped towers. They cover a variation in the shape and number of cross-arms, as well as the number of conductors carried by the transmission towers (from two to eight). For the guyed towers, different supporting guys' configurations are considered including guys connected to cross-arms, guys connected to the transmission tower bridge, and guys connected to the tower's bridge, and conductor's cross-arms. In addition, the chosen systems' spans range between 200 and 480 (m), which covers the common spans used by the industry for lattice towers. Different insulator configurations, such as suspension and V-suspension insulators, with various lengths are used.

Tower T1's height is 44.36 (m) and is supported by four guys attached to the tower through two guys' cross-arms. Two conductor bundles are connected to the line's cross-arms using a 4.27 (m) insulator at a height of 38.23 (m). One ground-wire is connected to the top of the tower. The conductors and ground-wire spans are 480 (m). The conductors and the ground-wire sags are 20 (m) and 13 (m), respectively. The geometric and material properties of the conductors, ground-wire, and supporting guys are provided by Shehata et al. (2005). Tower T2's height is 46.57 (m) and is supported by four guys attached to the tower's bridge as shown in Fig. 7-2. Three conductor bundles are connected to the lines' cross-arms and bridge using a 4.27 (m) suspension and V-suspension insulators. Two ground-wires are attached to the top of the tower. The lines have a span of 460 (m) and a sag of 16 (m).

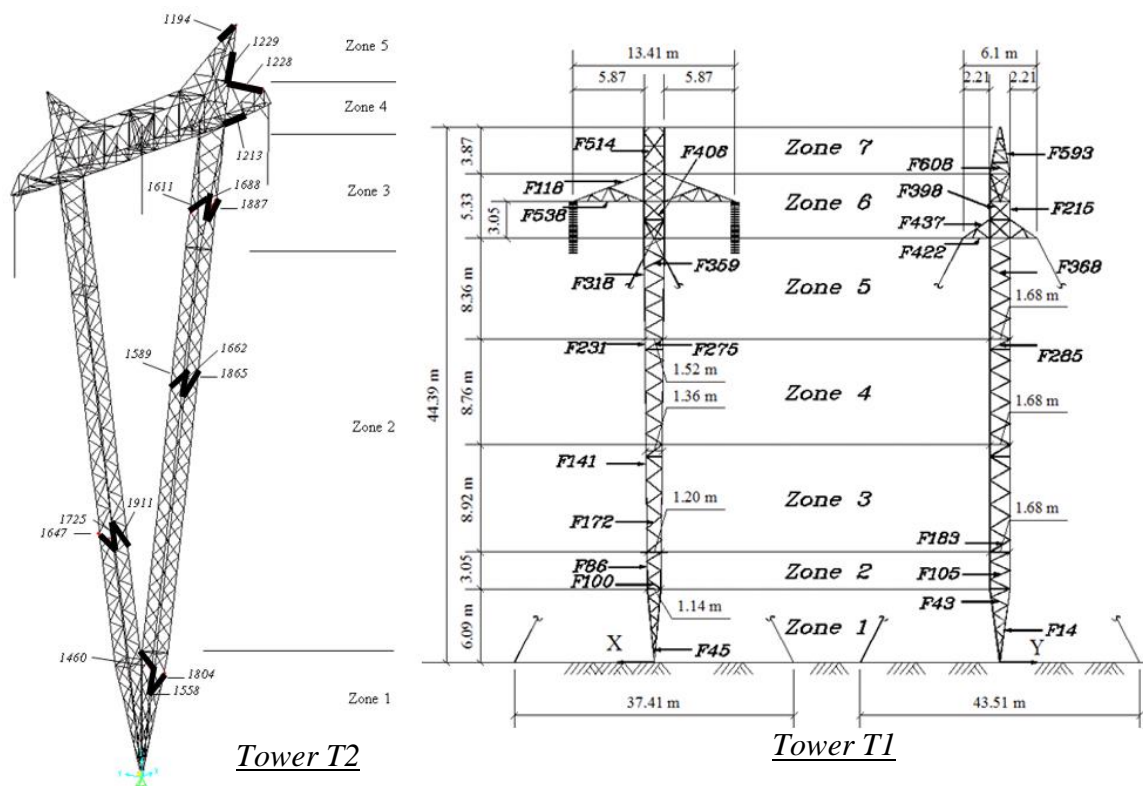


Fig. 7-2 Guyed Towers T1 and T2

The overall height of the self-supported tower T3 is 47.5 (m). The conductors' cross-arms are located at a height of 35.1 (m) and have a width of 13.4 (m). Conductor bundles are connected to the tower at three locations. Each of the outer left and right conductors is attached to a suspension insulator of 4.27 (m). The middle bundle is attached to the tower's bridge using a V-suspension insulator, each 5.9 (m) long. Two ground-wires are attached to the top of the tower. The transmission line span is 420 (m). The material and geometric properties of the conductors and ground-wire are provided by Altamas (2011). For tower T4, the overall height of the tower is 54.7 (m). The tower has six cross-arms on which conductors are carried. The lower cross-arms are located at a height of 34.2 (m), while the upper cross-arms are located at a height of 49.6 (m). The middle cross-arms are

located at a height of 41.9 (m) with a total width of 14.3 (m). The transmission line spans are 213 (m). Each of the six conductor bundles is attached to a single insulator of 2.4 (m) long, which is allowed to swing in two perpendicular planes. The ground-wires are attached to the top of the tower. The material and geometric properties of the conductors and ground-wires are provided by Altalmas (2011) and Altalmas et al. (2012).

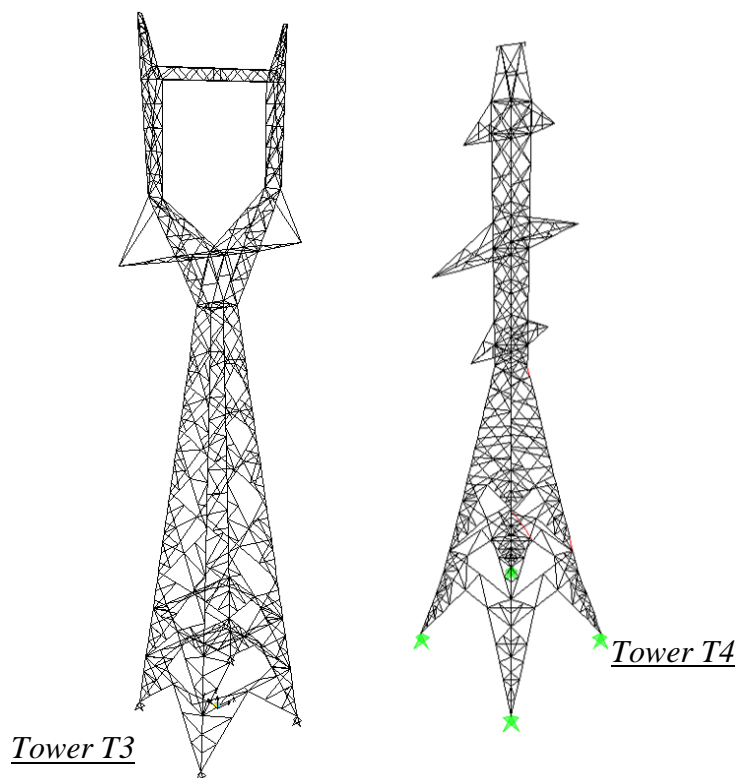


Fig. 7-3 Self-supported Towers T3 and T4

The numerical simulation of each of the four transmission line systems consists of the tower of interest and two towers from each side, which are included in order to properly simulate the stiffness of the whole system. As such, the nonlinear three dimensional finite element model includes five transmission towers with six bays of transmission lines (conductors and ground-wires). Such a number of spans was recommended by Shehata et

al. (2005) and Hamada (2009), in order to accurately account for the forces transferred from the lines to the middle tower (tower of interest).

7.2.1 Finite Element Modelling

The transmission line systems used in the current study are simulated using nonlinear three dimensional finite element models developed using the program SAP 2000 (CSI Inc. 2010). The transmission tower members are modelled using two-noded, three dimensional frame elements. The element takes into account the geometric nonlinear effects. Each member is modelled using one element. Rigid connections are assumed between chord members in order to simulate the typically used multi-bolted connections. Hinged connections are assumed for diagonal members to simulate single-bolted connections used to connect those members to the chord members. A two-noded, nonlinear, three dimensional cable element is used to model the transmission lines and the supporting guys. The element has three translational degrees of freedom at each node. The cable element nonlinear formulation accounts for tension stiffness and geometric nonlinearities resulting from large displacements and the P-delta effect. More details regarding the finite element model are provided by Hamada et al. (2010) and Hamada and El Damatty (2011).

7.2.2 F2 Tornado Wind Field

CFD simulation conducted by Hangan and Kim (2008) and used by Hamada et al. (2010) to obtain the three dimensional F2 tornado wind field is employed in the current study. The CFD simulations were conducted in a steady state manner. The F2 tornado wind

field is given as a function of the cylindrical coordinates r , θ , and Z . It has an approximate path width of 400 (m), accompanied with an outside gust front width of 2,400 (m). Vertical profiles for tangential, radial, and vertical velocity components at the near ground (100 m) region are provided in Fig. 7-4 to Fig. 7-6. The vertical profiles of the three velocity components are provided at various radial distances r . As shown in the figures, for radial distance $r < 200$ (m), the tornado wind profile is significantly different than the conventional boundary wind profile. Near the tornado center, the vertical location of the peak tangential velocity becomes very close to the ground. Also, away from the tornado center, the vertical location of the peak radial velocity becomes quite close to the ground. In addition, the radial velocity changes direction with height, where negative values shown in the figures imply velocities acting in an inward direction while positive values mean velocities acting in the outward direction. The vertical component acts in an upward direction and is characterized by a zero value at ground level. It is obvious from the figures that the tangential, radial, and axial velocity components change significantly with the location relative to the tornado center. The vertical wind profiles of the three velocity components vary for different values of radial distance r . The maximum tangential gust velocity, which incorporates the tornado translation velocity of the F2 tornado, is 78 m/sec and occurs at a radius $r = 96$ m and a height $Z = 22$ m. The maximum radial velocity is 49 m/sec and corresponds to a radius $r = 146$ m and a height $Z = 6$ m. The maximum vertical velocity is 37 m/sec and corresponds to a radius $r = 171$ m and a height $Z = 127$ m.

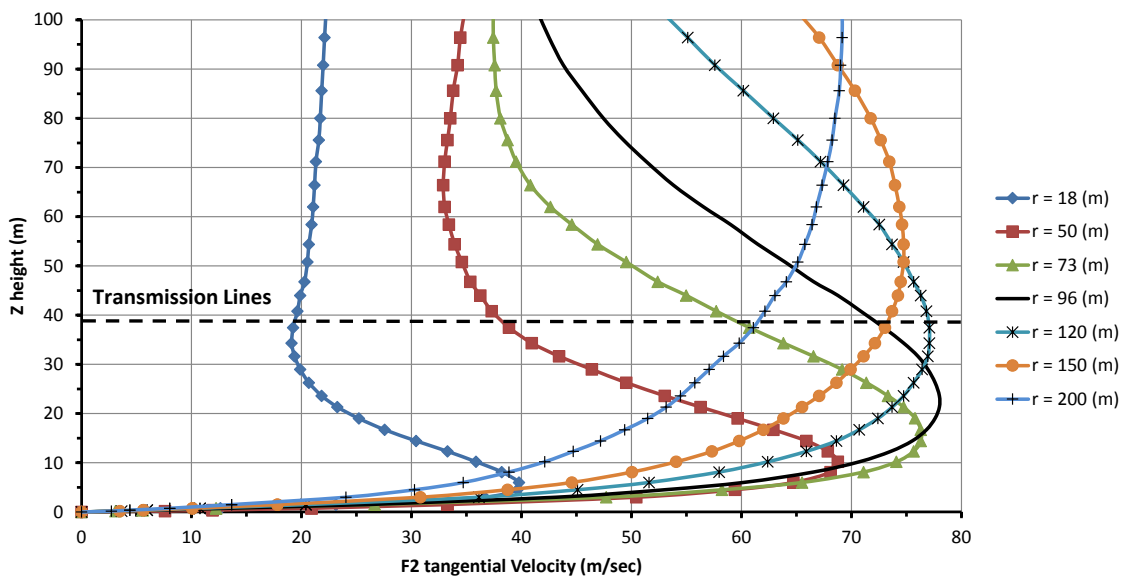


Fig. 7-4 Vertical profile of tangential velocity component for different radial distances “r” from tornado center – F2 Tornado

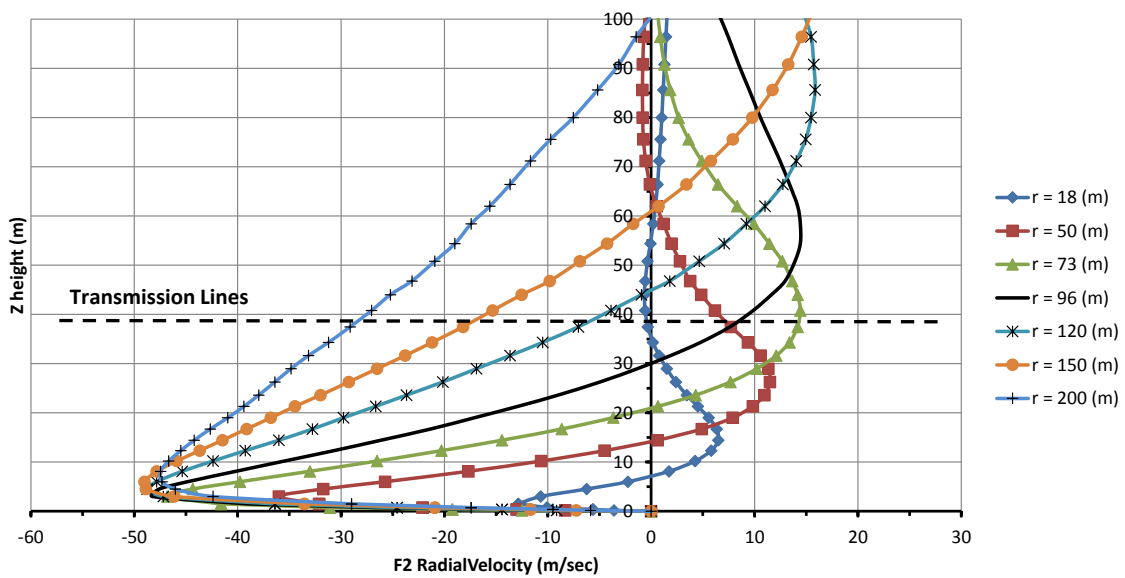


Fig. 7-5 Vertical profile of radial velocity component for different radial distances “r” from tornado center – F2 Tornado

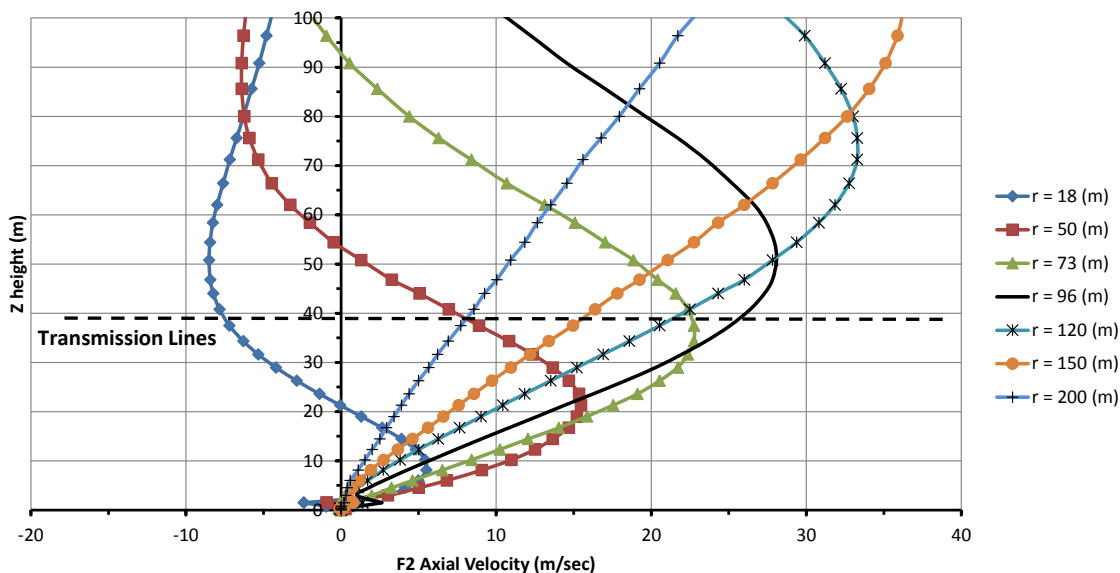


Fig. 7-6 Vertical profile of axial (vertical) velocity component for different radial distances “ r ” from tornado center – F2 Tornado

7.3 Parametric study

As mentioned before, the critical load cases developed in this chapter are based on extensive parametric studies conducted on the four transmission line system described earlier. The analyses of the towers T1 and T3 were conducted previously and were reported by Hamada et al. (2010), Hamada and El Damatty (2011), and Altalmas (2011), respectively. The analyses of the towers T2 and T4 are conducted in the current study. Only analyses under F2 tornado loading are considered since the aim is to develop load cases simulating this level of tornadoes. The self-weight of the towers and the lines are included in the analyses. The parametric study for each transmission line system involves a large number of quasi-static analyses by considering different values for the tornado location (R and θ) as shown in Fig. 7-7; R and θ are the relative tornado location with respect to the tower of interest. Combinations of thirteen values for R and sixteen values

for θ are considered in each parametric study. Each combination represents a different load case for the lines and the tower of interest. The considered values for R are 50, 75, 90, 100, 125, 150, 200, 250, 300, 350, 400, 450, and 500 (m) and for the angles θ are 0, 30, 45, 60, 90, 120, 135, 150, 180, 210, 225, 240, 270, 300, 315, and 330°.

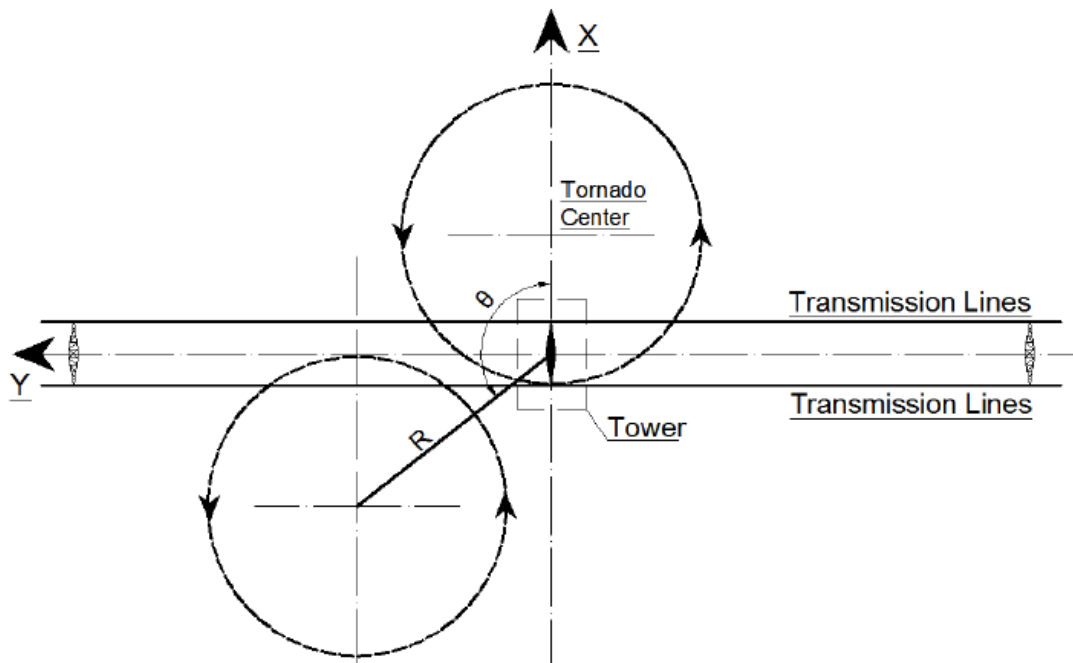


Fig. 7-7 Tornado Configurations R and θ Relative to the Tower of Interest

The four parametric studies reveal that the internal forces in all transmission tower members change significantly with the variation of the parameters R and θ . Different types of transmission tower members, either chord or diagonal members, have independent critical tornado configurations R and θ that lead to the peak (compression or tension) internal forces in those members. By examining all the results of the parametric studies, a number of critical tornado configurations (R and θ) that lead to peak forces in

the main body of the towers as well as in the cross-arms areas are identified in the current study. These identified tornado configurations are described in the next two subsections.

7.3.1 Critical tornado configuration on transmission tower's main body

Three critical values for R are identified. In addition, four critical values of θ are identified for each value of R . Those critical configurations are:

$$R = 100 \text{ (m), with } \theta = 0^\circ, 90^\circ, 180^\circ, \text{ and } 270^\circ$$

$$R = 125 \text{ (m), with } \theta = 30^\circ, 150^\circ, 210^\circ, \text{ and } 330^\circ$$

$$R = 150 \text{ (m), with } \theta = 60^\circ, 120^\circ, 240^\circ, \text{ and } 300^\circ$$

A discussion is carried out below to highlight the reason the above configurations are critical. According to Fig. 7-4 to Fig. 7-6, the relative distance to the tower of interest R of 100, 125, 150 (m) coincides with maximum tangential, radial, and vertical velocities on the tower of interest. To assess the effect of the lines on the forces transmitted to the towers, the variation of transmission lines transverse, vertical, and longitudinal reactions with respect to R and θ are shown in Fig. 7-8 to Fig. 7-11, respectively. In the following discussion, lines' reactions represent the conductors and ground-wire forces that are inverted on the tower of interest. An analogy can be made between a self-supported lattice transmission tower and a cantilever beam, as well as between a guyed tower and an overhanging beam. In both cases, due to tornadoes, the beam will be subjected to distributed loads acting on the tower members and concentrated loads representing the forces (reaction) from the lines transferred to the tower.

- Cases of $R = 100$ (m) and $\theta = 0^\circ$ and 180° : these tornado locations relative to the tower of interest lead to a large distributed loads along the tower height with maximum values close to the ground followed by a monotonic decrease similar to the wind velocity profile shown in Fig. 7-4 and 5. The distributed load on tower is accompanied with both minimum transverse and significant longitudinal reactions from the lines as depicted from Fig. 7-8 and 11, respectively. The minimum lines' transverse reaction is due to the opposite wind directions, almost counter balancing each other, on the spans adjacent to the tower of interest. The significant lines' longitudinal reaction is due to unbalanced loads on the spans adjacent to the tower of interest.
- Cases of $R = 100$ (m) and $\theta = 90^\circ$ and 270° : similar to the previous case, a large distributed load following the same trend is exhibited along the tower height. In this case, a significant transverse lines' reaction exists with a minimum longitudinal reaction, as depicted from Fig. 7-8 and 11.
- Cases of $R = 125$ (m) and $\theta = 30^\circ, 150^\circ, 210^\circ,$ and 330° : These tornado locations lead to larger distributed loads along the tower height, especially in the upper region. As shown in Fig. 7-4 and Fig. 7-5, the tangential velocity profile has a significant wind speed that extends from a height of 20 (m) to 50 (m). In addition, the radial velocity component has a maximum value near the ground and decreases with height till it reaches almost a zero value at the cross-arms height. The transverse loads on the adjacent spans of the towers almost counter balance each other and lead to a minimum transverse reaction, as depicted from Fig. 7-8. Similar to the case of $R = 100$ (m) and $\theta = 0^\circ$ and 180° , the unbalanced loads on

the adjacent spans result in a significant longitudinal reaction from the lines, as shown in Fig. 7-11 and Fig. 7-12.

- Cases of $R = 150$ (m) and $\theta = 60^\circ, 120^\circ, 240^\circ,$ and 300° : the distributed loads along the tower height follows the same discussion for $R = 125$ (m). For $\theta = 60^\circ,$ and 240° ; a significant high transverse reaction from the lines is observed accompanied with a significant longitudinal reaction, as depicted from Fig. 7-8 to Fig. 7-12.

Further discussions regarding the behaviour of transmission lines under tornadoes are provided by Hamada et al. (2010), Hamada and El Damatty (2011), and Altalmas (2011).

7.3.2 Critical tornado configuration on cross-arms

This section is divided into two subsections 3.2.1 and 3.2.2. Subsection 3.2.1 assess the critical tornado configurations that lead to the maximum transverse force applied on the supporting tower from the transmission lines. Subsection 3.2.2 discusses the critical tornado configurations that lead to the maximum longitudinal force for the lines.

7.3.2.1 Cases of maximum transverse reactions of the conductors

The extensive parametric study results are used to evaluate the maximum transverse (perpendicular to the lines) reactions of the transmission lines on the supporting towers.

The main objective is to identify the critical tornado configuration R and θ that lead to the maximum transverse reactions of the lines. The transverse and vertical reactions of all the considered thirteen values of R and the corresponding sixteen values of θ are calculated for each conductor and ground-wire of towers T1, T2, T3, and T4. The variation of the

transverse and vertical reactions with R and θ is shown to follow the same trend for all cases with change only in magnitudes. Thus, only the results for one transmission line system, transmission tower T1, are presented in Fig. 7-8 and Fig. 7-10, where the variations with R and θ of transverse and vertical reactions are plotted, respectively. As shown in Fig. 7-8, the transmission line's transverse reaction varies significantly with R and θ . Based on the results of the study, the maximum transmission line's transverse reaction is found to be associated with tornado configuration: $R = 250$ (m) and $\theta = 60^\circ$ and 240° .

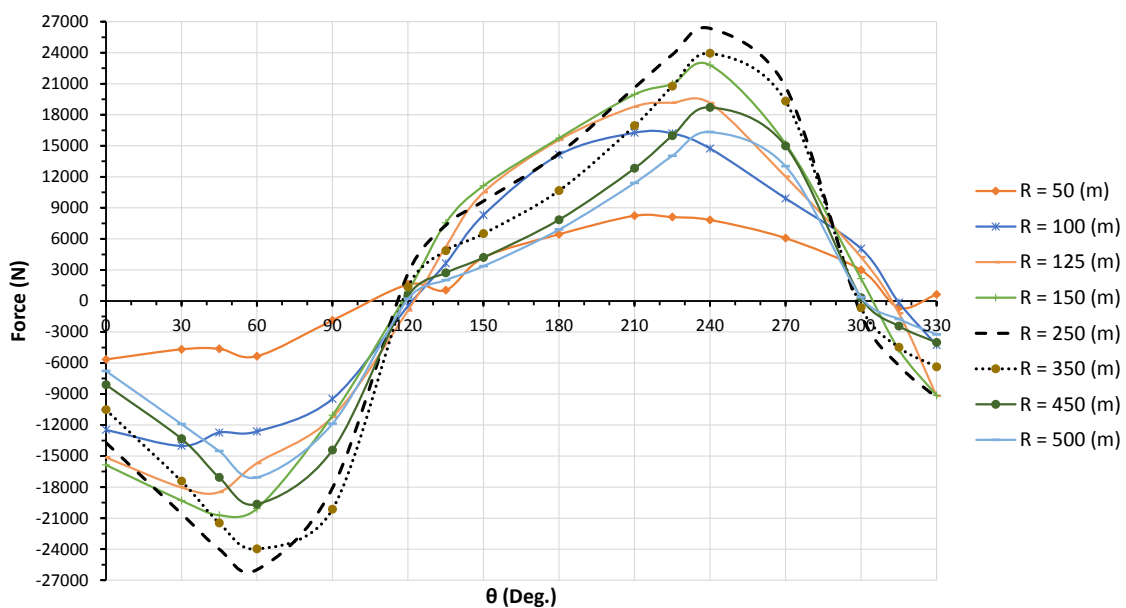


Fig. 7-8 Variation of Transmission Line's Transverse Reaction with R and θ (T1 Tower)

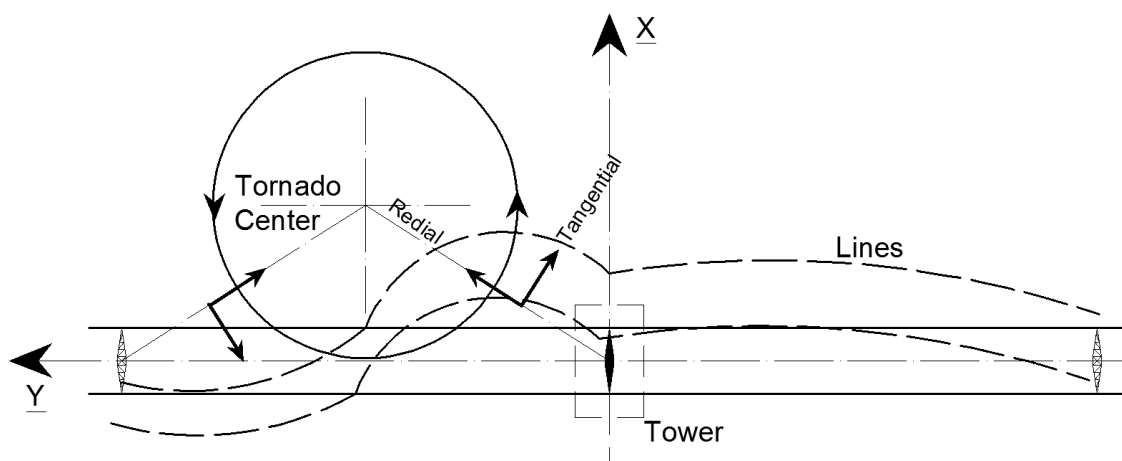


Fig. 7-9 Schematic View of Critical Tornado Configuration $R = 250$ (m) and $\theta = 60^\circ$ (T1 Tower)

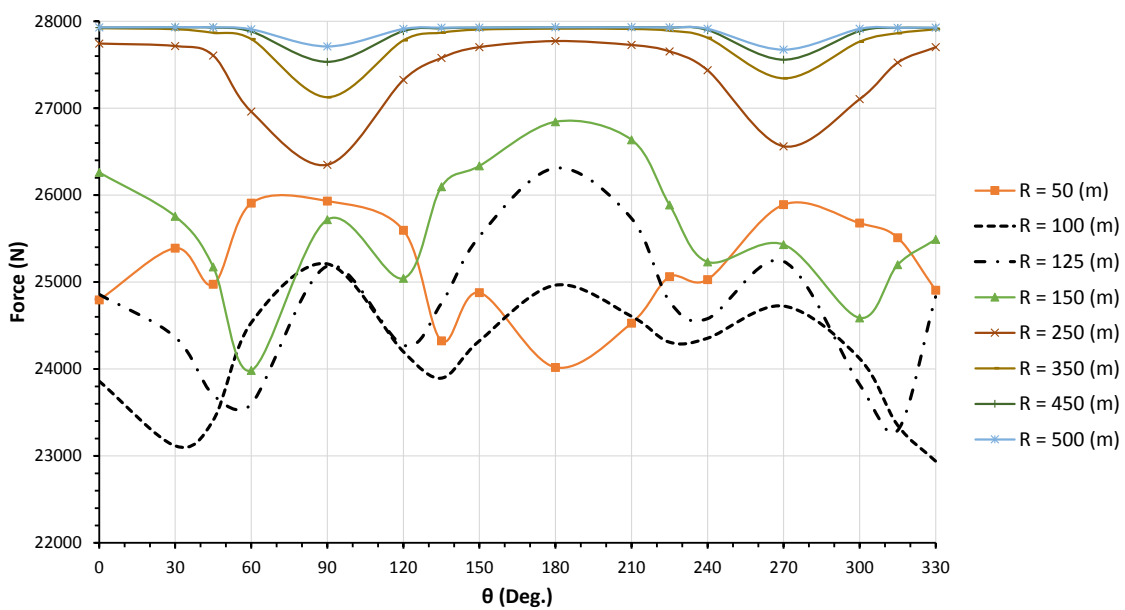


Fig. 7-10 Variation of Transmission Line's Vertical Reaction with R and θ (T1 Tower)

The maximum transverse reaction critical configuration ($R = 250$ (m) and $\theta = 60^\circ$) can be explained in view of the schematic shown in Fig. 7-9. The angle $\theta = 60^\circ$ and 240° leads to a maximum resultant of the tangential and radial velocity components, as shown in Fig. 7-9. For this tornado location, the transverse velocity profile along the tributary length (mid-span to mid-span of adjacent conductors) carried by the tower of interest is unidirectional. This is found to happen regardless of the span length.

The weight of the conductors and ground-wires is considered as a main component in the design of the lines' cross-arms and the tower. The uplift force generated by F2 tornado is found to be always less than the gravity of the lines and, therefore, no vertical uplift movement is anticipated for the lines. There is a 20% reduction in the vertical reaction of the wire due to some tornado configurations, as shown in Fig. 7-10.

7.3.2.2 Cases of maximum longitudinal reactions of the conductors

Longitudinal reactions of transmission lines lead to an important loading case which is caused by the unbalanced tornado loads on the adjacent spans of the tower of interest. Hamada and El Damatty (2011) concluded that these cases can lead to compression forces in the transmission tower's cross-arms that are not typically considered in the design of these tower sections. There was evidence of failure of a transmission tower during a downburst event as a result of an unbalanced load case as reported by Shehata and El Damatty (2008). The results of one conductor for transmission line system T1 are shown in Fig. 7-11, and for transmission line system T2 are shown in Fig. 7-12. As shown in both figures, the variation of the longitudinal reactions with R and θ is following the same trend with difference in magnitudes. The results show that the critical

tornado configurations that give the maximum transmission lines longitudinal reactions are as follows:

$$R = 450 \text{ (m)}, \text{ with } \theta = 90^\circ \text{ and } 270^\circ$$

$$R = 125 \text{ (m)}, \text{ with } \theta = 0^\circ \text{ and } 180^\circ$$

The results also indicate that the longitudinal reaction can reach up to 40% of the maximum transverse reaction. This can be concluded from Fig. 7-12, as the maximum longitudinal reaction of transmission line T2 is 11,071 (N), while the maximum transverse reaction is 28,859 (N).

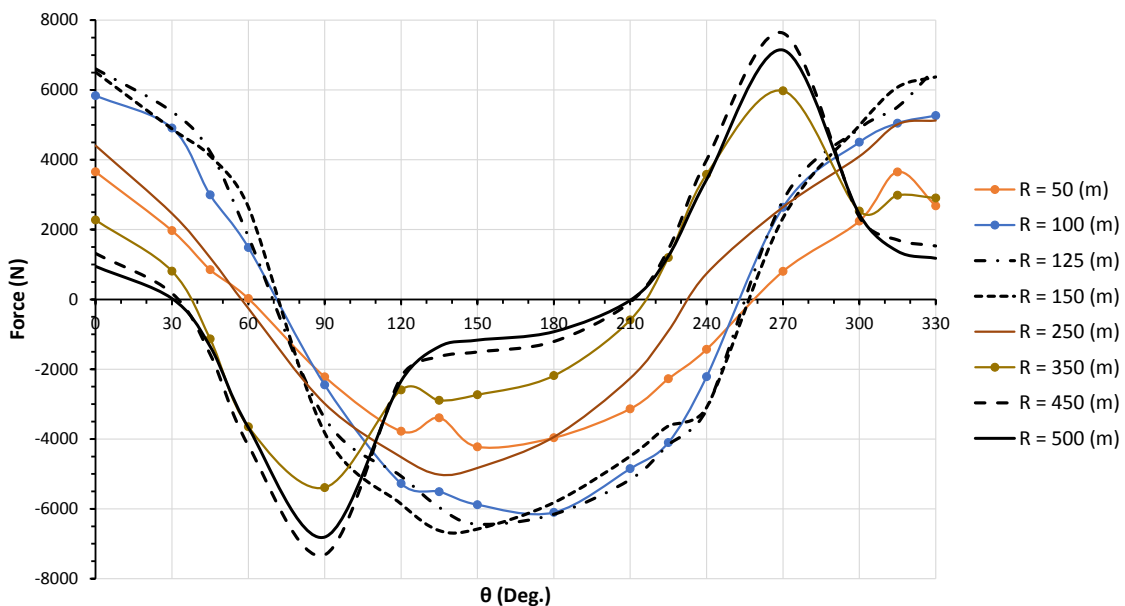


Fig. 7-11 Variation of Transmission Line's Longitudinal Reaction with R and θ (T1 Tower)

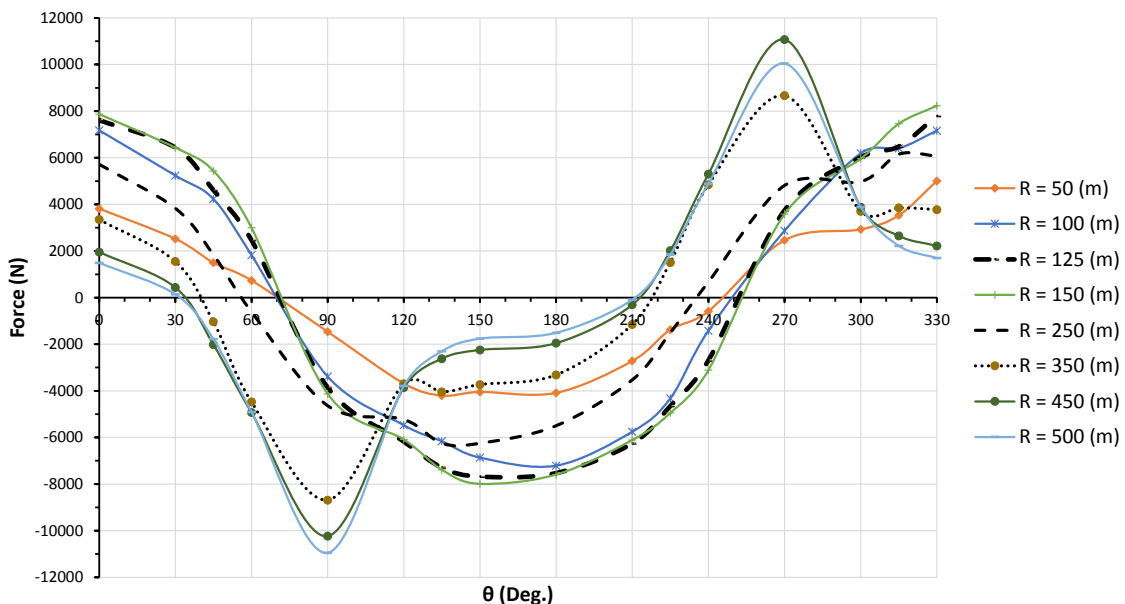


Fig. 7-12 Variation of Transmission Line's Longitudinal Reaction with R and θ (T2 Tower)

7.4 Velocity Profiles for Critical Load Cases for the Towers – Tower Profiles

The basic velocity profiles of the twelve recommended load configurations reported in Section 3.1 are resolved from the tangential and radial directions into the Cartesian coordinates (X and Y), where X is the direction perpendicular to the lines and Y is the direction parallel to the lines. The vertical components of the basic velocity profiles are along the Z direction. After careful examination of the X, Y, and Z basic velocity profiles along the height of the towers for the twelve cases, it is found that they can be described in view of five tower velocity profiles denoted as profiles A to G. Those six tower

profiles are illustrated in Appendix I and a curve fit equations is provided to describe each one of them.

Table 7-1 Recommended Twelve Case of Loading of Transmission Towers and Lines for Peak Internal Forces in the Tower of Interest

Distance from tornado center R (m)																	
Load Case #	Tornado config. R=100 (m)				Load Case #	Tornado config. R=125 (m)				Load Case #	Tornado config. R=150 (m)						
	Tornado config. θ	Applied tower velocity (m/s)				Cables transverse velocity (m/s)	Tornado config. θ	Applied tower velocity (m/s)			Cables transverse velocity (m/s)	Tornado config. θ	Applied tower velocity (m/s)			Cables transverse velocity (m/s)	
		x	y	z				x	y				z	x	y		z
1	0°	A	-B	G	H	5	30°	C	-D	G	L	9	60°	B	-F	0.75 G	P
2	90°	B	A	G	I	6	150°	F	B	0.80 G	M	10	120°	D	C	0.75 G	Q
3	180°	-A	B	G	J	7	210°	-C	D	G	N	11	240°	-B	0.80 F	0.75 G	R
4	270°	-B	-A	G	K	8	330°	-F	-B	0.80 G	O	12	300°	-0.80 D	-C	0.75 G	S

A profile of wind velocity acting along the transverse direction of the transmission lines is also associated with each one of the twelve load cases. Also by examining those profiles, it is found that they have twelve different shapes and those are denoted by profiles H to S and are illustrated in Appendix II together with the curve fitting equations describing each one of them. The tower profile designation describing the three velocity components of the wind field along the height of the towers as well as describing the variation of the transverse velocity along the spans of the conductors adjacent to the tower of interest are given in Table 7-1 for the twelve load cases. It should be noted, that for some diagonal members, it is found that the peak internal forces occur when the conductors and ground-wires forces are not included. As such, it is recommended that those twelve load cases be repeated twice; firstly with inclusion of both conductors and ground-wires and the secondly without the inclusion of both the conductors and ground-wires.

7.5 Velocity Profiles for Critical Load Cases for Cross-arms – Line Profiles

The twelve load cases presented above embrace all configurations leading to peak forces in members of the main body of a tangent lattice transmission tower. However, the analyses indicate that other tornado configurations can lead to peak forces in members of the towers' cross-arms. The internal forces in the cross-arm members depend mainly on the forces transmitted from the conductors to the tower as a result of the wind loads acting on those conductors. It should be noted that the longitudinal forces result from the case where the wind loads acting on two spans adjacent to a tower are unequal. This case leads to a variation in the conductor's internal tension forces between the two spans and, consequently, a resultant longitudinal force is transferred to the cross-arms through the insulators. As such, the critical tornado configurations for the cross-arms are those leading to maximum values for the transverse and longitudinal forces transmitted from the conductors to the tower.

Table 7-2 Recommended Six Case of Loading of Transmission Towers and Lines for Maximum Longitudinal and Transverse Reactions of Transmission Lines

Maximum Longitudinal Reaction												Maximum Transverse Reaction					
Load Case #	Tornado config. R=450					Load Case #	Tornado config. R=125					Load Case #	Tornado config. R=250				
	Tornado config. θ	Applied tower velocity			Cables transverse velocity (m/s)		Tornado config. θ	Applied tower velocity			Cables transverse velocity (m/s)		Tornado config. θ	Applied tower velocity			Cables transverse velocity (m/s)
		x	y	z				x	y	z				x	y	z	
13	90°	C1	C2	--	C6	15	0°	C3	- C4	C5	C8	17	60°	0.8 C4	0.5 C3	0.25 C5	C10
14	270°	- C1	- C2	--	C7	16	180°	- C3	C4	C5	C9	18	240°	- 0.8 C4	-0.5 C3	0.25 C5	C11

The parametric studies conducted on the four lines predict six critical load cases for the cross-arm members (reported in Subsection 7.3.2.1 and Subsection 7.3.2.2). Those cases are described in Table 7-2, where the values of the radial distance R and the angle θ are

provided for each case. As shown in the table, the variation of the three velocity components along the height of a tower can be represented by four basic profiles (C1 to C4). Those line profiles are presented graphically and are described mathematically in Appendix III. Similar to the load cases for the main body of the tower, each load case for the cross-arm is associated with a specific profile for transverse velocity acting along the conductor spans adjacent to the tower of interest. Those profiles are denoted in Table 7-2 as C6 to C11 and are illustrated in Appendix IV.

7.6 Steps of Applying Critical Load Cases on Transmission lines

The steps below describe how the above developed critical tornado profiles can be applied to a transmission line system in order to predict the response of a tangent tower to F2 tornadoes:

- 1) The tower, the conductors, the ground-wires, and the supporting guys of guyed towers are modelled as described in Section 2.1 using any available commercial software. At least two conductors' spans from each side of the tower of interest should be included in the analyses. As shown in Appendix II and IV, the conductor loads are provided for a distance of 500 (m) from each side of the tower. Beyond this distance, the loading should be maintained constant with a value corresponding to that at the 500 (m) distance.
- 2) For each load case,
 - i. The velocity profiles in the X, Y, and Z directions are used to evaluate the velocities at the nodal points of the tower and supporting guys.

- ii. The lines velocity profile is used to evaluate the transverse velocity at the conductors and ground-wire nodal points.
 - iii. The horizontal and vertical forces acting on the nodal points of the tower, conductors, ground-wire, and supporting guys are evaluated using the procedures specified in the design code or manual of practice employed by the user (e.g. ASCE 2010).
 - iv. Nonlinear (with geometric nonlinearity included) elastic static analysis is conducted for the transmission line system.
 - v. Tower`s members peak internal forces are evaluated.
- 3) Envelop of the tower`s members peak internal force resulting from all critical cases is evaluated.

7.7 Verification using different towers configurations

The load cases presented above are developed based on extensive parametric studies conducted on four different tangent lattice transmission line systems. The approach adopted to verify the adequacy of those load cases involves considering two other independent and different transmission line systems. As extensive parametric study is conducted for those two lines by moving the tornado in space (at different R and θ values). For each specific value of R and θ , a nonlinear analysis is conducted for the three dimensional finite element model of the transmission line system and the internal forces in the members of the tower of interest are recorded. The peak forces in the members obtained from the entire parametric studies are determined.

Meanwhile, the lines are analyzed nonlinearly under the 18 load cases proposed in this chapter and the envelope for the peak forces in various members of the tower due to those load cases are determined. The peak forces obtained from both the critical load cases analyses and the parametric study are compared together. The proposed load cases would be considered conservative if they estimate peak internal forces exceeding those resulting from the extensive parametric studies. It is considered here that the load cases are acceptable even if the parametric studies give higher peak forces as long as the difference is less than 5%.

7.7.1 Description of the Two Transmission Line Systems

The two transmission lines systems employed for verification are generic self-supported and guyed transmission tower systems used by several hydro companies. The towers are labelled as T5 (self-supported) and T6 (guyed) and are shown in Fig. 7-13. Tower T5 height is 51.81(m) and has six conductors' bundles connected to the line's cross-arms using a 2.4 (m) insulator strings. Two ground-wires are connected to the top of the tower. The transmission line system spans are 450 (m). The conductors and ground-wires sags are 20 and 12 (m), respectively. Tower T6 height is 43.44 (m) and is supported by eight guys attached to the cross-arms as shown in Fig. 7-13. Three conductor's bundles are connected to the cross-arms using a 4.27 (m) insulator. Two ground-wires are attached to the top of the tower. The transmission line system spans are 400 (m) and conductors and ground-wires sags are 16 and 11 (m), respectively.

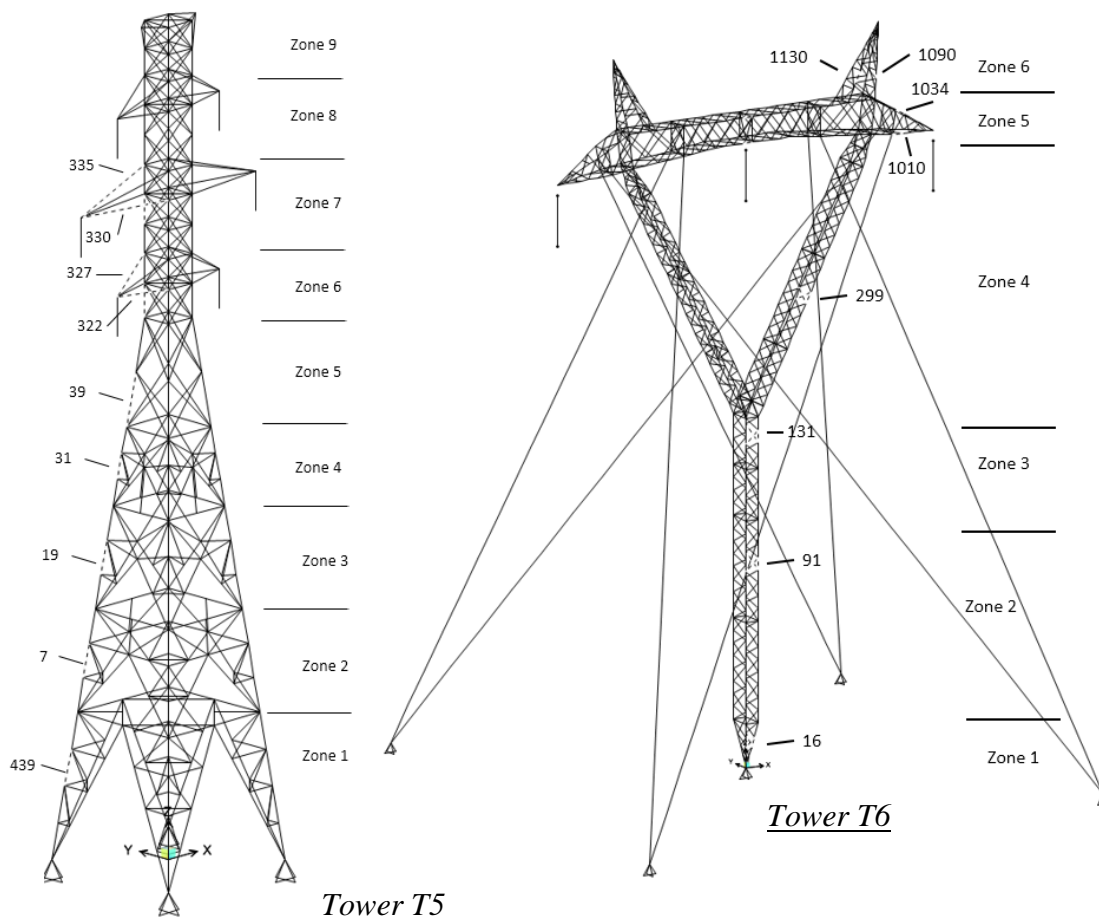


Fig. 7-13 Verification Transmission Towers – Tower T5 and T6

7.7.2 Analysis and Discussion

Towers T5 and T6 are divided into different zones as shown in Fig. 7-13. For each zone, some chord and diagonal members are selected to present the results. In addition, the results are shown for several chord and cross-arm's upper and lower chord members. For each selected member, the peak internal forces resulting from the critical load cases and the extensive parametric studies analyses are reported in Table 7-3 and 4.

The following observations can be concluded:

- The critical tornado configurations (R and θ) that lead to peak internal forces in the two systems coincide with the counterpart values reported earlier in the chapter.
- For chord members, the peak internal forces due to the equivalent F2 loading cases are higher than the parametric study results with a maximum difference of 14%.
- For cross-arms members, the peak internal forces due to the extensive parametric study are 5% higher than the peak internal forces obtained from the equivalent F2 tornado loading cases. This is within the limit set as acceptable difference.

Table 7-3 Parametric Study and Equivalent Loading Cases Results for Tower T5

Member			Parametric Study		Critical Load Cases	Critical Load Cases / Parametric Study	
No.	Type	Peak Axial Force (kN)	<i>Tornado</i>	Peak Axial Force (kN)	%		
Zone 1	439	Chord	-811	$R = 125$ $\theta = 180$	-873	108	
Zone 2	7	Chord	-743	$R = 125$ $\theta = 210$	-802	108	
Zone 3	19	Chord	-654	$R = 150$ $\theta = 210$	-691	106	
Zone 4	31	Chord	-649	$R = 150$ $\theta = 210$	-678	104	
Zone 5	39	Chord	-701	$R = 150$ $\theta = 210$	-719	103	
	Tower	47	Chord	-526	$R = 150$ $\theta = 240$	-565	108
Zone 6	Conductor	327	Upper Chord	14	$R = 400$ $\theta = 270$	14	98
		322	Lower Chord	-32	$R = 150$ $\theta = 0$	-30	95
	Tower	59	Chord	-243	$R = 150$ $\theta = 210$	-276	113
Zone 7	Conductor	335	Upper Chord	25	$R = 150$ $\theta = 0$	24	97
		330	Lower Chord	-65	$R = 125$ $\theta = 0$	-61	95

Table 7-4 Parametric Study and Equivalent Loading Cases Results for Tower T6

Member			Parametric Study	Critical Load Cases	Critical Load Cases / Parametric Study	
No.	Type	Peak Axial Force (kN)	<i>Tornado</i>	Peak Axial Force (kN)	%	
Zone 1	16	Chord	-368 $\frac{R = 125}{\theta = 150}$	-351	95	
Zone 2	91	Chord	-1076 $\frac{R = 125}{\theta = 180}$	-1032	96	
Zone 3	131	Chord	-1259 $\frac{R = 125}{\theta = 180}$	-1221	97	
Zone 4	299	Chord	-488 $\frac{R = 125}{\theta = 180}$	-465	95	
Zone 5	Conductors Cross-arms	1034	Upper Chord	24 $\frac{R = 125}{\theta = 0}$	25	105
		1010	Lower Chord	-23 $\frac{R = 125}{\theta = 0}$	-26	114
Zone 6	1090	Chord	-51 $\frac{R = 125}{\theta = 0}$	-58	114	

7.8 Conclusion

The current study summarizes the major findings of research conducted during the past six years on the effect of F2 tornadoes on tangent lattice transmission line systems. It also builds on this research to develop critical load cases for the analysis of such systems under F2 tornadoes. The study focuses on F2 tornadoes since they are shown to have a cumulative frequency of occurrence of 86%. In the current chapter, the F2 tornado wind field is discussed, where the tangential, radial, and vertical basic velocity profiles of such events are described. Transmission line systems that are commonly used by utility companies and covers different transmission lines variation aspects are used in the current study. The description of the nonlinear three dimensional finite element modelling of the different transmission lines is provided. Based on the results of extensive parametric studies, a number of critical tornado configurations (R and θ) that

lead to peak forces in the transmission tower members are identified. For transmission towers' main body, three critical values for R , combined with four critical values of θ for each value of R , are identified. Those critical configurations are:

$$R = 100 \text{ (m), with } \theta = 0^\circ, 90^\circ, 180^\circ, \text{ and } 270^\circ$$

$$R = 125 \text{ (m), with } \theta = 30^\circ, 150^\circ, 210^\circ, \text{ and } 330^\circ$$

$$R = 150 \text{ (m), with } \theta = 60^\circ, 120^\circ, 240^\circ, \text{ and } 300^\circ$$

For transmission tower's cross-arms, critical tornado configurations that lead to the maximum transverse and longitudinal forces transferred from the lines to the transmission towers are identified. Critical tornado configurations leading to maximum transverse reactions are:

$$R = 250 \text{ (m) and } \theta = 60^\circ \text{ and } 240^\circ$$

and critical tornado configurations of maximum longitudinal reactions are:

$$R = 450 \text{ (m), with } \theta = 90^\circ \text{ and } 270^\circ$$

$$R = 125 \text{ (m), with } \theta = 0^\circ \text{ and } 180^\circ$$

For each of the above eighteen critical load configurations, the velocity wind fields have been resolved from the tangential and radial directions into the Cartesian directions aligned parallel and perpendicular to the transmission lines. Each critical configuration represents a load case and the vertical profile for the three perpendicular velocity components along the height of the tower are provided for each case. In addition, the

corresponding horizontal profile for the transverse velocity acting on the lines are given for each load case. These equivalent load cases represent an envelope for the effect of F2 tornadoes on transmission line systems, and can be applied by a structural engineer in the design process of lattice tangent transmission line structures. Validation for these developed load cases is conducted by considering two independent transmission line systems and conducting extensive parametric studies for each system. The results indicate that the developed critical load cases lead to peak internal forces in the transmission tower members that are either higher or within less than 5% lower than the values predicted by the detailed parametric studies. It should be noticed that these cases do not include the effect of debris on transmission line structures that might happen during large tornado events.

7.9 Acknowledgment

The authors gratefully acknowledge Hydro One Inc. for the in-kind support, the collaboration, and the financial support provided for this research. The second author is indebted to the Vanier Canada Graduate and the Natural Science and Engineering Research Council of Canada (NSERC) for the financial support provided for this research.

7.10 References

Altalmas, A., El Damatty, A. A., and Hamada, A. (2012). "Progressive failure of transmission towers under tornado loading." Annual Conference of the Canadian Society for Civil Engineering 2012: Leadership in Sustainable Infrastructure, CSCE 2012, June 6,

2012 - June 9, Canadian Society for Civil Engineering, Edmonton, AB, Canada, 2220-2229.

Altalmas, A. (2011). "Behaviour of self-supported transmission lines under tornado loading." M.E.Sc. thesis, School of Graduate and Postdoctoral Studies, University of Western Ontario, London, Ont.

American Society of Civil Engineers. (2010). "Guidelines for electrical transmission line structural loading." ASCE manuals and reports on engineering practice, no. 74 (3rd ed.), American Society of Civil Engineers.

Baker, G. L., and Church, C. R. (1979). "Measurements of core radii and peak velocities in modeled atmospheric vortices." *J. Atmos. Sci.*, 36, 2413-2424.

Behncke, R.H., and White, H. B. (2006). "Applying Gust Loadings to Your Lines." Proceedings of the 9th International Conference on Overhead Lines, American Society of Civil Engineers (ASCE), Fort Collins, Colorado

Church, C. R., Snow, J. T., Baker, G. L., and Agee, E. M. (1979). "Characteristics of tornado-like vortices as a function of swirl ratio: A laboratory investigation." *J. Atmos. Sci.*, 36, 1755-1776.

Church, C. J., Snow J. T., and Agee, E. M. (1977), "Tornado vortex simulation at Purdue University." *Bull. Amer. Meteor. Soc.*, 58, 900-908.

CIGRÉ (Conseil International des Grands Réseaux Électriques/ International Council on Large Electrical Systems) SC-22 WG22-06 (2006). "Review of IEC 826: Loading and Strength of Overhead Lines. Part 3: Analysis of Recent Transmission Line Failures." Scientific Committee B2 on Overhead Lines.

CIGRÉ (Conseil International des Grands Réseaux Électriques/ International Council on Large Electrical Systems) (2009). "Overhead line design guidelines for mitigation of severe wind storm damage." Scientific Committee B2 on Overhead Lines, B2. 06.09.

Davies-Jones, R. P. (1973). "The dependence of core radius on swirl ratio in a tornado simulator." *J. Atmos. Sci.*, 30, 1427-1430.

Dempsey, D., and White, H. B. (1996). "Winds wreak havoc on lines." *Transmission & Distribution World*, 48(6), 32 - 42.

El Damatty, A. A., and Hamada, A. (2013). "Behaviour of guyed transmission line structures under tornado wind loads - Case studies." *Electrical Transmission and Substation Structures 2012: Solutions to Building the Grid of Tomorrow*, November 4, 2012 - November 8, American Society of Civil Engineers (ASCE), Columbus, OH, United states, 193-204.

Fujita, T. T., and Pearson, A. D. (1973). "Results of FPP classification of 1971 and 1972 tornadoes." *8th Conference on Severe Local Storms (abstracts only)*, USA, 609.

Hamada, A. (2009). "Analysis and behaviour of guyed transmission line structure under tornado wind loading." M.E.Sc. thesis, School of Graduate and Postdoctoral Studies, University of Western Ontario, London, Ont.

Hamada, A., Damatty, A. A. E., Hangan, H., and Shehata, A. Y. (2010). "Finite element modelling of transmission line structures under tornado wind loading." *Wind and Structures*, 13(5), 451-469.

Hamada, A., and El Damatty, A. A. (2011). "Behaviour of guyed transmission line structures under tornado wind loading." *Computers and Structures*, 89(11-12), 986-1003.

Hamada, A., and El Damatty, A. A. (2012). "Analysis and Behaviour of Guyed Transmission Lines under Tornado Wind Loads – Case Studies." *Annual Conference of the Canadian Society for Civil Engineering 2013: General Conference, CSCE 2013*, May 29, 2013 - June 1, Canadian Society for Civil Engineering, Montreal, QC, Canada.

Hangan, H., and Kim, J. (2008). "Swirl ratio effects on tornado vortices in relation to the Fujita scale." *Wind and Structures*, 11(4), 291-302.

- Holmes, J. D., and Oliver, S. E. (2000). "An empirical model of a downburst." *Eng.Struct.*, 22(9), 1167-1172.
- Ishac, M.F., and White, H.B. (1994). "Effect of tornado loads on transmission lines." *Proceedings of the 1994 IEEE Power Engineering Society Transmission and Distribution Conference*, 10-15 April 1994, IEEE, Chicago, IL, USA, 521-527.
- Kareem, A. (2010). "Bluff Body Aerodynamics and Aeroelasticity: A Wind Effects Perspective." *Journal of Wind Engineering*, 7(1), 30-74.
- Letchford, C. W., and Chay, M. T. (2002). "Pressure distributions on a cube in a simulated thunderstorm downburst. Part B: Moving downburst observations." *J.Wind Eng.Ind.Aerodyn.*, 90(7), 733-753.
- Lund D. E., and Snow, J. (1993). "The tornado: its structure, dynamics, prediction and hazards." *Geophys. Monogr. Ser.*, 79, 297-306.
- Newark, M.J. (1984). "Canadian tornadoes, 1950-1979." *Atmospheric-Ocean*, 22, 243-253.
- Rotunno, R. (1979). "A Study in tornado-like vortex dynamics." *J. Atmos. Sci.*, 36, 140-155.
- Sarkar, P., Haan, F., Gallus, Jr., W., Le, K., and Wurman, J. (2005). "Velocity measurements in a laboratory tornado simulator and their comparison with numerical and full-scale data." *37th Joint Meeting Panel on Wind and Seismic Effects*, Tsukuba, Japan, May 2005.
- Savory, E., Parke, G. A. R., Zeinoddini, M., Toy, N., and Disney, P. (2001). "Modelling of tornado and microburst-induced wind loading and failure of a lattice transmission tower." *Eng.Struct.*, 23(4), 365-375.
- Shehata, A. Y., and El Damatty, A. A. (2008). "Failure analysis of a transmission tower during a microburst." *Wind and Structures*, 11(3), 193-208.

Shehata, A. Y., El Damatty, A. A., and Savory, E. (2005). "Finite element modeling of transmission line under downburst wind loading." *Finite Elements Anal.Des.*, 42(1), 71-89.

Wan, C., and Chang, C. (1972). "Measurement of the velocity field in a simulated tornado-like vortex using a three dimensional velocity probe." *J. Atmos. Sci.*, 29, 116-127.

Wang, H., James, D., Letchford, C. W., Peterson, R., and Snow, J. (2001). "Development of a prototype tornado simulator for the assessment of fluid-structure interaction." First American Conference on Wind Engineering, Clemson, SC.

7.11 Appendices

7.11.1 Appendix I

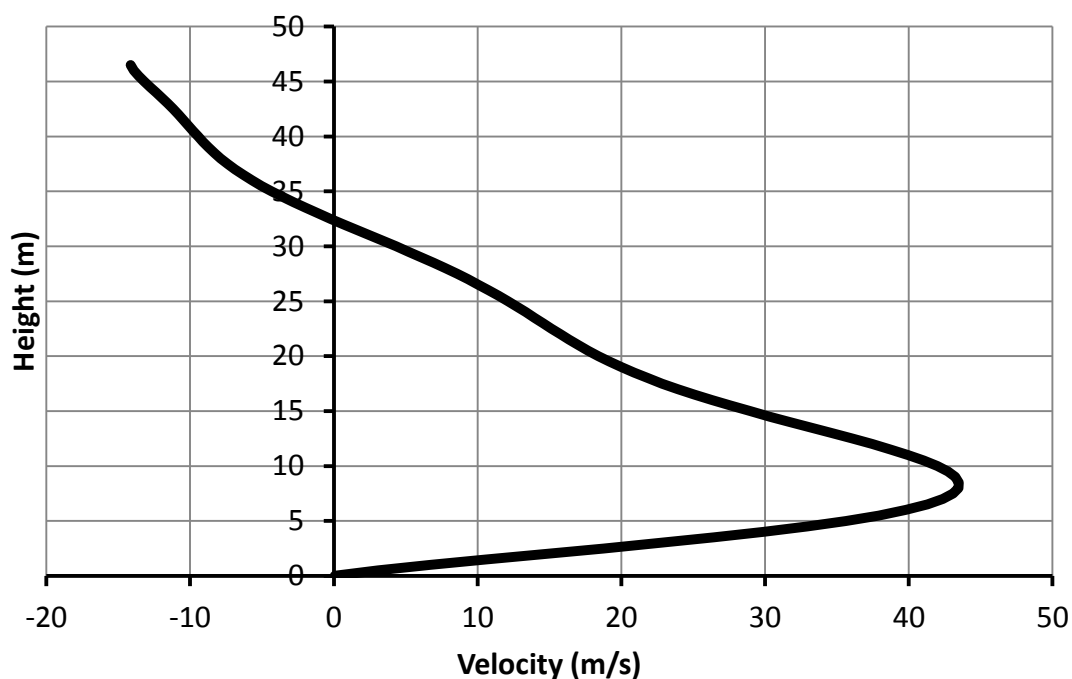


Fig. 7-14 Tower Velocity Profile A along Tower Height – F2 Tornado

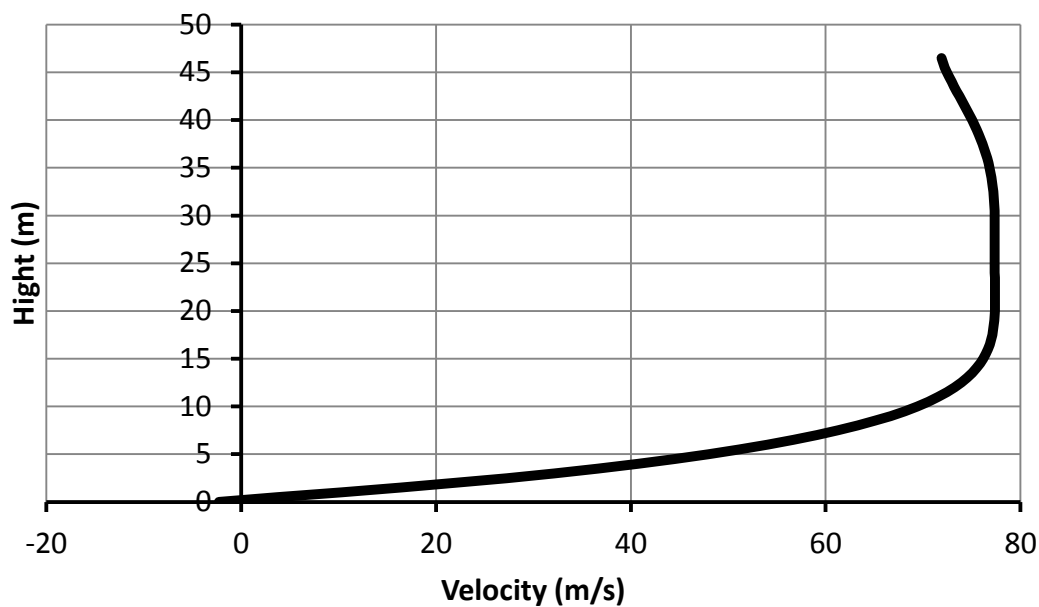


Fig. 7-15 Tower Velocity Profile B along Tower Height – F2 Tornado

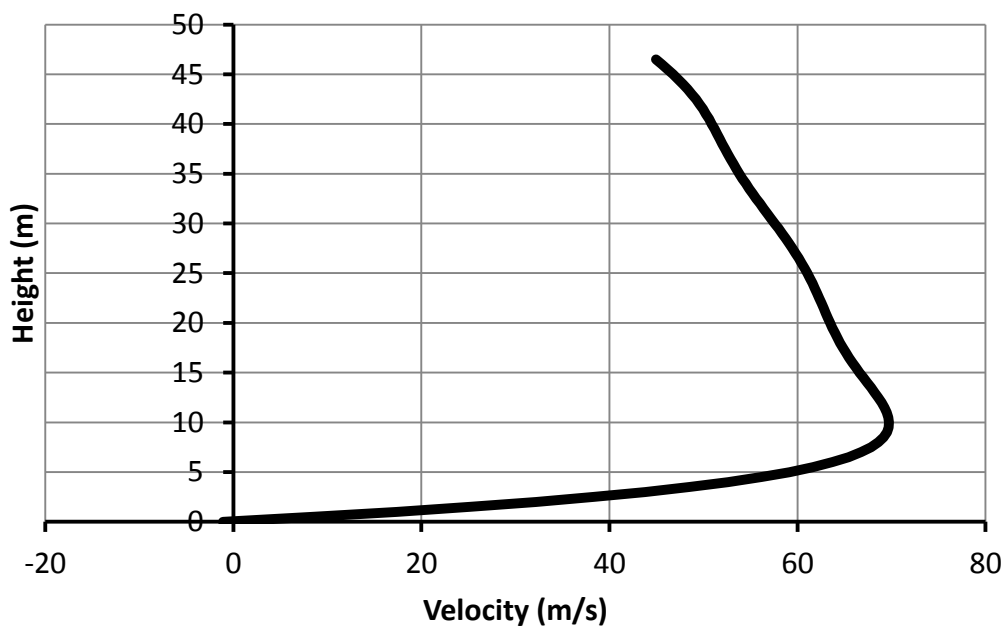


Fig. 7-16 Tower Velocity Profile C along Tower Height – F2 Tornado

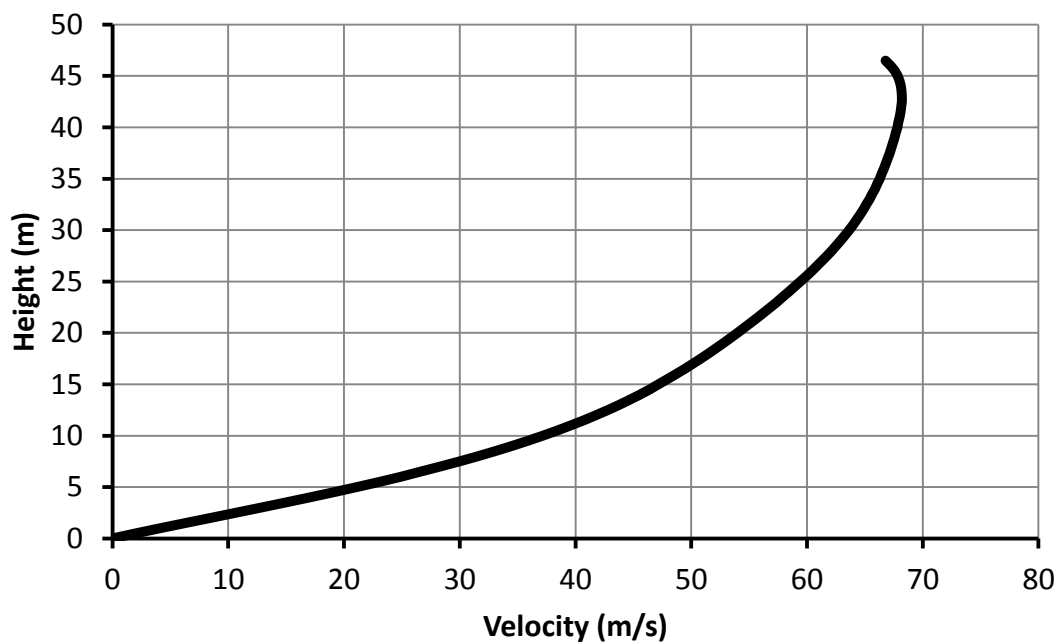


Fig. 7-17 Tower Velocity Profile D along Tower Height – F2 Tornado

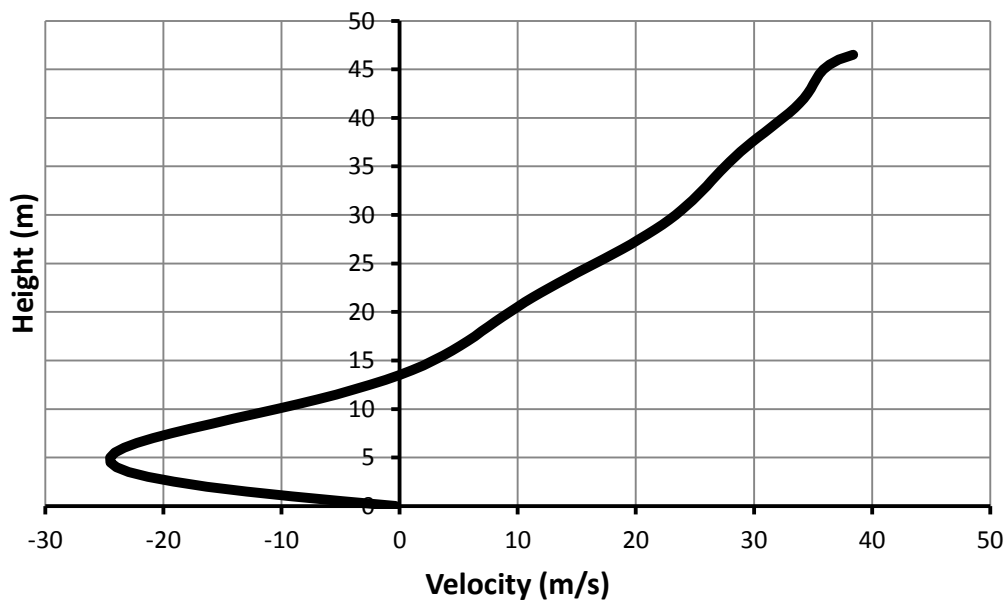


Fig. 7-18 Tower Velocity Profile F along Tower Height – F2 Tornado

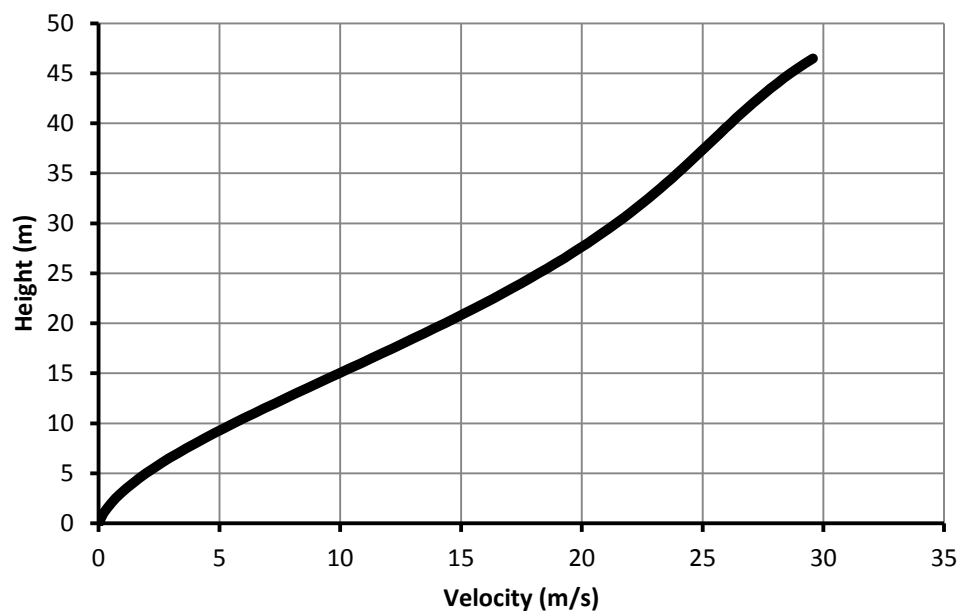


Fig. 7-19 Tower Velocity Profile G along Tower Height – F2 Tornado

Tower profiles' equations (limited for towers with maximum height of 50 m):

“x” is the height from ground and “y” is the velocity

Tower Profile A

$$y = 3.40z^8 - 3.35z^7 - 18.44z^6 + 19.99z^5 + 24.18z^4 - 24.57z^3 - 5.28z^2 - 17.646z + 13.34$$

$$z = (x - 24) / 14.56$$

Tower Profile B

$$y = 1.76z^5 - 7.95z^4 + 10.98z^3 - 6.24z^2 + 1.42z + 77.27$$

$$z = (x - 18.65) / 13.51$$

Tower Profile C

$$y = 0.79z^8 + 0.29z^7 - 7.34z^6 + 4.23z^5 + 10.27z^4 - 5.98z^3 - 4.62z^2 - 7.54z + 61.57$$

$$z = (x - 24) / 14.56$$

Tower Profile D

$$y = 0.22z^7 - 0.56z^6 + 0.76z^5 + 1.34z^4 - 0.63z^3 - 4.65z^2 + 9.14z + 62.80$$

$$z = (x - 28.84) / 12.04$$

Tower Profile E

$$y = 0.88z^{10} - 1.19z^9 - 3.63z^8 + 6.66z^7 + 0.62z^6 - 8.61z^5 + 4.59z^4 + 7.29z^3 - 7.22z^2 - 2.99z + 75.75$$

$$z = (x - 24) / 14.56$$

Tower Profile F

$$y = 3.38z^9 - 0.047z^8 - 20.95z^7 + 5.36z^6 + 39.19z^5 - 14.32z^4 - 22.65z^3 + 3.27z^2 + 22.73z + 14.99$$

$$z = (x - 24) / 14.56$$

Tower Profile G

$$y = 0.006z^5 + 0.29z^4 + 0.03z^3 - 1.87z^2 + 7.34z + 19.63$$

$$z = (x - 27) / 11.27$$

7.11.2 Appendix II

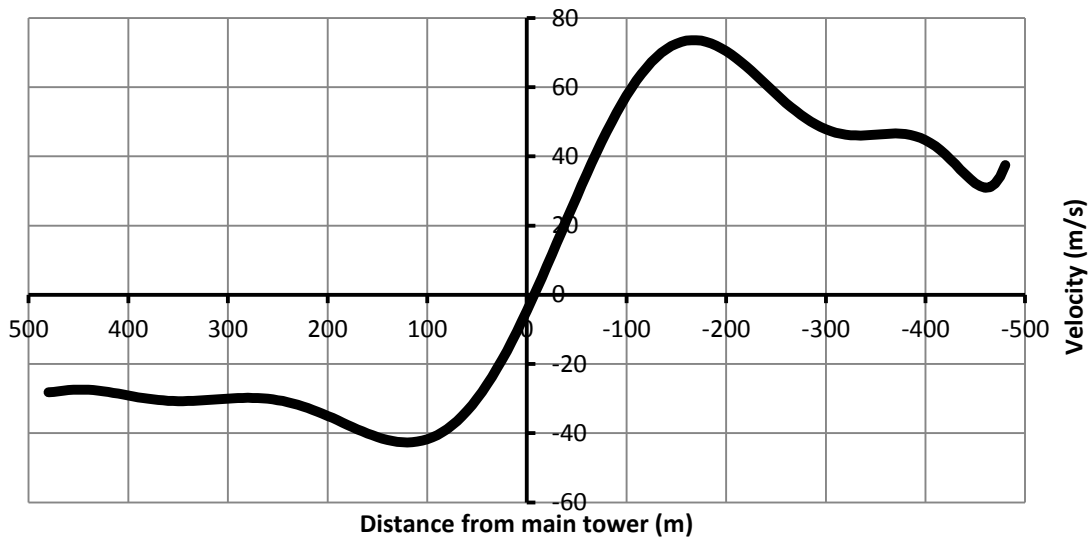


Fig. 7-20 Line Velocity Profile H – F2 Tornado Transverse Velocity Profile along the Lines

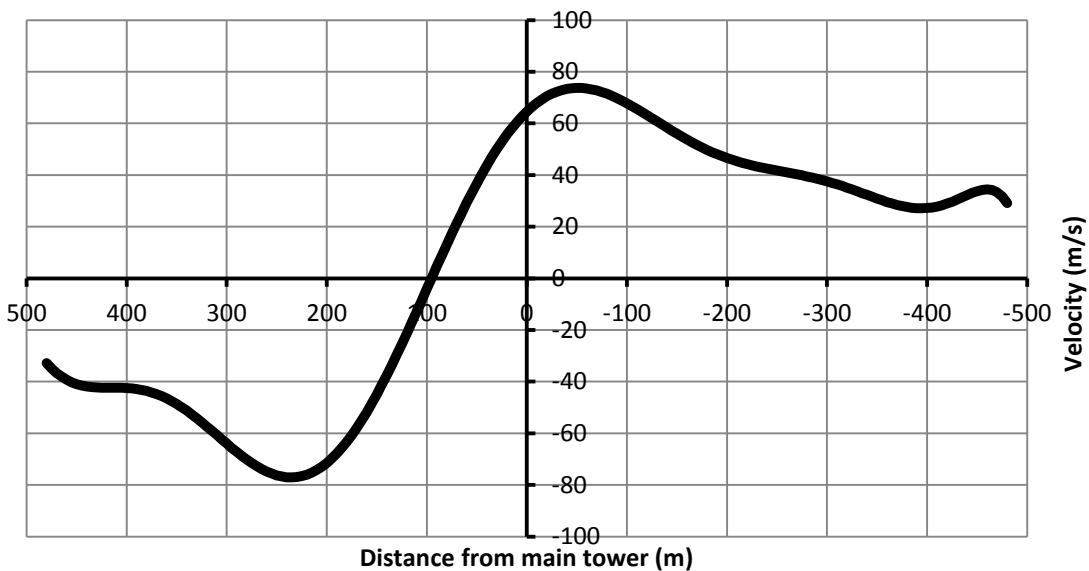


Fig. 7-21 Line Velocity Profile I – F2 Tornado Transverse Velocity Profile along the Lines

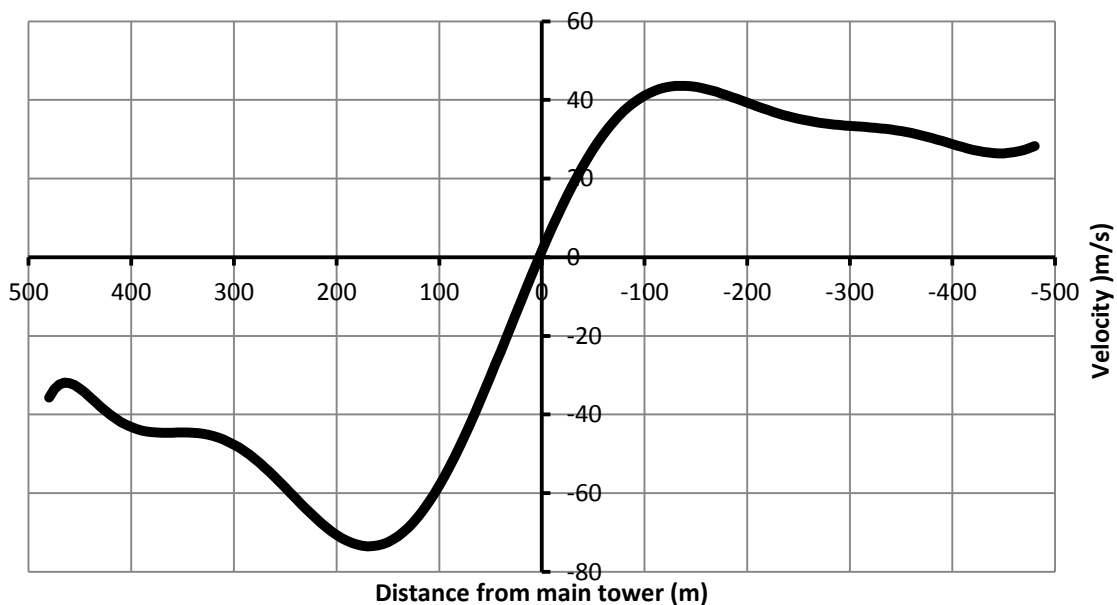


Fig. 7-22 Line Velocity Profile J – F2 Tornado Transverse Velocity Profile along the Lines

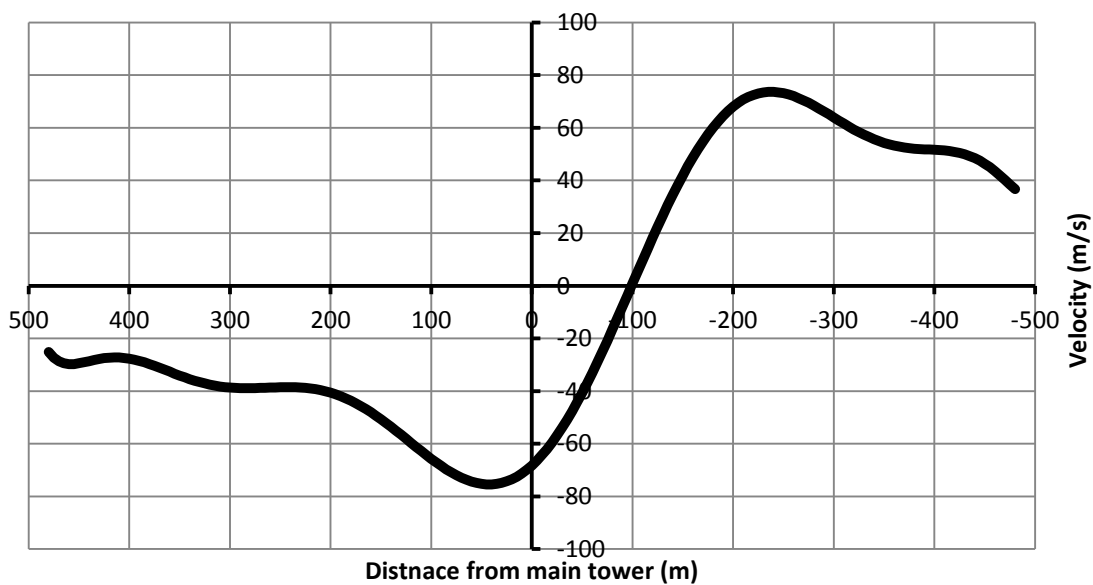


Fig. 7-23 Line Velocity Profile K – F2 Tornado Transverse Velocity Profile along the Lines

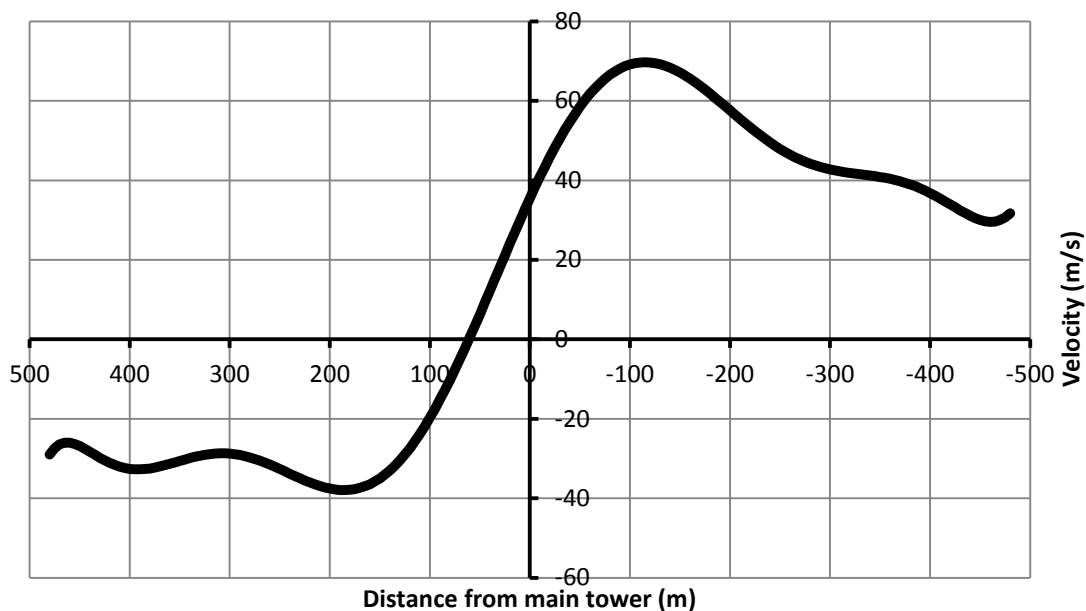


Fig. 7-24 Line Velocity Profile L – F2 Tornado Transverse Velocity Profile along the Lines

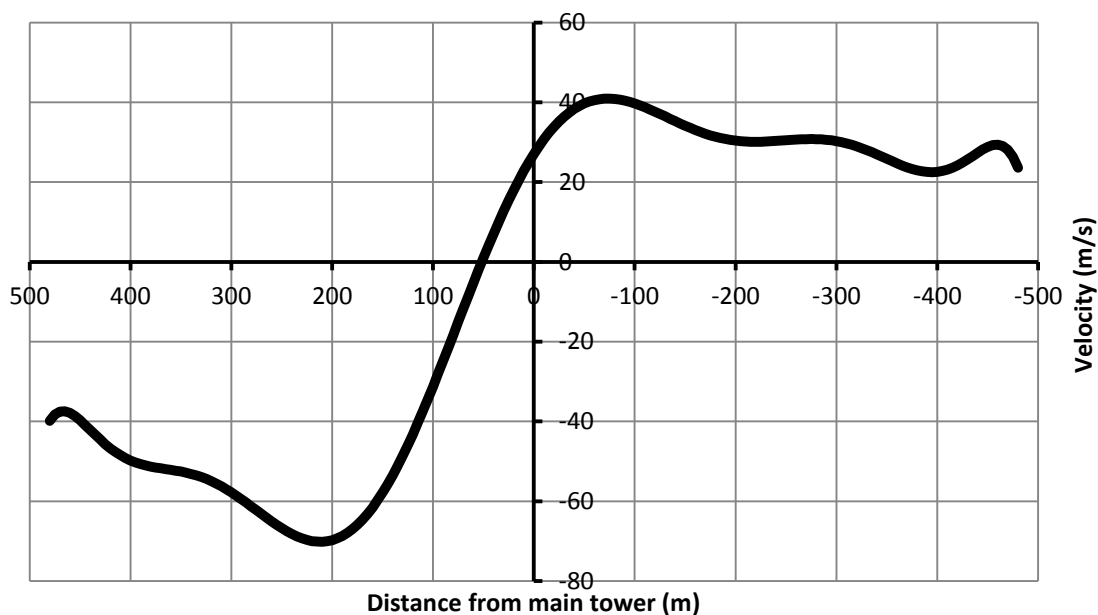


Fig. 7-25 Line Velocity Profile M – F2 Tornado Transverse Velocity Profile along the Lines

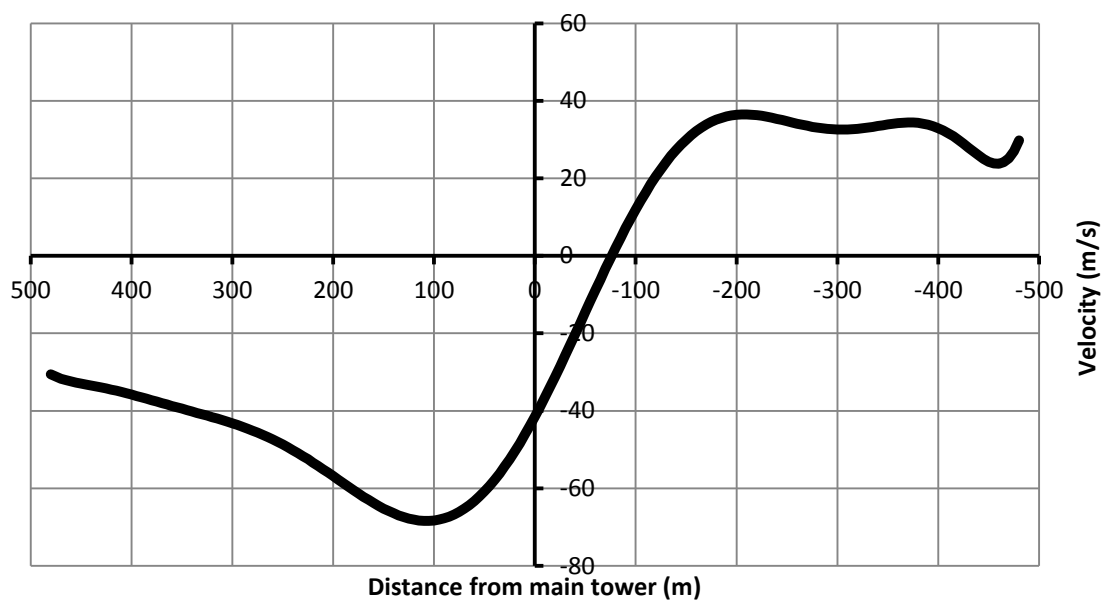


Fig. 7-26 Line Velocity Profile N – F2 Tornado Transverse Velocity Profile along the Lines

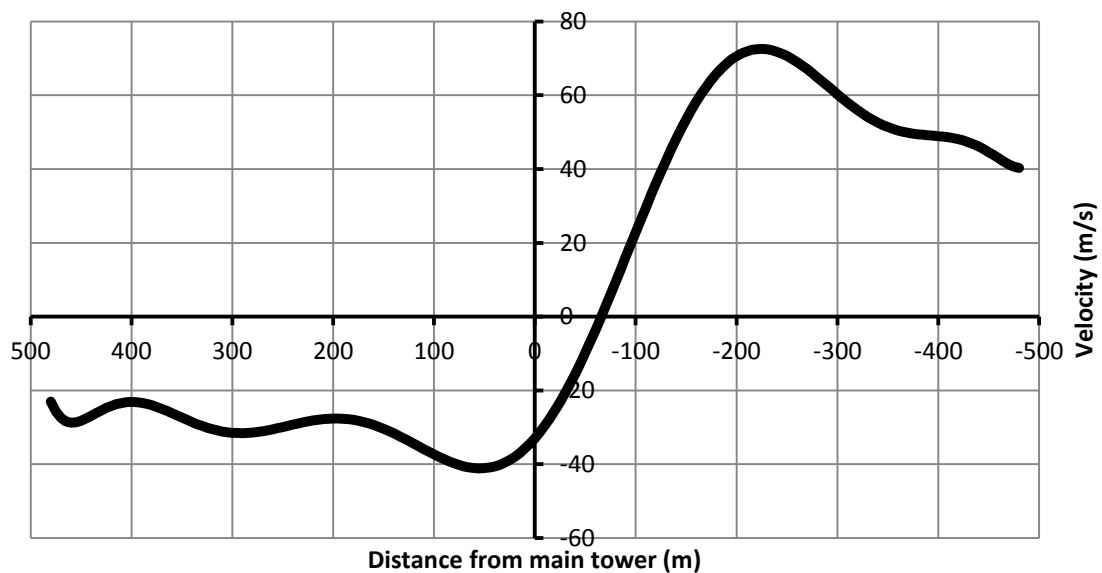


Fig. 7-27 Line Velocity Profile O – F2 Tornado Transverse Velocity Profile along the Lines

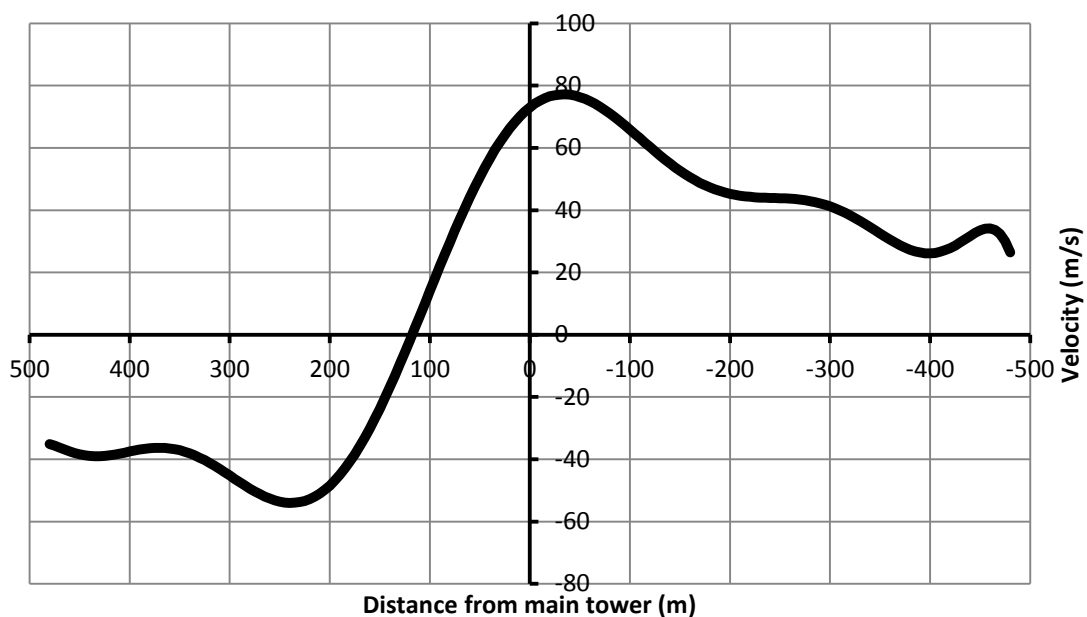


Fig. 7-28 Line Velocity Profile P – F2 Tornado Transverse Velocity Profile along the Lines

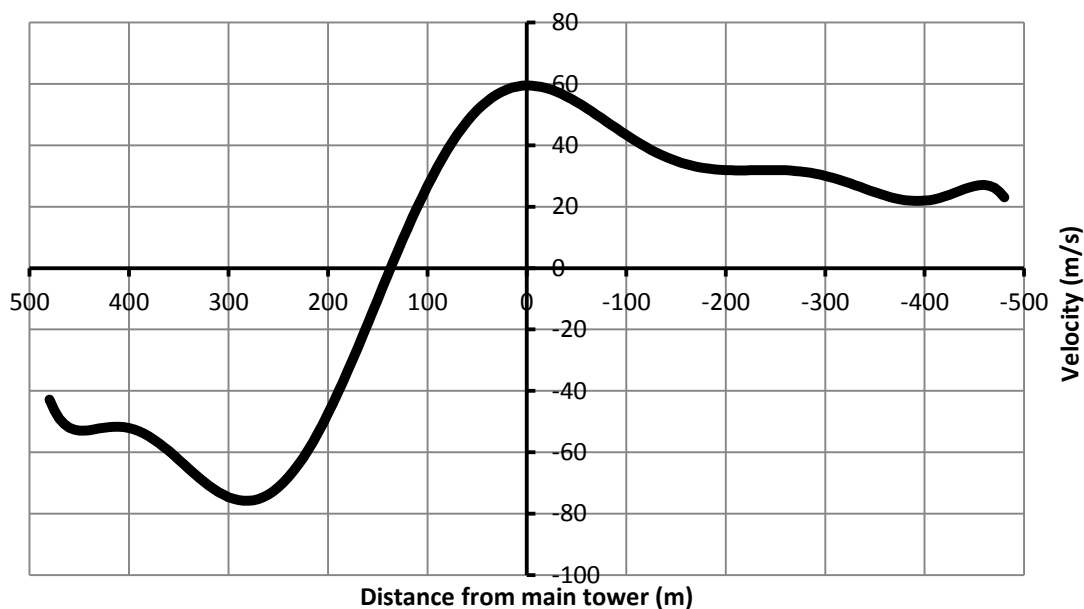


Fig. 7-29 Line Velocity Profile Q – F2 Tornado Transverse Velocity Profile along the Lines

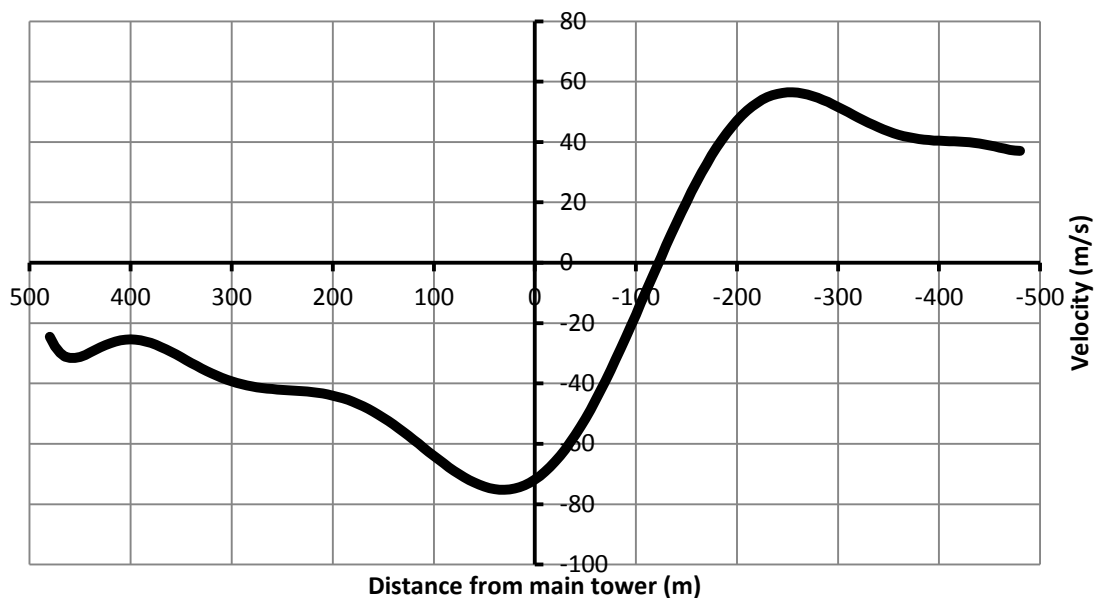


Fig. 7-30 Line Velocity Profile R – F2 Tornado Transverse Velocity Profile along the Lines

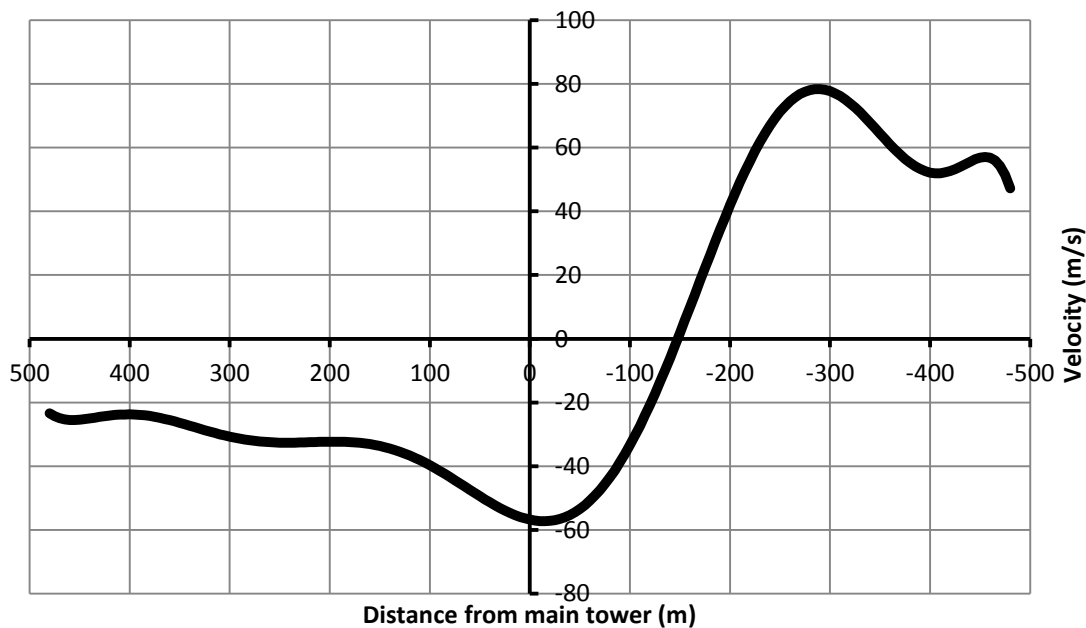


Fig. 7-31 Line Velocity Profile S – F2 Tornado Transverse Velocity Profile along the Lines

Line Profiles' equations:

“x” is the distance from the tower of interest and “y” is the velocity

Line Profile H

$$y = 11.03z^{10} - 14.80z^9 - 82.85z^8 + 106.22z^7 + 227.91z^6 - 277.77z^5 - 277.67z^4 + 326.1z^3 + 135.81z^2 - 179.2z - 4.63$$

$$z = x / 290.95$$

Line Profile I

$$y = -11.56z^{10} + 9.01z^9 + 98.63z^8 - 50.64z^7 - 319.06z^6 + 75z^5 + 483.07z^4 + 22.1z^3 - 329.88z^2 - 108.16z + 64.60$$

$$z = x / 290.95$$

Line Profile J

$$y = -8.91z^{10} - 12.23z^9 + 68.19z^8 + 89.77z^7 - 190.18z^6 - 242.93z^5 + 231.96z^4 + 300.68z^3 - 110.44z^2 - 176.64z + 1.63$$

$$z = x / 290.95$$

Line Profile K

$$y = 14.68z^{10} + 5.15z^9 - 123.23z^8 - 27.54z^7 + 387.4z^6 + 34.28z^5 - 561.56z^4 + 37.36z^3 + 364.55z^2 - 101.71z - 68.25$$

$$z = x / 290.95$$

Line Profile L

$$y = -4.77z^{10} - 12.96z^9 + 38.92z^8 + 93.58z^7 - 118.1z^6 - 245.83z^5 + 164.87z^4 + 289.26z^3 - 109.29z^2 - 160.24z + 35.49$$

$$z = x / 290.95$$

Line Profile M

$$y = -16.11z^{10} - 0.58z^9 + 122.12z^8 + 10.37z^7 - 341.96z^6 - 52.67z^5 + 434.45z^4 + 113.88z^3 - 239.91z^2 - 115.94z + 27.05$$

$$z = x / 290.95$$

Line Profile N

$$y = 7.99z^{10} - 9.74z^9 - 59.14z^8 + 70.31z^7 + 163.44z^6 - 186.72z^5 - 212.23z^4 + 229.09z^3 + 135.79z^2 - 141.31z - 41.49$$

$$z = x / 290.95$$

Line Profile O

$$y = 14.27z^{10} + 5.02z^9 - 113.93z^8 - 27.15z^7 + 338.48z^6 + 34.59z^5 - 457.7z^4 + 32.46z^3 + 267.23z^2 - 91.89z - 32.95$$

$$z = x / 290.95$$

Line Profile P

$$y = -16.26z^{10} + 9.59z^9 + 130.24z^8 - 56.82z^7 - 390.33z^6 + 99.39z^5 + 539.35z^4 - 22.71z^3 - 338.53z^2 - 74.08z + 73.02$$

$$z = x / 290.95$$

Line Profile Q

$$y = -1.57z^{10} + 17.62z^9 + 22.55z^8 - 119.16z^7 - 110.32z^6 + 273.3z^5 + 241.58z^4 - 223.35z^3 - 234.15z^2 - 1.52z + 59.48$$

$$z = x / 290.95$$

Line Profile R

$$y = 13.69z^{10} + 9.14z^9 - 109.9z^8 - 56.95z^7 + 333.52z^6 + 109.64z^5 - 475.42z^4 - 44.17z^3 + 316.41z^2 - 64.31z - 71.85$$

$$z = x / 290.95$$

Line Profile S

$$y = -4.46z^{10} + 19.59z^9 + 21.07z^8 - 135.27z^7 - 1.92z^6 + 319.85z^5 - 119.66z^4 - 278.51z^3 + 185.28z^2 + 19.50z - 56.78$$

$$z = x / 290.95$$

7.11.3 Appendix III

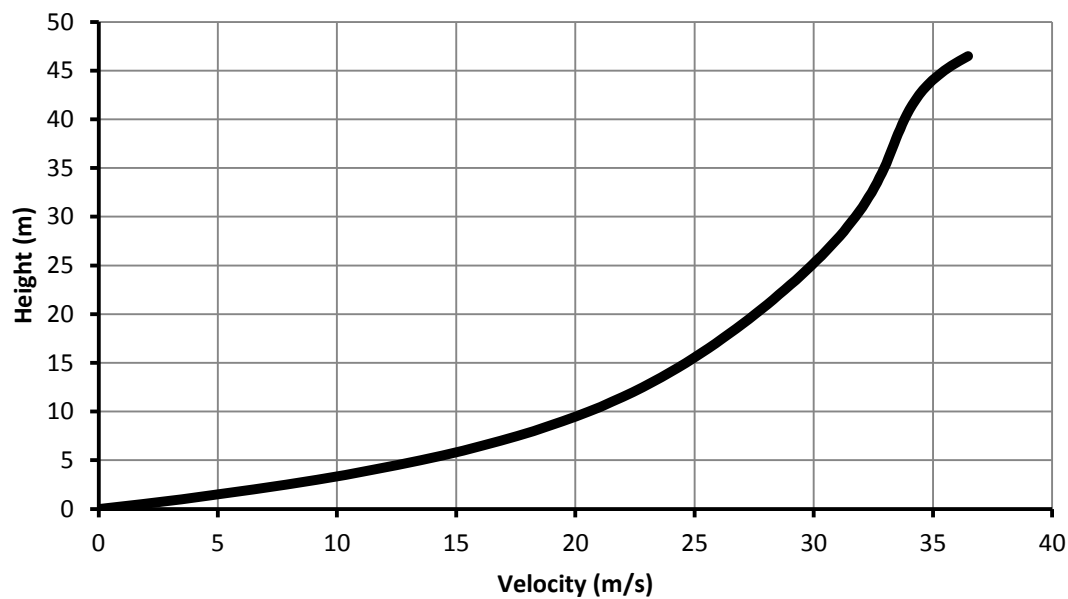


Fig. 7-32 Tower Velocity Profile C1 along Tower Height – F2 Tornado

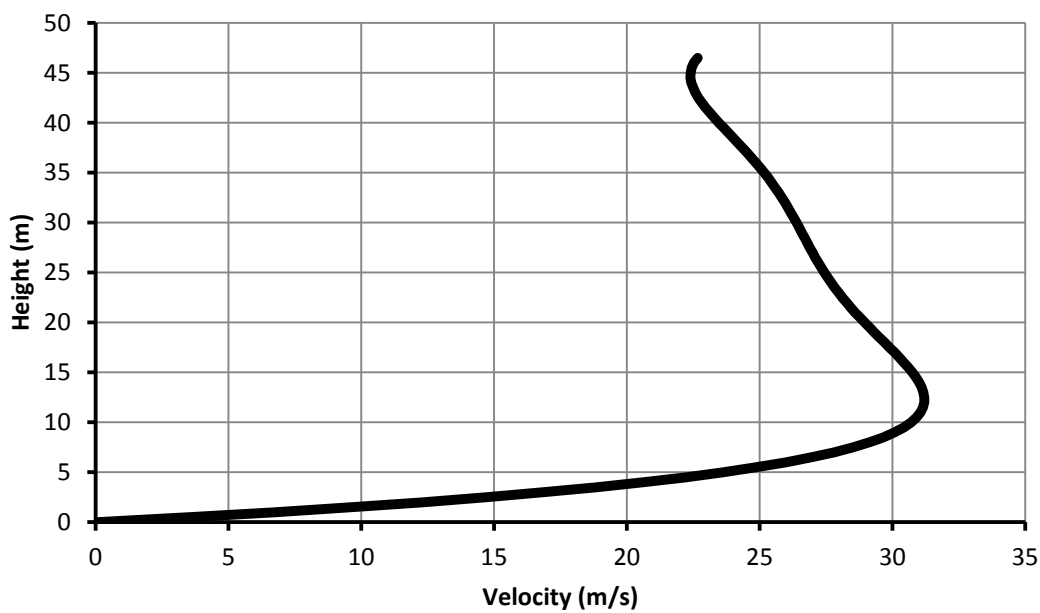


Fig. 7-33 Tower Velocity Profile C2 along Tower Height – F2 Tornado

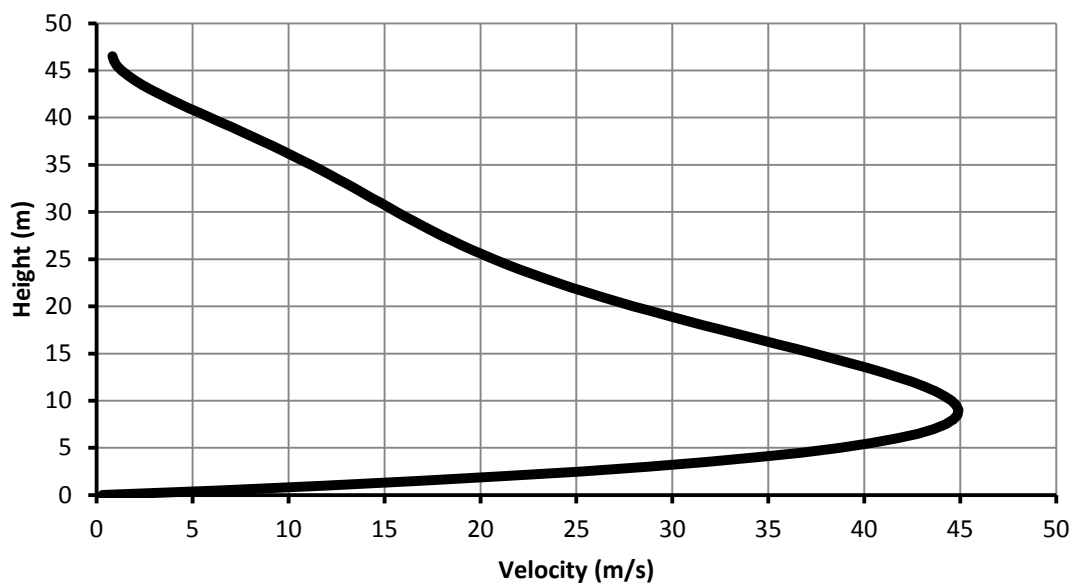


Fig. 7-34 Tower Velocity Profile C3 along Tower Height – F2 Tornado

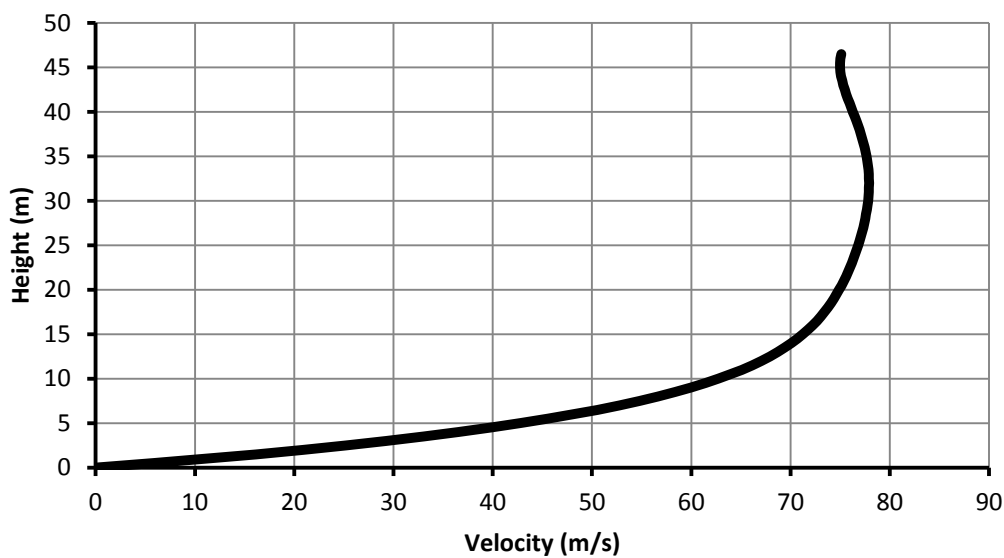


Fig. 7-35 Tower Velocity Profile C4 along Tower Height – F2 Tornado

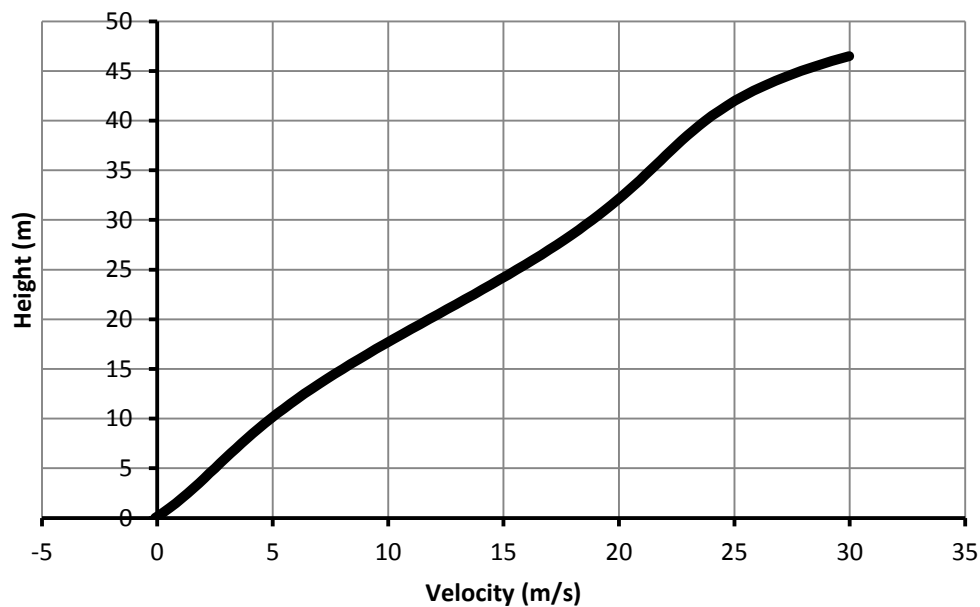


Fig. 7-36 Tower Velocity Profile C5 along Tower Height – F2 Tornado

Tower Profiles' equations (limited for towers with maximum height of 50 m):

“x” is the height from ground and “y” is the velocity

Tower Profile C1

$$y = 0.34z^5 + 0.38z^4 - 0.27z^3 - 1.87z^2 + 4.04z + 31.37$$

$$z = (x - 28.84) / 12.04$$

Tower Profile C2

$$y = 0.76z^5 + 0.07z^4 - 1.86z^3 - 0.03z^2 - 2.39z + 26.62$$

$$z = (x - 18.65) / 13.50$$

Tower Profile C3

$$y = 1.10z^5 - z^4 - 3.68z^3 + 4.39z^2 - 11.48z + 18.41$$

$$z = (x - 27.06) / 11.27$$

Tower Profile C4

$$y = 0.82z^5 - 0.17z^4 - 1.07z^3 - 3.05z^2 + 1.78z + 77.66$$

$$z = (x - 28.84) / 12.04$$

Tower Profile C5

$$y = 0.56z^5 + 0.34z^4 - 2.29z^3 - 0.87z^2 + 10.53z + 13.48$$

$$z = (x - 22.20) / 13.67$$

7.11.4 Appendix IV

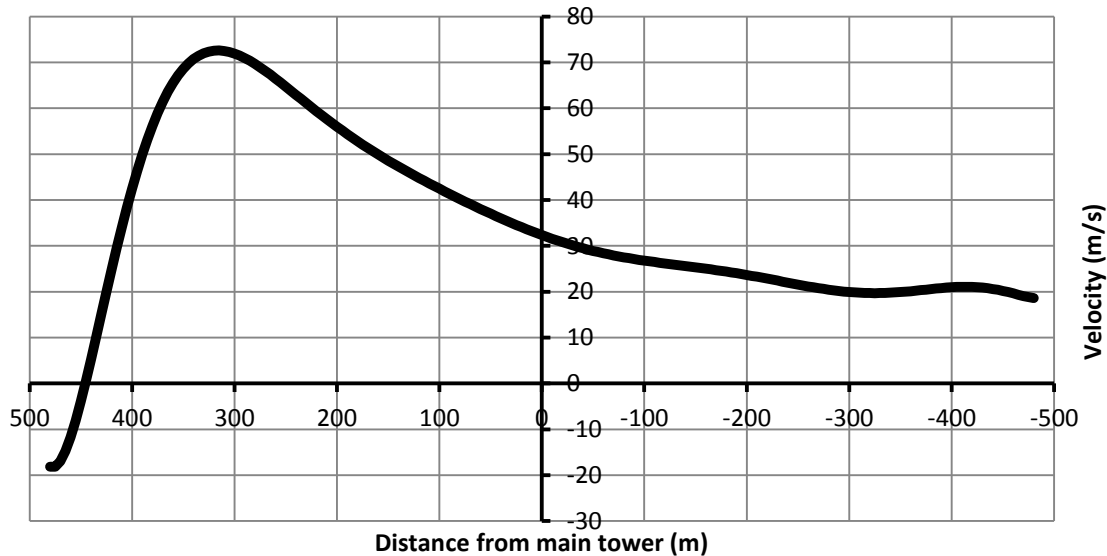


Fig. 7-37 Line Velocity Profile C6 – F2 Tornado Transverse Velocity Profile along the Lines

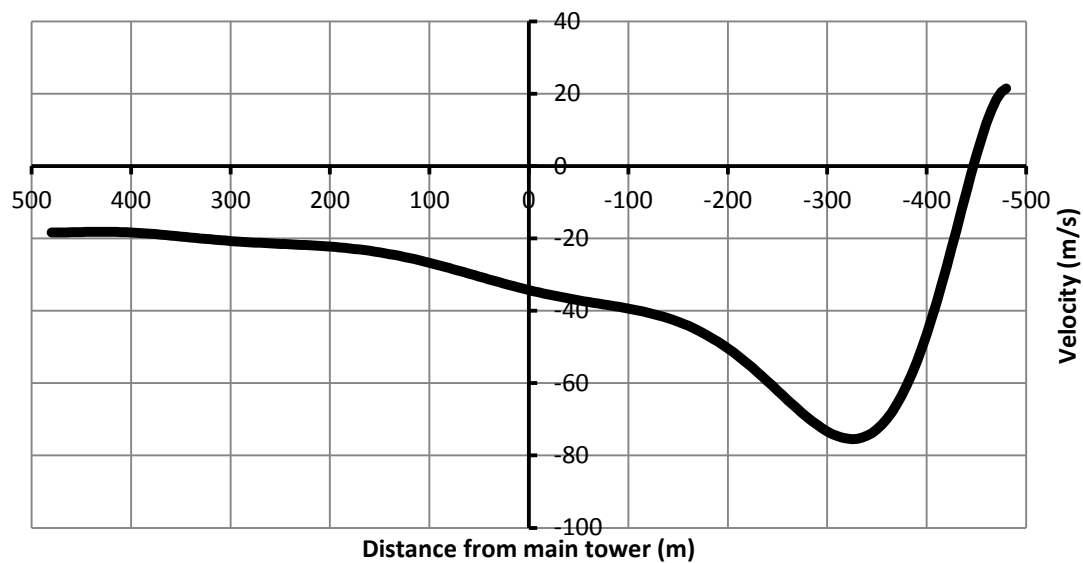


Fig. 7-38 Line Velocity Profile C7 – F2 Tornado Transverse Velocity Profile along the Lines

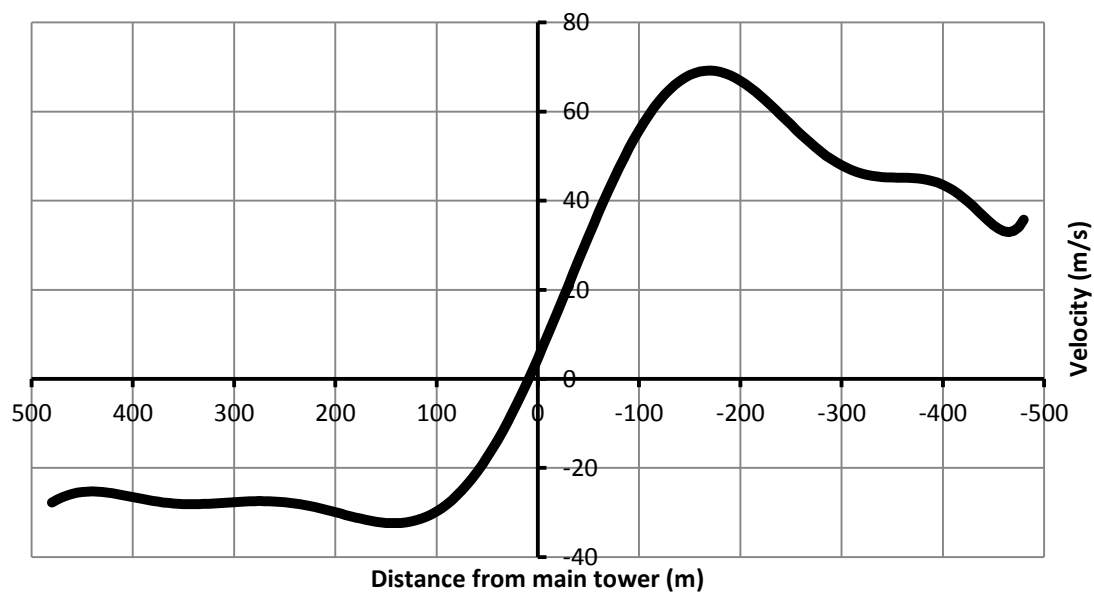


Fig. 7-39 Line Velocity Profile C8 – F2 Tornado Transverse Velocity Profile along the Lines

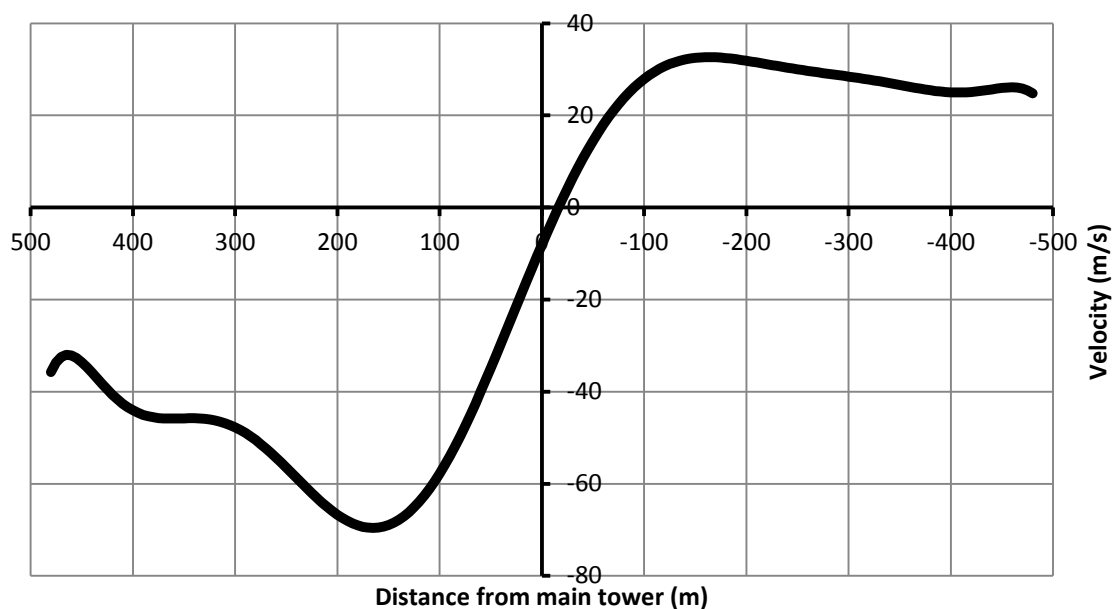


Fig. 7-40 Line Velocity Profile C9 – F2 Tornado Transverse Velocity Profile along the Lines

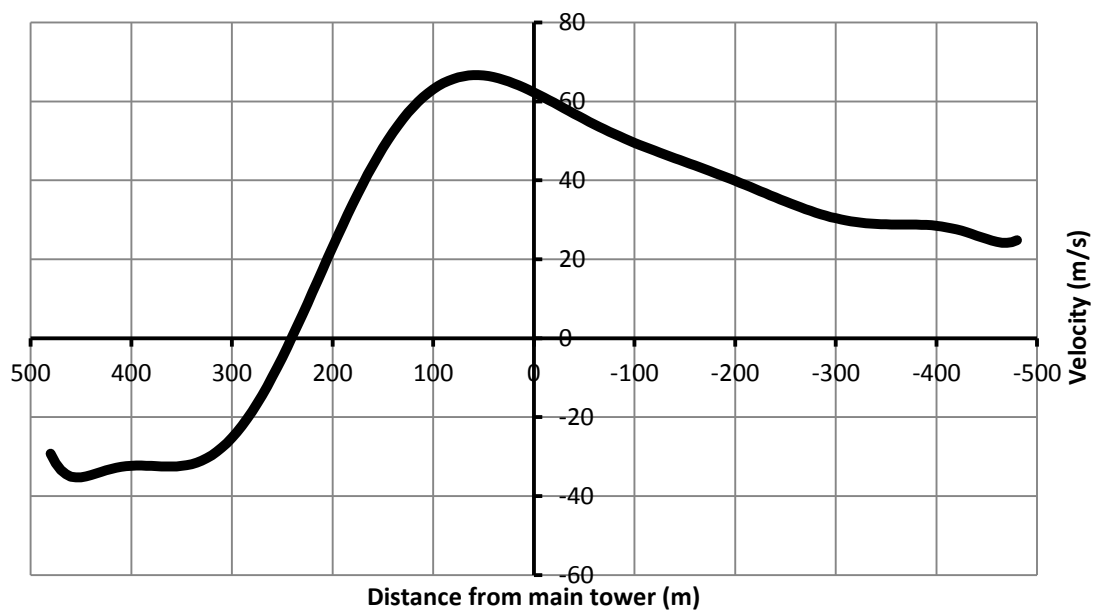


Fig. 7-41 Line Velocity Profile C10 – F2 Tornado Transverse Velocity Profile along the Lines

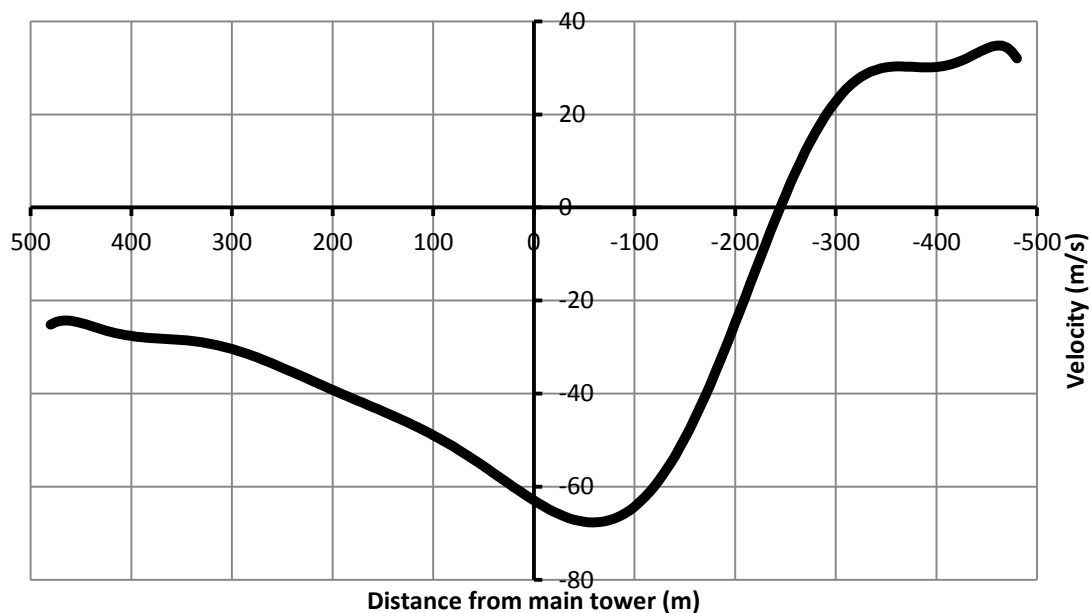


Fig. 7-42 Line Velocity Profile C11 – F2 Tornado Transverse Velocity Profile along the Lines

Line Profiles' equations:

“x” is the distance from the tower of interest and “y” is the velocity

Line Profile C6

$$y = 4.24z^{10} + 6.59z^9 - 22.15z^8 - 33.44z^7 + 32.92z^6 + 42.77z^5 - 23.38z^4 - 14.39z^3 + 21.63z^2 + 23.94z + 32.32$$

$$z = x / 290.95$$

Line Profile C7

$$y = -1.53z^{10} + 7.21z^9 + 0.19z^8 - 38.05z^7 + 32.32z^6 + 51.19z^5 - 59.69z^4 - 14.39z^3 + 16.66z^2 + 19.48z - 34.26$$

$$z = x / 290.95$$

Line Profile C8

$$y = 7.37z^{10} - 10.49z^9 - 56.68z^8 + 76.62z^7 + 159.01z^6 - 205.91z^5 - 195.19z^4 + 253.02z^3 + 91.63z^2 - 151.59z + 4.65$$
$$z = x / 290.95$$

Line Profile C9

$$y = -8.94z^{10} - 9.19z^9 + 64.74z^8 + 68.86z^7 - 168.41z^6 - 190.76z^5 + 187.92z^4 + 243.14z^3 - 77.22z^2 - 150.83z - 8.13$$
$$z = x / 290.95$$

Line Profile C10

$$y = 8.23z^{10} + 6.68z^9 - 58.09z^8 - 50.49z^7 + 138.5z^6 + 139z^5 - 106.61z^4 - 158.58z^3 - 40.11z^2 + 36.64z + 62.32$$
$$z = x / 290.95$$

Line Profile C11

$$y = -7.28z^{10} + 6.38z^9 + 51.75z^8 - 49.62z^7 - 123.38z^6 + 139.24z^5 + 92.02z^4 - 161.05z^3 + 44.40z^2 + 39.48z - 62.94$$
$$z = x / 290.95$$

CHAPTER 8

CONCLUSIONS AND RECOMMENDATIONS

8.1 Summary

The research conducted in this thesis presents a significant progress in the subject of structural behaviour of transmission line structures under tornado loading. Chapter 1 covers a literature review for the research conducted on this subject. The research conducted previously by the author in his M.E.Sc. dissertation is also summarized. The tornado wind field used in the previous M.E.Sc. study and the current study is based on computational fluid dynamics simulations conducted and validated by other researchers. The wind field represents the steady-state of a tornado with open smooth terrain. In his M.E.Sc. thesis, the author established a procedure to scale the wind field in order to simulate an F2 tornado and to estimate the wind forces acting on transmission line systems due to this type of extreme wind events. In the previous research conducted by the author, the modelling and prediction of the behaviour of transmission line systems was conducted using a commercial analysis software.

The research reported in Chapter 2 of the current dissertation is conducted using this previous model. Two transmission line systems are considered as case studies in this chapter and analyses are conducted to compare the internal forces in the tower members due to an F2 tornado to those associated with normal wind loads, downbursts, and the available guideline for tornado loading on transmission line structures. The purpose of

this chapter was to assess the significance of tornado loading compared to other type of wind events.

In this thesis, the author has developed a comprehensive in-house numerical model for the analysis of transmission lines under tornadoes. This was done incrementally in two chapters of the thesis. In Chapter 3, the formulation of a special cable element is extended to include the geometric nonlinear effect. This curved element consists of four nodes and thus can model efficiently the curved shaped of the conductors and ground-wire of a transmission line. A simulation for the insulators connecting the conductors to the transmission towers is developed in this chapter using a three dimensional nonlinear spring system. In Chapter 5, a nonlinear finite element is developed for the simulation of the towers, where three dimensional frame element are used to model the tower members. The element includes the geometric nonlinear effect. This is combined with conductors' model developed in Chapter 3 and the tornado wind field obtained from the CFD simulations to form a comprehensive numerical tool for the simulation of an entire transmission line system. In addition, two failure models are incorporated for the tower member in order to study the failure and the progressive collapse of transmission towers under tornadoes. This numerical development was used to conduct a number of studies. In Chapter 3 and 4, the behaviour of the conductors under F2 tornado loading was investigated. In Chapter 5, the progressive failure of two different transmission line systems under F2 tornadoes was assessed as case studies.

In Chapter 6, a unique aeroelastic model was designed and constructed. The physical model was tested at the Boundary Layer Wind Tunnel Laboratory (BLWTL) and the

results of the test were used to validate the developed numerical model. Finally, in Chapter 7, the numerical model was used to develop a set of load configurations simulating the critical effect of F2 tornadoes on lattice transmission line structures.

8.2 Conclusions

The following conclusions are drawn from the study:

- Comparing the internal forces due to F2 tornado to the those resulting from conventional wind load, downbursts, and the high intensity wind load cases recommended by CIGRE, it is concluded that the F2 tornado forces exceed the peak forces resulting from these loads .
- For the cross-arm members, the peak internal forces are found to be associated with a tornado located at a relatively far distance from the tower.
- Accounting for the flexibility of the tower and the insulator is very important in predicting the behaviour of the conductors especially under the unbalanced loading cases caused by tornadoes.
- An assessment is conducted for the validity of the recommendation made in some codes of practice and design manuals to neglect the tornado loads applied to transmission lines, such as conductors and ground-wire. The results show that the peak internal forces in chord members increase by 22 to 140 % due to the inclusion of the line loads in the analysis of transmission line systems under tornadoes.

- The transverse F2 tornado force and wind velocity distributions on transmission lines, such as conductors and ground-wires, are highly non-uniform, vary nonlinearly, and change directions within one line span. The vertical (uplift and downdraft) velocity component of F2 tornadoes is significant and can be up to 40% of the transverse velocity component.
- The length of transmission tower's cross-arms has a significant effect on the conductor's reactions associated with tornado loads. For the same tower, differences of 32% and 47% in the longitudinal and transverse reactions, respectively, are reported due to a horizontal distance of 29 (m) between the two edge conductors. This difference in lines' reactions leads to an additional torsional moment on the supporting towers.
- Significant longitudinal line's reaction leads to an out-of-plan bending effect on the tower's cross-arms and, consequently, compression forces in some members that are not typically considered in the design. Accordingly, the current study investigates the effect of different parameters on the longitudinal reactions of transmission lines. The study shows that the longitudinal reactions:
 - a) have a nonlinear variation with the magnitude of the applied F2 tornado wind load.
 - b) change significantly and in a nonlinear manner with both the value of the initial pretension force and sag, and the length of the insulator springs attached to the line.
 - c) vary linearly with a change in the conductor's self-weight

- The numerical model predicts that two considered guyed transmission tower systems, L1 and L2, cannot withstand the maximum velocity of an F2 tornado. However a significant difference in the tornado capacity is shown between the two systems. While system L1 is predicted to fail at 84% of the maximum tornado velocity, system L2 is predicted to fail at only 54%. Also, the failure modes predicted for the two systems are different; system L1 fails by bending while system L2 fails by shear. Despite the fact that the two systems have almost equal conductors' span and they were initially designed under similar environmental loads (without considering tornadoes), significant difference in tornado capacity and failure modes is observed. The main reason affecting the failure mode, whether it is bending and shear, is the location of the guys relative to the conductors. This difference in tornado behaviour between the two systems can be attributed to the difference in the geometric configuration of the towers, in the number of conductor bundles, and in the width of the conductors' cross-arm. As a result of the localized nature of tornadoes, a system with wide cross arms will have different forces acting on the parallel conductor lines. This can lead to a torsion effect on the tower.
- The assumption made regarding the post yield tension behaviour has no significant effect on the failure velocity. Assuming that the tension members maintain their post yield strength compared to losing their strength has increased the failure velocity by about 8% and 10% for systems L1 and L2, respectively.
- Due to the localized nature of tornadoes, the forces acting on a transmission tower depend on the location of the tornado relative to tower. Thus, the failure velocity

of the same tower can vary based on the location of the tornado. For the two considered critical tornado locations, a difference of 11% is observed in the failure velocities for system L1. This is reduced to only 3% for system L2.

- The inclusion of geometric nonlinearities is shown to alter the failure velocity of systems L1 and L2 by 8% and 17%, respectively. Because of the larger flexibility of system L2, the geometric nonlinear effect is shown to have a more pronounced effect for this system.
- For the thirty seven test wind speeds used for the aeroelastic test, no instabilities are found for the tested guyed transmission towers or lines. The general dynamic response of the tower follows an exponential curve, similar to the variation in the applied wind load.
- The resonant components of the dynamic response are more significant and noticeable in low wind speeds. With increasing the wind speeds, these resonant components become less distinguished and in some cases vanishes.
- The measured resonant frequencies of the aeroelastic model match those expected by the numerical model of the full tower.
- In terms of the resonant peaks of the tower's dynamic response and their correspondent frequencies, no significant differences are for the case with and without conductors. The resonant peaks almost have the same frequencies for both cases. The magnitude of the dynamic response is different due to the conductor's loads. This can be explained in view of both the high aerodynamic damping of the conductors and the significant difference in the natural frequencies between the conductors and the supporting towers. In addition, most

of the conductor's load path is transferred by the supporting guys to ground supports.

- The conductors' oscillations under fluctuating wind affect the resonant component of the conductors' cross-arms. Such effect is noticed in the mid-tower straining actions response at low wind speeds, and become less distinguished with the increase of the wind speed.
- The variation of the transmission tower straining actions with the increase of the wind speed follows an exponential curve, similar to the applied wind load.
- For the case of towers only and the case of towers with conductors, a very good agreement is found between the measured straining actions of the aeroelastic model and the calculated values using the in-house numerical model.
- The inclusion of the conductors changes the transmission towers response under wind loads, with increase or decrease of the internal forces of the tower. The conductors reaction decrease the internal forces in the towers main body, while increase the supporting guys and conductor's cross-arms straining actions. In addition, the conductors exhibit a longitudinal force on the supporting towers' cross-arms due to the unbalanced wind loading on the conductors. This longitudinal reactions change the structural response and force distribution in the different components of the transmission tower.
- Based on the results of extensive parametric studies, a number of critical tornado configurations (R and θ) that lead to peak forces in the transmission tower members are identified. For transmission towers' main body, three critical values

for R , combined with four critical values of θ for each value of R , are identified.

Those critical configurations are:

$R = 100$ (m), with $\theta = 0^\circ, 90^\circ, 180^\circ,$ and 270°

$R = 125$ (m), with $\theta = 30^\circ, 150^\circ, 210^\circ,$ and 330°

$R = 150$ (m), with $\theta = 60^\circ, 120^\circ, 240^\circ,$ and 300°

- For transmission tower's cross-arms, critical tornado configurations that lead to the maximum transverse and longitudinal forces transferred from the lines to the transmission towers are identified. Critical tornado configurations leading to maximum transverse reactions are:

$R = 250$ (m) and $\theta = 60^\circ$ and 240°

and critical tornado configurations of maximum longitudinal reactions are:

$R = 450$ (m), with $\theta = 90^\circ$ and 270°

$R = 125$ (m), with $\theta = 0^\circ$ and 180°

- There is a lack of information and procedures in the transmission line's codes of design and manuals of practice regarding the estimation of tornado forces on transmission lines systems. Accordingly, eighteen critical load configurations have been recommended in the current thesis. Each critical configuration represents a load case and the vertical profile for the three perpendicular velocity components along the height of the tower are provided for each case. In addition, the corresponding horizontal profile for the transverse velocity acting on the lines are given for each load case. These equivalent load cases represent an envelope for the effect of F2 tornadoes on transmission line systems, and can be applied by

a structural engineer in the design process and failure investigations of lattice tangent transmission line structures.

8.3 Recommendation for Future Work

The following recommendations are added for future work which would extend the results presented in this thesis:

- Fluid numerical model for HIW and normal wind should be combined with the structural model developed by the author in the current thesis. A fluid-structure interaction scheme should be incorporated into the combined numerical models in order to account for the variation of the wind fields resulting from the structure's motion.
- The developed aeroelastic model should be tested under simulated tornado and downburst events in WindEEE research institute. The results of the aeroleastic tests in WindEEE research institute should be used to calibrate and validate the developed wind-structure numerical models.
- Propose two design levels for transmission lines under HIW. Level I is an operational level, which assures that under moderate intensity HIW, no damage is anticipated to happen to any structural member of the tower. Level II is a no-collapse level, which assures that the tower does not collapse under strong intensity HIW. This economical design procedure will ensure that power interruptions do not occur under moderate HIW. It will also minimize the duration of power interruptions after a strong intensity HIW.

CURRICULUM VITAE

Name: Ahmed (Mahdy) Hamada

Post-Secondary Education and Degrees:

Doctor of Philosophy 2010-2014
 Department of Civil and Environmental Engineering
 Faculty of Engineering
 The University of Western Ontario
 London, Ontario, Canada

Masters of Engineering Science 2008-2009
 Department of Civil and Environmental Engineering
 Faculty of Engineering
 The University of Western Ontario
 London, Ontario, Canada

Bachelor of Engineering Science 1999-2004
 Department of Civil and Environmental Engineering
 Faculty of Engineering
 Alexandria University
 Alexandria, Egypt

Honours and Awards:

Vanier Canada Graduate Scholarship
 2011-2014
 Natural Science and Engineering Research Council of Canada
 (NSERC), Canada

Graduate Award in Structural Engineering
 2013-2014
 Department of Civil and Environmental Engineering
 The University of Western Ontario, Canada

Ontario Graduate Scholarship (OGS) – international
 2011-2012
 Ontario Graduate Scholarship, Canada

MITACS Accelerate Ph.D. Fellowship/Award
 2010-2011
 Federal and Provincial Funded Research Network, Canada

1st Place, Graduate Student Civil Seminar Competition 2010
 Department of Civil and Environmental Engineering
 The University of Western Ontario, Canada

Nominated for the Outstanding Teaching Assistant Award
2009, 2010, 2011, 2012, 2013
The University of Western Ontario, Canada

The government Award of Excellence in Undergraduate Studies
(Dean's List)
1999-2004
Alexandria University, Egypt

**Academic
Appointments:**

Research Engineer/Assistant
2008-2014
Department of Civil and Environmental Engineering
The University of Western Ontario, Canada

Teaching Assistant
2008-2014
Civil and Environmental Engineering Department
The University of Western Ontario, Canada

Instructor – Civil Engineering Design Project (CEE 4441)
2013-2014
Department of Civil and Environmental Engineering
The University of Western Ontario, Canada

Western Certificate in University Teaching and Learning
2013
The University of Western Ontario, Canada

Instructor – Structure Theory IV (CEE 3341b)
2013
Department of Civil and Environmental Engineering
The University of Western Ontario, Canada

Teaching Assistant
2004-2007
Department of Civil and Environmental Engineering
Faculty of Engineering – Alexandria University, Egypt

**Professional
Appointments:**

Structural Designer
2008-2014
London, Ontario, Canada

Structural Engineer
2004-2007
Egyptian Consultant Union – ECU
Alexandria, Egypt

Technical Committees:

American Society of Civil Engineers (ASCE) Task Committee, Manual of Practice No. 74: Guidelines for Electrical Transmission Line Structural Loading, USA

Teaching Committees:

Graduate Education Council – Mentorship and professional Development Committee, The University of Western Ontario, Canada

Publications

Journal Articles

A. Hamada, A.A. El Damatty (2011), “*Behaviour of Guyed Transmission Line Structures under Tornado Wind Loading*”, Computer and Structures, Vol. **89**, Issues 11-12, 986-1003

A. Hamada, A.A. El Damatty, H. Hangan, and A. Y. Shehata (2010), “*Finite Element Modelling of Transmission Line Structures under Tornado Wind Loading*”, Wind and Structures, Vol. **13**, No. 5, 451-469

Peer-reviewed Conference Papers

(A. Hamada is the presenting author unless noted by underline)

A. A. El Damatty, A. Elawady, **A. Hamada**, W. E. Lin (2014), “*State-of-the-Art Knowledge about Behaviour of Transmission Line Structures under Downbursts and Tornadoes*”, 2014 International Conference on Advances in Wind and Structures (AWAS14) - ACEM14, Busan, Korea, Montreal, Canada, 24-28 August, 2014

A. Hamada, A. A. El Damatty (2014), “*Nonlinear Formulation of Four-Noded Cable Element and Application to Transmission Lines under Tornadoes*”, 2014 International Conference on Advances in Wind and Structures (AWAS14) - ACEM14, Busan, Korea, Montreal, Canada, 24-28 August, 2014

A. A. El Damatty, A. K. Elawady, **A. Hamada**, (2014), “*Resilience of transmission lines to localized high intensity wind events*”, proceedings (Abstract and Presentation)

ASCE –Engineering Mechanics Institute Conference, McMaster University, Hamilton, ON, Canada, August, 2014

A. Hamada, A. A. El Damatty (2013), “*Seismic Analysis of L-shaped High and Low Rise Buildings – Comparison with NBCC 2005 and NBCC 2010*”, CSCE 2013 General Conference, Montreal, Canada, May 2013

A. Hamada, A. A. El Damatty (2013), “*Analysis and Behaviour of Guyed Transmission Lines Under Tornado Wind Loads – Case Studies*”, CSCE 2013 General Conference, Montreal, Canada, May 2013

A. A. El Damatty, **A. Hamada**, A. El Awady (2013), “*Development of Critical Load Cases Simulating the Effect of Downbursts and Tornadoes on Transmission Line Structures*”, proceedings (Keynote speaker paper) of the Eighth Asia-Pacific Conference on Wind Engineering, Chennai, India

A.A. El Damatty, **A. Hamada** (2012), “*Behaviour of Guyed Transmission Line Structures under Tornado Wind Loads – Case Studies*”, ASCE – Structural Engineering Institute – Electrical Transmission and Substation Structures Conference, Columbus, Ohio, USA, November 2012

A.Altalmas, A. A. El Damatty, and **A. Hamada** (2012), “*Progressive Failure of Transmission Towers under Tornado Loading*”, CSCE 3rd International Structural Specialty Conference, Edmonton, Canada, June 2012

A.A. El Damatty, M.M. Hassan, A.Y. Shehata, **A. Hamada** (2010), “*Recent Advances in High Intensity Wind Structural Problems*”, Seventh Alexandria International Conference on Structural and Geotechnical Engineering, Alexandria, Egypt, December 2010

Selected Engineering Research Projects

A. Hamada, (2013), “*Computational Fluid Dynamics Simulations of Tall Buildings with Different Corner geometries*”, Computational Wind Engineering CEE 9527, Department of Civil and Environmental Engineering, The University of Western Ontario, London, Ontario, Canada

A. Hamada, (2010), “*Plastic Analysis and Design of Fixed Offshore Structures*”, The University of Western Ontario, London, Ontario, Canada

A. Hamada, (2009), “*Performance Based Design of 35-Storey Concrete Building*”, Computational Wind Engineering CEE 9550, Department of Civil and Environmental Engineering, The University of Western Ontario, London, Ontario, Canada